UPOL Studies in Analytical Chemistry

Novel electrochemical sensors for analysis of biological active compounds

Soodabeh Hassanpour

Palacký University
Olomouc

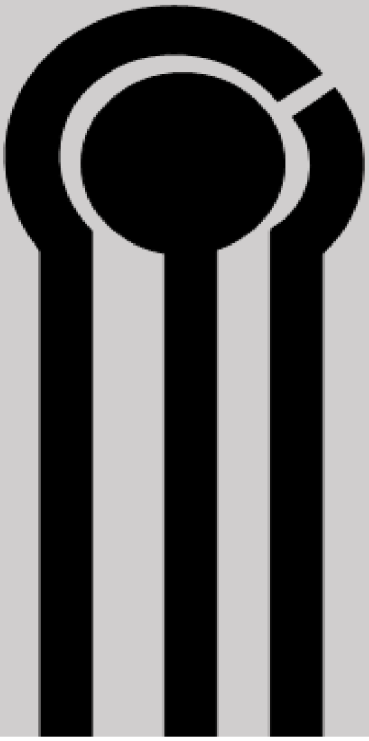

PALACKÝ UNIVERSITY IN OLOMOUC

Faculty of Science

Department of Analytical Chemistry

DOCTORAL THESIS

Novel electrochemical sensors for analysis of biological active compounds

Author of the thesis:	Soodabeh Hassanpour, MSc.
Field of study:	Analytical Chemistry
Supervisor:	Assoc. Prof. RNDr. Jan Petr, Ph.D.

Olomouc 2023

Declaration

This dissertation results from my investigations, observations, and experiments, except where otherwise stated. All sources of literature are correctly cited. The adapted figures were reproduced with the permission of the original journals. I agree that the work is made available online in the library of the Department of Analytical Chemistry, Faculty of Science, Palacký University in Olomouc.

In Olomouc on .....

…….

Handwritten signature

Acknowledgements

First and foremost, I would like to express my special and sincere thanks to my supervisor, doc. RNDr. Jan Petr, Ph.D., for giving me a home in his lab and supports me over the years. I am deeply grateful for his guidance, scientific advice, continuous support, endless patience, and the opportunities he has afforded me. Under his mentorship, I have learned the particulars of grant writing, which is an invaluable tool as my career progresses. I want to thank my friends in our group for their kind help at the beginning of my life in the Czech Republic and the time we spent together in our office.

My appreciation also goes out to my parents and sisters for their encouragement and support throughout my studies. Last and foremost, I would like to offer my special thanks to a very special person, my husband, Navid, for his continued and unwavering love, support, and understanding during my pursuit of a Ph.D. degree that made completing the thesis possible. You were always around when I thought it was impossible to continue; you helped me keep things in perspective and stood by me through the ups and downs. I greatly value his contribution and sincerely appreciate his belief in me. Words would never say how grateful I am to you.

Bibliographic Information

Author:	Soodabeh Hassanpour, MSc.
Title of Thesis:	Novel electrochemical sensors for analysis of biological active compounds
Type of Thesis:	Doctoral
Department:	Department of Analytical Chemistry
Supervisor:	Assoc. Prof. RNDr. Jan Petr, Ph.D.
Academic Year:	2022/2023
Keywords:	(Bio)sensors, Screen-printed electrodes, Disposable, Dasatinib, Single-walled carbon nanotubes, Horseradish peroxidase, Hydrogen peroxide, Molecularly imprinted polymer, Poly(tyrosine)-Chitosan; Bioelectrocatalyst, Genosensor, Haemophilus influenza, DNA bio-assay, citrate capped silver nanoparticle
Number of Pages:	108
Number of Appendices:	1
Language:	English

Abstract

Recently, medical organizations and research disciplines have switched to employing affordable biosensors. Biosensors have become more critical in drug development, drug identification, bio-medicine, food safety, security, protection, and ecological research. It has directly contributed to developing specialized and reliable diagnostic equipment that uses biological sensing components as biosensors. Different analytes, biological receptors, and transducer concepts are used in biosensors. In recent years, innovative sensing platforms have been developed employing screen-printed electrodes (SPEs), which are inexpensive, simple, and quick mass production through thick film technology.

During my Ph.D., I concentrated on designing, constructing, and validating several SPE-based (bio)sensors to identify biologically active compounds important for healthcare applications, demonstrating their significant potential as a suitable sensing platform. I created (bio)sensors for a variety of analytes, from nucleic acid to small molecules, with specific modification strategies to endow the platforms with selectivity toward the species of interest. I developed disposable electrochemical (bio)sensors in two papers based on modifying with single-walled carbon nanotubes (SWCNT) and molecularly imprinted polymers. In the first case, SWCNT-modified SPCE as disposable electrochemical sensors was proposed for quick determination of dasatinib in pharmaceutical formulations, demonstrating an excellent boosting effect on the oxidation response of dasatinib. The sensor was able to monitor different dasatinib concentrations with a limit of detection of 0.06 µM. In the second paper, the SPE surface was modified with poly tyrosine-chitosan and combined with a self-assembly surface molecular imprinting approach to develop horseradish peroxidase (HRP)-imprinted biosensor. Additionally, the molecularly imprinted electrochemical biosensor for determination of HRP was expanded for the detection of H_2O_2 as

enzymatic substrates. The HRP-imprinted biosensor was determined H_2O_2 and HRP with detection limits of 2.18 nM and 9.39×10^{-8} mg/ml (2.34 pM), respectively.

The last paper was related to developing a DNA-based bio-assay for determining *Haemophilus influenza* through bioconjugation of citrate-capped silver nanoparticles with pDNA toward target sequences detection. The ultra-sensitive fabricated optical genosensor was detected the synthesized probe (SH-5′-AAT TTT CCA ACT TTT TCA CCT GCA T-3') of *Haemophilus influenza* with great selectivity and sensitivity after hybridization with cDNA with the low limit of quantification of 1 zM (zeptomolar). Finally, the designed genosensor is a significant diagnostic strategy for detecting *Haemophilus influenza* with great selectivity.

Contents

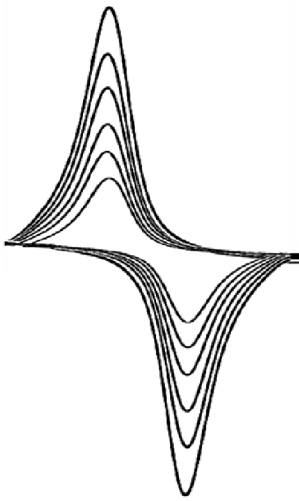

CHAPTER 1: INTRODUCTION

Biosensors as analytical instruments connect a biological, biochemical, or chemical recognition element with a transducer in which the recognition part can interact directly or indirectly with an analyte [1]. The use of sensors and biosensors in detecting and monitoring different analytes in clinical analysis, medical diagnosis, environmental monitoring, and food safety has grown in popularity in recent years. They are preferred over traditional methods like immunoassays, spectroscopy, and chromatography techniques because of their high sensitivity, quick analysis time, and lower cost [2, 3]. Additionally, they may be utilized by the general population to examine complicated materials without tedious sample preparation. Such sensors can be found in various powerful devices, including glucose biosensors, cholesterol test kits, and some blood analyzers [4].

The versatility, low cost, small size, and portability for *in-situ* applications provided by screen-printed technology added significant merits to electrochemical biosensors. Nowadays, the creation of miniaturized electrochemical biosensors for detecting various analytes is made possible by disposable screen-printed carbon electrodes (SPCEs) produced using thick-film technology [5, 6]. SPCEs, as an alternative to the standard electrochemical setups using conventional electrodes, are available for electrochemical applications due to their easy and quick activating procedure, disposability, small size, high chemical stability, portability, wide electrochemical window, low background current with an economical substrate, and no need for time-consuming processes. One of the most notable benefits of SPCEs, besides the significant cost reduction, is the ability to analyze a trace amount of sample solution by replacement of large cells and bulky electrodes [7, 8]. In light of these indications, the works presented herein pursued the development of electrochemical SPCEs-based sensors and biosensors to monitor a number of biologically active compounds.

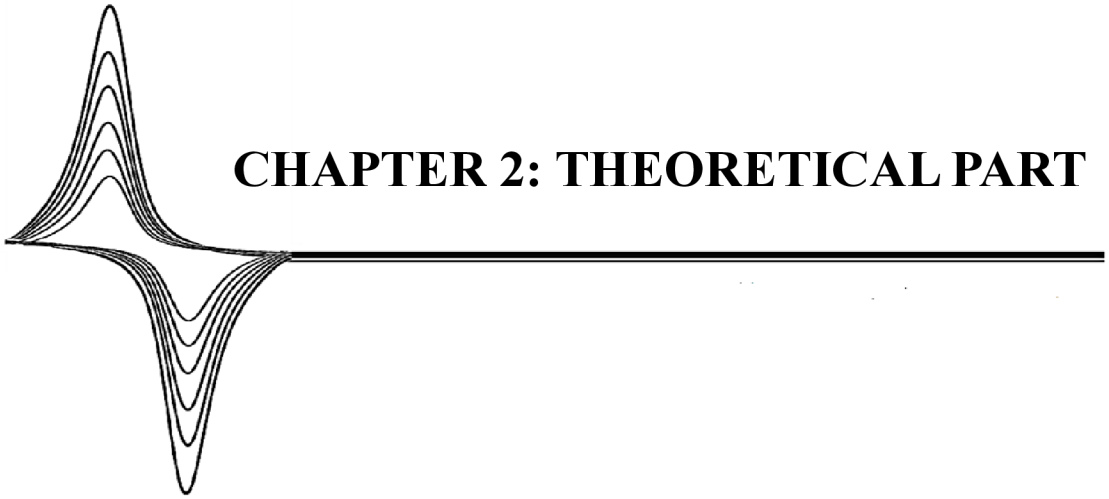

CHAPTER 2: THEORETICAL PART

Sensors and Biosensors

Historically, the contemporary idea of biosensors, in which an enzyme was combined with an electrode to create a biosensor, was introduced by Clark and Lyons [9]. Since the invention of Clark and Lyons in 1962 made it possible to access simple, rapid, and precise biosensor for glucose, the area of biosensors has rapidly expanded [10]. So far, the development of biosensors for diverse analytes in fields including medicine, healthcare, the environment, and industry has been the subject of countless investigations. A biosensor can be used to monitor non-biological or biological substances. The fact that biosensors do not need sample preparation is one of the key factors contributing to their growing popularity. Disposable biosensors, however, are incredibly helpful for testing things like blood glucose for persons with diabetes [11]. Biosensors as analytical instruments connect a biological, biochemical, or chemical recognition element with a transducer in which the recognition part can interact directly or indirectly with an analyte [1]. Interaction of the analyte with the recognition part causes the alteration of biological responses into signals and then emits the signals by the transducer; consequently, signals are amplified. This conversion of a biological event into a readout is proportional to the concentration of a specified analyte in sample [1].

Biosensors are often classified into three main parts: biorecognition elements (bioreceptor), transducers, and a signal processor (Fig. 2.1). The most crucial step in the manufacture of a biosensor is the selection of an appropriate transducer, bioreceptor, and their immobilization on a sensing platform during detection of analyte (such as proteins, DNAs, metabolites, human samples, food, or environmental samples). We can modify the sensing platform throughout the construction process by functionalizing any component according to the conditions of our experiment [12]. The biorecognition component is an important part of a biosensor that selectively

reacts with the target analyte, lessens interferences from other species in a sample, and needs careful consideration throughout the selection and immobilization processes. Bioreceptors can be made in a lab or directly taken from live systems (such as an antibody, aptamer, nucleic acid, whole cells, or enzyme). Transducers are an extremely important parts of a biosensor since they are known to transform the produced biological signals into detectable signal that may be either optical or electrochemical. The analyte concentration often affects the signal strength produced during biological contact with it. Then, the signal is then collected, amplified, and displayed by a signal processor. Depending on the transducer or biorecognition element biosensors may be divided into numerous categories [13]. Biosensors are categorized into electrochemical, optical, thermal, and piezoelectric biosensors based on the transducer surface employed to create the sensing platform. Electrochemical biosensors are the most commonly studied among the other four due to their outstanding sensitivity, speed, and cost-effectiveness for identifying analytes [12].

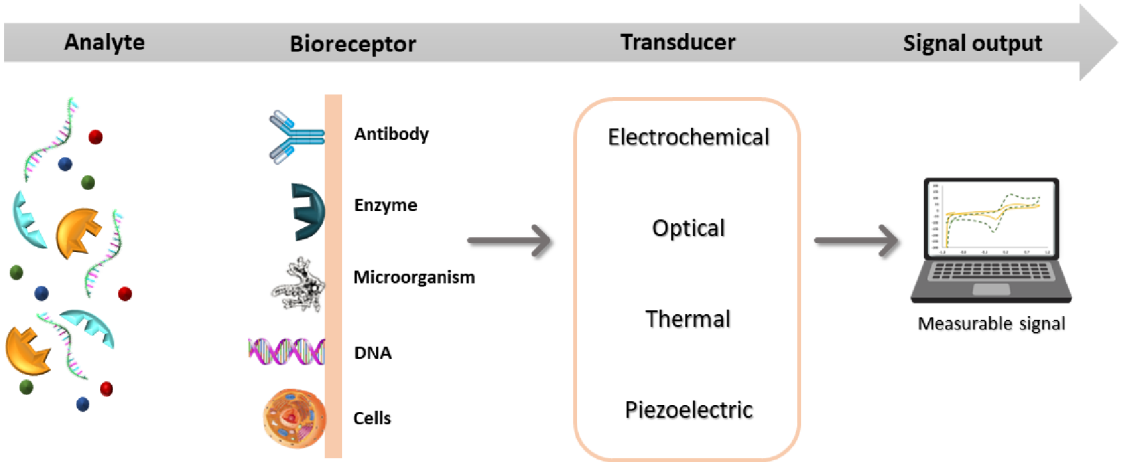

Fig. 2.1 | Biosensor components. Schematic illustration of biosensor operation principles: target analyte detection by the corresponding biorecognition element followed by signal transduction method and output.

Electrochemical Sensors and Biosensors

In electrochemical sensors and biosensors, the electrode functions as a transducer [14]. The sensing ability of a sensor depends on the measurement of currents and/or voltages that are produced by a recognition event between the interest analytes and the immobilized or chemically modified receptor on the electrode [15]. The main methods used to operate electrochemical transducers include cyclic voltammetry (CV), differential pulse voltammetry (DPV), square wave voltammetry (SWV), linear sweep voltammetry (LSV), electrochemical immittance/impedance spectroscopy (EIS), amperometry, etc [16]. The electrochemical sensors and biosensors are shown in Fig. 2.2, together with the measurable signals they produce using various transduction methods. The following sections describe the transduction techniques used in this research.

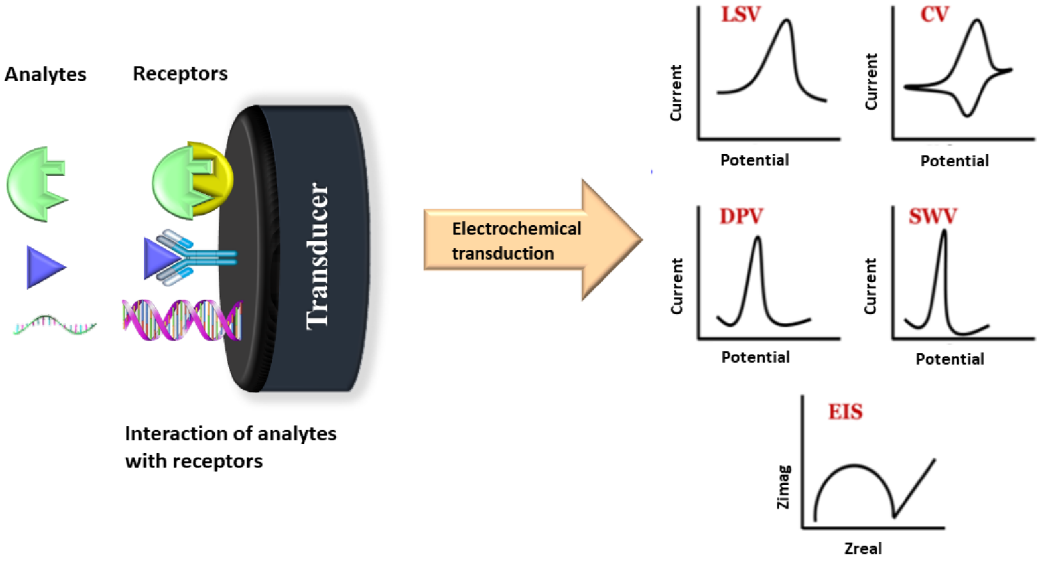

Fig. 2.2 | Electrochemical (bio)sensor and its measurable signals.

Voltammetric techniques

Voltammetric measurements provide the current output vs. potential after imposing a potential ramp. Typically, these procedures are carried out in quiescent solutions. The potential sweep generates voltammetric peaks in the presence of electroactive species, including quantitative and qualitative data about the redox processes. As the potential of the peaks depends on the nature of the redox groups, it may be utilized to get qualitative data about the molecules. These methods are, in fact, the most used for gathering qualitative information on electrochemical processes. On the other hand, the concentration of electroactive species in the solution can be related to measuring voltammetric peaks regarding current, area, or charge [17].

The Randles-Sevcik equation, which defines the influence of the scan rate on the peak current, may provide quantitative and kinetic information on voltammetric processes [18]. At 25°C, the simplified Randles-Sevcik model yields equation 1.

$$I_p = (2.687 \times 10^5) n^{3/2} A.C(D.v)^{1/2} \qquad \text{Eq. 1}$$

Where n is the electron stoichiometry, I_p denotes the peak current, A is the electrode area (cm^2), D is the electroactive species diffusion coefficient (cm^2/s), C is the electroactive species concentration (mol/cm^3), and v is the potential scan rate (V/s). The D, A, or n may be calculated theoretically using the relationships given by this equation and the known experimental values [18].

Equation 1 shows that the current is directly proportional to C and enhances with $v^{1/2}$, indicating that the reaction is regulated by mass-transport (diffusion). To evaluate the diffusion coefficient, linear plots of I_p *vs.* $v^{1/2}$, for constant C value, should pass through the origin and exhibit a gradient. Moreover, the slope of the I_p *vs.* $v^{1/2}$ plots for species where D is known (or may be estimated) gives insight into the stoichiometry of the redox process or A. It is occasionally feasible to find a non-linear relationship between I_p *vs.* $v^{1/2}$, which points to a process that is not regulated

by diffusion and may contain adsorbed intermediates [18-20]. The linear sweep voltammetry (LSV) method is the simplest method for measuring potential variation. It is based on a single potential ramp that changes over time from a start potential (E_{begin}), where electrochemical activity is typically absent, to a final potential (E_{end}), where the reaction is mass transport-controlled. Several significant analytical methods, including cyclic voltammetry, pulse voltammetry, and stripping voltammetry are built on the foundation of this methodology [14].

Cyclic Voltammetry

Cyclic voltammetry (CV) is an adaption of the linear sweep voltammetry, by cycling the potential between two vertices, creating a triangular potential waveform (Fig. 2.3A) that produces the cyclic voltammograms (Fig. 2.3B). CV can operate in single or multicycle modes depending on the information needed.

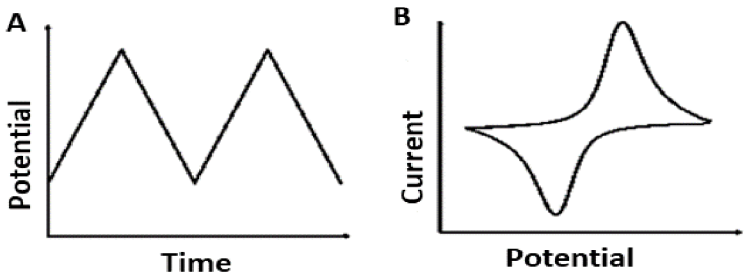

Fig. 2.3 | Cyclic voltammetric technique. (A) The potential cycling waveform. (B) An example of a typical cyclic voltammogram for a reversible redox process.

Cyclic voltammetry has become a key and commonly utilized technique in several fields of electroanalytical chemistry. Because of the quick availability of considerable information on redox processes and the kinetics of heterogeneous electron transfer reactions, CV is the first experiment performed in electroanalytical research. CV is a fast voltage scan technique in which the voltage scan direction is reversed. The resultant current is measured while the applied voltage

at the working electrode is applied in both forward and reverse orientations. The coupled redox reactions' reversibility is shown by the potential cycling, which reveals whether a system is based on reversible, quasi-reversible, or irreversible processes [14]. In cyclic voltammetry, the measured parameters are anodic and cathodic peak currents (I_{pa} and I_{pc}), anodic and cathodic peak potentials (E_{pa} and E_{pc}), and half peak potentials ($E_{p/2}$) at which the cathodic and anodic currents reach half of their peak value [21]. For a simple reversible pair, the I_{pa} and I_{pc} values should be the same, signifying a quick process. However, the reactions coupled to the electrode process might have an impact on the ratio between those values. Peaks potential might yield further information, which is indicating the formal potential of the redox process. The voltammetric peak-to-peak separation analysis indicates process reversibility. The peak-to-peak separation (ΔE_p) for a reversible process is ~ 57 mV at 25 °C (2.22 (RT/F)) and is independent of scan rate. In contrast, the peak-to-peak separation in electrochemical quasi-reversible or irreversible processes is greater and is reliant on the scan rate for potential sweep. Furthermore, the individual peaks in this example are small and far dispersed. The E_p shifts with the scan rate in completely irreversible systems, which is generated by a gradual electron exchange between the electroactive molecule and the working electrode [18, 21, 22].

Differential Pulse Voltammetry

In differential pulse voltammetry (DPV), the surface of working electrode is exposed to fixed-amplitude pulses, short pulses with a length of 10–100 ms and an amplitude of 1–100 mV with an increasing-potential ramp (Fig. 2.4A). In this method, the current is measured at two various times: before (I_1) and after applying the pulse (I_2). The difference between I_2 and I_1 ($\Delta I = I_2 - I_1$) is generating highly sensitive voltammetric peak and plotting the current difference vs the applied voltage (Fig. 2.4B). During the half-wave potential of the reduction or oxidation reaction,

the differential pulse voltammogram reaches a maximum. The DPV is very useful for determining inorganic or organic trace concentrations, resulting in voltammetric peaks with heights that are exactly proportional to the concentration of the target analytes (equation 2) [14, 23, 24].

$$I_p = \frac{nFAD^{1/2}C}{\pi^{1/2}(t-\tau')^{1/2}}\left(\frac{1-\alpha}{1+\alpha}\right) \qquad \text{Eq. 2}$$

Where $\alpha = \exp[(nF/RT)(\Delta E/2)]$. The term $(1 - \alpha)/(1 + \alpha)$ explains the effect of ΔE, pulse amplitude, on I_p max.

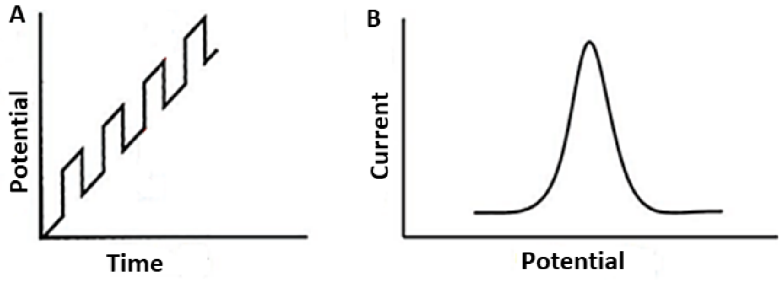

Fig. 2.4 | Differential pulse voltammetry. (A) Potential waveform of pulses superimposed on staircase. (B) Typical DPV voltammogram for oxidation of a target analyte.

Square Wave Voltammetry

Barker was the one who invented square wave voltammetry (SWV) [25]. SWV is the fastest and most sensitive pulse voltammetric technique, and a square wave pulse is followed by a staircase wave to apply the potential in a square waveform. The SWV waveform of the current-potential curve is a regular square wave superimposed on the base of staircase potential and applied to the working electrode. The current is doubled during each square wave cycle, once at the end of the forward pulse, the first current (I_1) is a positive current related to the oxidation and the other at the end of the reverse pulse, the second current (I_2) is a negative current related to the reduction. The difference between I_1 and I_2 is plotted versus the base potential (Fig. 2.5). The final signal has a stronger signal than I_1 and I_2 since it is the difference between I_2 and I_1, which have the opposite

sign [23, 26]. SWV's main benefit is its speed. When square wave and differential pulse voltammetry were compared for reversible and irreversible situations, the square wave currents were 4 and 3.3 times greater, respectively, than the corresponding differential pulse response. Due to its good selectivity and high sensitivity, SWV has been frequently used in recent years to create electrochemical biosensors to identify diseases and environmental pollutants [23, 26].

Fig. 2.5 | Square wave voltammetry. (A) square-wave form and (B) typical voltammogram for square wave

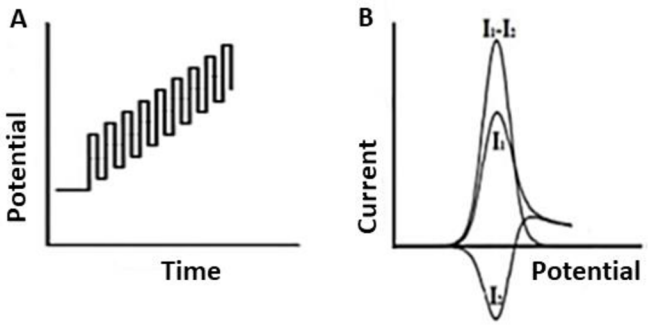

voltammetry.

Electrochemical Platform Setup

Electrochemical platforms are typically made up of three electrodes including working electrode (WE), auxiliary or counter electrode (CE), and reference electrode (RE) that are part of an electrochemical cell. An ionic material, usually a salt in solution, is needed for electrochemical experiments since it serves as the supporting electrolyte and ensures conductivity [23, 27]. To conduct electrochemical studies, a variety of setup and equipment options are available. The most popular configuration relies on the usage of a standard three-electrode cell. However, the analytical field's demands forced this configuration to downsize, become more portable, and combine all the components into a single system, leading to screen-printed electrodes-based systems.

Conventional three-electrode system

A three-electrode cell arrangement typically consists of a beaker with a capacity of 5 to 50 mL that contains the three electrodes submerged in supporting electrolyte. There are also more comprehensive systems that include gas management, such as oxygen removal, temperature control, and magnetic stirrers together with the correct cover (Fig. 2.6). Due to the considerable adaptability of these systems, it is simple to change the cell components based on the analytical goal and/or the kind of sample. Glass is frequently used as a cell material because it is inexpensive, transparent, chemically inert, and impermeable; however, quartz and teflon are potential alternative materials [27].

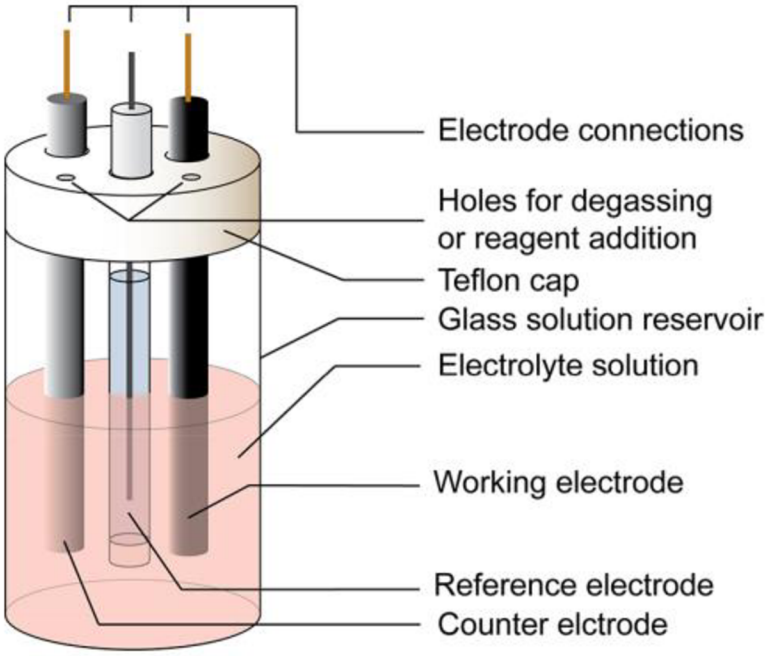

Fig. 2.6 | Schematic illustration of the conventional electrochemical cell. The electrodes are inserted through holes in the cell cover [28].

Using the reference electrode, a consistent and well-known voltage is applied to the working electrode. Reference electrodes include the standard hydrogen electrode, the calomel

electrode (Hg_2Cl_2/Hg), and silver/silver chloride (Ag/AgCl). Due to the explosive nature of hydrogen and its difficulty in preparation and maintenance, the calomel and Ag/AgCl electrodes are used more frequently than the standard hydrogen electrode [27, 29]. Typically, auxiliary electrodes are constructed from inert substances like gold, platinum, and carbon. Every half-reaction that occurs on the working electrode causes the auxiliary electrode to do the opposite half-reaction. This is accomplished by adjusting the voltage of the auxiliary electrode. Moreover, the working electrode's surface is often greater than the auxiliary electrode's. The happening half-reaction at the working electrode shouldn't be hindered by the half-reaction at the auxiliary electrode, which should happen quickly enough. The working electrode acts as the transducer component in bioelectrochemical or biochemical processes, since it should produce a repeatable response with a good signal-to-noise ratio. There are several working electrodes, including platinum electrodes, gold electrodes, carbon paste electrodes, silver electrodes, screen-printed electrodes, etc. The target species' redox behavior, which specifies the needed potential window and the background currents of the supporting electrolyte, should be taken into account while choosing the appropriate WE. While choosing this component, consideration should be given to factors including toxicity, cost, mechanical qualities, and electrical conductivity. A potentiostat or galvanostat and the related software are also necessary as the fundamental equipment for electrochemical experiments [23, 27, 29]. Although these platforms are adaptable and inexpensive, they still have a complicated mounting system that makes it difficult to do *in-situ* analyses, making it tough to work outside of a laboratory. In this aspect, screen-printed electrodes resolve the issues with these standard setups.

Screen-printed electrodes system

Screen-printed electrodes (SPE), a new class of compact, disposable, sensitive, and selective devices, have emerged due to the electroanalytical limitations and practical challenges related to the traditional solid electrodes. Nowadays, electroanalysis uses these transducers extensively to create biosensors and electrochemical sensors, demonstrating their usefulness for a variety of applications. The thick-film method used to create SPEs involves sequentially depositing conductive and nonconductive layers onto an insulating support (printing substrate) with the help of the right screen-printing equipment. This approach enables the large-scale manufacture of low-cost, highly repeatable devices, which is particularly beneficial in fabricating numerous electrodes or electrode array structures [30, 31]. Various inks or pastes are deposited on the printing substrate using a suitable screen with open-mesh areas. The ability to employ multiple screens and inks results in different SPE types that may be created based on the analytical goal. As seen in figure 2.7, a squeegee is used to print SPEs, forcing the ink to flow through the open-mesh regions and depositing the pattern onto the substrate for the printing surface. The finished devices are produced by applying curing stages of appropriate temperature between the printing of each pattern. Hence, the substrate keeps rather durable ink layers that range in thickness from 20 to 100 µm [31].

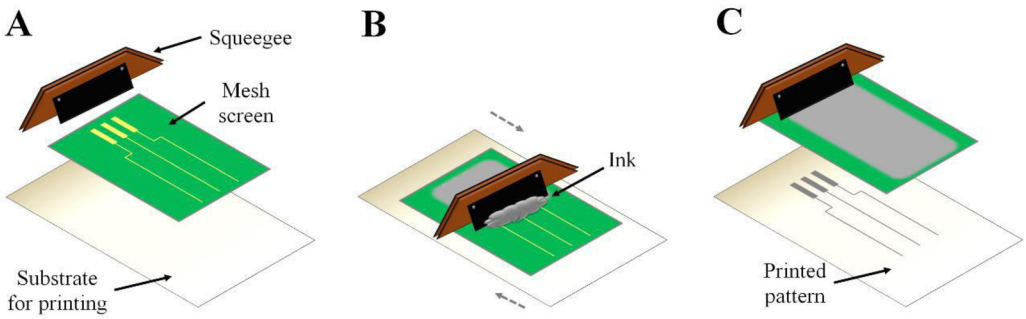

Fig. 2.7 | Screen-printing procedure. (A) Components for screen-printed electrodes fabrication, squeegee, porous screen, and substrate. (B) Ink is printed on a screen using squeegee traversing. (C) Ink deposited as screen-printed electrode pathways pattern on the substrate surface [32].

The rising reputation of SPEs as effective electroanalytical instruments has resulted in many commercially accessible electrodes of various materials and designs throughout the years. Figure 2.8 depicts a typical commercially available SPEs arrangement employed in our experiment. These SPEs have a three-electrode configuration, with an Ag/AgCl reference electrode, an auxiliary carbon electrode, and a working electrode (4-mm diameter) made of carbon, gold, platinum, silver, or other types of conductive inks.

Besides design adaptability, the SPE configuration has remarkable advantages in the electroanalytical sector. SPEs are affordable and may be used either as disposable or reusable devices. Additionally, because they do not require highly experienced staff or time-consuming sample preparation methods, these platforms are simple and suited for *in-situ* and real-time applications outside the laboratory. Moreover, the low power consumption, rapid response, high sensitivity, and ability to function at room temperature broaden the variety of applications for these devices. Furthermore, the appropriate modifications to SPEs give a chance to increase the devices' specificity and sensitivity to the target analytes [30, 33].

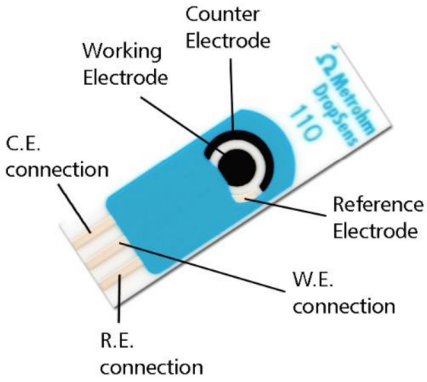

Fig. 2.8 | Commercially available screen-printed carbon electrodes used in this PhD thesis (WE 4-mm diameter).

Modifications of (bio)sensors

Achieving high selectivity, sensitivity, repeatability, and stability is a significant problem in the creation of biosensors. Surface modifications are crucial for the appropriate immobilization of bioreceptors, noise reduction, and improved sensitivity. Furthermore, surface functionalization reduces unintended non-specific binding of the analyte or other components to the surface [34]. Furthermore, the biomolecules' conformation on the surface significantly impacts the selectivity and sensitivity of a biosensor. In other words, the performance of biosensors is greatly affected by the materials utilized for surface modification and the surface chemistry or functionalization approach employed in bioreceptor immobilization [34]. The analytical performance of the biosensors can also be marked by metal coatings, polymers, enzymes, and reactive groups, among other things. Several different electrode modifications and combinations have been developed recently as a result of numerous research with the goal of achieving a reasonable selectivity and sensitivity [35]. Some of the electrode alterations are briefly summarized here.

Carbon-based Nanomaterials

Carbon is widely employed in electrochemistry because of its unique qualities such as a large potential window, chemical inertness, and compatibility for many types of analysis [36]. The development of carbon nanotechnology has led to materials with a high surface-to-volume ratio, high electrical conductivity, biocompatibility, chemical stability, and robust mechanical strength that are suitable for application in electrochemical sensing of different chemicals [37]. Carbon nanotubes [38], graphene [39], diamond nanoparticles [40], and carbon nanofiber-modified electrodes [41] were used to produce a superior analytical performance for a number of analytes.

Metallic Silver Nanoparticles

Silver nanoparticles (AgNPs) have received much attention due to their distinct optical properties and high extinction coefficients [42]. Due to their excellent chemical stability, thermal, catalytic activity, and electrical conductivity of AgNPs, their use in biosensors increased the detection limit of the target [43]. Due to their ease of manufacture, lower cost, and higher extinction coefficients than gold nanoparticles of comparable average size, AgNPs are gaining popularity for their use in optical sensors [44, 45]. Target biomolecule detection was shown to be improved using nanoparticle-conjugated probes. In different sensors, including surface plasmon resonance, spectroscopic, and electrochemical detections, Ag nanoparticle-conjugated biomolecules exhibit high stability and sensitivity toward the target molecular validation [46].

Molecularly Imprinted Polymers (MIPs)

The molecular imprinting process used to make sensors involves the polymerization of specific functional monomers in the presence of template molecules. This template is then removed from the resultant polymer matrix, yielding a film packed with complementary cavities in the size and shape of the template molecule. The electrochemical signals resulting from this film's interaction with a media containing analyte molecules can be employed for sensing. Using relatively inexpensive polymers with excellent specificity is a benefit of this approach. Fig. 2.9 depicts the desorption of the template using a solvent such as PBS at pH 7.2 or a combination of solvents such as water, methanol, etc [16].

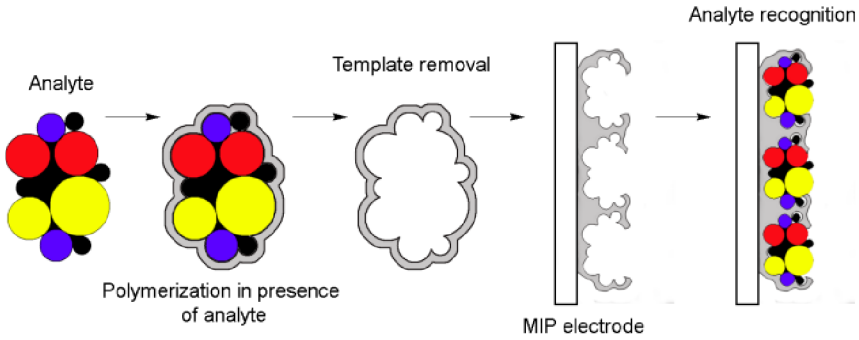

Fig. 2.9 | Schematic illustration of a MIP electrode.

Metal-Organic Frameworks (MOFs)

Metal-organic frameworks, as high-surface-area materials, are 1D, 2D, or 3D inorganic–organic porous hybrid materials made up of rigid metal clusters or metal ions and flexible organic linkers that have shown promise in chiral sensing due to their design flexibility and structured porosity cages [47]. Due to their numerous novel properties, including an ultra-high surface area of up to 10,000 m^2 g^{-1}, non-toxic nature, high porosity, outstanding thermal and chemical stability, available cavities, and tunnels, MOFs are attractive for enantioselective sensors. The porous nature of MOFs helps preconcentrate the target, resulting in increased sensitivity. The chirality of the framework, channel size exclusion, host-guest chemistry in the MOF cavity, target-specific signal response, and hydrogen bonding or special coordination of analytes to the framework all contribute to the selectivity of MOF-based sensors [47, 48].

Enzymes

Enzymes are the most common biological components used as bioreceptors in the construction of biosensors, allowing for a variety of quantifiable responses [49]. The chosen enzyme must have catalytic functions to convert the target analyte, which is a fundamental need for biosensor fabrication. Moreover, cofactors (a non-protein chemical product, such as NAD^+ or

oxygen), controlled temperature, medium pH, and ionic strength are occasionally crucial and necessary for regulating enzyme activity and subsequent catalytic conversion of the substrates. Several types of enzymes can be categorized based on the kind of reactions they catalyze. The most popular ones utilized to develop electrochemical biosensors are oxidoreductases, which catalyze redox reactions, and hydrolases, which accomplish substrate hydrolysis [50].

Immobilization is used to couple the enzyme to the surface of the transducer. Such electrodes are known as enzyme electrodes [51]. Immobilization is "the physical confinement or localization of enzymes in a specific region of space while retaining their catalytic activities, and which can be used repeatedly and continuously." Proper enzyme immobilization can increase the lifespan of a biosensor. The nature of the enzyme and the related substrate, as well as the arrangement of the transducer, influence the selection of immobilization techniques. Proper enzyme immobilization on the electrode surface improves sensor sensitivity, analytical specificity and stability [52].

There are five types of immobilization procedures, including adsorption (chemical and physical), covalent bonding/attachment, entrapment, cross-linking, microencapsulation. Combining these immobilization procedures is frequently utilized, such as bonding/attachment followed by cross-linking [52-54].

Adsorption is a simple approach that requires no chemicals; an enzyme is placed onto the surface of the transducer. Without reagents, it provides a cost-effective and easy approach for disposable biosensors. Adsorption is classified as either physical or chemical. Physical adsorption happens, for example, through the creation of van der Waals bonds or electrostatic connections and in hydrogen bridges where the bonding force is difficult to manage. Chemical adsorption is more powerful adsorption with covalent bonds [53, 54].

Entrapment is a relatively primary experimental method. It consists of the physical retention of the enzyme in the interior cavities of a porous or gel matrix. With this approach, the bioreceptor typically does not change structurally; instead, significant diffusional barriers are created for the analyte towards the molecules of the bioreceptor, leading to more extended sensor response times [50].

Covalent bonding/attachment is a strong bond between the enzyme and the transducer's surface. It happens via functional groups such as amines, carboxyls, and alcohols, which are not required for the enzyme's catalytic activity. Covalent bonding/attachment necessitates gentle circumstances such as temperature and pH within the physiological range. The procedure has the benefit of not releasing the enzyme during the measurement [53].

Cross-linking is the most popular method for enzymatic stabilization on electrode surfaces. This approach effectively immobilizes the biocatalysts by forming intermolecular bonds between the enzyme molecules with the help of bifunctional agents (dialdehydes, diiminoesters, and diisocyanates). The most used bifunctional substance for enzymatic crosslinking is glutaraldehyde (GA). However, it is known that this substance can cause protein denaturation, necessitating the use of proteins with a high concentration of lysine residues, such as serum albumins, to prevent the loss of enzymatic function. Adding a drop of an enzyme- and crosslinking-reagent-containing solution on the WE surface may achieve this immobilization in a single modification step. Crosslinking also frequently yields positive outcomes regarding shelf-life stability, with studies revealing sensors with a viability of a few weeks or even months [53, 54].

Enzyme microencapsulation relies on using semi-permeable membranes to enclose biomolecules in contact with the electrode surface. The analytes and reaction products can flow through these membranes without washing the bioreceptors. This method may be used for

membranes made of cellulose acetate, collagen, and Nafion, among other materials. However, some encapsulations need unfavorable circumstances to form, affecting the biocatalyst activity. The influence of the medium conditions on the stability of enzyme immobilization is minimal [50, 53].

DNA

DNA-based biosensors, also known as genosensors, have been widely used for detection due to their high sensitivity, specificity, low cost, simplicity, and minimizing ability [55]. The most crucial procedure in the manufacturing of DNA-based biosensors is the hybridization of DNA, in which ssDNA (single-stranded DNA) immobilizes on the surface nanoparticle and target DNA (cDNA) binds to it to create a double-stranded helix (ds-DNA) [56, 57]. With the advancement of nanotechnology, new types of nanoparticles are being used for the immobilization of thiolated DNA probes with extraordinary properties such as high adsorption power, large surface area, and biocompatibility [42].

Biosensor in healthcare and pharmaceutical

Chemical sensors and biosensors have been developed to replace expensive and complicated healthcare analytical devices with compact and widely used sensors for healthcare applications. Biosensors and chemical sensors are garnering interest in the healthcare and pharmaceutical areas due to practical and low-cost analytical techniques, their potential to provide continuous and real-time physiological and chemical information, and noninvasive measurements of biochemical markers in human biofluids [58]. Clinical analyses require reliable and fast analytical techniques and tools. For this purpose, chemical sensors and biosensors can be appropriate options because of their simplicity, specificity, capability of continuous monitoring and providing rapid

results, potentially low cost, and portability [59]. Up to date, High Performance Liquid Chromatography (HPLC) [60], Mass Spectrometry [61], and Enzyme Linked Immunosorbent Assay (ELISA) [62] are some of the most used and standardized assays for analyte detection and quantification. Even in complex fluids, these approaches provide excellent sensitivity and selectivity toward various analytes. They are also highly repeatable and reliable, a crucial quality for clinical diagnosis. However, the drawbacks of these approaches include the need for specialized personnel and equipment, sample processing, which increases the volume of samples that must be collected, and the prolonged analysis time. To overcome these constraints, research is concentrating on automating biosensors, turning them into a competitive technology that will abandon the laboratory bench in favor of portable devices integrated into an uncomplicated, user-centered setup. To meet the rising demand and new needs, biosensors should be compatible with large-scale production, made of cost-effective materials, robust, and reliable. For point-of-care applications in-home testing, new biosensing platforms for improved detection devices should be miniaturized systems, implantable, or in-field deployable. The application of nanomaterials, including carbon nanotubes (CNTs) and dendritic fibrous nano-silica, paved the way for new opportunities for biosensing technology, together with new techniques like MIPs (molecularly imprinted polymers) for the fabrication of highly sensitive biosensors [63-65].

CHAPTER 3: AIMS

Aim of the thesis

The primary objective of the research presented herein is to develop new sensors and biosensors for determining biologically active compounds with interest in the analytical field. This Ph.D. thesis entails achieving the following objectives:

- Development of method for determination of anticancer drug Dasatinib based on single-walled carbon nanotube-modified SPCEs

- Development of biosensing method for detection of *haemophilus influenza* based on citrate capped silver nanoparticles conjugated with pDNA

- Development of horseradish peroxidase bound to poly(tyrosine)-chitosan polymeric scaffold as a molecularly imprinted polymer for monitoring of hydrogen peroxide

CHAPTER 4: EXPERMINTAL PART

A disposable electrochemical sensor based on single-walled carbon nanotubes for the determination of anticancer drug dasatinib

Introduction

Dasatinib (DAS) or N-(2-chloro-6-methylphenyl)-2-(6-(4-(2-hydroxyethyl)-piperazin-1-yl)-2-methyl-pyrimidin-4-ylamino) thiazole-5-carboxamide monohydrate (Fig. 4.1) is an orally accessible multitargeted inhibitor to kinases of the SRC family (sarcoma), PDGFR-β5 (platelet-derived growth factor receptor), c-KIT (receptor tyrosine kinase), and BCR-ABL [66]. Dasatinib is also a tyrosine kinase inhibitor; it can help block tyrosine kinase. It is a conventional anticancer drug for treating chronic myelogenous and acute lymphoblastic leukemia [67]. It is also beneficial for treating prostate cancer, nonHodgkin's lymphoma, and metastatic breast cancer with many side effects. Despite a remarkable improvement in patient survival, some adverse effects of dasatinib, such as cardiovascular, hematologic, gastrointestinal, endocrine, and pulmonary toxicity, have been described. Some gastrointestinal side effects are nausea and vomiting, diarrhea, stomach discomfort, hemorrhagic colonic ulcers, acute hepatitis, anorexia, dyspepsia, and gastrointestinal bleeding resulting from platelet failure [68]. Due to its toxicity and substantial consumption of DAS, it is essential to accurately and quickly determine its concentration in the therapeutic window [69]. In this context, electrochemical techniques are excellent options, and voltammetric techniques are inexpensive, sensitive, and selective. Because of these benefits, voltammetric methods have often been employed to study redox reactions and analyze inorganic and organic compounds using a variety of electrodes.

There are few studies on the voltammetric determination of dasatinib. Moghaddam *et al.* [70], and Kalambate *et al.* [71], reported that dasatinib was electrochemically detected at Fe_3O_4-SWCNTs 1-hexyl-3-methylimidazolium tetrafluoroborate-based paste electrode and Pd@Pt/MWCNT (mesoporous core-shell NPs supported on MWCNT) glassy carbon electrode, respectively. However, preparation of these electrodes (including synthesis of nanoparticles) took place approximately 20 hours. Moreover, the reproducibility of the preparation is also the question since the nanostructured surface can be easily modified by external conditions. Thus, taking advantage of the merits of the SPCEs, we propose a fast determination method for DAS in pharmaceutical tablets using disposable SWCNT-modified screen-printed carbon electrodes based on the DAS oxidation signal. The technique is low-cost, sensitive, robust, and fast for screening of pharmaceutical samples at the point-of-care level.

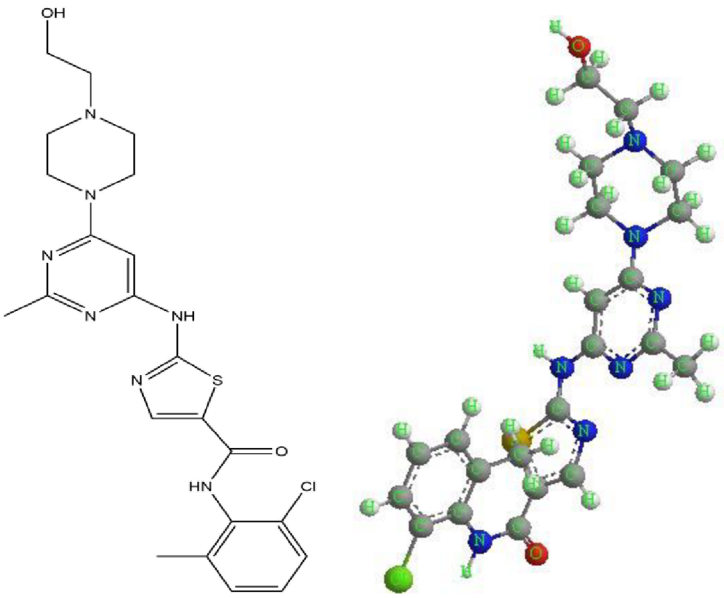

Fig. 4.1 | 3D-chemical structure of Dasatinib or N-(2-chloro-6-methyl-phenyl)-2-(6-(4-(2-hydroxyethyl)-piperazin-1-yl)-2-methylpyrimidin-4-ylamino) thiazole-5-carboxamide monohydrate.

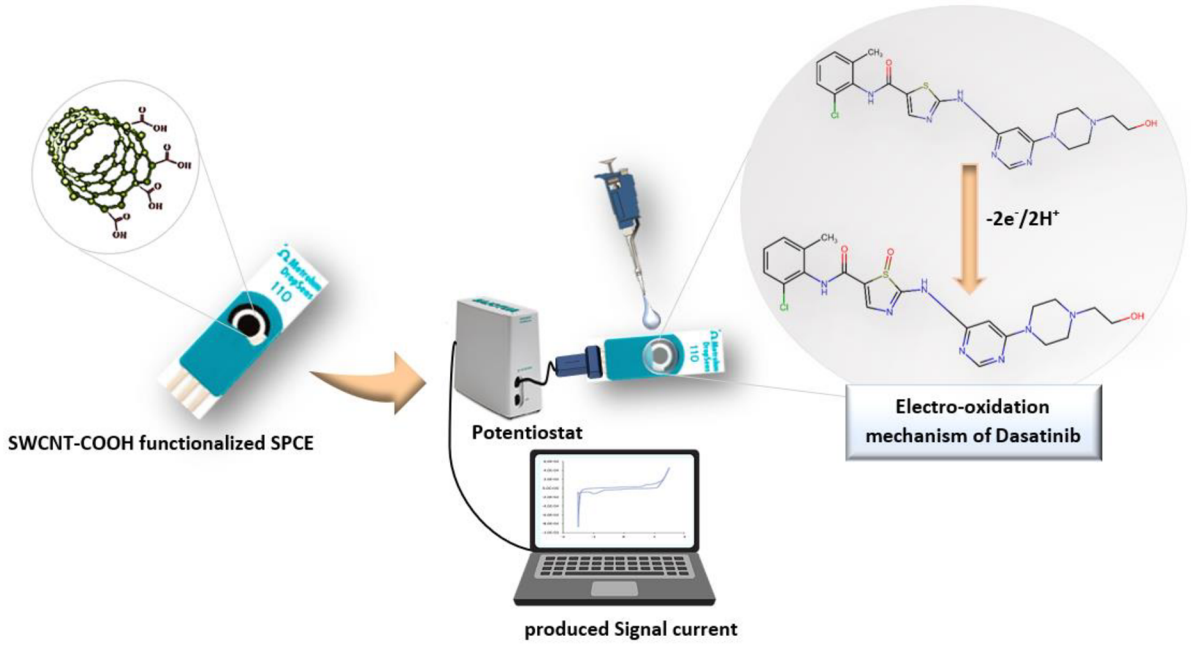

Scheme. 4.1 | *Electrochemical sensing of Dasatinib with SWCNT-modified screen-printed carbon electrode.*

Chemical and reagents

Boric acid (99.50%, ACS reagent), phosphoric acid (≥85%, ACS reagent), acetic acid (≥99.8%, ACS reagent), and methanol (≥99.8%, ACS reagent) were supplied from Sigma Aldrich (St. Louis, MO). The dasatinib drug was purchased from Sigma Aldrich (Prague, Czech Republic). All solutions were prepared using ultrapure water (resistivity of 18.2 MΩ cm, MilliQ, Millipore, France). The Olomouc University Hospital kindly provided samples of the dasatinib tablet. Commercial buffer solutions with pH levels of 4.0, 7.0, and 10.0 were used to calibrate the pH electrode. All experiments were done at room temperature.

Britton–Robinson buffer was prepared by an equal volume of 40 mM H_3BO_3:H_3PO_4:CH_3COOH. The pH was adjusted to 3 to 10 with 0.1 mM NaOH. The 100 µM dasatinib stock solution was prepared by dissolving it into ethanol/water (1:1) solution

and ultrasonication for 30 minutes. Britton–Robinson buffer was used as the supporting electrolyte. The drug solutions were kept at 4°C. For dasatinib detection, 60 µL of dasatinib solution was cast on the surface of SPCE and analyzed using electrochemical methods.

Preparation of standards and samples calibration

Britton–Robinson buffer solution pH 5.0 was selected as the optimum buffer pH. Hence, dasatinib concentrations varying from 0.1 µM to 100 µM were prepared in Britton–Robinson buffer solution pH 5.0. Then, for the actual sample, 9.7 mg of the powdered dasatinib tablet was dissolved in 2 mL 50% aqueous ethanol (35°C) and sonicated for 15 min. After filtration, 30 µL of the solution was diluted in Britton–Robinson buffer solution (pH=5.0) and used to analyse actual samples using the standard addition method of 40 µL of the dasatinib tablet solution was mixed with 20 µL of various concentrations of standard solutions.

For dasatinib quantitation, all electrochemical measurements (CV and SWV) were made on the surface of SPCEs. SWV was chosen as a more sensitive electrochemical method with a much lower background current, a higher current sensitivity, and a better resolution than CV. Under optimal conditions, signals were recorded for square-wave voltammetric investigation in the potential range of 0.2 – (+1.5) V with 10.0 Hz using SWCNT- modified SPCEs. All experiments were repeated three times.

Instruments

Electrochemical measurements were performed on the Metrohm Potentiostat PGSTAT101 AUTOLAB (Prague, Czech Republic) with NOVA 2.1 software. Six different screen-printed electrodes were purchased from Metrohm Dropsens (Prague, Czech

Republic). The screen-printed electrochemical cell consists of a carbon working electrode (4-mm diameter), a silver or Ag/AgCl reference electrode, and an auxiliary carbon electrode. SPCE studies included electrodes for bare, single-walled carbon nanotubes (SWCNT)-modified, graphene (GPH)-modified, graphene oxide (GPHOX)-modified, and carbon nanotubes (CNT)-modified SPCEs. For DPV measurements, the step potential of 0.005 V and the scan rate of 100 mVs^{-1} were applied. The 10.0 Hz frequency was also used for SWV measurements. The surface morphology of the screen-printed carbon electrodes was characterized by Hitachi SU6600 SEM (Hitachi, Japan) scanning electron microscope (SEM). EDS (Energy dispersive spectroscopy) coupled with the SEM equipment was also employed to analyze the chemical compositions of the SPCEs.

Results and Discussion

Characterization of SPCEs

SEM images of SPCEs were performed to investigate the surface morphology of the working electrode modified with nanoparticles. Fig. 4.2A shows the surface of a bare screen-printed carbon electrode with a smooth morphology. But modification of the electrode surface with graphene oxide (GPHOX)/graphene nanoparticles (GPH) demonstrates stable and monolayer structures (Fig. 4.2B-C). Notably, carbon nanotube (CNT)/single-walled carbon nanotubes modified SPCEs exhibit a compact film with a tubular distribution structure of nanotubes on the surface of the screen-printed carbon electrodes (Fig. 4.2D-E). The surface of the SWCNT-SPCE was very uneven, which can be helpful in the enhancement of the electrode surface area. Subsequently, these results confirmed that the SPCE was modified with single-walled carbon nanotubes, which altered the electrode surface activity. Also, these results validate that the dispersion of SWCNT on

the surface of the screen-printed carbon electrode was performed successfully. Also, the EDS of the SWCNT-modified working electrode is presented in Fig. 4.2F.

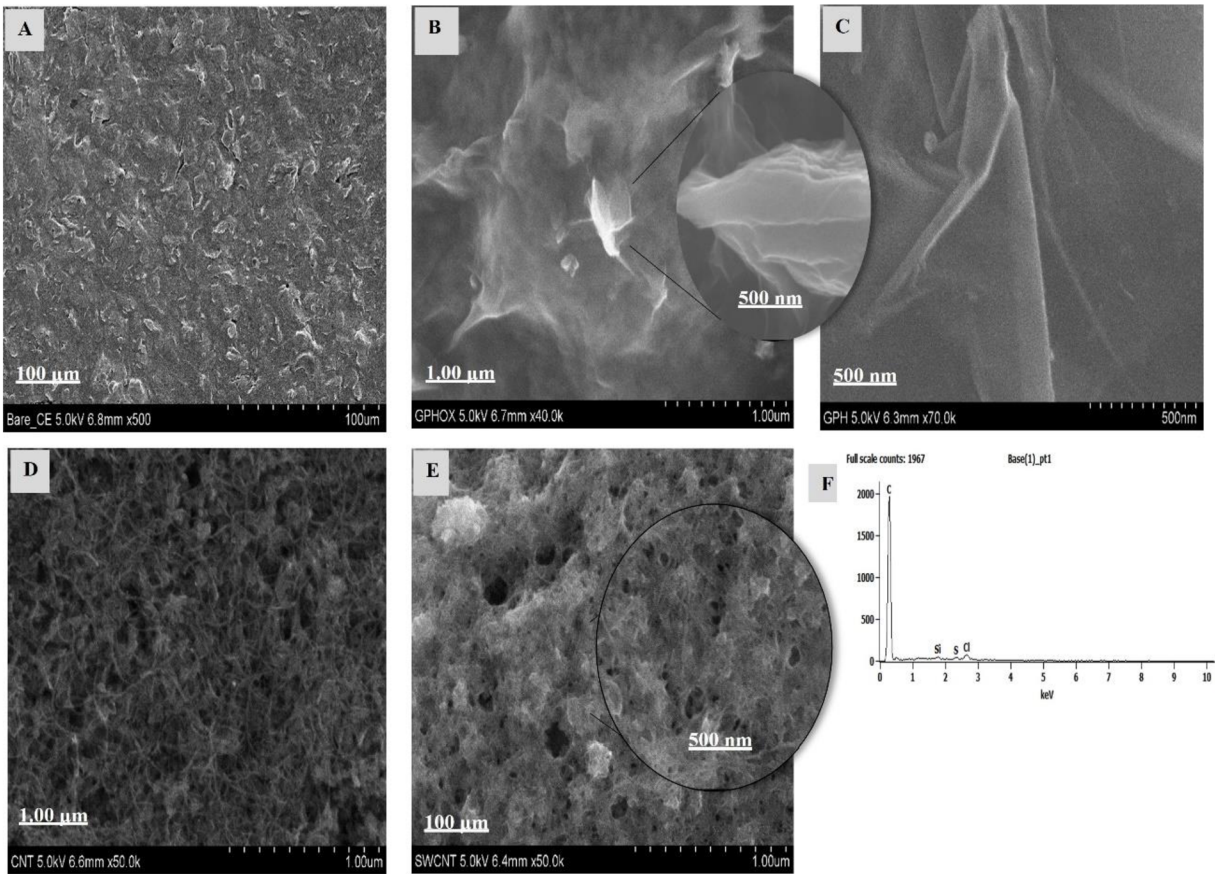

Fig. 4.2 | SEM images of working electrodes: (A) Bare carbon electrode; (B) Graphene oxide modified carbon electrode; (C) Graphene modified carbon electrode; (D) Carbon nanotubes modified carbon electrode; (E) Single-walled carbon nanotubes modified carbon electrode, and (F) EDS spectra of SWCNT.

SWCNT-modified SPCE as the optimal SPCE for dasatinib quantitation

This work aims to select the best SPCE for studying DAS oxidation behavior and fast determination of it in a pharmaceutical sample. The electrochemical behavior of DAS has been analyzed by measuring the cyclic voltammetry at different modified SPCEs at various pHs. In cyclic voltammetry, 100 M DAS showed an oxidation peak at 0.6 V to 0.8 V depending on the pH and type of SPCE when the potential range was between -1.5 and 1.5 V, with a scan rate of 100 mV s^{-1} in a 40 mM Britton–Robinson (BR) buffer. The

absence of a reduction peak for DAS on the reverse scan, as shown in Fig. 4.3, indicated that the oxidation process is irreversible. These peaks refer to the anodic oxidation of dasatinib using bare and modified SPCEs.

Various types of SPCEs, including those based on bare carbon, modified SWCNTs, CNTs, GPH, or GPHOX, were evaluated as different working electrodes. The signal intensity obtained using various electrodes in accordance with the applicable approach is shown in Fig. 4.3A. The SWCNT-modified SPCE was shown to give a greater peak intensity with a sharper peak. In contrast, the others exhibited broadened peaks, especially GPH and GPHOX-modified SPCEs. Hence, this kind of electrode proved to be the best. The difference in the electric charges of SWCNT-COOH-SPCE (negative charge due to the loss of the carboxylic group's proton) and the positive charge of DAS at this pH (pH 5.0) could explain the sensitivity of this compound's behavior over the electrode. The anodic peak current rose at the SWCNT-modified SPCE compared to the bare SPCE in Fig. 4.3B, showing the critical function of single-walled carbon nanotubes. This can be related to the increment of the active surface area of the electrode due to modification with SWCNTs which has a large surface area of about 600 m^2g^{-1}, high electrical conductivity, and the accumulation of DAS on the surface of the modified SPCE. It shows the crucial role of SWCNTs in the oxidation process and electrode activity. SWCNTs can accelerate the electron transfer rate with excellent electrocatalytic behavior toward the oxidation of dasatinib.

To comprehend the interaction and oxidation behavior of DAS over the SPCE, it is crucial to understand how the positive charge of the DAS molecule changes with pH. Dasatinib API has two basic ionization constants (pKa), which are 6.8 and 3.1, and one weakly acidic pKa, which is 10.8, in a saturated solution in water with a pH of approximately 6.0 [72]. In this way, this study evaluated the effect of the pH values over a

broad range from 3.0 to 10.0 of the BR buffer on the 100 µM dasatinib electrochemical behavior through cyclic voltammetry. It was observed that for DAS compound, peak 1_a broadened as the supporting electrolyte's pH rose, and the voltammogram at pH 9.0 and pH 10.0 revealed two successive charge transfer processes, peak 1_a at E_p1_a = +0.61 V and peak 2_a at E_p2_a = +0.94 V for pH 9.0 and peak 1_a at E_p1_a = +0.46 V and peak 2_a at E_p2_a = +0.81 V for pH 10.0 (Fig. 4.4A). The buffer pH considerably influenced the anodic peak currents (*Ipa*) at the surface of SWCNT-COOH-SPCE. It was observed that with increasing pH, the peak current of the modified SWCNT electrode at pH 5.0 is higher than that of other types of SPCE and pH (Fig. 4.3B), probably related to the large effective surface area of SWCNTs. The *Ipa* of dasatinib steadily increased with the increment of pH from 3.0 to 5.0. They decreased afterward because of the peak broadening. The anodic peak current of dasatinib reaches a maximum at pH 5.0 (Fig. 4.4C). Also, with a rise in pH, the anodic peak potential of dasatinib slightly shifted toward the negative. According to these findings, protons have participated in their electrode reaction processes. Ep versus pH was plotted with a slope of approximately −0.0602 V. (Fig. 4.4B). Therefore, it was concluded that both peaks signify irreversible processes involving two protons and two electrons.

This finding is consistent with the known electrochemical reactions of dasatinib, as demonstrated by other research. It is well known that two electron and two proton processes contribute to the oxidation of dasatinib. It is suggested that dasatinib's thiazole moiety is involved in its oxidation. This may be referred to the creation of sulfoxide due to the transfer of two electrons and two protons from the sulfur atom of the thiazole ring in the presence of Britton-Robinson buffer (Fig. 4.3C) [73].

Then, the carryover effect was evaluated on bare and SWCNT-modified electrodes. The Britton–Robinson buffer and dasatinib signals were assessed on the same electrode. The RSD of the peak current was 14% for the bare carbon electrode and 0.2% for the SWCNT-modified electrode. Therefore, SWCNT-COOH-SPCEs were used in further studies.

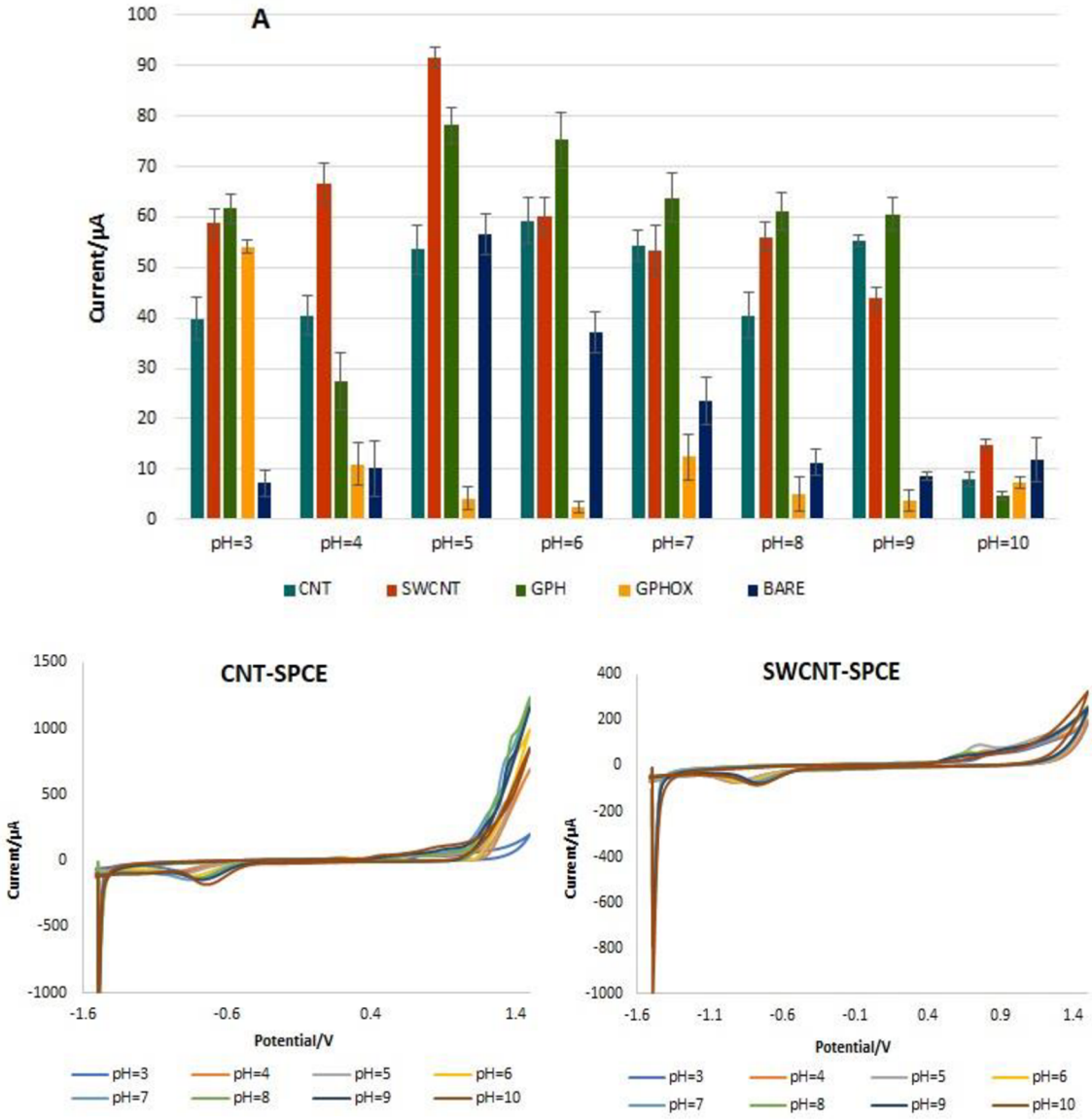

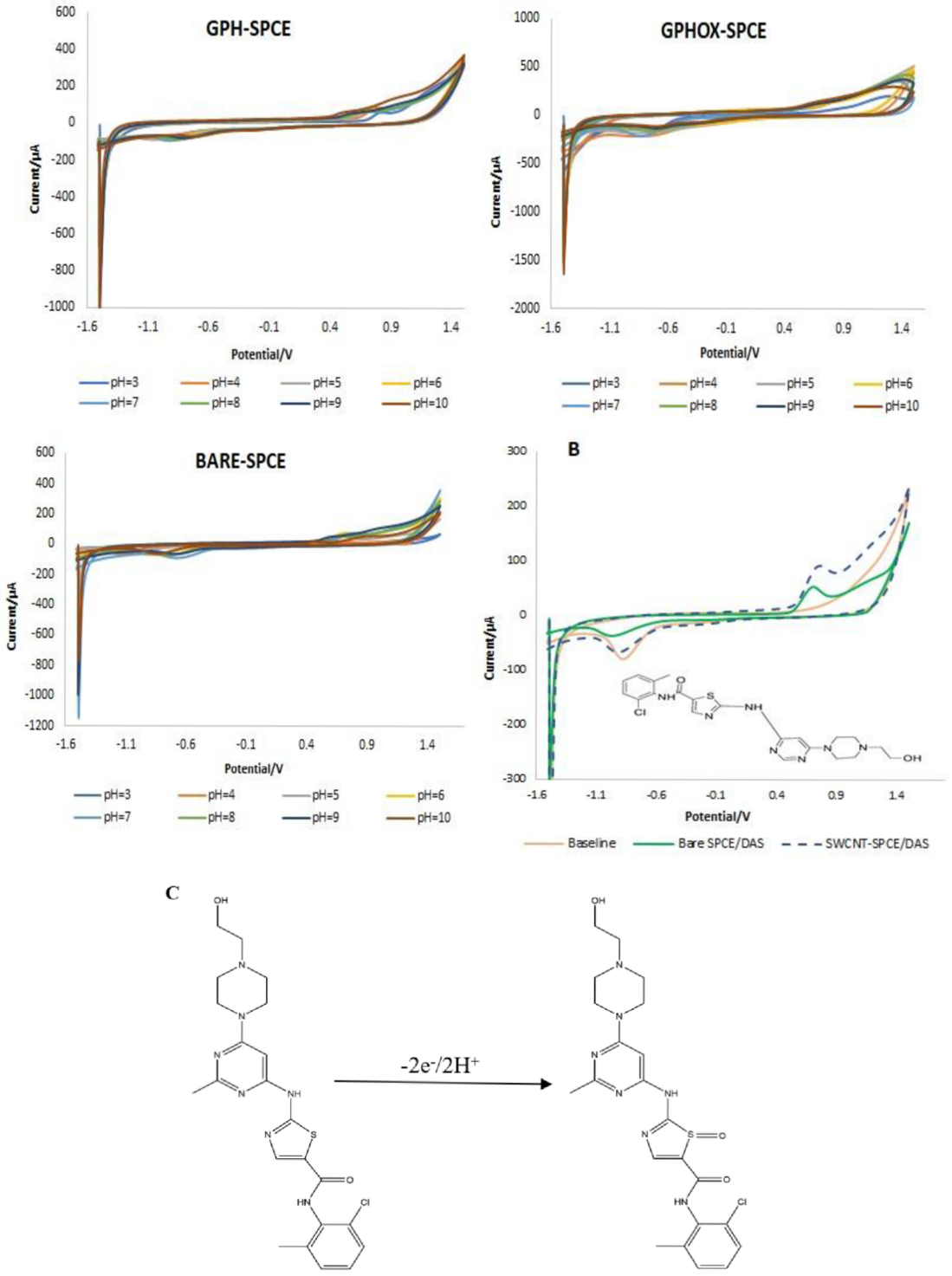

Fig. 4.3 | (A) Histogram of various types of SPCE at different pHs of Britton-Robinson buffer for detection of DAS using CV techniques. (B) The CVs of bare and SWCNT-modified SPCE in the presence (b) of 100 µM DAS (pH 5.0). (C) Electrochemical oxidation mechanism of dasatinib at SWCNT-modified SPCE.

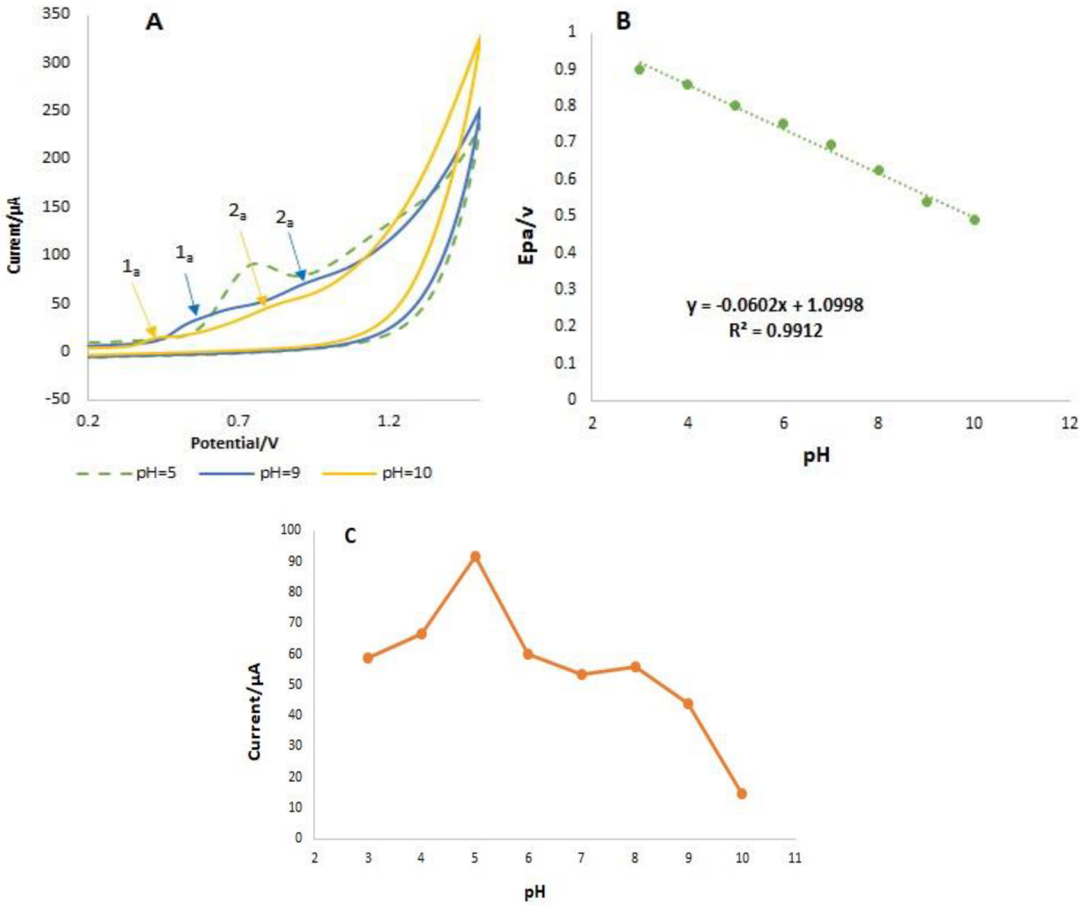

Fig. 4.4 | (A) Cyclic voltammograms in 100 µM DAS at pH 5.0, 9.0, and 10.0. (B) Effect of pH (pH 3.0–10.0) on the peak potential obtained at SWCNT- modified SPCE in Britton-Robinson buffer solution at a scan rate of 100mV.s^{-1}. (C) Variation in the peak potentials of DAS with pH of the buffer at SWCNT- modified SPCE.

Effect of scan rate at SWCNT-modified SPCE

The effect of the scan rate on DAS electrooxidation was evaluated in the range of 20–200 mVs^{-1} on the surface of the SWCNT-modified electrode using the CV technique (Fig. 4.5A). The dependence of Neperian logarithm of peak current on the Neperian logarithm of sweep rate (*ln* I_p *versus ln v*) is linear in which slope is 0.7499 ± 0.02 (Fig. 4.5B). It is indicated that the kinetics of the electrode process was controlled by adsorption, so the anodic oxidation of DAS on the surface of the SWCNT-COOH-SPCE is an adsorption-controlled electrochemical process. It is established that a slope is less than 0.5

is related to diffusion-controlled electrode processes, but if the slope is close to 1.0, the electrode process is adsorption-controlled [2, 27, 74-77]. It is described by the following equation [78]:

$\ln I_p/\mu A = 0.7499 \ln v(V/s) + 5.5469 (R^2 = 0.9947)$ Eq. 1

According to Fig. 4.5C, the peak currents were found to increase with increasing the scan rate, with a shift in the oxidation peak potential of DAS towards a more positive window (anodic area) which confirms the irreversible nature of electrode processes. Fig. 4.5C shows the dependence of *Epa* on the Neperian logarithm of the scan rate (*Epa versus ln v*). If the electrochemical reaction is irreversible, then the *Epa* is independent of the scan rate. Therefore, it can be deduced that heterogeneous electron transfer in DAS electrooxidation is irreversible because *Epa* increases with increasing scan rate. By increment of scan rate, the anodic peak potential (*Epa*) shifted towards more positive values, and a linear relationship was witnessed in the range of 20–200 $mVs^{-1,}$ as shown in Fig. 4.5C. The equation of this behaviour can be expressed as:

$Epa (V) = 0.0449 Ln v(V s^{-1}) + 0.8526 (R^2 = 0.9954)$ Eq. 2

Additionally, for an adsorption-controlled and irreversible electrode process, the following Laviron equation between E_{pa} *versus ln v* can be used to determine the value of the reaction's total electron transfer coefficient [79]:

$$Ep = \left(\frac{RT}{2\alpha nF}\right) \ln v + \text{constant}$$ Eq. 3

Where α is the electron-transfer coefficient, n is the number of electrons, and v is the potential sweep rate. The other symbols have their usual meaning. Taking F = 96485 C mol−1, T = 298 K, and R = 8.314J K−1 mol−1, in this study, employing the dependence of

anodic peak potential on the logarithm of the potential sweep rate (the slope = 0.0449), the value of total electron transfer coefficient (αn) was calculated to be 0.28 for DAS electrooxidation.

α can be calculated based on the equation Ep/2−Ep=1.875 (RT/αF) [79, 80], where Ep and Ep/2 are the peak potential and the potential at which the current (Ip) is equal to half its peak value (Ip/2) in cyclic voltammogram, respectively. The value of α equals 0.13. Furthermore, the shape factor in the irreversible system is given by |Ep − Ep/2| = 47.7/αn (mV) [81-83], from which the number of electrons transferred in the electrochemical reaction of DAS (in the presence of Britton-Robinson buffer) were found to be approximately 2 (n=2.1).

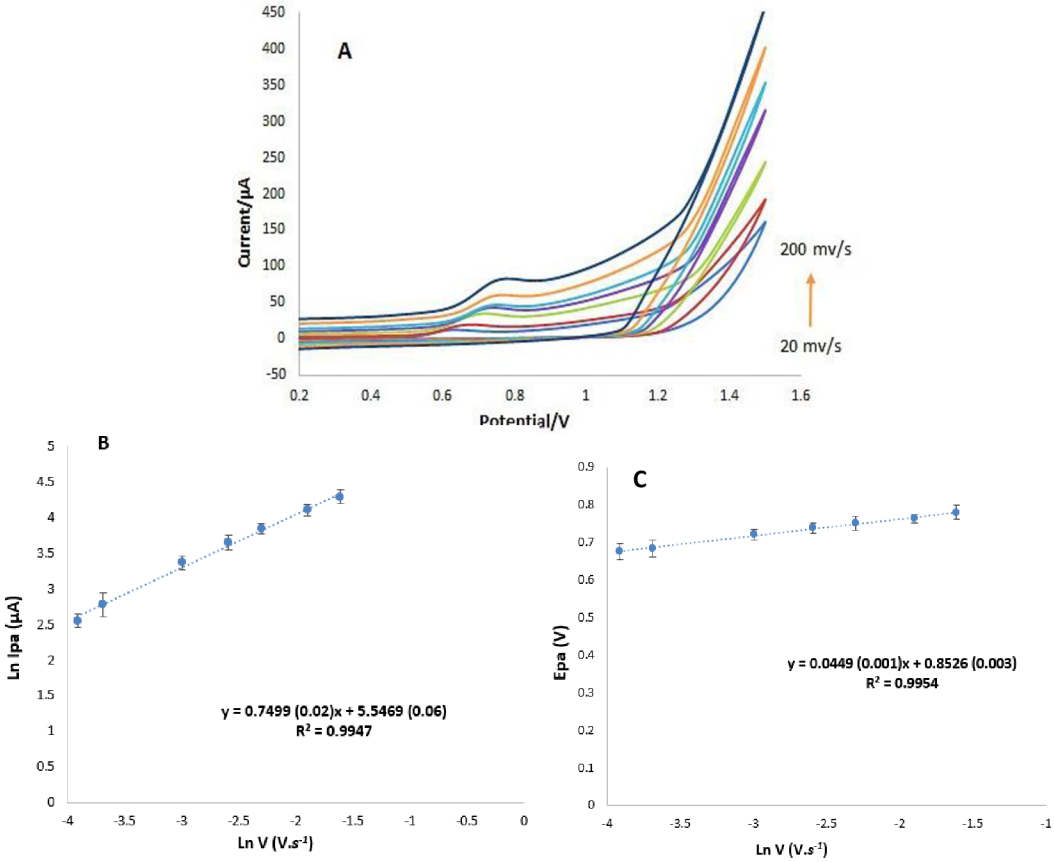

Fig. 4.5 | The effect of scan rate (A) CV of 100 µM dasatinib at SWCNT-modified SPCE; Britton-Robinson buffer pH 5.0; scan rates 20, 25, 50, 75, 100, 150, 200 $mV.s^{-1}$. (B) The plot of ln Ipa (Napierian logarithm of oxidation peak currents) versus ln V (Napierian logarithm of scan rates). (C) Dependency of oxidation Epa (peak potentials) versus ln V.

Optimized experimental SWCNT-modified SPCE

The calibration curve in Fig. 4.6A-B shows that the oxidation signal is linearly associated with dasatinib in the concentrations range of 0.1 - 100 µM, with a correlation coefficient of 0.9975. The limit of detection (LOD), calculated as signal/noise = 3.3, was estimated to be 0.06 µM. The limit of quantitation (LOQ), calculated as signal/noise = 10, was 0.19 µM. Based on the obtained results, the developed electrochemical sensor had relatively high sensitivity and good linearity. The linear range for determining DAS tablet solutions (as actual samples) was investigated from 0.1 to 100 µM with a correlation coefficient of 0.999 (Fig. 4.6C). The LOD, calculated as signal/noise = 3.3, and LOQ, calculated as signal/noise = 10, were estimated to be 0.07 µM and 0.22 µM, respectively (Table. 4.1). The amount of dasatinib found was 70 mg/tablet, representing a relative error of 6 %.

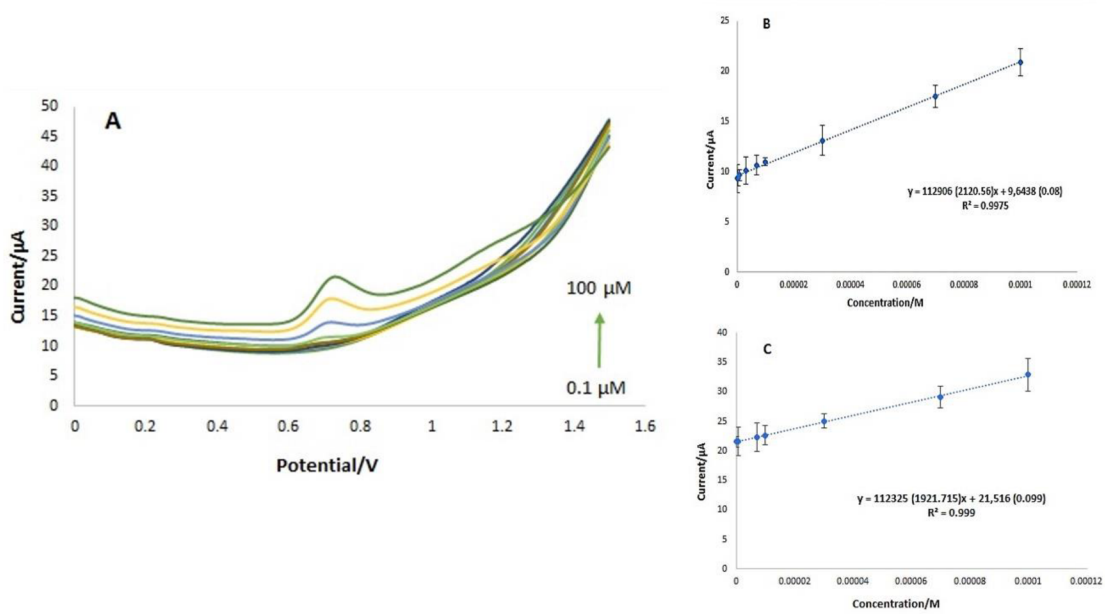

Fig. 4.6 | (A) Concentration effect of DAS detection by SWV method in concentration range (100, 70, 30, 10, 7, 3, 0.7, 0.3, and 0.1 µM) in Britton-Robinson buffer pH 5.0 by SWCNT-modified SPCEs. Step potential= 0.005V, Scan rate= 100mV/s. (B) Calibration curve related to SWV analysis of DAS. (C) Calibration curve related to SWV analysis of real sample dasatinib tablet solutions.

Table. 4.1 | Linear range, limits of detection, limits of quantification and correlation coefficient (R^2) calculated from DAS calibration curves obtained in BR buffer pH 5.0, and tablet sample.

Sample	Linear range (µM)	LOD (µM)	LOQ (µM)	R^2
Buffer	0.1 - 100	0.06	0.19	0.9975
Tablet	0.1 - 100	0.07	0.22	0.999

Therefore, the carbon-based screen-printed electrodes, a new generation of electrodes, were used to determine the anticancer drug dasatinib. According to the obtained results, modification of SPCEs with nanomaterials resulted in a better response for dasatinib than the bare ones. And among the different types of modified SPCEs, single-walled carbon nanotube-modified electrodes gave the highest peak currents for dasatinib detection. SWCNTs improve the electrochemically active area and enhance the electronic transfer attributes. The tubular structure of SWCNTs on the SPCE surface was very uneven, which led to the enhancement of the surface area of the electrode. The developed platform showed a good electrochemical response towards dasatinib with LODs of 0.06 µM. The established electrochemical sensor is among the superior reported electrochemical sensors (Table. 4.2) in terms of repeatability, low detection limit, and broad linear range. It should be highlighted that the excellent performance of the SWCNT was related to its outstanding properties like high electrical conductivity and large surface area, which pave the way for fast electrons. The results showed that the developed electrochemical sensor also had relatively high sensitivity and good linearity in detecting dasatinib in actual samples, too. Consequently, the single-walled carbon nanotube-modified screen-printed electrodes could

be used for the sensitive and quick analysis of electrochemically active pharmaceutical substances.

Table. 4.2 | Comparison of developed electrochemical sensors for the sensitive determination of Dasatinib.

Type of electrode	Modification	pH	RSD	Linear range	Limit of detection	Ref.
Carbon paste	ZnO NP/1-butyl-3-methylimidazolium tetrafluoroborate	5.0	3.78%	1.0–1200 µM	0.5 µM	[84]
Glassy carbon	Au-NPs/rGO/ds-DNA	4.80	3.1%	0.03–5.5 µM	0.009 µM	[85]
Pencil graphite	-	3.0	5.80%	0.0092 – 1.0 µM	0.0028 µM	[86]
Glassy carbon	-	3.4	2.1%	0.2–2.0 µM	0.13 µM	[73]
Carbon paste	Pt/MWCNTs-1-butyl-3-methylimidazoliumhexafluoro phosphate-	8.0	-	5.0– 500 µM	1.0 µM	[87]
Screen-printed carbon	SWCNT	5.0	1.89%	0.1-100 µM	0.06 µM	This work

Reproducibility, Selectivity, and Stability of the sensor

Six sensors were chosen randomly to detect dasatinib under the same experimental conditions. The proposed method's repeatability (relative standard deviation) was assessed by measuring SWVs of 100 µM DAS in Britton–Robinson buffer pH 5.0 (intraday stability) through a SWCNT-modified electrode. The relative standard deviation (RSD%) was 1.89% to determine DAS in one day.

The interference study serves a significant role in analytical chemistry. To this end, the sensor's selectivity for determining DAS was investigated through the influences of some co-existing interferences like different organic and inorganic compounds such as lactose, sucrose, glucose, SO_4^{2-}, and CO_3^{2-} in the real samples. Fig. 4.7 displays the SWV measurements of DAS and its mixtures with various interfering species. As can be seen, these compounds had almost no effect on the peak current of DAS, with a difference of less than 1.8% in peak current (%ΔI) between the peak current of DAS with and without interference. It demonstrated that the suggested sensor is highly selective for dasatinib detection. It should be noted that using glucose as an interfering agent broadened the DAS peak and showed two consecutive charge transfer reactions (Fig. 4.7A).

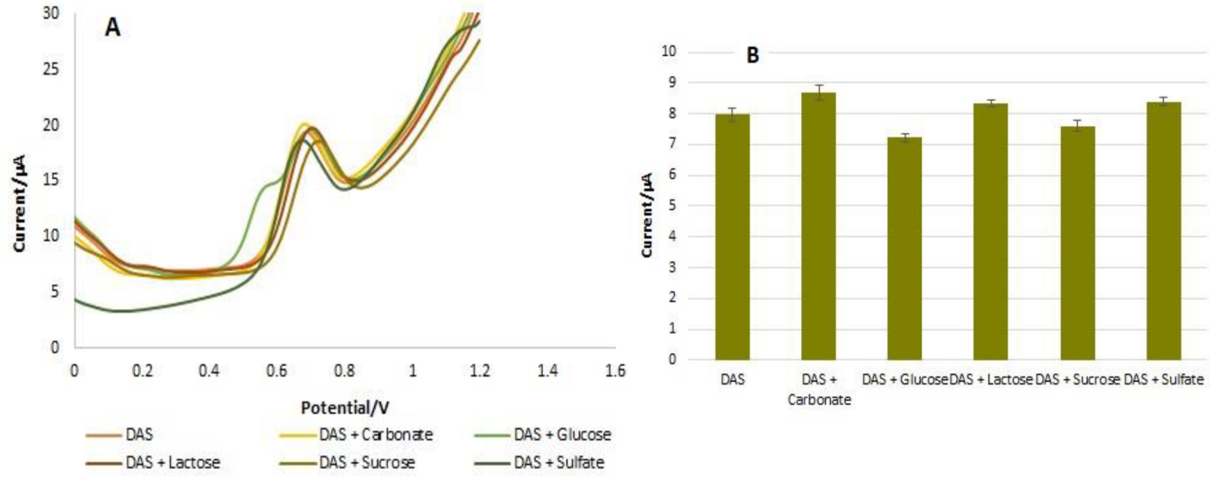

Fig. 4.7 | (A) Interference effect of lactose, sucrose, glucose, SO_4^{2-}, and CO_3^{2-} on determination of DAS by SWV method on SWCNT-COOH-SPCEs in supporting electrolyte Britton-Robinson buffer pH 5.0. (B) Histogram of interference effect.

Conclusion

Herein, sensitive individual electrochemical determination of dasatinib is introduced on a SWCNT-modified SPCE platform. Compared to other electrochemical sensors with

various nanoparticles modification such as GPH, GPHOX, CNT, and bare electrodes, the SWCNT-modified SPCE showed an excellent function for dasatinib detection.

Dasatinib could demonstrate an irreversible signal with good sensitivity at a surface of SWCNT-modified SPCE compared to others. SWCNTs-modified SPCE showed good catalytic activity of the oxidation signal of the DAS anticancer drug and improved its signal. This work has exhibited that dasatinib has only one oxidation peak at about +0.8 V at SWCNT-modified SPCE in Britton Robinson buffer solution, pH 5.0, and the electrochemical oxidation happens through step by two electrons and protons. The quantitative measurement of dasatinib with the SWV technique was optimized to voltammetric parameters. The developed platform showed a great electrochemical response towards DAS with an excellent detection limit and selectivity. Also, based on the results, there was a good linear relationship between the concentration range of DAS and its oxidation peak current. The results showed that our sensor could detect low dasatinib concentrations in tablet solutions (as actual samples).

pDNA conjugated with citrate capped silver nanoparticles towards ultrasensitive bio-assay of haemophilus influenza in human biofluids: A novel optical biosensor

Introduction

Haemophilus influenza (*H. influenza*) is a gram-negative coccobacillus which produces polysaccharide capsules. There are 6 serotypes from A to F based on type of capsular antigen [88]. Capsulated strains are resistant towards phagocytosis, whereas non-capsulated strains have less resistance and invasive features [89]. *Influenza* causes respiratory infections including bronchitis, acute otitis media, pneumonia, and sinusitis. Furthermore, it leads to invasive infections like meningitis, septic arthritis, and cellulite [90]. Hence, sensitive and fast determination of *H. influenza* is of paramount significance in medical microbiology. There are numerous techniques for diagnosis of *H. influenza* such as Polymerase chain reaction (PCR), latex particle agglutination (LAT), and culture. The latex particle agglutination and culture techniques are usually employed for clinical diagnosis of viruses [91, 92]. *H. influenza* is still a fastidious bacterium and its growing needs compound nutrition. Replication of this virus takes long time, so in culture technique it may takes long period of time up to weeks. A more sensitive method than culture and LAT is PCR but it also has some limitations. Some disadvantages of these methods are being laborious, time-consuming, low specificity and sensitivity as well as requiring developed high-price instruments and expert technicians [93].

Because of limitations of conventional techniques, biosensors have been advanced for specific and more sensitive detection of *H. influenza* [94]. Genosensors are usually applied for detection of infectious diseases [95, 96]. Recently, DNA-based biosensors or genosensors have been

widely utilized for detection because of their great sensitivity, specificity, low-cost, simplicity as well as minimization ability [55]. Hybridization of DNA is the most significant process in the fabrication of DNA-based biosensors in which ssDNA (single-stranded DNA) immobilizes on the on the surface nanoparticle and target DNA (cDNA) bind to it for forming double-stranded helix (ds-DNA) [56, 57]. By emerging of nanotechnology, various kinds of nanoparticles are applied for immobilization of thiolated DNA probe with exceptional attributes like great adsorption power, great surface area and biocompatibility. Among the metallic nanoparticles, AgNPs (silver nanoparticles) have been broadly examined mostly because of their unique and optical characteristics as well as excellent extinction coefficients [42]. AgNPs draw lots of interests for its application in optical sensors because of their simple and cheap fabrication besides their greater extinction coefficients than those of gold nanoparticles with the similar average size [44, 45]. In addition, the high surface area of silver nanoparticles is completely appropriate for modification and fabricate useful components in colorimetric determination of some analytes including, metal ions [97], pesticides [98], thiols [99], amino acids [100], DNA [101], proteins [102], small molecules [103], enzymes [44] as well as food and environmental contaminants [104-106].

In present research, an innovative optical DNA-based biosensor using citrate capped silver nanoparticles for detection of *H. influenza* gene was developed. The purpose of this study is design a spectrofluorometeric and UV/Vis spectrophotometric technique for sensitive determination of *H. influenza*. The developed method not only has acceptable linear range but also it is simple and cost-efficient technique in comparison with conventional methods.

Chemical and reagents

Sodium acetate (CH_3COONa), sodium chloride (NaCl), DTT (Dithiotrietol), silver nitrate ($AgNO_3$), $NaBH_4$ (sodium borohydride), trisodium citrate ($Na_3C_6H_5O_7$) were purchased from

Sigma-Aldrich (Ontario, Canada). The oligonucleotide sequences achieved from Takapouzist Co. (Iran) include:

- Probe single strand DNA (ssDNA): SH-5′-AAT TTT CCA ACT TTT TCA CCT GCA T-3'
- Complementary target DNA: 5′-ATG CAG GTG AAA AAG TTG GAA AAT T-3'
- 1-base mismatched target DNA: 5′-ATG GAG GTG AAA AAG TTG GAA AAT T-3'
- 2-base mismatched target DNA: 5′-AGG GAG GTG AAA AAG TTG GAA AAT T-3'
- 3-base mismatched target DNA: 5′-AGG GAG GTG AGA AAG TTG GAA AAT T-3'

Dilution of oligonucleotides was performed using Tris−HCl buffer (0.1 M, pH~7.4). DTT solution was made ready using 500 mM DTT and 10 mM sodium acetate (pH~5.2).

Instruments

Transmission electron microscopy (TEM) was carried out by Philips CM30 electron microscope operated at 200 kV (Adelaide, Australia). Dynamic light scattering (DLS) was evaluated using zeta potential instrument Malvern Instruments Ltd (Zetasizer Ver. 7.11, MAL1032660, England) for size distribution and zeta potential. Field emission scanning electron microscope (FE-SEM) (Hitachi-SU8020, Czech) with an operating voltage of 3 kV was performed to appraise the modified electrode surface and particles morphology. The chemical composition of the modified electrodes was investigated using energy dispersive spectroscopy (EDS). Overall these instruments have three major components-laser, sample and light detector UV-VIS spectrophotometer achieved by shimadzu UV-1800 UV-VI spectrophotometer with a resolution

of 1 nm. Fluorescence spectra and intensity measurements were done employing a Jasco FP-750 Spectrofluorometer (Japan) equipped 1.0 cm quartz cells and a 150 W xenon lamp.

Synthesis of citrate capped silver nanoparticles

In order to synthesis the citrate capped silver nanoparticles, in an ice bath (approximately 0 °C) 400 mL of trisodium citrate (1.06 mM) solution, as a capping/stabilizing agent, was completely mixed with 25 mL of silver nitrate solution (5 mM). Next, 2500 µL of 100 mM $NaBH_4$ aqueous solution as a reducing agent was drop wisely added to the mixed solution over 5 min. This was led to immediate color alteration to light yellow. The prepared solution was vigorously stirred about 1 h and 45 min under dark condition until the color was shiny yellow which confirms the end of reaction and Cit/AgNPs formation. Then, the ice bath was removed and solution was kept in dark condition overnight to attain room temperature. The synthesized Cit/AgNPs were centrifuged at 6000 rpm for 15 min.

Citrate ions are usually utilized as a reductant and stabilizer in synthesis of metal nanoparticles and makes powerful surface interaction with AgNPs. Adding citrate ions to the silver solution leads to the citrate ions complication with silver nanoparticles. The complexity of citrate ions with AgNPs serves significant role in dictating shape and size of AgNPs. Citrate ions effects the growth of particle through compounding with positively charged dimers of Ag^+.

Results and Discussion

TEM, FE-SEM and DLS analysis of citrate capped AgNPs

The mechanism of Cit/AgNPs formation and supportive proof of morphologies and characteristics of silver nanoparticles was provided by TEM (transmission electron microscopy). TEM is continuously the first method employed for determination of the size and nanoparticle size distribution [107]. TEM images recorded using the holey carbon grid which are shown in Fig. 4.8. The TEM micrographs of synthesized citrate capped silver nanoparticles clearly show the AgNPs are discrete, monodisperse, and spherical in environment with average particle size under 10 nm.

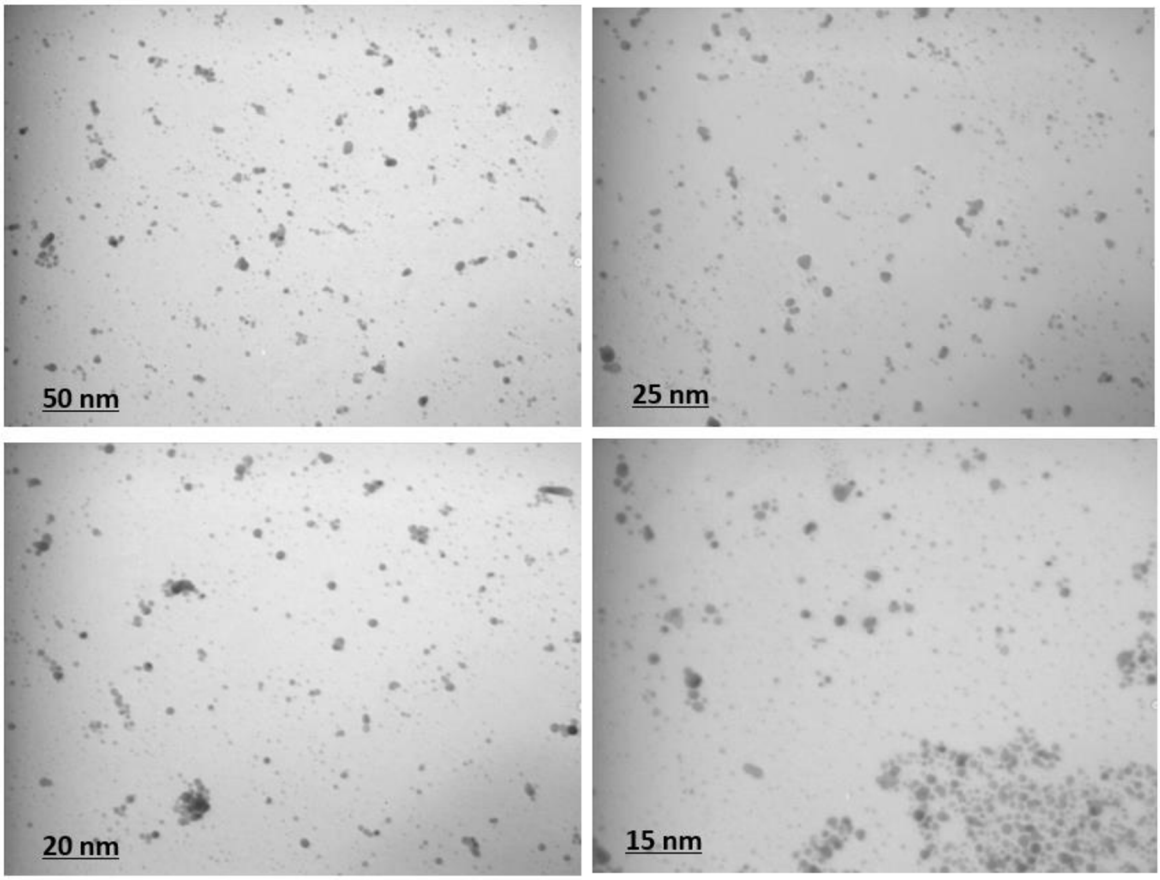

Fig. 4.8 | TEM images of Cit/AgNPs in various magnifications.

Surface morphology of Cit/AgNPs was characterized by FE-SEM (field emission scanning electron microscope) and chemical compositions of nanoparticles were analyzed by EDS (energy dispersive spectroscopy). As shown in Fig. 4.9A, AgNPs have uniform spherical structure. According to the standard theory of colloids, the stability of colloids depends on the equilibrium between the van der Waals interaction and the coulombic repulsion of the charged particles the charged particles [108]. According to Fig. 4.9B, sharp and large peaks from citrate and sodium appear due to the existence of sodium citrate and sodium borohydride in the structure of Cit/AgNPs.

A

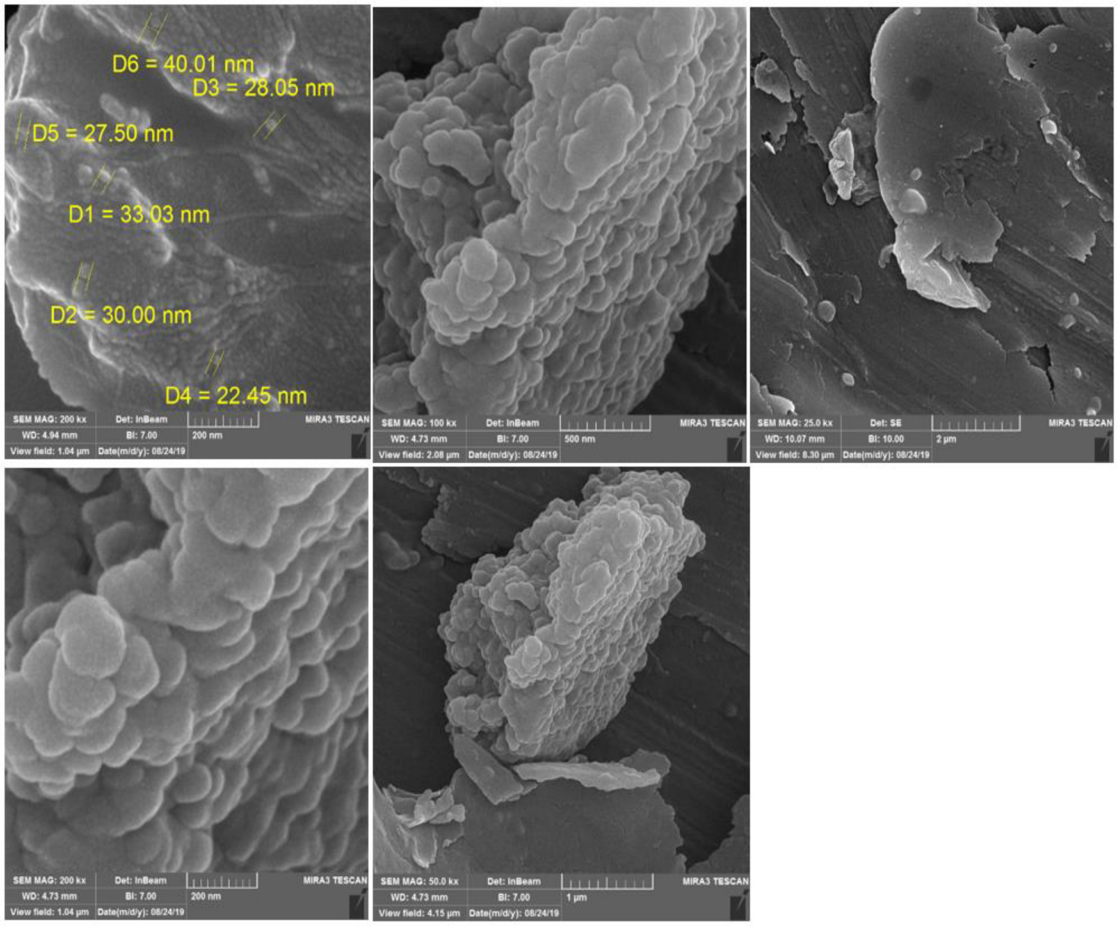

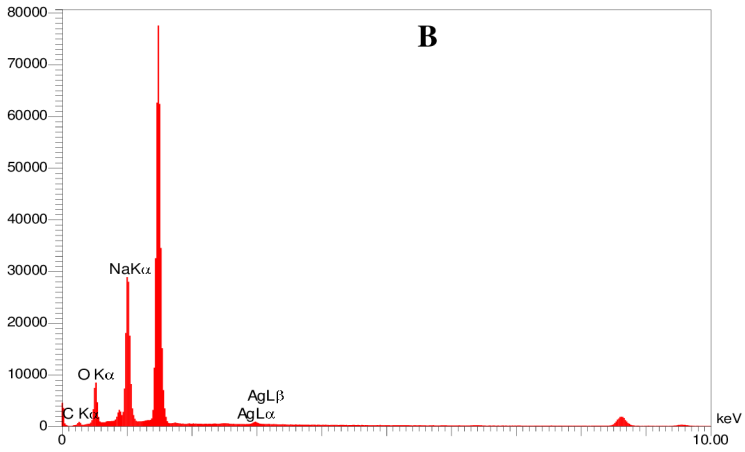

Fig. 4.9 | (A). FE-SEM images of Cit/AgNPs in various magnification. (B). EDS spectra of Cit/AgNPs.

DLS (dynamic light scattering) is a powerful technique which depends on the interaction of light with particles. This technique can be employed for measurements of narrow particle size distributions especially in the range of 2–500 nm [109]. For determination of citrate capped AgNPs hydrodynamic sizes and zeta potential were evaluated (Fig. 4.10). The average particle size of synthesized Cit/AgNPs was 2.27 nm. Furthermore, Cit-AgNPs exhibits fluorescence emission in the range of 400–600 nm. This may be due to citrate in the structure of this probe with the maximum excitation and emission wavelength at 370 nm and 420 nm, respectively UV–Vis spectra revealed that maximum absorption of Cit-AgNPs is around 397 nm.

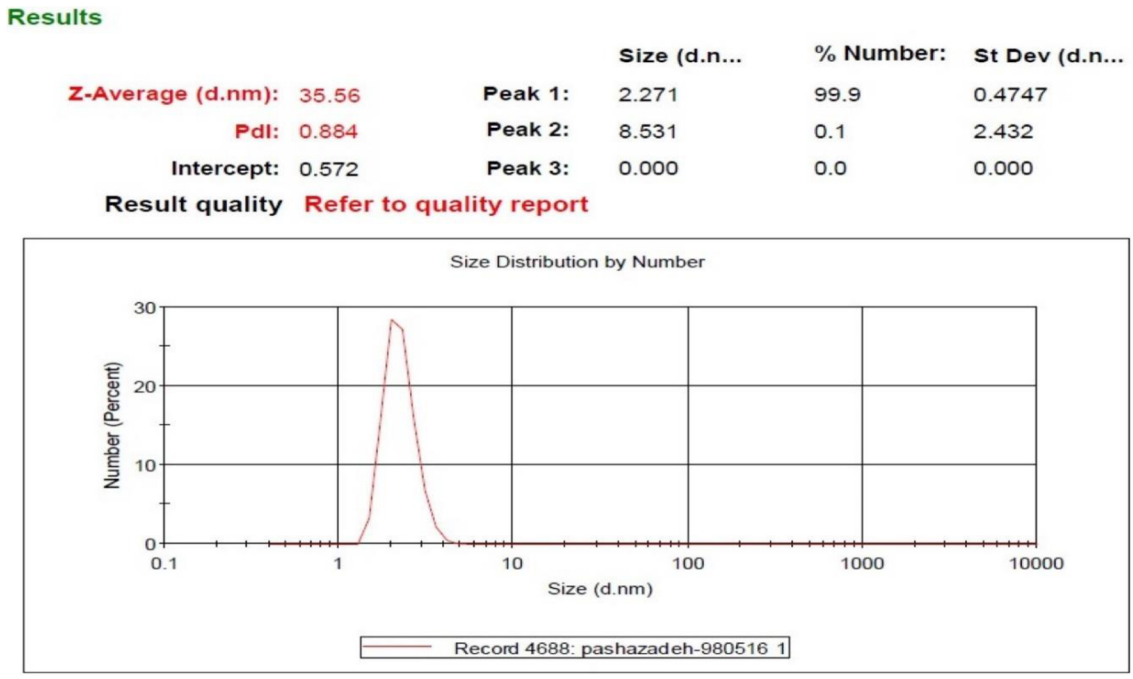

Fig. 4.10 | Size distribution analysis of Cit/AgNPs via DLS.

Preparation of optical biosensor

pDNA is one of the most significant element in genosensing. For this purpose, pDNA was activated through combination with DTT. DTT (dithiotrietol) is usually employed as a deprotecting or decreasing agent for thiolated-probe DNA. The sulfur atoms in terminal of thiolated DNA have potential for forming dimers especially in the existence of oxygen. Thiol groups oxidation prevented by DTT. So, it is applied as a protecting agent [110, 111]. Therefore, DTT (0.01 M) and sodium acetate (0.01 M) were prepared with deionized water. Then, 15 µL of pDNA (SH-5′-AAT TTT CCA ACT TTT TCA CCT GCA T-3') was mixed with 100 µL DTT/sodium acetate solution. After 15 min, 200 µLof ethyl acetate was added and for 5 min vortexed. The prepared solution was centrifuged for 10 min at 8000 rpm and supernatant was removed. Subsequently, 200 µL of Cit/AgNPs was added to the prepared pDNA solution and incubated for 2 h at 45$^{\circ C}$ for spectrofluorometery and 200 µL of diluted Cit/AgNPs (1/2 concentration) was also another microtube of prepared pDNA and incubated which was applied for UV–vis

spectrophotometery. 10 μL of NaCl (1 M) was added to 300 μL of mixed Cit/AgNPs-pDNA and Cit/AgNPs for increment of quality and stability of nanoparticles. Then, the prepared solutions were pipetted in the cuvettes and data was recorded both by spectrofluorometer in range of 400−750 nm wavelength and UV-VIS spectrophotometer in range of 250−700 nm spectral range. Fluorescence emission and excitation spectra of Cit/AgNPs and Cit/AgNPs-pDNA are demonstrated in Fig. 4.11A. The excitation peaks for Cit/AgNPs and Cit/AgNPs-pDNA were observed at 439 and 438 nm, respectively. The fluorescence spectrum of Cit/AgNPs was similar to that of Cit/AgNPs-pDNA; although, the fluorescence intensity was declined by pDNA. As can be seen in Fig. 4.11B, momentous alteration in UV–vis spectra was happened after addition of pDNA which appeared at 470 nm. All of the genosensor preparation steps was shown in Scheme. 4.2.

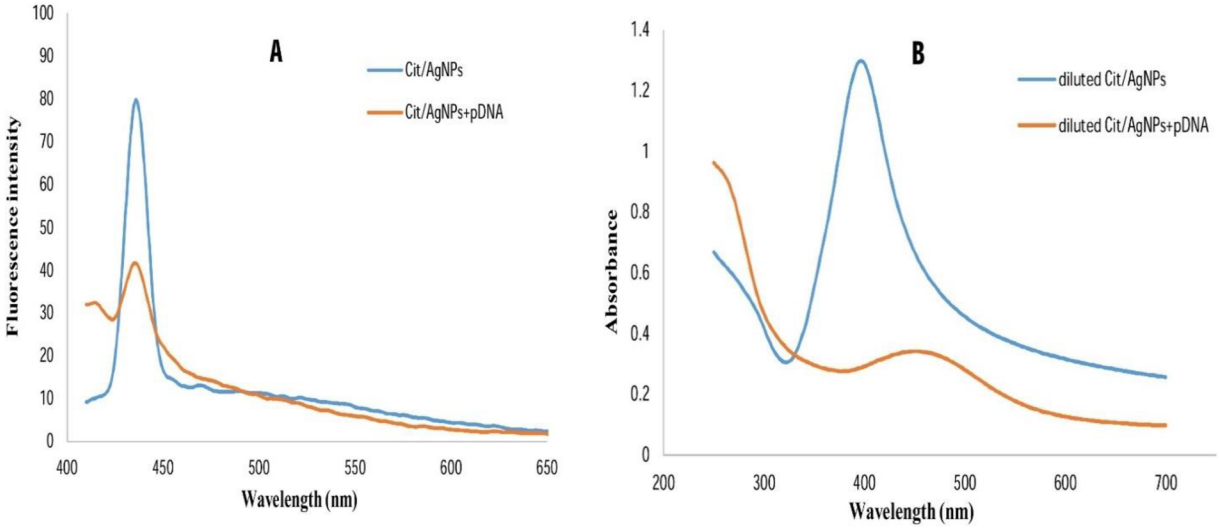

Fig. 4.11 | A) Fluorescence spectra of Cit/AgNPs and Cit/AgNPs-pDNA. B) UV/Vis absorbance spectrum of Cit/AgNPs and Cit/AgNPs-pDNA.

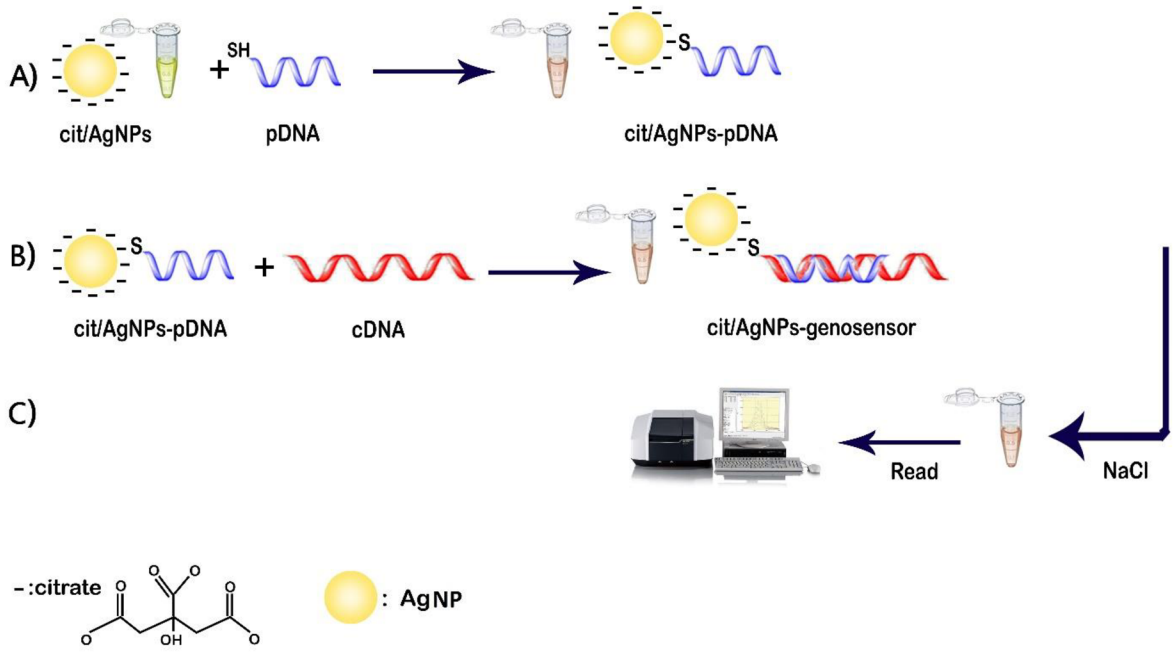

Scheme. 4.2 | Illustration of preparation steps of genosensor.

Optimization of hybridization time

Hybridization leads to quick and effective binding of DNA strands. In this study, pDNA hybridized with its specific DNA (cDNA (complementary target sequences)). Oligonucleotides were successfully immobilized on the surface of Cit/AgNPs due to interaction of AgNPs surface with oligonucleotides binding groups. Thiol groups of oligonucleotides result in increment of binding affinity of them to the surface of nanoparticles, which leads to greater stability of Ag nanoparticle probes [45]. The Cit/AgNPs have stability toward salt concentration (NaCl). So, they are stable against aggregation by NaCl concentration. This hybridization process was associated with color alteration, red-shifting as a result of assembly of particle which can be seen by naked eye in the form of yellow to pale red color change (Fig. 4.12A). To evaluate the hybridization and optimum incubation time, Cit/AgNPs functionalized with pDNA (SH-5′-AAT TTT CCA ACT TTT TCA CCT GCA T-3') solution (Cit/AgNPs-pDNA) and incubated with 15 µL of cDNA (5′-ATG CAG GTG AAA AAG TTG GAA AAT T-3') at different incubation times (2, 5, 10, 15, and 20 min). In this part, 10 µL of NaCl was added to enhance the AgNPs stability and inhibted their aggregration. After insertion of 10 µl NaCl, UV–vis spectra were recorded at different time (251,015 and 20 min). Obtained results demonstrated that the optimum cDNA incubation time was 2 min. As revealed in Fig. 4.12, the location of peak is absolutely similar with previous section.

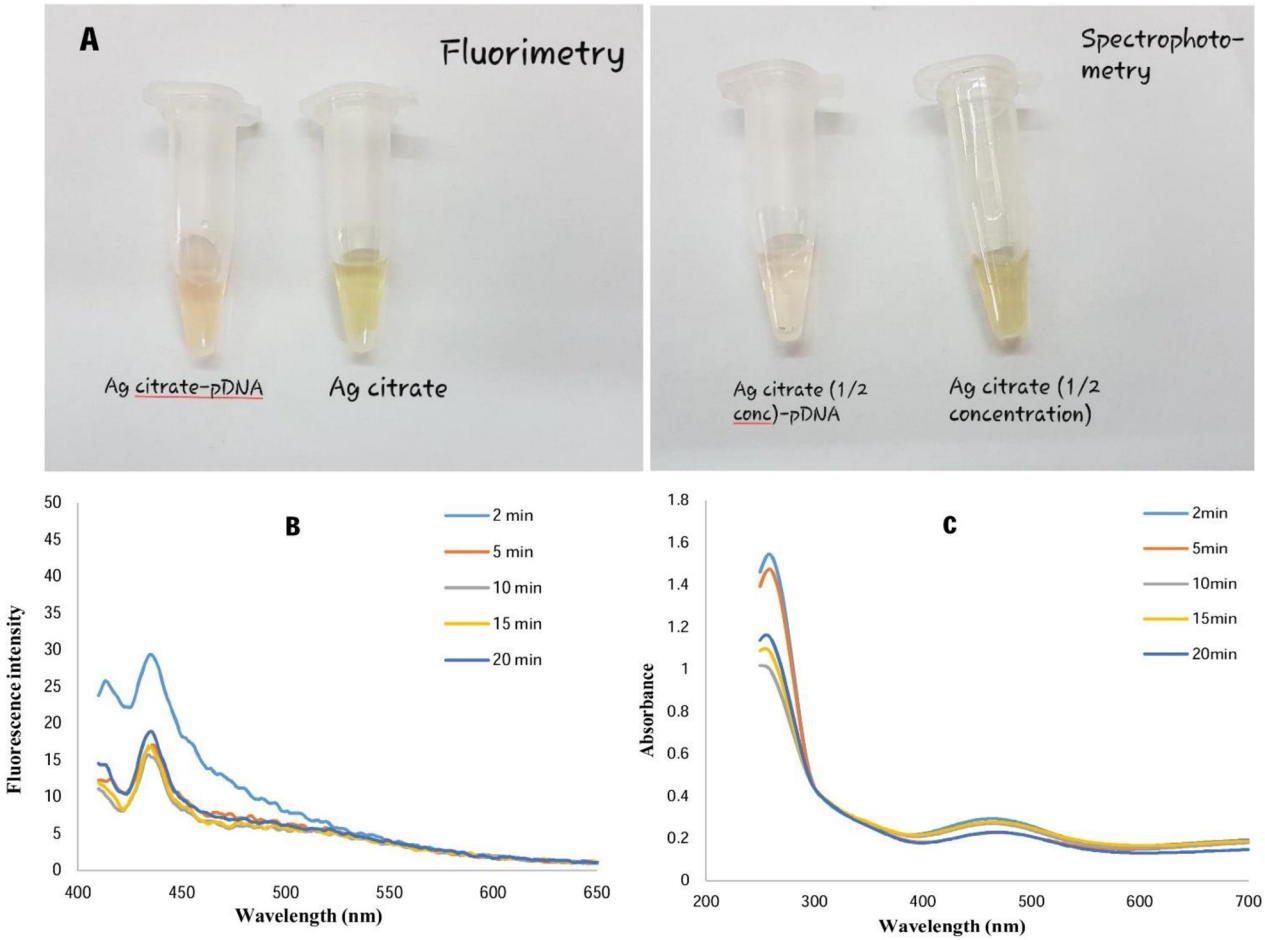

Fig. 4.12 | (A) color alteration of Cit/AgNPs from yellow to pale red after hybridization with pDNA. Fluorescence excitation (B) and UV/Vis absorbance (C) spectrum in various hybridization time (2,5,10,15, and 20 min).

Analytical study

Sensitivity is one of the significant parts of the genosensors. In order to evaluate the sensitivity of prepared genosensor, various concentration of cDNA (10^{-6},10^{-9},10^{-12},10^{-15},10^{-17} and 10^{-21} M) was applied with 2 min incubation time. Same as the previous section, 10 µL of NaCl was added for increasing quality and stability of AgNPs. 15 µL of these concentrations were added to the prepared Cit/AgNPs-pDNA and incubated at 37°C for 2 min. As exhibited in Fig. 4.13, the maximum peak was recorded for concentration 10^{-6} M and it was thoroughly predictable.

According to decrease of cDNA concentration, the intensity of the excited fluorescence and absorbed signal was decreased. According to the results, in spite of recorded signals downward mobility, the developed optical genosensor can be employed for determination of cDNA, target sequence, up to the concentration of 1 zM for both spectrofluorometer and UV–vis spectrophotometer. Dynamic linear ranges for both were between 1 µM-1 zM and regression equations recorded for spectrofluorometery and UV–vis spectrophotometery respectively were:

$y = -1.7625$ (*Haemophilus influenza*) $+ 23.969$ $R^2 = 0.8412$ Eq. 4

$y = -0.0885$ (*Haemophilus influenza*) $+ 1.1295$ $R^2 = 0.8692$ Eq. 5

Briefly, the designed DNA based biosensor not only possess great sensitivity but also has easy and low-cost construction.

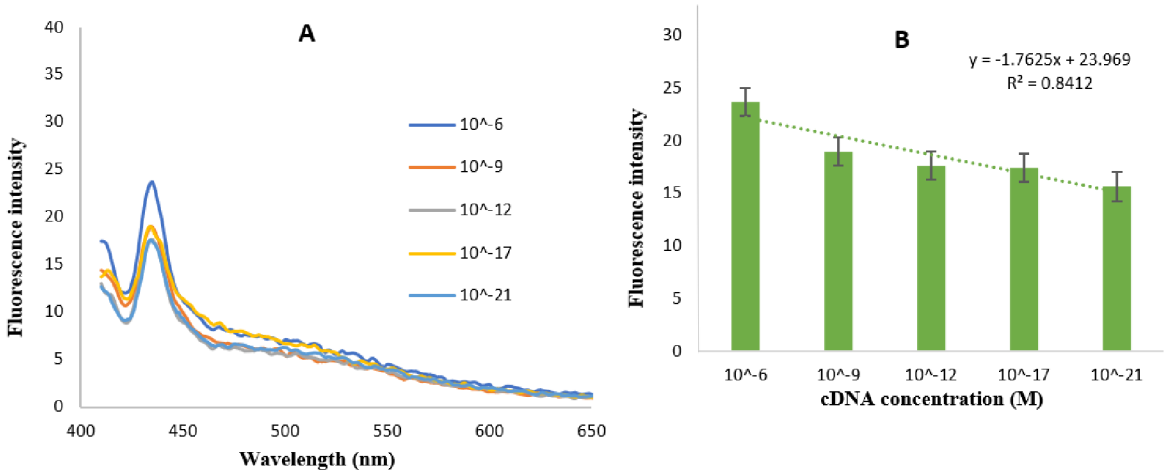

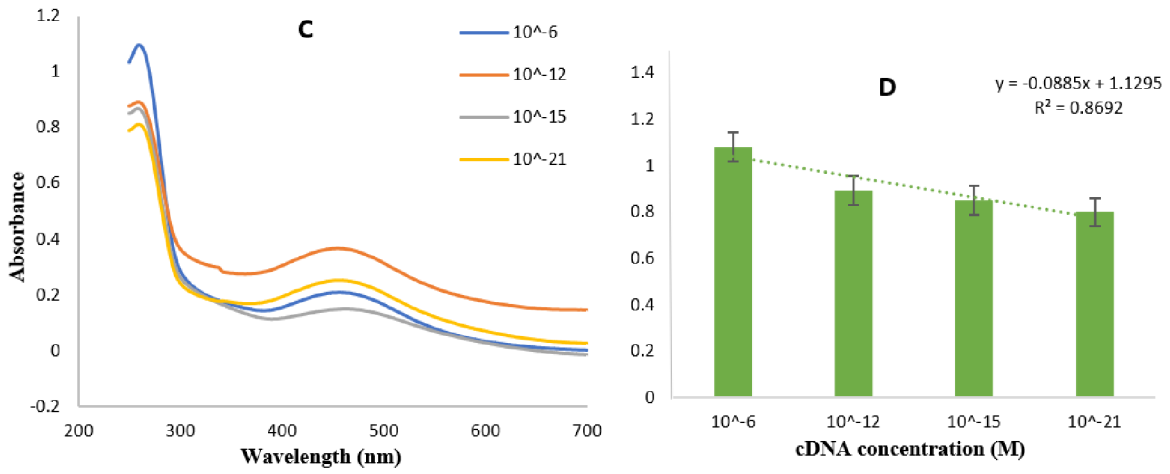

Fig. 4.13 | Fluorescence excitation (A) and UV/Vis absorbance (C) spectrum of genosensor after hybridization with a variety of cDNA concentrations (10^{-6},10^{-9},10^{-12},10^{-15},10^{-17} and 10^{-21} M) in the 400−750 nm and 250−700 nm spectral ranges, respectively. Histograms of peak intensity versus concentration of cDNA (C and D).

Selectivity

One of the remarkable merits of biosensors is its selectivity. Hence, a perfect biosensor should have power to distinguish similar analytes. For evaluate the selectivity, we designed three mismatch sequences (mismatch 1: 5′-ATG GAG GTG AAA AAG TTG GAA AAT T-3', mismatch 2: 5′-AGG GAG GTG AAA AAG TTG GAA AAT T-3', mismatch 3: 5′-AGG GAG GTG AGA AAG TTG GAA AAT T-3'). Alike with analytical study, the designed genosensor was incubated with 15 µL mismatch primers and fluorescence excitation and UV/Vis absorbance was recorded for comparison with cDNA hybridization. The selectivity of genosensor was evaluated in spectral ranges 400−750 nm and 250−700 nm, respectively. As showed in Fig. 4.14, in the presence of mismatched DNAs, fluorescence excitation had significant reduction, whereas, UV/Vis absorbance was considerably increased from mismatch one to mismatch three. These results has

exact agreement with different reported studies that the dsDNA intensity is more than that of ssDNA.

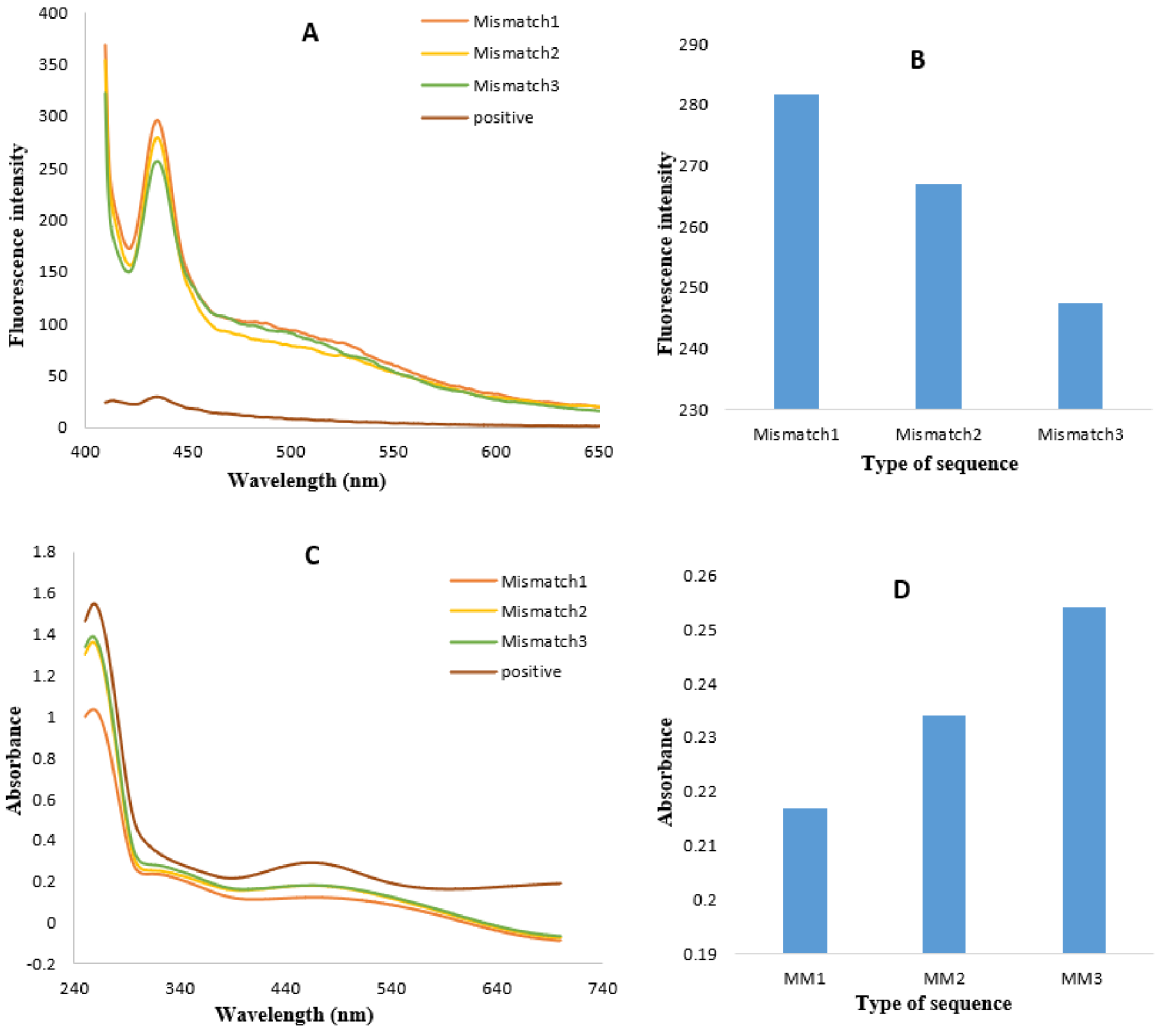

Fig. 4.14 | Fluorescence excitation (A) and UV/Vis absorbance (C) spectrum of hybridization with mismatch cDNAs (Mismatch1, Mismatch2, Mismatch3) in the 400−750 nm and 250−700 nm spectral ranges, respectively. Histograms of peak intensity versus type of sequence (B and D).

Stability

One of the ways to increase the genosensors stability is employing silver nanoparticles. Silver nanoparticles draw a lot of attention in optical biosensors because of their simple and low-cost fabrication as well as great extinction coefficients. In addition, AgNPs has great superficial

area which can be suitably modified [44, 45]. The stability of developed genosensor was measured in two steps. At first, intraday stability of synthesized Cit/AgNPs was examined at regular 2 -h interval time. According to Fig. 4.15A-B, the fluorescence excitation and UV/Vis absorbance of Cit/AgNPs were decreased respectively during each 2 h interval time. In the second step, the stability of developed genosensor was evaluated similar to that of Cit/AgNPs. As displayed in Fig. 4.15C-D, the fluorescence excitation of engineered genosensor was increased respectively during each 2 -h interval time; whereas, its UV/Vis absorbance was decreased. Therefore, the synthesized Cit/AgNPs has acceptable stability. The genosensor has stability for use within 4 h. Finally, designed platform has appropriate stability despite its easy fabrication.

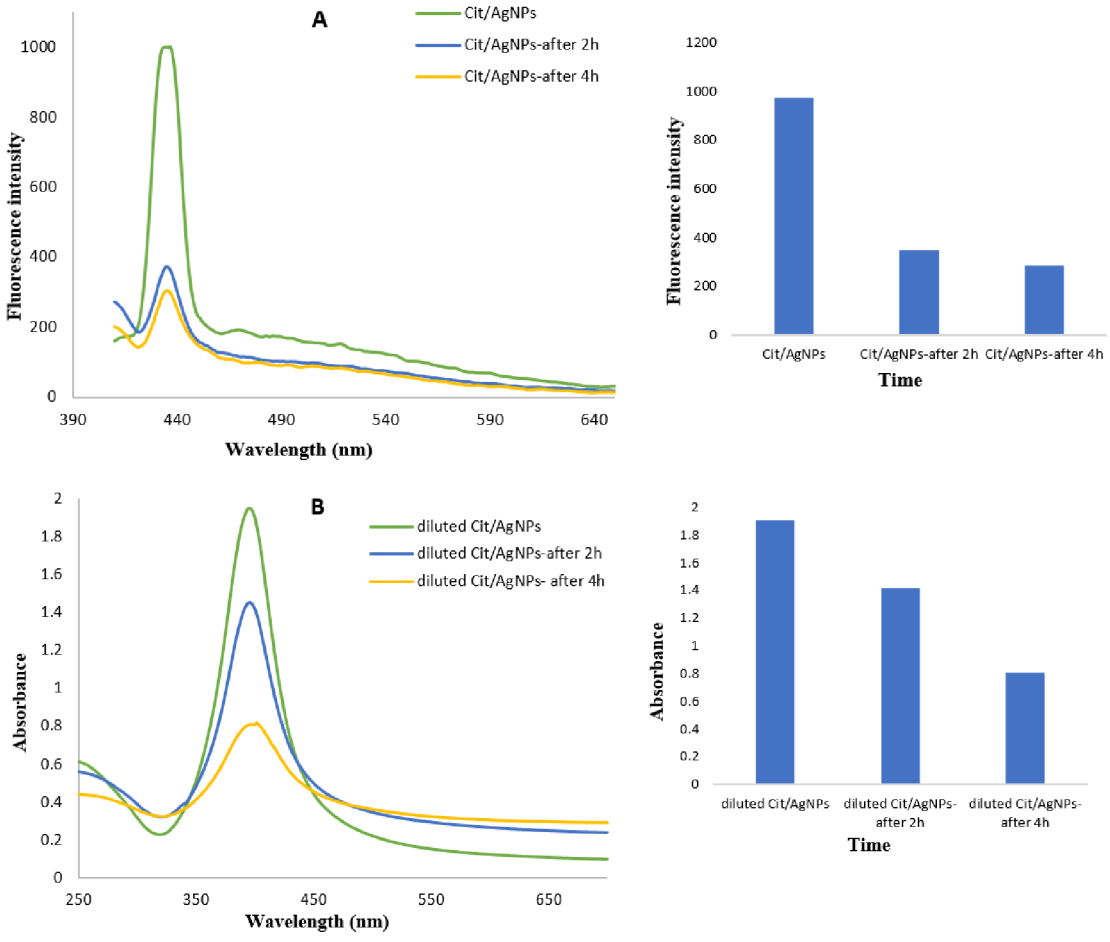

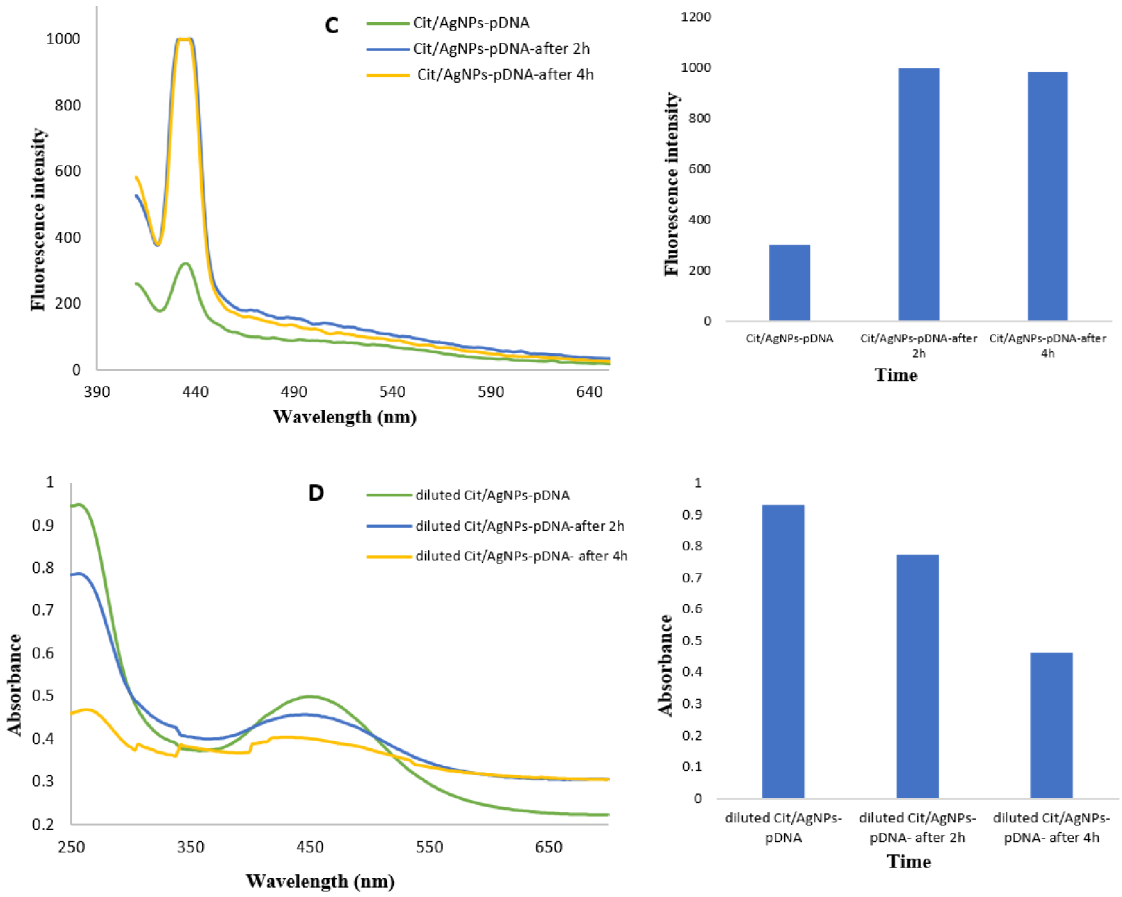

Fig. 4.15 | Fluorescence excitation (A–C) and UV/Vis absorbance (B–D) of Cit/AgNPs and Cit/AgNPs-pDNA, respectively, at regular 2 -h interval time.

Conclusion

A unique method for the analysis of DNA hybridization was developed to detect *Haemophilus influenza*. The technique was based on spectrofluorometeric and UV/Vis spectrophotometric which detected hybridization of DNA using citrate capped silver nanoparticles conjugation as a transducer. The LLOQ (low limit of quantification) of DNA sample was 1 zM using 15 µL of probe and 200 µL of Cit/AgNPs. The fabricated platform not only is rapid and simple, but also it is cost-efficient, convenient and only a small volume of sample is required. Therefore, this technique has potential applications in clinical diagnosis field. Fast and specific

determination of pathogenic bacteria could be a great alternative for hard-growing bacteria diagnosis.

Bioelectrocataytic behavior horseradish peroxidase bound to green polymeric scaffold of poly(tyrosine)-chitosan as molecularly imprinted polymer toward monitoring of H_2O_2 in human biofluids

Introduction

Molecular imprinting, which leads to creating particular recognition sites in polymer matrices, recently became a broadly employed technique for developing robust and durable biosensors for diagnostics, industry, and environmental analysis[112]. The goal of molecular imprinting based on the "lock-and-key" idea is to create specialized target molecular locks to match target molecules as "key" templates. The approach has been extensively used in electrochemical sensors [113]. The study of protein recognition and rebinding characteristics is typically the primary focus of conventional MIPs (molecularly imprinted polymers) made with initiators, cross-linkers, functional monomers, and template molecules. However, these MIPs likely have limitations, including slow target analyte binding kinetics, small binding capacities, deficient template removal, and inadequate site accessibility for the template molecules [114, 115].

Surface imprinting is a common and widely used approach for imprinting biomolecules such as proteins, with the diffusion problem alleviated through template-polymer contact. Hence, high-affinity recognition sites on the substrate's surface can be obtained [116]. The merits of MIP-based electrochemical biosensors include great sensitivity and selectivity, reusability, low cost, automation, ease of preparation, mechanical/chemical stability, and miniaturization[64]. The preparation process for MIP-based electrochemical biosensors can be carried out without catalysts, initiators, or cross-linkers, which are essential functional components in conventional MIP procedures. Thus, a simple and affordable process emerges as a promising approach for MIP

formation. By adjusting the charge and deposition mode, electropolymerization provides the capacity to precisely regulate the film thickness and compactness on the transducer surface.

In several enzyme-substrate processes, hydrogen peroxide (H_2O_2) serves as an enzymatic intermediate and functions as a potent oxidant. Since H_2O_2 plays a significant role in several redox processes in biological systems, the quick and precise detection of trace amounts of H_2O_2 is critical in clinical applications[117-119]. Horseradish peroxidase (HRP) is a plant-source essential heme-containing enzyme that has been extensively researched for over a century. It is a glycoprotein with an approximate molecular weight of 42,000 Da, belonging to the class III classical secretory plant peroxidases. It contains two different metal center iron (III) protoporphyrin IX (ferriprotoporphyrin IX) situated at the active site[120, 121]. It is described as oxidoreductase enzymes utilizing H_2O_2 as the electron acceptor for peroxides reduction and oxidization of a broad range of inorganic and organic compounds[122].

In this work, we proposed a new matrix of poly(Tyr)-CS on the disposable screen-printed carbon electrodes for surface imprinting of the HRP enzyme. Additionally, using imprinted film as matrices that HRP has immobilized based on the strong interaction between poly(Tyr)-CS MIP film and HRP, a molecularly imprinted electrochemical biosensor for determination of HRP can be expanded for the detection of H_2O_2 as enzymatic substrates. In other words, using the MIP film can create a bi-analyte biosensor for the enzyme and its substrate. The chief aspects of this work have been highlighted. The application of poly(Tyr)-CS film is an economical, facile, and green matrix for constructing a sensitive HRP surface molecular imprinting electrochemical biosensor, which results in facilitating the electron transfer and enhancing the bioelectrocataytic activity of the HRP on H_2O_2. The fabricated MIPs have dramatically improved the current intensity and enhanced sensitivity for determining H_2O_2 in human plasma samples.

Chemical and reagents

Chitosan, L-tyrosine (L-Tyr), H_2O_2 (≥30%), potassium ferrocyanide, potassium ferricyanide, potassium chloride, bovine serum albumin (BSA), and HRP (type II) were purchased from Sigma Aldrich (Prague, Czech Republic). 0.1 M phosphate buffer saline solution (PBS) was prepared by dissolving Na_2HPO_4 (0.1 M) and NaH_2PO_4 (0.1 M) in ultrapure water. Ultrapure water with a resistivity of 18.2 M.cm (MilliQ, Millipore, France) was used to prepare all solutions. Human plasma samples were kindly provided by the University Hospital in Ostrava. Commercial buffer solutions with pH levels of 4.0, 7.0, and 10.0 were used for calibration of the pH electrode.

Instruments

The Metrohm Potentiostat PGSTAT101 AUTOLAB was used for electrochemical measurements (Prague, Czech Republic). The NOVA 2.1 software was used to run the system on a computer. Three-electrode screen-printed carbon electrodes DRP-C110 (bare carbon) were purchased from Metrohm Dropsens (Prague, Czech Republic). The screen-printed electrochemical cell comprises a carbon working electrode (4-mm diameter), a silver or Ag/AgCl reference electrode, and an auxiliary carbon electrode. A scanning electron microscope (SEM), Hitachi SU6600 SEM (Hitachi, Japan), was used to analyse the surface morphology of the screen-printed carbon electrodes. The electrode components were identified using an EDS (energy dispersive spectroscopy) paired with SEM equipment.

Electroanalytical measurements

The electrochemical characteristics of the imprinted biosensor were characterized using different electrochemical methods, including CV and DPV. $Fe(CN)_6^{4-}/Fe(CN)_6^{3-}$ was selected as the electroactive probe solution for evaluating the HRP response.

The imprinted polymer was electrochemically characterized using CV scanning in 0.01 M $Fe(CN)_6^{4-}/Fe(CN)_6^{3-}$ containing 0.1 M KCl at the potential range of -1.2 to 1.0 V and a sweep rate of 30 $mV.s^{-1}$. Furthermore, DPV at potentials between -1.2 and 0.0 V with a step potential of 0.005 mV *and* chronoamperometry with an applied potential of -0.66 V was employed to evaluate and determine H_2O_2 using molecularly imprinted biosensor in 0.1 M PBS solution (pH 8.0) containing various concentrations of H_2O_2. All experiments were conducted at room temperature and repeated three times.

Electropolymerization of L-Tyr supported CS on the SPCE surface

The electropolymerization of 10 mM L-Tyr in PBS (pH = 7.4) utilizing the CV method produced poly(Tyr). The modification procedure was performed in the potential range of -1.0 to 1.0 V (10 repetitive cycles), and the scan rate was 100 $mV.s^{-1}$. After the electropolymerization of poly(Tyr) on the SPCE surface, deionized water was used to rinse the modified electrode to remove any unabsorbed substances. According to Fig. 4.16A, the creation of poly(Tyr) led to an anodic peak at 0.6 V and a reduction peak at -0.8 V. As the number of CV scans rose, the peak current also increased, exhibiting the formation of an electroconductive polymer film on the electrode surface. In the second step, the SPCE was moved into 0.1 M HCl containing 2 mg/mL CS, and 20 repetitive cycles were performed in the potential range from -1.0 V to 0.15 V and sweep rate of

100 mV.s^{-1} (Fig. 4.16B). A thin film of poly(Tyr)-CS film was created on the surface of a screen-printed carbon electrode.

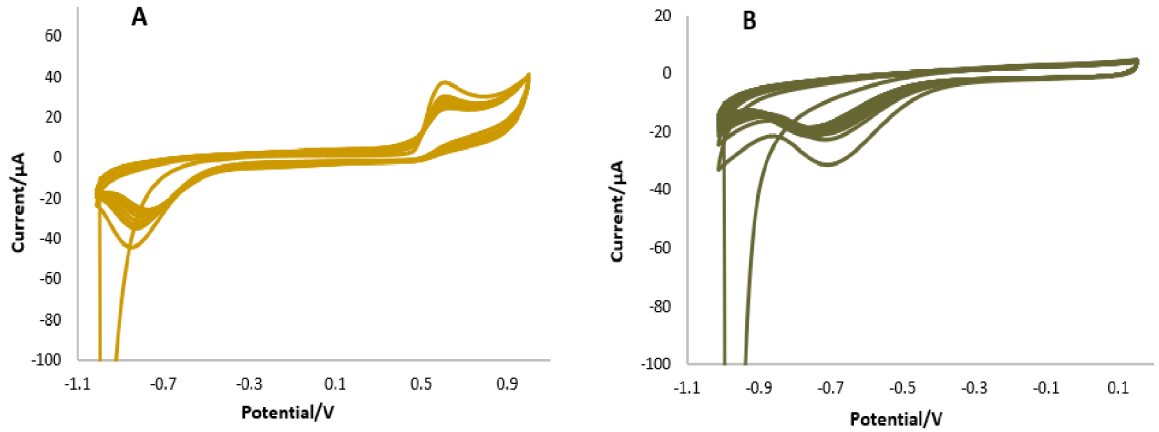

Fig. 4.16 | A) CVs of poly(Tyr) on the surface of SPCE in the presence of 0.1 M *PBS* (pH=7.4) containing 27 mM *L-Tyr* at scan rate of 100 mV s^{-1}. Number of cycles is 10. B) CVs of CS on the surface of SPCE in the presence of 0.1 M *HCl* containing 2 mg/mL CS at scan rate of 100 mV s^{-1}. Number of cycles is 20.

Preparation of MIP/ poly(Tyr)-CS modified biosensors

The combination of poly(Tyr)-CS electropolymerization with the self-assembly surface molecular imprinting approach led to the protein (HRP) imprinting in poly(Tyr)-CS. The poly(Tyr)-CS/SPCE were submerged in PBS (pH=6) containing 1 mg/mL HRP after the electropolymerization. They lasted 24 hours in a refrigerator at 4°C. The HRP template molecules were easily immobilized on the poly(Tyr)-CS matrix through hydrogen binding interaction. The modified electrode (HRP/poly(Tyr)-CS/SPCE) was immersed in 1.0 M hydrochloric acid solution for a period to eliminate the binding template HRP. The imprinted electrode (MIP/poly(Tyr)-CS/SPCE) was thoroughly rewashed with ultrapure water after that. Electrochemical techniques like CV and DPV were applied to ensure that the template had been properly removed. Prior to usage, the MIP/poly(Tyr)-CS/SPCE electrode was kept at 4 °C in a refrigerator.

Results and discussion

Morphological and structural characterization of prepared imprinted biosensor

The morphology of the modified SPCE and the imprinted layer was further examined using SEM. EDS was used to perform an elementary analysis as well. Fig. 4.17 display the SEM image of the poly(Tyr)-CS/SPCE, HRP/poly(Tyr)-CS/SPCE, MIP/poly(Tyr)-CS/SPCE, and bare SPCE. The surface of bare SPCE was smooth and flat, as seen in Fig. 4.17D. A notable homogeneous monodispersed spherical structure was seen when poly(Tyr)-CS was modified on SPCE (Fig. 4.17A), which is ideal for macromolecular loading effectiveness, and the average size of spherical beads was around 60 nm. Such polymer's monodispersed spherical beads have increased surface area and pore volume, which results in high imprinting effectiveness and enhanced noncovalent bonding interaction strength. Fig. 4.17B exhibits that HRP protein molecules have been assembled on the surface of the monodispersed spherical poly(Tyr)-CS film, which made the surface uneven and undulant. Additionally, the EDX demonstrates that P and Fe elements were not initial polymer film, and P and Fe peaks can be seen in the enzyme-immobilized film. These alterations showed that HRP had been successfully immobilized on the poly(Tyr)-CS film. The change in film shape caused by eliminating the HRP template molecules is apparent in Fig. 4.17C.

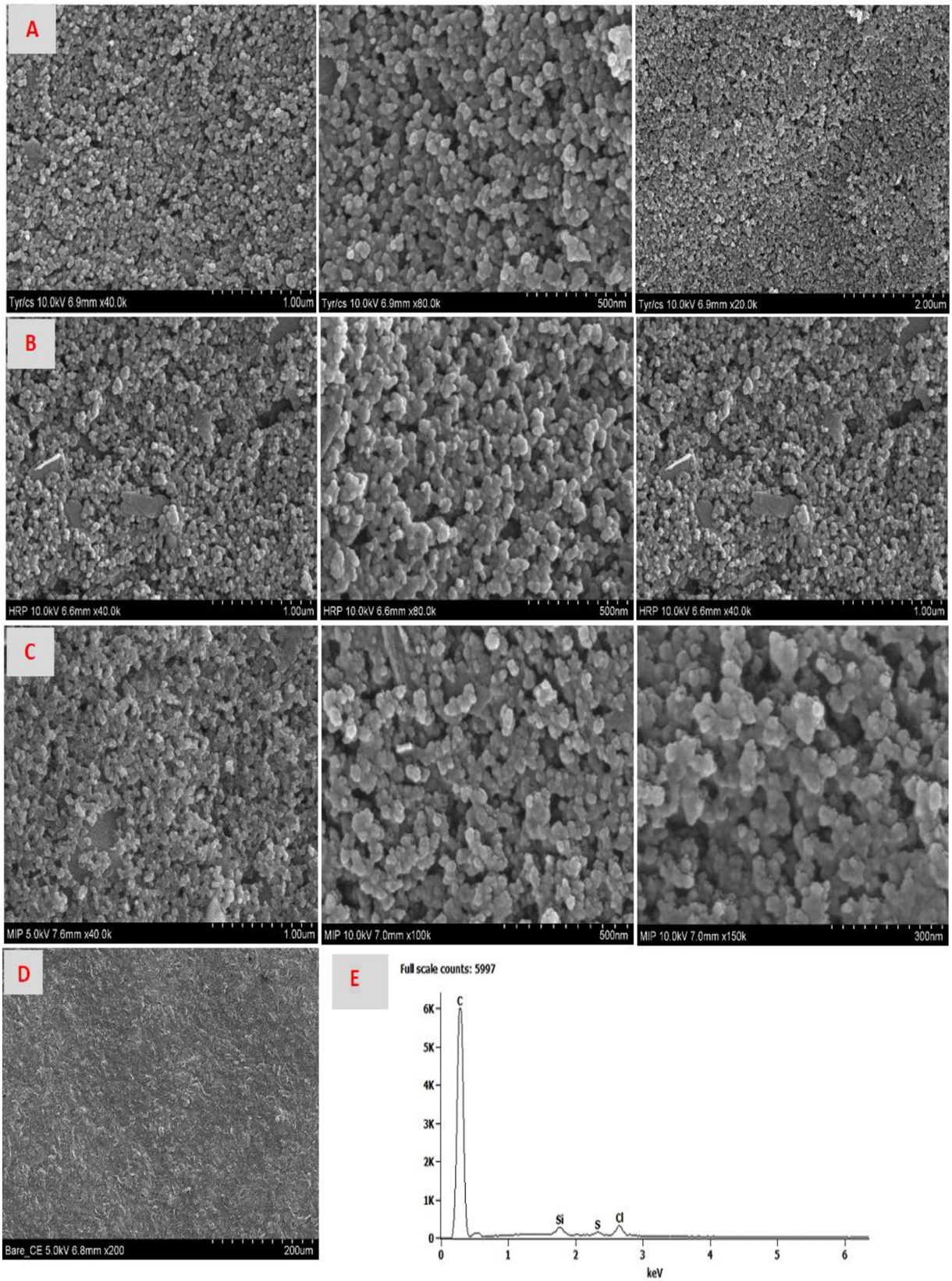
A
Tyr/cs 10.0kV 6.9mm x40.0k 1.00um
Tyr/cs 10.0kV 6.9mm x80.0k 500nm
Tyr/cs 10.0kV 6.9mm x20.0k 2.00um
B
HRP 10.0kV 6.6mm x40.0k 1.00um
HRP 10.0kV 6.6mm x80.0k 500nm
HRP 10.0kV 6.6mm x40.0k 1.00um
C
MIP 5.0kV 7.6mm x40.0k 1.00um
MIP 10.0kV 7.0mm x100k 500nm
MIP 10.0kV 7.0mm x150k 300nm
D
Bare_CE 5.0kV 6.8mm x200 200um
E
Full scale counts: 5997
C
Si
S
Cl
6K
5K
4K
3K
2K
1K
0
0
1
2
3
4
5
6
keV

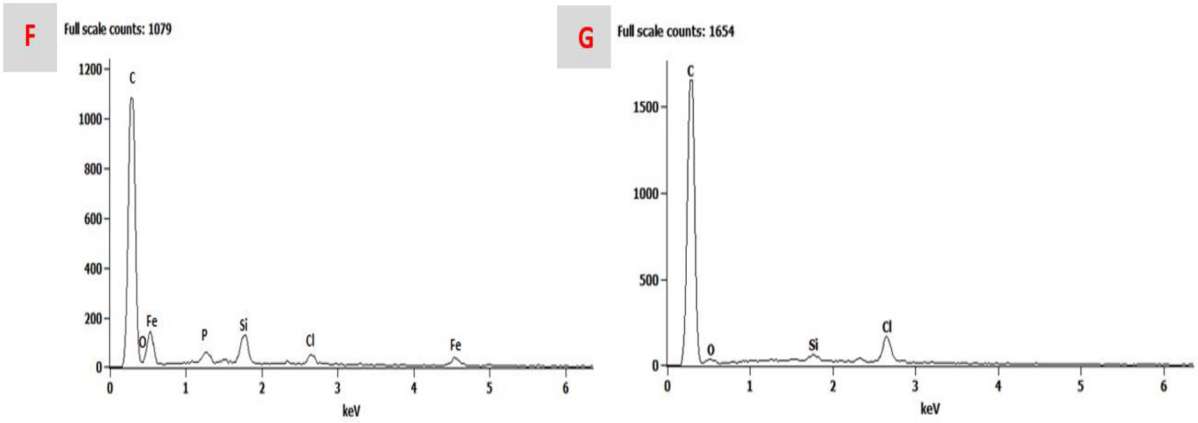

Fig. 4.17 | Scanning electron microscopy of (A) poly(Tyr)-CS/SPCE, (B) HRP/poly(Tyr)-CS/SPCE, and (C) MIP/poly(Tyr)-CS/SPCE, (D) bare SPCE, and EDXs of (E) poly(Tyr)-CS/SPCE, (F) HRP/poly(Tyr)-CS/SPCE, and (G) MIP/poly(Tyr)-CS/SPCE, respectively.

The possible mechanisms of the electropolymerization of poly(Tyr)-CS film

The suggested process of electropolymerization of poly(Tyr)-CS is that L-tyrosine polymerization starts in the first step by providing an oxidation potential, leading to the production of a radical cation on the carbon-containing amine group. It has been demonstrated that an NH group-containing monomer may be electropolymerized on the SPCE surface to create a conducting film by the formation of a covalent bond (N-C) between the NH group and carbon electrode [123, 124]. Since CS is positively charged when dissolved in acid (HCl in the current study), the electron-withdrawing oxygen-containing groups on poly(Tyr) in the second step are advantageous to the combination with CS from an electrostatic point of view. The findings, therefore, demonstrate that tyrosine may interact with hydrophilic CS via $-NH_3^+$ and -OH side groups, allowing for the formation of a specific self-assembly network between the tyrosine monomer and CS chains (Scheme. 4.3) [124, 125].

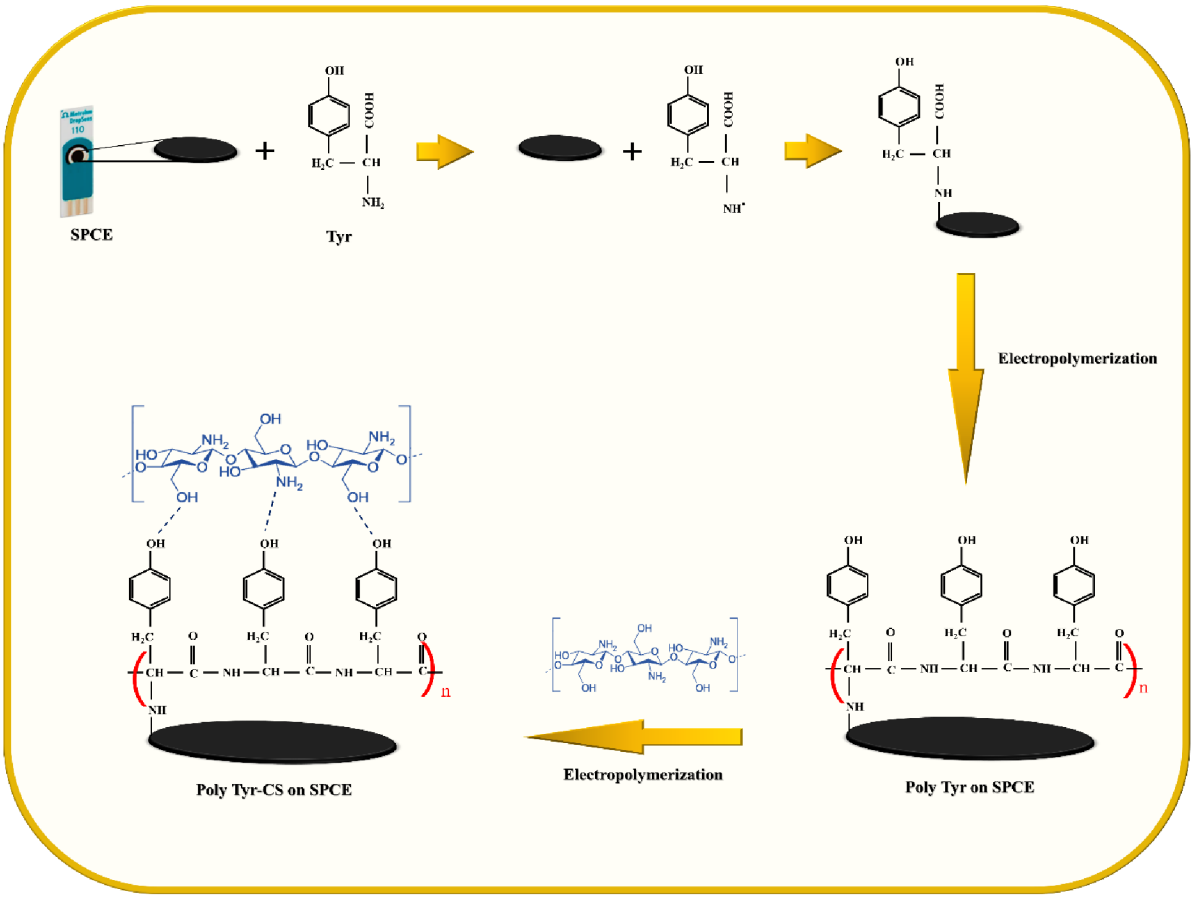

Scheme. 4.3 | *Electropolymerization procedure of tyrosine supported chitosan on the screen-printed carbon electrode.*

Optimization of biosensor responses

Electrochemical characterization of developed imprinted biosensor

Scheme 4.4 depicts the fabrication of the HRP electrochemical imprinted biosensor (MIP/poly(Tyr)-CS/SPCE). A new imprinting preparation method was used to ensure the diffusion and elution of the HRP biomacromolecule on the surface of the created modified electrode [122, 126-129]. In this strategy, pre-assembly of the poly(Tyr)-CS film onto the SPCE surface before binding of HRP rather than the conventional method of tyrosine and CS electropolymerization in the presence of the HRP template was carried out. CV was employed for the characterization of preparation procedures of the imprinted biosensor in a 0.01 M $Fe(CN)_6^{4-}/Fe(CN)_6^{3-}$ solution

containing 0.1 M KCl as a supporting electrolyte. Fig. 4.18 showed that the redox peaks were enhanced when SPCE was modified by poly(Tyr)-CS compared to the bare SPCE, suggesting that the high electrical conductivity and unique characteristics of the poly(Tyr)-CS/SPCE *can* expedite the electron flow of probe involving $Fe(CN)_6^{4-}/Fe(CN)_6^{3-}$. Template HRP molecules were trapped in the poly(Tyr)-CS matrix through hydrogen bond interaction between the –NH groups of the poly(Tyr)-CS film and the -COOH groups of the HRP template molecules. Consequently, when the HRP molecule was bounded, the peak current of the prepared electrode reduced drastically, implying the successful assembly of HRP that allows electron transport to be retarded because of weak conductivity. However, after the removal of the template protein molecules from the polymer matrix, the specific imprinting cavity for HRP molecule determination was reconstructed. The imprinted sites were evidently generated following the elution of the template protein, which let the probe molecules diffuse into the electrode surface via the imprinted layer's pores [122, 128, 129]. As a result, the peak current was enhanced, indicating that HRP biomacromolecules were successfully removed. CV can keep track of the template elution from the matrix.

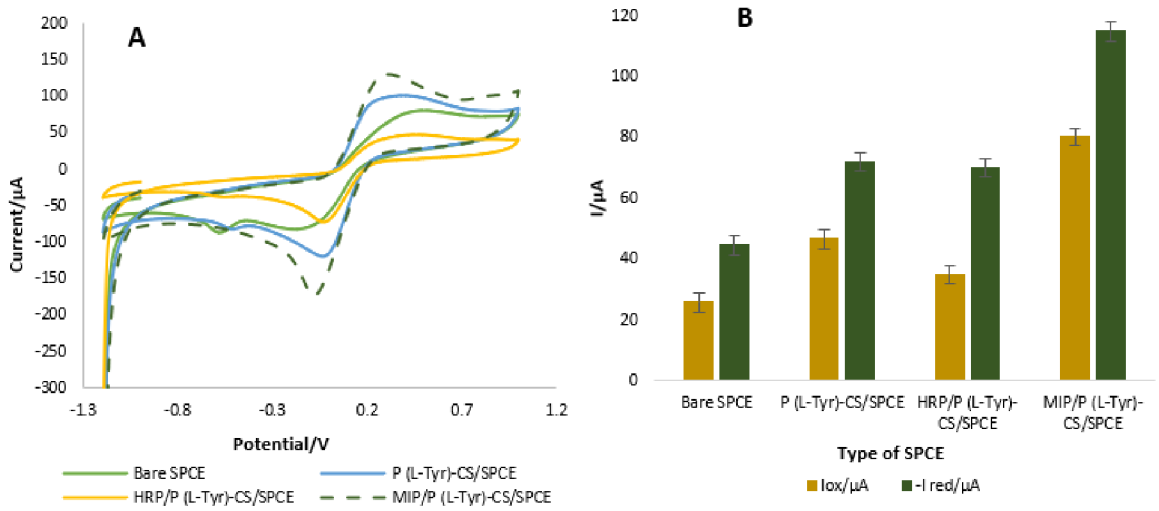

Fig. 4.18 | A) CVs of preparation steps of imprinted polymer in 0.01 M $Fe(CN)_6^{4-}/Fe(CN)_6^{3-}$+0.1 M KCl at a sweep rate of 30 mV/s. B) peak currents variation versus type of modified electrodes (n = 3, SD = 3.01).

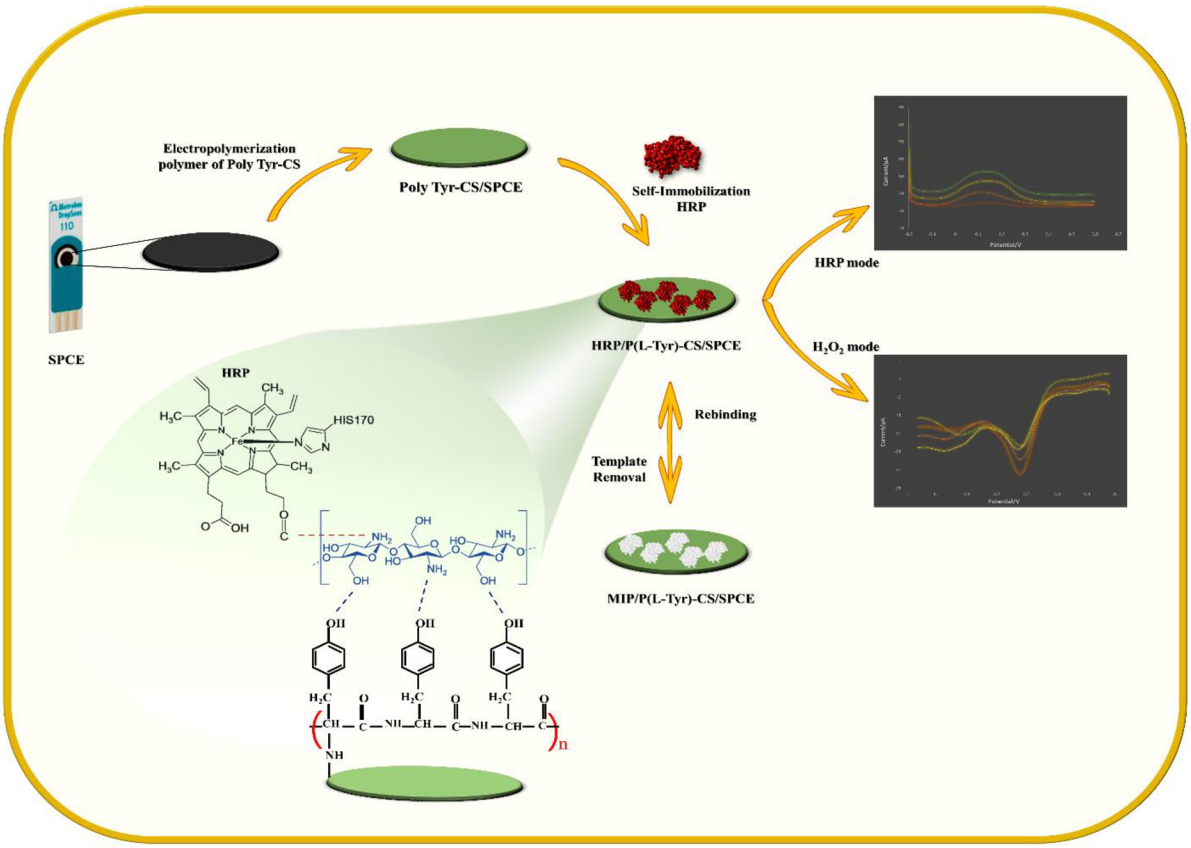

Scheme. 4.4 | *The preparation process of MIP/poly(Tyr)-CS/SPCE biosensor.*

The template removal time is critical in achieving the optimal MIP-based sensor. The adequate time allows for the template extraction from the polymeric matrix. The electrode surface was exposed to 1.0 M HCl, and the exposure time was between 5 and 40 min (Fig. 4.19). The peak current rose when the electrode surface was soaked in 1.0 M HCl for 20 minutes. These findings show that the HRP has begun to be removed from the polymeric matrix. However, after 20 min, the CV current fell and remained stable until 40 min. As shown in Fig. 4.19B, a 20-min immersion in 1.0 M HCl was sufficient to remove HRP from the polymeric matrix.

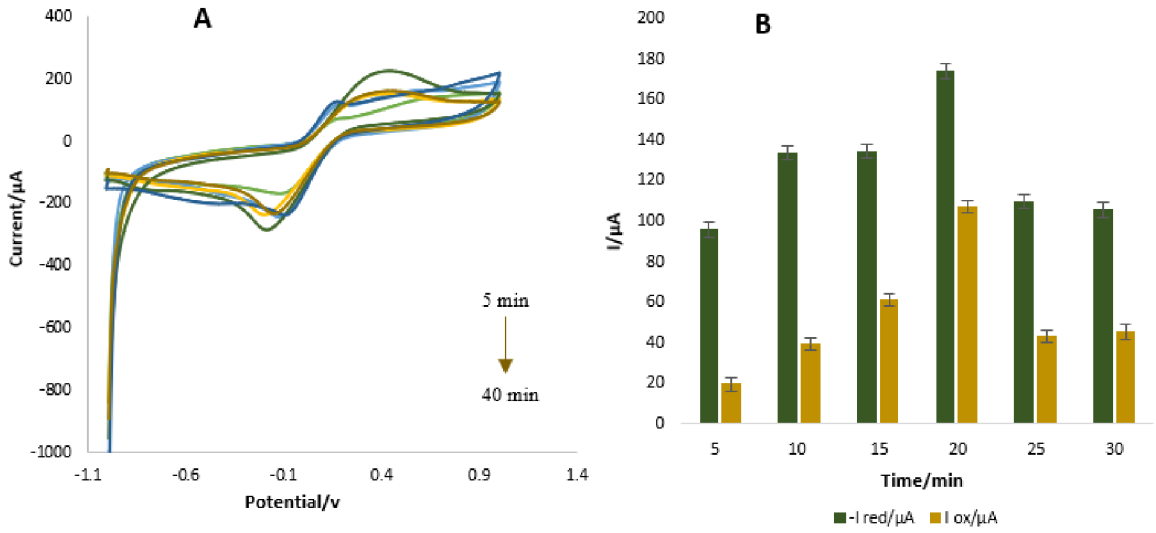

Fig. 4.19 | A) CVs of HRP/poly(Tyr)-CS/SPCE imprinted polymer at different *removal time (5,10,15,20,30, and 40 min)* in 0.01 M $Fe(CN)_6^{4-}/Fe(CN)_6^{3-}$+0.1 M KCl at a sweep rate of 0.1 V/s. B) peak currents variation versus template removal time with HCl (n = 3, SD = 3.33).

Kinetic studying

CVs of poly(Tyr)-CS modified SPCE were obtained at various sweep rates in the range of 10 to 500 $mV.s^{-1}$ in $Fe(CN)_6^{4-}/Fe(CN)_6^{3-}$ solution for the kinetic study. Peak currents increased with increasing scan rate, as shown in Fig. 4.20. According to Fig. 4.20D, the dependence of the Neperian logarithm of peak current on the Neperian logarithm of sweep rate (*ln Ip versus ln v*) is linear $\ln Ip_a = 0.1845 \ln v + 5.1798$ ($R^2 = 0.9951$), in which the slope is 0.1845 ± 0.003. A slope close to 1.0 is believed to be the electrode process is adsorption-controlled, and a slope less than 0.5 is thought to be diffusion-controlled by Fick's law [130, 131]. Hence, this indicates that the electrochemical reaction at poly(Tyr)-CS/SPCE surface was controlled by diffusion. Fig. 4.20C demonstrates the dependence of peak potential on the Neperian logarithm of the scan rate (E_{pa} *versus ln v*) and that the electron transfer has an irreversible nature with a positive shifting in the anodic and cathodic peak positions, respectively. The linear relation between E_{pa} *versus ln v* can be expressed as $E_{pa} = 0.0932 \ln v + 0.6717$ ($R^2 = 0.9843$). As for a diffusion-controlled and

irreversible electrode process, according to Laviron [79], E_{pa} can be calculated using the following equation:

$$Ep = (\frac{RT}{2\alpha nF}) \ln v + \text{constant} \quad \text{Eq. 6}$$

In the above equation, E_p is the peak potential, α is the electron-transfer coefficient, n is the number of electrons, T is the temperature (298 K), F is the Faraday constant (96485 C mol^{-1}), and R is the universal gas constant (8.314 J K^{-1} mol^{-1}). In this study, the value of αn was calculated to be 0.13 for $[Fe(CN)_6]^{3-/4-}$. Furthermore, the value obtained for n from $|Ep - E_p/2| = 47.7/\alpha n$ (mV) irreversible system [81-83] is $1.03 \approx 1$.

Moreover, the special surface of SPCE covered with poly(Tyr)-CS should be investigated to assess the effective electrode surface coverage. To calculate the value of Γ^* as surface coverage of a modified electrode, the slope of peak currents on scan rates (I_p *vs.* V) was examined using Equation. 5 (Fig. 4.20B) [132]:

$$I_p = (n^2 F^2/4RT)\, vA\Gamma^* \quad \text{Eq. 7}$$

Where A is the electrode surface area ($A=\pi r^2=0.1256$ cm^2), ν is the potential sweep rate, and Γ* represents the surface coverage of the modified electrode (M/cm^2). The surface coverage of poly(Tyr)-CS/SPCE was attained as 1.25×10^{-5} $cm^2 \cdot s^{-1}$, which supplies an effective surface for the HRP immobilization and generation of the imprinted polymer.

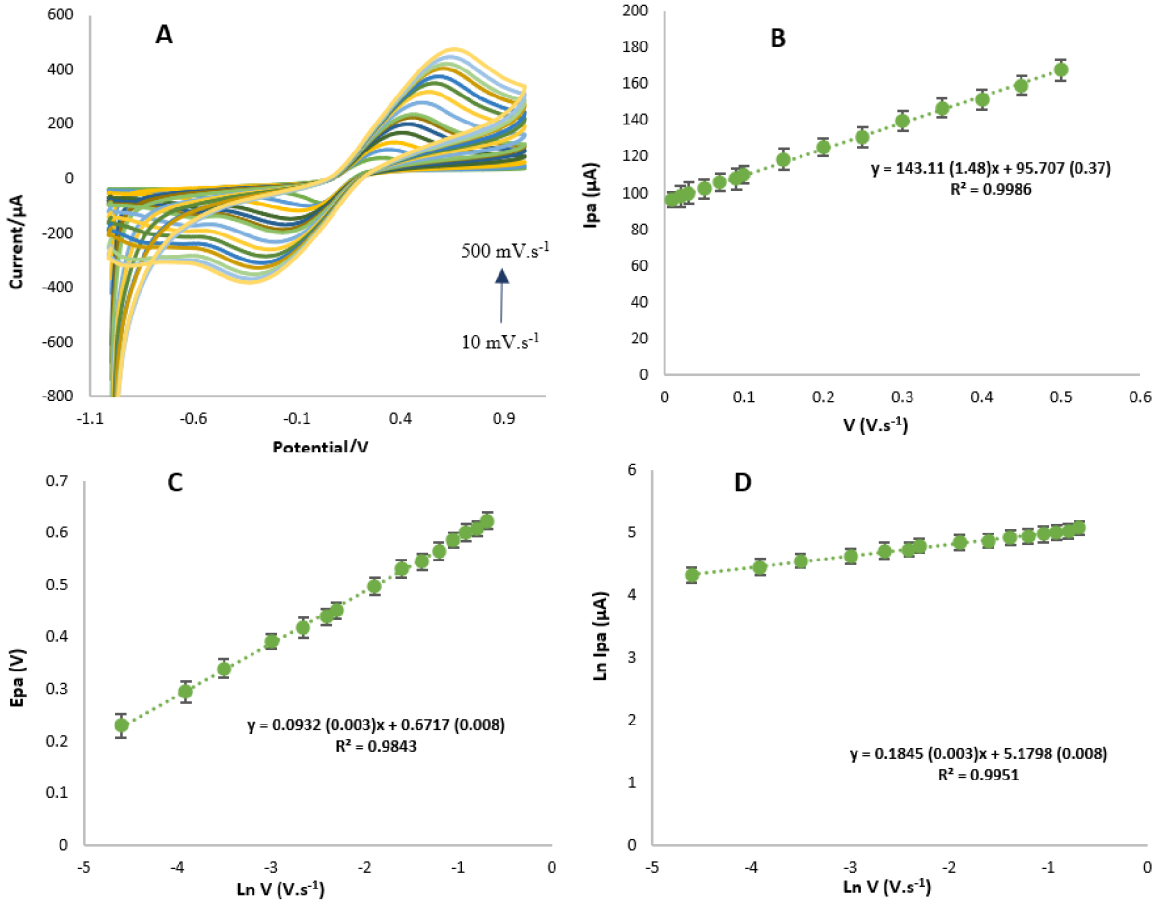

Fig. 4.20 | A) CVs of poly(Tyr)-CS/SPCE in 0.01 M $Fe(CN)_6^{3-}$ /$Fe(CN)_6^{4-}$ + 0.1M KCl at various sweep rates (10, 20, 30, 50, 70, 90, 100, 150, 200, 250, 300, 350, 400, 450, and 500 mV/s). B) The dependency of I_p versus v. C) Variation of E_p versus Lnv. D) Variation of lnIp versus Lnv.

HRP determination by the MIP/poly(Tyr)-CS/SPCE

Highly sensitive determination of the target is critical for molecularly imprinted sensors. This study has investigated the application of MIP/poly(Tyr)-CS/SPCE to detect HRP at various concentrations using the DPV method with 0.01 M $Fe(CN)_6^{3-}$ /$Fe(CN)_6^{4-}$ containing 0.1 M KCl as an electrochemical probe. According to Fig. 4.21A, the current response of the imprinted biosensor reduced as HRP concentration rose. This was caused by the entrance of the template molecule into imprinted sites, retarding electron transfer to the created cavity and obstructing the probe molecule's ability to diffuse through the imprinting layer. A correlation exists between the

concentration of HRP and the decreased peak current. As exhibited in Fig. 4.21B, there was a good dynamic linear range from 1.0 ×10^{-8} to 1.0 ×10^{-1} mg/mL to be displayed with a linear regression equation ΔI (μA)=0.1679 C_{HRP}+2.8954 (R^2=0.9729) with the LOD of 9.39 × 10^{-8} mg/ml (2.34 pM) (S/N=3.3) and a quantitation limit (LOQ) of 2.84 × 10^{-7} mg/ml (7.11 pM) (S/N=10).

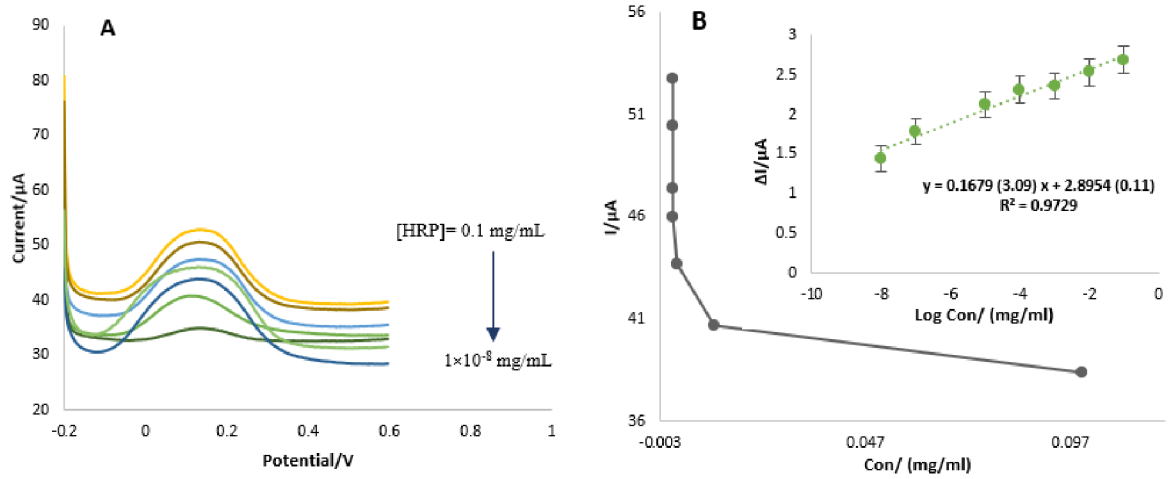

Fig. 4.21 | A) DPV of MIP/poly(Tyr)-CS/SPCE in different concentration of HRP (0.1, 10^{-2}, 10^{-3}, 10^{-4}, 10^{-5}, 10^{-7}, and 10^{-8} mg/mL in 0.01M $Fe(CN)_6^{3-}$/$Fe(CN)_6^{4-}$ + 0.1M KCl. B) Calibration curve of the corresponding peak currents of MIP/poly(Tyr)-CS/SPCE versus concentrations of HRP (n = 3, SD = 2.03).

Bioelectrocatalytic *activity* of HRP-imprinted biosensor

Anaerobic oxidase via the ferric-ferrous cycle provides the basis for the bioelectrocatalytic activity of HRP. A typical reduction substrate for the HRP process is H_2O_2. The bioelectrocatalytic mechanism of HRP for H_2O_2 reduction comprises two fundamental steps: i) Through two-electron oxidation, the heme moiety transforms into an intermediate known as compound I, and ii) two sequential one-electron reductions allow the enzyme to return to its resting state utilizing compound II, a second intermediate [133]. Using CV and DPV techniques (Fig. 4.22), the electrocatalytic performance of the HRP-imprinted biosensor (1 mg/ml HRP) for H_2O_2 reduction was investigated in 0.1 M PBS solution with different concentrations of H_2O_2. The influence of pH on the biosensing behavior of the HRP-imprinted biosensor was examined in the pH range of

4.0 to 8.0 in the presence of H_2O_2 to develop effective biosensing for H_2O_2 reduction. The current response reached its maximum at pH 8.0, as shown in Fig. 4.22C. Thus, HRP's enzyme activity reached its peak. Consequently, 0.1 M PBS solution pH 8.0 has been used to investigate H_2O_2 reduction for the first time. The CV curve represented -0.66 V as the reduction potential for H_2O_2 (Fig. 4.22D). Using the DPV method, the current response was studied at H_2O_2 concentrations ranging from 10 nM to 1 mM. The reduction peak current progressively rose as the concentration of H_2O_2 successively increased, demonstrating that the immobilized HRP/poly(Tyr)-CS/SPCE had a bioelectrocatalytical activity to H_2O_2 reduction in 0.1 M PBS with pH 8.0 (Fig. 4.22A). The obtained linear range by DPV was 10 nM to 1 mM with regression equation $-I(\mu A) = 1.061\ C_{[H2O2]}(mM) + 7.4934$ ($R^2 = 0.9945$). The limit of detection for the detection of H_2O_2 using the HRP-imprinted biosensor was estimated to be 2.18 nM (S /N=3.3), and LOQ was 6.60 nM (S/N=10) for DPV.

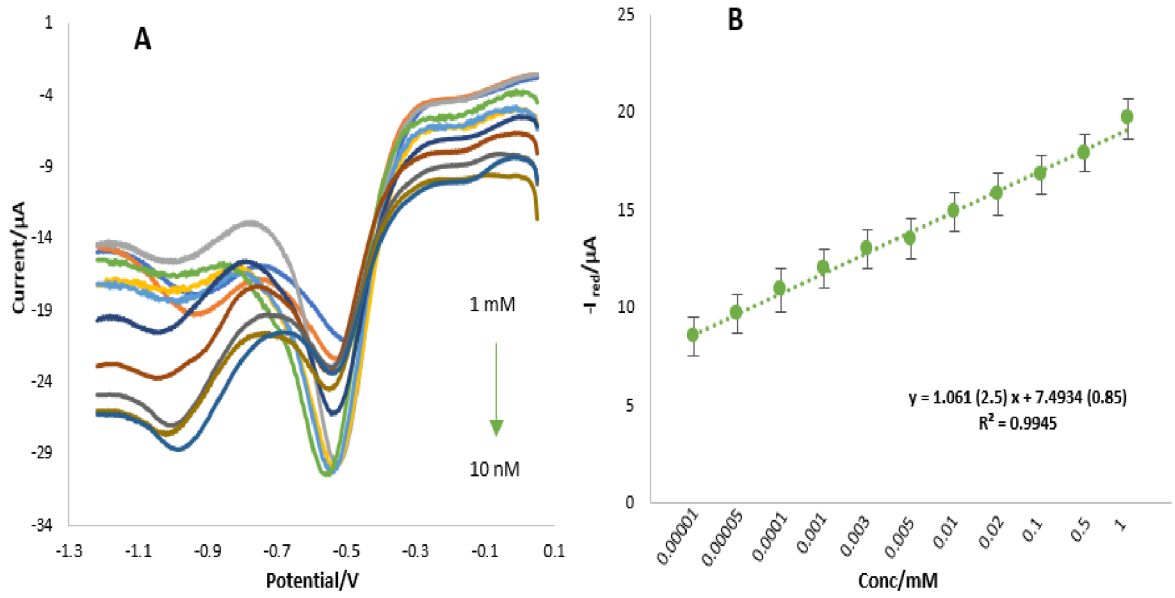

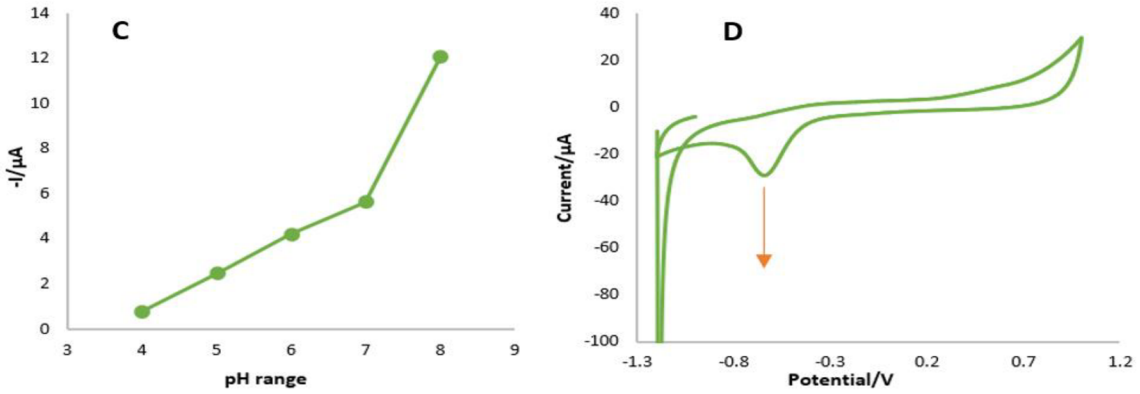

Fig. 4.22 | A) DPVs of HRP/poly(Tyr)-CS/SPCE to different concentrations of H_2O_2 from 10 nM to 1 mM in 0.1 M PBS (pH = 8.0). B) Histogram of HRP/poly(Tyr)-CS/SPCE (n = 3, SD = 1.01). C) Calibration of pH effect on H_2O_2 reduction by HRP-imprinted biosensor in 1 mM H_2O_2 solution including 0.1 M PBS with different pH (4.0 - 8.0) at a sweep rate of 30 mV/s (n = 3, SD = 0.6). D) CV of HRP/poly(Tyr)-CS/SPCE in 1 mM H_2O_2 solution including 0.1 M PBS (pH = 8.0) at a sweep rate of 30 mV/s.

H_2O_2 measurement using electrochemical biosensors has been the subject of several investigations (Table. 4.3). A few studies have employed molecularly imprinted polymer-electrochemical biosensors to determine H_2O_2. However, most researchers have used different types of nanoparticles as matrices for biosensor development. It should be noted that creating these platforms takes more time and involves more procedures, including creating working electrodes such as carbon paste and carbon cloth electrodes and synthesizing nanoparticles. However, the environmentally friendly poly(Tyr)-CS film offers a simple, accessible, and affordable matrix for the creation of molecularly imprinted polymer-electrochemical biosensors. As shown in Table. 4.3, the performance of the proposed molecularly imprinted biosensor has a lower LOD than those of previously published electrochemical biosensors for the precise determination of trace amounts of H_2O_2.

Table. 4.3 | Analytical performance comparison of the available biosensors for determination of H_2O_2.

Materials	Electrodes	Detection methods	Linear range	LOD	Ref.
Pt-MWCNT	SPCE	Chronoamperometry	10–100 µM	10 µM	134
HRP/toluidine blue/graphite	Ceramic electrode		0.429 µM–0.455 mM	0.171 µM	135
CS/HRP-poly(L-DOPA)	Au-plated Au (Au_{plate}/Au) electrodes		0.001–1.25 mM	0.1 µM	136
MnO_2	CPE[1]		0.04–1.91 µM	0.012 µM	137
MnOOH nanorod arrays	Carbon cloth electrode		20 µm–9.67 mM	3.2 µM	138
HRP/NH_2-Hf-BTB-MOL[2]/MWNTs			7.5 µM to 1500 µM	0.87 µM	139
PEDOT:PSS[3]	SPCE		1-100 µM	0.97 µM	140
PtNPs-CDs/IL-GO	GCE[5]	Amperometry	1–900 µM	0.1 µM	141
HRP/PTMSPA[4]@GNR			1×10^{-5}–1×10^{-3} M	0.06 µM	142
PtNPs/ethyl cellulose			0.05 µM–2.22 mM	0.01 µM	143
$Co_3S_4/CuCo_2O_4$			0.001–4.03 mM	17 µM	144
Pd/HRP/f-GR	Graphite electrode		25 µM–3.5 mM	0.05 µM	145
AgNiNP/RGO	Paper electrode		0.003–13 mM	0.91 µM	146
Boron-doped graphene nanosheets	RDE[6]		1.0–20.0 mM	3.8 µM	147
HRP/PAN-PNMThH	GCE	Chronoamperometry	5.0 µM–60.0 mM	3.2 µM	148
HRP/C-Dots/LDHs			0.1–23.1 µM	0.04 µM	149
NiO/GR			0.25–4.75 mM	0.7664 µM	150
EFK8-SWNT- hemoglobin			20–960 µM	7.54 µM	151
MIP/P(β-CD)			1–15 µM	0.4 µM	129
$ZnFe_2O_4/g\text{-}C_3N_4$			5–200 µM	1 µM	152
CoS/RGO			0.1–2542.4 µM	42 nM	153
Nanographene-coated rice-like manganese dioxide nanorods/graphene			0.002–4.44 mM	0.2 µM	154
HRP/Hap5-fCNT			1.0×10^{-5} – 2.34×10^{-4} M	1.91 µM	155
Ag-Cu nanoalloys		Cyclic voltammetry – Electrochemical impedance spectroscopy	2.0 – 9.61 mM	152 µM	156
HRP/Bi-AgNPs		Differential pulse voltammetry	0.02–1.0 µM	0.06 µM	157
MIP/MPBA[7]/AuNPs			0.6–20 µM	0.16 µM	158

MIP/polyaniline nanotubes			0–10 µM and 10–90 µM	0.01 µM	[122]
MIP/Poly toluidine blue			1 µM –40 mM	1 µM	[159]
MIP/poly(Tyr)-CS	SPCE		10 nM–1 mM	2.18 nM	This work

Real sample analysis

Using the DPV technique, the developed HRP-imprinted biosensor was also successfully employed toward the sensitive detection of H_2O_2 in unprocessed human plasma samples (Fig. 4.23A). Different concentrations of H_2O_2, ranging from 5 nM to 1 mM, were spiked into human plasma samples to examine the practical use of the MIP-based biosensor. These concentrations were then measured using the DPV method. As shown in Fig. 4.23B, the HRP-imprinted biosensor is capable of measuring H_2O_2 in the concentration range of 5 nM to 1 mM, and the calibration curve for the linear regression equation is $-I(\mu A) = 0.8822\ C_{[H2O2]}(mM) + 2.0266$ ($R^2 = 0.994$). The LOD (S/N=3.3) for the detection of H_2O_2 in unprocessed human plasma samples using HRP-imprinted biosensor was calculated to be 1.50 nM, and the LOQ (S/N=10) was 4.56 nM.

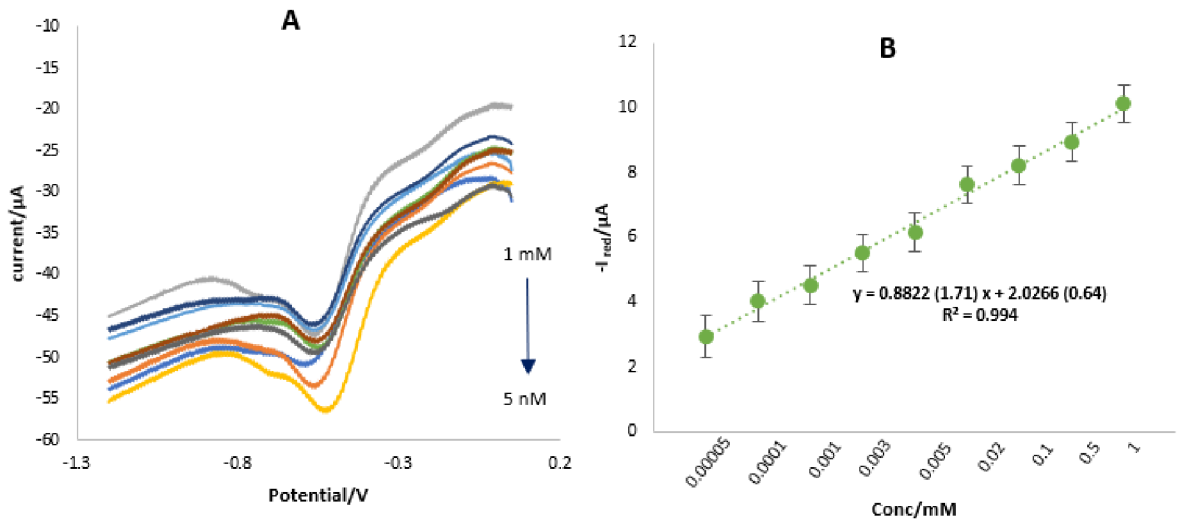

Fig. 4.23 | A) DPV response of HRP/poly(Tyr)-CS/SPCE towards sensitive determination of H_2O_2 in untreated human plasma samples with different concentration. B) Calibration curve (n = 3, SD = 0.6).

Stability, repeatability, and selectivity of the developed molecularly imprinted biosensor

The imprinted biosensor showed good stability and repeatability. CVs of poly(Tyr)-CS/SPCE were measured in 0.01 M $Fe(CN)_6^{3-}$ /$Fe(CN)_6^{4-}$ containing 0.1 M KCl at different cycles (1,5,10, and 50) to evaluate the stability of the polymer layer on the SPCE surface. Good stability was found after 10 cycles, as shown in Fig. 4.24A-B, indicating that the suggested polymer film is stable. The findings show that the peak current of poly(Tyr)-CS/SPCE remained almost steady after 10 cycles. However, after 50 cycles, there was a drastic change in the oxidation and reduction potentials of the proposed polymer film. Redox peak currents and potentials were discovered to have altered, confirming the limited stability of poly(Tyr)-CS after 50 cycles. The findings show that the electropolymerization of poly(Tyr)-CS is highly stable throughout a range of 10 sweep rates. Hence, after 10 cycles, this polymer is not an acceptable matrix for subsequent applications. poly(Tyr)-CS can therefore be employed in the disposal. The repeatability of MIP/poly(Tyr)-CS/SPCE was examined using 0.1 mg/ml HRP by the DPV method in six cycles of a binding-elution-rebinding test of the protein-modified electrode, and the calculated RSD (relative standard deviation) was 3.96% (Fig. 4.24C-D).

The selectivity of the HRP/poly(Tyr)-CS/SPCE for H_2O_2 was investigated in the presence of potential interfering electroactive agents such as ascorbic acid (AA), dopamine (DA), uric acid (UA), and glucose (GL) with DPV technique. Fig. 4.24E-F shows the voltammetric response signals of 1mM H_2O_2 in PBS solution (pH 8.0) by the addition of 0.1 mM of each interfering specie. The HRP-imprinted biosensor reduced the interference effect to 1 mM H_2O_2 by GL 16.41 %, UA 17.21 %, and AA 23.76 %, which exhibited negligible effects on the H_2O_2 response. This implies that the interfering agents have almost no effect on the analyte response. Therefore, it displayed the high selectivity of the designed HRP-imprinted biosensor toward the

determination of H_2O_2. However, voltammetric responses can be detected by dopamine (1 mM H_2O_2), indicating dopamine can engage in the redox process of H_2O_2 (51.11 %), thus interfering with H_2O_2 measurement.

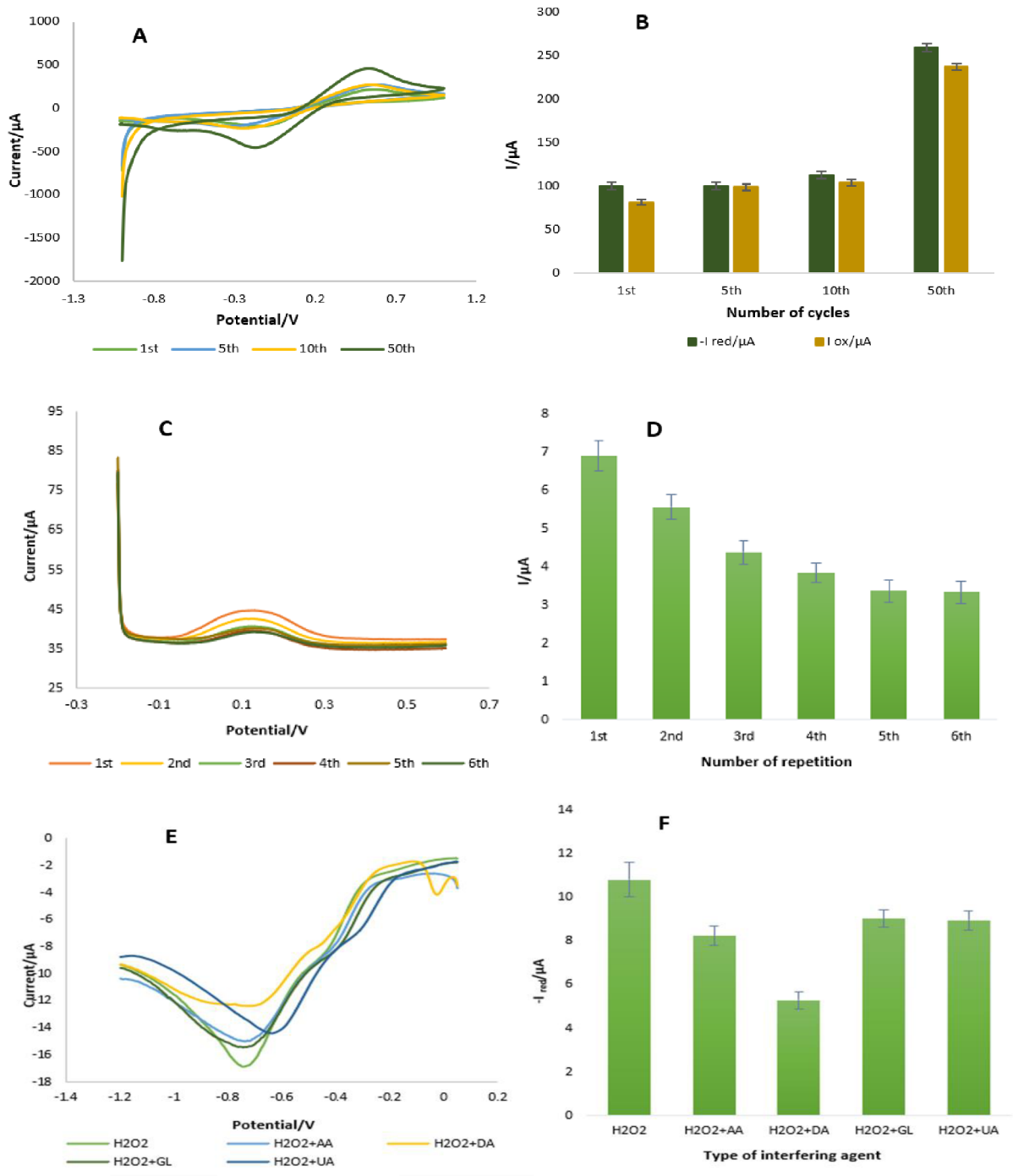

Fig. 4.24 | A) Stability of poly(Tyr)-CS/SPCE were recorded in 0.01 M $Fe(CN)_6^{3-}$ /$Fe(CN)_6^{4-}$ + 0.1M KCl at a sweep rate of 100 mV/s with different cycle numbers (1,5,10, and 50). B) variation of current versus cycle number (n = 3,

SD = 3.86). C) Repeatability of MIP/poly(Tyr)-CS/SPCE was recorded in 0.1 mg/ml HRP solution for six cycles. D) Current versus cycle number variation (n = 3, SD = 0.31). E) Effects of interfering species on the voltammetric determination of 1 mM H_2O_2 with HRP/poly(Tyr)-CS/SPCE in PBS solution pH=8 in the presence of ascorbic acid, glucose, dopamine, and uric acid as interfering agents. F) Variation of I_p H_2O_2 versus the type of interfering agents (n = 3, SD = 0.5).

Conclusion

A unique, simple, and sensitive HRP-imprinted biosensor employing poly(Tyr) and CS matrices as MIPs was created by combination with a self-assembly surface molecular imprinting strategy on the disposable screen-printed carbon electrode. Using poly(Tyr)-CS film as an affordable, simple, and environmentally friendly matrix for constructing a sensitive HRP surface molecular imprinted electrochemical biosensor allows for easier electron transfer and increases the HRP's bioelectrocatalytic activity on H_2O_2. In addition, the poly(Tyr)-CS film produced a high surface area and coverage for the successive re-binding of HRP targets. The molecularly imprinted biosensor not only demonstrated good sensitivity for the template protein HRP determination in a linear range from 1.0×10^{-8} to 1.0×10^{-1} mg/mL with LOD of 9.39×10^{-8} mg/ml (2.34 pM) and LOQ of 2.84×10^{-7} mg/ml (7.11 pM) but also exhibited excellent bioelectrocatalytic behavior toward H_2O_2 reduction in pH=8.0 within the linear range of 10 nM to 1 mM and the limit of LOD and LOQ of 2.18 nM and 6.60 nM, respectively. Moreover, the prepared imprinted biosensor was employed for the detection of H_2O_2 in unprocessed human plasma. The suggested approach demonstrates a suitable framework for the biological analysis of H_2O_2 in actual samples and quantitative determination of HRP.

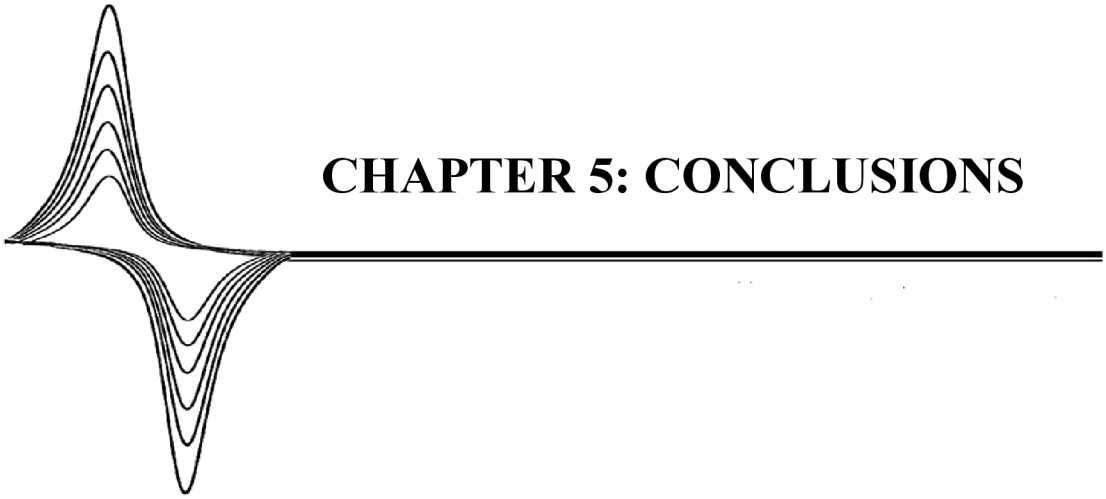

CHAPTER 5: CONCLUSIONS

This thesis briefly describes screen-printed electrodes and devices with potential applications in bioelectronics. I focused on the development of portable and disposable (bio)sensors for detecting distinct biologically active compounds important for biomedical applications.

In the first part, SWCNT-modified SPCE as disposable electrochemical sensors was suggested for fast quantification of dasatinib in pharmaceutical formulations, demonstrating an excellent boosting effect on the oxidation response of dasatinib. At optimized pH 5.0 Britton-Robinson buffer, SWCNT-modified SPCEs showed 94% recovery with optimum electrooxidation activity. The oxidation currents exhibited linear relation with dasatinib concentration in the 0.1–100 µM. Based on the results, a limit of detection of 0.06 µM was obtained in the standard solution. The SWCNT-modified SPCEs have been applied to analyze dasatinib in pharmaceutical tablet samples.

In the second part, a sensitive and specific approach was developed for the determination of *Haemophilus influenza* using DNA based bio-assay through bioconjugation of citrate capped silver nanoparticle with pDNA toward target sequences detection. The synthesized probe (SH-5′-AAT TTT CCA ACT TTT TCA CCT GCA T-3') of *Haemophilus influenza* was detected with great sensitivity and selectivity after hybridization with cDNA (5′-ATG CAG GTG AAA AAG TTG GAA AAT T-3'). The ultra-sensitive fabricated optical DNA-based bio-assay was showed the low limit of quantification of 1 zM for DNA sample using 15 µL of probe and 200 µL of Cit/AgNPs. It has potential for bacterial determination both in clinical and environmental specimens. To evaluate the selectivity of developed DNA based biosensor, three mismatch sequences were applied. Finally, the designed genosensor is a significant diagnostic strategy for detection of *Haemophilus influenza* with great selectivity.

The last part of the thesis focused on the development a highly selective and sensitive electrochemical horseradish peroxidase-imprinted biosensor based on the combination of poly tyrosine-chitosan film electropolymerization on the surface of screen-printed electrodes and a self-assembly surface molecular imprinting approach. The HRP-imprinted biosensor showed a highly bioelectrocatalytical behavior toward hydrogen peroxide reduction in 0.1 M PBS with pH 8.0 and could be used in the voltammetric determination of H_2O_2 in the linear range of 10 nM to 1 mM with a limit of detection and limit of quantification of 2.18 nM and 6.60 nM, respectively. The molecularly imprinted biosensor also exhibited great sensitivity for HRP and was successfully applied for recognition with various concentration ranges of HRP from 1.0×10^{-8} to 1.0×10^{-1} mg/mL with LOD and LOQ of 9.39×10^{-8} mg/ml (2.34 pM) and 2.84×10^{-7} mg/ml (7.11 pM) by differential pulse voltammetry, respectively. The designed electrochemical imprinted biosensor was utilized to detect H_2O_2 in an unprocessed human plasma sample.

To conclude, I concentrated on creating functionalization techniques to design sensitive and selective (bio)sensors for specific analytes and demonstrated their detection in complex media. The screen-printed electrodes were employed to develop cost-effective disposable and portable devices for home care or in-field applications accompanied by various modification techniques for more selective target detection. I investigated numerous factors to enhance the functionalization approach and sensing range, resulting in highly effective (bio)sensors for all applications.

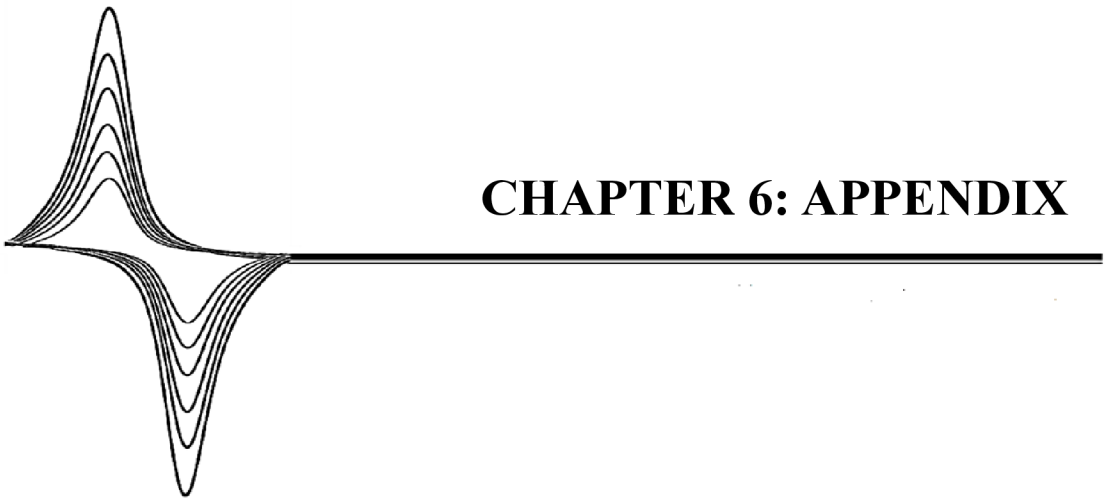

CHAPTER 6: APPENDIX

List Of Abbreviations

SPE	Screen-printed electrode
SPCE	Screen-printed carbon electrode
WE	Working electrode
CE	Counter/auxiliary electrode
RE	Reference electrode
CV	Cyclic voltammetry
DPV	Differential pulse voltammetry
SWV	Square wave voltammetry
LSV	Linear sweep voltammetry
EIS	Electrochemical impedance spectroscopy
MIP	Molecularly Imprinted Polymer
DAS	Dasatinib
SWCNT	Single-walled carbon nanotube
CNT	Carbon nanotube
GPH	Graphene
GPHOX	Graphene oxide
DFNP	Dendritic fibrous nanoparticle
Cit/AgNPs	Citrate capped silver nanoparticles
HRP	Horseradish peroxidase
H_2O_2	Hydrogen peroxide
LOQ	Limit of quantitation
LOD	Limit of detection
LLOQ	Low limit of quantification

Soodabeh Hassanpour, MSc.

Czech Republic | soodabeh.hassanpour01@upol.cz, soodabehhassanpour@yahoo.com | +420 605-881-208 | Linkedin | Google Scholar

RESEARCH INTERESTS

-Development of electrochemical biosensors for POC applications
-Developing micro/nanosensors
-Biosensors integrated into microfluidics
-Screen printing
-Designing flexible, printable, and wearable biosensors
-Application of nanomaterials for designing biosensors
-BioMEMS

EDUCATION

11/2019-Present **Ph.D. Candidate in Analytical Chemistry**
Palacký University Olomouc, Czech Republic
Dissertation: Novel electrochemical (bio)sensors for analysis of biologically active compounds

10/2015–10/2017 **MSc. Cellular and Molecular Biology-Biochemistry,** Top-Researcher honors
University of Tabriz, Iran
Thesis: Preparation of electrochemical sensors based on functionalized mesoporous silica nanoparticles with amine/iron oxide nanoparticles and their application for the detection of some small biomolecules

10/2010–01/2014 **BSc. Cellular and Molecular Biology-Biotechnology**
University of Tabriz, Iran

PROFESSIONAL EXPERIENCES

2019 - Present **Ph.D. Student**
Palacký University Olomouc, Czech Republic
• Developed innovative MIP (molecularly imprinted polymer) based biosensors for high-precision diagnosis.
• Designed protocols for enantioselective electrochemical biosensors to detect D-amino acids.
• Proficient in utilizing Capillary Electrophoresis for chiral separation of antidepressant and antihistamine drugs.
• Skilled in designing 3D models of microfluidics using Autodesk Fusion 360 software and fabricating them using 3D printers.
• Synthesized nanoparticles and prepared nanocomposites and polymeric films for electrode modification.
• Entrapped enzymes into dendritic silica nanoparticles to create enzymatic biosensors.
• Designed protocols for enzymatic and nonenzymatic electrochemical biosensors to detect cancer biomarkers, viruses, drugs, and pesticides.
• Crafted compelling project proposals and secured funding from reputable agencies.
• Conducted statistical analysis on data sets to derive meaningful insights for the research projects.
• Led a group of researchers in a project that resulted in one published review paper and two under-review original research papers.

2016 - 2019 **Research Assistant**
Pharmaceutical Analysis Research Center, Tabriz University of Medical Sciences, Iran
• Designed and developed a range of biosensors, including electrochemical, paper-based, and optical sensors using AUTOLAB and PalmSens 4c systems.
• Entrapped enzymes into mesoporous silica nanoparticles to create enzymatic biosensors.
• Developed immunosensors for cancer biomarker detection and genosensors for virus detection.
• Designed and fabricated various electrochemical sensors for detecting drugs, amino acids, and pesticides.
• Synthesized and utilized various conductive inks to create flexible and wearable sensors.
• Synthesized nanoparticles and prepared nanocomposites for electrode modification.
• Conducted statistical analysis on data sets using Excel.
• Managed lab inventory and procurement of equipment and services through negotiations.
• Mentored and trained undergraduate and postgraduate students in biosensor development and analysis techniques.

TEACHING EXPERIENCE

2021–2022	“Imunoanalytics” course to MSc. Students, Palacký University Olomouc, Czech Republic
2020–2021	“Immunoanalysis of low-molecular-weight compounds” course to MSc. Students, Palacký University Olomouc, Czech Republic

PROJECTS, GRANTS AND AWARDS

	As Principal Investigator (PI)	
2022	The Ministry of Education, Youth and Sports Czech Republic, Doctoral Student Grant Competition, “Chirality-based electrochemical sensors: new approaches for enantiomer discrimination project”, DSGC-2021-0176	56,398 EUR
	As Main Applicant	
2019-2023	Fischer Scholarship, Palacký University Olomouc	12,611 EUR /year
2022	Erasmus+ Scholarship for the research stay at the University of Copenhagen, Denmark	2,200 EUR
	As Member	
2023	Palacký University Olomouc, project IGA_PrF	
2022	Palacký University Olomouc, project IGA_PrF	
2020-2021	Czech Science Foundation, Improving sensitivity in chiral separations by capillary electrophoresis connected with ESI-MS or ICP-MS project	
2021	Palacký University Olomouc, project IGA_PrF	
2020	Palacký University Olomouc, project IGA_PrF	
2018-2019	Tabriz University of Medical Sciences, Conductive nano/bio-inks for the design of different biosensors project	

CONFERENCES

09/2022	12th International Symposium of Drug Analysis, 32nd International Symposium on Pharmaceutical and Biomedical Analysis, DA-PBA 2022, Mons, Belgium (Poster) "A new platform for enzymatic enantioselective biosensing of amino acids in human plasma using the D-amino acid oxidase enzyme encapsulated in dendritic silica"
06/2022	Advances in Chromatography and Electrophoresis & Chiranal 2022, Olomouc, Czech Republic (Poster) "Enzymatic chiral biosensing of tyrosine in human plasma using the D-amino acid oxidase enzyme entrapped in dendritic silica nanoparticles"
04/2022	4th Cross-Border Seminar on Electroanalytical Chemistry (CBSEC), Prague, Czech Republic (Oral) "Nanomaterials modified conductive ink-based electrochemical immunosensor for monitoring CA125 protein in plasma samples"
07/2021	e-MSB 2021: 37th International Symposium on Microscale Separations and Bioanalysis (Poster) "Preconcentration of DNA in A 3D-Printed Microfluidic Device"
10/2020	24th International Conference on Miniaturized Systems for Chemistry and Life Sciences (MicroTAS 2020) online workshop

TECHNICAL SKILLS

-Autodesk Fusion 360
-Chem Draw
-Corel
-NOVA 1.10 and NOVA 2.1.2
-ChemStation Agilent
-Microsoft Office

TRAINING

11/2022-04/2023	Electro-membrane extraction (EME) with chiral Capillary Electrophoresis, University of Copenhagen, Denmark Supervisors: Prof. Jorg P. Kutter and Prof. Stig Pedersen-Bjergaard

THESIS PUBLICATIONS

1 **S. Hassanpour**, J. Petr, *A disposable electrochemical sensor based on single-walled carbon nanotubes for the determination of anticancer drug dasatinib*, Monatshefte für Chemie-Chemical Monthly (2023) 1-9. doi: 10.1007/s00706-023-03043-w

2 S. Hassanpour, N. Niaei, J. Petr, *Metal–Organic Frameworks-Based Analytical Devices for Chiral Sensing and Separations: A Revie (2012–2022)*, Chemosensors 11(1) (2023) 29. doi: 10.3390/chemosensors11010029

3 **S. Hassanpour**, A. Saadati, M. Hasanzadeh, *pDNA conjugated with citrate capped silver nanoparticles towards ultrasensitive bio-assay haemophilus influenza in human biofluids: A novel optical biosensor*, Journal of Pharmaceutical and Biomedical Analysis 180 (2020) 113050. doi: 10.1016/j.jpba.2019.113050

4 **S. Hassanpour**, M. Hasanzadeh, J. Petr, *Bioelectrocataytic behavior horseradish peroxidase bound to green polymeric scaffold of poly(tyrosine)-chitosan as molecularly imprinted polymer toward monitoring of H_2O_2 in human biofluids*, RSC advances, submitted with article number RA-ART-03-2023-001905.

SELECTED PUBLICATIONS (GOOGLE SCHOLAR H INDEX 16, 7190 citations)

1 M.B. Behyar, H. Kholafazad-kordasht, **S. Hassanpour**, M. Hasanzadeh, *An innovative electrically conductive biopolymer based on poly (β-cyclodextrin) towards recognition of ascorbic acid in real sample: Utilization of biocompatible advanced materials in biomedical analysis*, Journal of Molecular Recognition 35(5) (2022) e2953.

2 **S. Hassanpour**, M. Hasanzadeh, *Label-free electrochemical-immunoassay of cancer biomarkers: Recent progress and challenges in the efficient diagnosis of cancer employing electroanalysis and based on point of care (POC)*, Microchemical Journal 168 (2021) 106424.

3 **S. Hassanpour**, B. Behnam, B. Baradaran, M. Hashemzaei, F. Oroojalian, A. Mokhtarzadeh, M. de la Guardia, *Carbon based nanomaterials for the detection of narrow therapeutic index pharmaceuticals*, Talanta 221 (2021) 121610.

4 A. Saadati, **S. Hassanpour**, M. Hasanzadeh, *Lab-on-fruit skin and lab-on-leaf towards recognition of trifluralin using Ag-citrate/GQDs nanocomposite stabilized on the flexible substrate: A new platform for the electroanalysis of herbicides using direct writing of nano-inks and pen-on paper technology*, Heliyon 6(12) (2020) e05779.

5 **S. Hassanpour**, H.J. Kim, A. Saadati, P. Tebon, C. Xue, F.W. van den Dolder, J. Thakor, B. Baradaran, J. Mosafer, A. Baghbanzadeh, *Thrombolytic agents: nanocarriers in controlled release*, Small 16(40) (2020) 2001647.

6 H. kholafazad Kordasht, **S. Hassanpour**, B. Baradaran, R. Nosrati, M. Hashemzaei, A. Mokhtarzadeh, M. de la Guardia, *Biosensing of microcystins in water samples; recent advances*, Biosensors and Bioelectronics 165 (2020) 112403.

7 A. Saadati, **S. Hassanpour**, M. Hasanzadeh, N. Shadjou, *Binding of pDNA with cDNA using hybridization strategy towards monitoring o Haemophilus influenza genome in human plasma samples*, International journal of biological macromolecules 150 (2020) 218-227.

8 F. Farshchi, M. Hasanzadeh, M. Feyziazar, A. Saadati, **S. Hassanpour**, *Electropolymerization of chitosan in the presence of CuNPs on the surface of a copper electrode: an advanced nanocomposite for the determination of mefenamic acid and indomethacin in human plasma samples and prevention of drug poisoning*, Analytical Methods 12(9) (2020) 1212-1217.

9 **S. Hassanpour**, A. Saadati, M. Hasanzadeh, *Sensitive monitoring of riboflavin in commercial multivitamins using poly (chitosan)-based nanocomposite*, Journal of Molecular Recognition 33(2) (2020) e2817.

10 F. Bahavarnia, A. Mobed, M. Hasanzadeh, A. Saadati, **S. Hassanpour**, A. Mokhtarzadeh, *Bio-assay of Acintobacter baumannii using DNA conjugated with gold nano-star: A new platform for microorganism analysis*, Enzyme and microbial technology 133 (2020) 109466.

11 A. Saadati, **S. Hassanpour**, F. Bahavarnia, M. Hasanzadeh, *A novel biosensor for the monitoring of ovarian cancer tumor protein CA 125 in untreated human plasma samples using a novel nano-ink: a new platform for efficient diagnosis of cancer using paper based microfluidic technology*, Analytical Methods 12(12) (2020) 1639-1649.

12 A. Mobed, M. Hasanzadeh, A. Saadati, **S. Hassanpour**, *Synthesis and electroanalytical behaviour of AgNPs/graphite conductive nano-ink towards biosensing of bacteria genome in human biofluids*, Analytical Methods 12(9) (2020) 1218-1228.

13 M. Feyziazar, M. Hasanzadeh, F. Farshchi, A. Saadati, **S. Hassanpour**, *An innovative method to electrochemical branching of chitosan in the presence of copper nanocubics on the surface of glassy carbon and its electrical behaviour study: A new platform for pharmaceutical analysis using electrochemical sensors*, Reactive and Functional Polymers 146 (2020) 104402.

14 A. Mobed, M. Hasanzadeh, N. Shadjou, **S. Hassanpour**, A. Saadati, M. Agazadeh, *Immobilization of ssDNA on the surface of silver nanoparticles-graphene quantum dots modified by gold nanoparticles towards biosensing of microorganism*, Microchemical Journal 152 (2020) 104286.

15 A. Mobed, F. Nami, M. Hasanzadeh, **S. Hassanpour**, A. Saadati, A. Mokhtarzadeh, *A novel nucleic acid based bio-assay toward recognition of Haemophilus influenza using bioconjugation and DNA hybridization method*, International journal of biological macromolecules 139 (2019) 1239-1251.

16 F. Bahavarnia, A. Saadati, **S. Hassanpour**, M. Hasanzadeh, N. Shadjou, A. Hassanzadeh, *Paper based immunosensing of ovarian cancer tumor protein CA 125 using novel nano-ink: a new platform for efficient diagnosis of cancer and biomedical analysis using microfluidic paper-based analytical devices (μPAD)*, International journal of biological macromolecules 138 (2019) 744-754.

17 A. Mobed, M. Hasanzadeh, **S. Hassanpour**, A. Saadati, M. Agazadeh, A. Mokhtarzadeh, *An innovative nucleic acid based biosensor toward detection of Legionella pneumophila using DNA immobilization and hybridization: A novel genosensor*, Microchemical Journal 148 (2019) 708-716.

18 A. Saadati, **S. Hassanpour**, M. Hasanzadeh, N. Shadjou, A. Hassanzadeh, *Immunosensing of breast cancer tumor protein CA 15-3 (carbohydrate antigen 15.3) using a novel nano-bioink: A new platform for screening of proteins in human biofluids by pen-on-paper technology*, International journal of biological macromolecules 132 (2019) 748-758.

19 A. Saadati, **S. Hassanpour**, M. de la Guardia, J. Mosafer, M. Hashemzaei, A. Mokhtarzadeh, B. Baradaran, *Recent advances on application of peptide nucleic acids as a bioreceptor in biosensors development*, TrAC Trends in Analytical Chemistry 114 (2019) 56-68.

20 **S. Hassanpour**, M. Hasanzadeh, A. Saadati, N. Shadjou, J. Soleymani, A. Jouyban, *A novel paper based immunoassay of breast cancer specific carbohydrate (CA 15.3) using silver nanoparticles-reduced graphene oxide nano-ink technology: A new platform to construction of microfluidic paper-based analytical devices (μPADs) towards biomedical analysis*, Microchemical Journal 146 (2019) 345-358.

21 M. Jafari, M. Hasanzadeh, E. Solhi, **S. Hassanpour**, N. Shadjou, A. Mokhtarzadeh, A. Jouyban, S. Mahboob, *Ultrasensitive bioassay of epitope of Mucin-16 protein (CA 125) in human plasma samples using a novel immunoassay based on silver conductive nano-ink: A new platform in early stage diagnosis of ovarian cancer and efficient management*, International journal of biological macromolecules 126 (2019) 1255-1265.

22 H. Ashrafi, **S. Hassanpour**, A. Saadati, M. Hasanzadeh, K. Ansarin, S.A. Ozkan, N. Shadjou, A. Jouyban, *Sensitive detection and determination of benzodiazepines using silver nanoparticles-N-GQDs ink modified electrode: A new platform for modern pharmaceutical analysis*, Microchemical Journal 145 (2019) 1050-1057.

23 **S. Hassanpour**, A. Saadati, M. Hasanzadeh, N. Shadjou, A. Mirzaie, A. Jouyban, *Direct writing of biocatalytic materials based on pens filled with high-tech enzymatic inks: "Do-it-Yourself"*, Microchemical Journal 145 (2019) 266-272.

24 F. Nami, A. Saadati, **S. Hassanpour**, M. Hasanzadeh, A. Hassanzadeh, *Bioassay of ovarian cancer tumor protein CA 125 using novel nano-ink on the flexible paper substrate: A new platform for efficient diagnosis of cancer*, International journal of biological macromolecules (2019).

25 A. Mirzaie, A. Saadati, **S. Hassanpour**, M. Hasanzadeh, M. Siahi-Shadbad, A. Jouyban, *Determination of proline in human plasma samples using the encapsulation of proline dehydrogenase enzyme in dendritic silica: a new platform for the enzymatic biosensing of amino acids*, Analytical Methods 11(36) (2019) 4609-4619.

26 A. Mobed, M. Hasanzadeh, M. Aghazadeh, A. Saadati, **S. Hassanpour**, A. Mokhtarzadeh, *The bioconjugation of DNA with gold nanoparticles towards the spectrophotometric genosensing of pathogenic bacteria*, Analytical Methods 11(33) (2019) 4289-4298.

27 A. Mobed, M. Hasanzadeh, **S. Hassanpour**, A. Saadati, M. Agazadeh, A. Mokhtarzadeh, *An innovative nucleic acid based biosensor toward detection of Legionella pneumophila using DNA immobilization and hybridization: A novel genosensor*, Microchemical Journal 148 (2019) 708-716.

28 **S. Hassanpour**, B. Baradaran, M. de la Guardia, A. Baghbanzadeh, J. Mosafer, M. Hejazi, A. Mokhtarzadeh, M. Hasanzadeh, *Diagnosis of hepatitis via nanomaterial-based electrochemical, optical or piezoelectrical biosensors: a review on recent advancements*, Microchimica Acta 185(12) (2018) 1-24.

29 M. Hasanzadeh, A.S. Nahar, **S. Hassanpour**, N. Shadjou, A. Mokhtarzadeh, *Immobilization of proline dehydrogenase on functionalized silica mesoporous nanomaterial towards preparation of a novel thermostable enzyme biosensor*, Journal of Nanoscience and Nanotechnology 18(11) (2018) 7786-7796.

30 M. Hasanzadeh, **S. Hassanpour**, A.S. Nahr, N. Shadjou, A. Mokhtarzadeh, S. Mahboob, *Electropolymerization of proline supported beta cyclodextrin inside amino functionalized magnetic mesoporous silica nanomaterial: one step preparation, characterization and electrochemical application*, Anal. Bioanal. Electrochem 10(1) (2018) 77-97.

31 **S. Hassanpour**, B. Baradaran, M. Hejazi, M. Hasanzadeh, A. Mokhtarzadeh, M. de la Guardia, *Recent trends in rapid detection of influenza infections by bio and nanobiosensor*, TrAC Trends in Analytical Chemistry 98 (2018) 201-215.

32 M. Hasanzadeh, **S. Hassanpour**, A. Saadati, N. Shadjou, A. Mokhtarzadeh, *Magnetic mesoporous silica/chitosan/polyproline: a novel nanocomposite toward sensing of some clinically relevant biomolecules*, Nano Life 7(03n04) (2017) 1750006.

33 A. Mokhtarzadeh, **S. Hassanpour**, Z.F. Vahid, M. Hejazi, M. Hashemi, J. Ranjbari, M. Tabarzad, S. Noorolyai, M. de la Guardia, *Nano-delivery system targeting to cancer stem cell cluster of differentiation biomarkers*, Journal of Controlled Release 266 (2017) 166-186.

34 M. Hasanzadeh, A.S. Nahar, **S. Hassanpour**, N. Shadjou, A. Mokhtarzadeh, J. Mohammadi, *Proline dehydrogenase-entrapped mesoporous magnetic silica nanomaterial for electrochemical biosensing of L-proline in biological fluids*, Enzyme and microbial technology 105 (2017) 64-76.

BOOK PUBLICATIONS

Book	A. Saadati, **S. Hassanpour**, N. Shadjou, M. Hasanzadeh, *Conductive inks: Synthesis and electroanalytical application*, LAP LAMBERT academic publishing (2022).
Book chapter	**S. Hassanpour**, A. Mokhtarzadeh, M. Hasanzadeh, M. Hejazi, B. Baradaran, *Nanomaterials for Use in Apta-Assays*, Handbook of Smart Materials in Analytical Chemistry (2019) 243-271.

REFERENCES

Dr. Jan Petr	jan.petr@upol.cz	Ph.D. supervisor, Palacký University Olomouc, Czech Republic
Dr. Petr Bednář	petr.bednar@upol.cz	Head of the Analytical Chemistry department, Palacký University Olomouc, Czech Republic
Prof. Jorg P. Kutter	jorg.kutter@sund.ku.dk	Erasmus+ traineeship supervisor, University of Copenhagen, Denmark
Prof. Stig Pedersen-Bjergaard	stig.pedersen-bjergaard@farmasi.uio.no	Erasmus+ traineeship supervisor, University of Copenhagen, Denmark
Dr. Mohammad Hasanzadeh	hasanzadehm@tbzmed.ir	MSc. supervisor, Tabriz University of Medical science, Iran

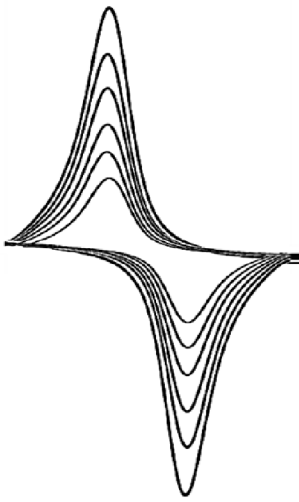

CHAPTER 7: REFERENCES

1. F. Bettazzi, G. Marrazza, M. Minunni, I. Palchetti and S. Scarano, *Comprehensive Analytical Chemistry*, 2017, **77**, 1-33.
2. S. Hassanpour, B. Baradaran, M. de la Guardia, A. Baghbanzadeh, J. Mosafer, M. Hejazi, A. Mokhtarzadeh and M. Hasanzadeh, *Microchimica Acta*, 2018, **185**, 1-24.
3. S. Hassanpour, B. Baradaran, M. Hejazi, M. Hasanzadeh, A. Mokhtarzadeh and M. de la Guardia, *TrAC Trends in Analytical Chemistry*, 2018, **98**, 201-215.
4. J. J. Gooding, *Electroanalysis: An International Journal Devoted to Fundamental and Practical Aspects of Electroanalysis*, 2008, **20**, 573-582.
5. L. M. Santiago, D. Bejarano-Nosas, P. Lozano-Sanchez and I. Katakis, *Analyst*, 2010, **135**, 1276-1281.
6. D. Mata, D. Bejarano, M. Botero, P. Lozano, M. Constantí and I. Katakis, *Electrochimica Acta*, 2010, **55**, 4261-4266.
7. Y. Koç, U. MORALI, S. Erol and H. AVCI, *Turkish Journal of Chemistry*, 2021, **45**, 1895-1915.
8. K. Mahato and J. Wang, *Sensors and Actuators B: Chemical*, 2021, **344**, 130178.
9. L. C. Clark Jr and C. Lyons, *Annals of the New York Academy of sciences*, 1962, **102**, 29-45.
10. B. R. Eggins, *Biosensors: an introduction*, Springer-Verlag, 2013.
11. J. Ding and W. Qin, *TrAC Trends in Analytical Chemistry*, 2020, **124**, 115803.
12. U. Jain, N. Chauhan and K. Saxena, *Multifaceted Bio-Sensing Technology*, 2023, 31-44.
13. A. Saadati, S. Hassanpour, M. de la Guardia, J. Mosafer, M. Hashemzaei, A. Mokhtarzadeh and B. Baradaran, *TrAC Trends in Analytical Chemistry*, 2019, **114**, 56-68.
14. O. A. Farghaly, R. A. Hameed and A.-A. H. Abu-Nawwas, *Int. J. Electrochem. Sci*, 2014, **9**, 3287-3318.
15. D. R. Thévenot, K. Toth, R. A. Durst and G. S. Wilson, *Analytical Letters*, 2001, **34**, 635-659.
16. H. R. S. Lima, J. S. da Silva, E. A. de Oliveira Farias, P. R. S. Teixeira, C. Eiras and L. C. C. Nunes, *Biosensors and Bioelectronics*, 2018, **108**, 27-37.
17. S. P. Kounaves, *Handbook of instrumental techniques for analytical chemistry*, 1997, 709-726.
18. A. J. Bard, L. R. Faulkner and H. S. White, *Electrochemical methods: fundamentals and applications*, John Wiley & Sons, 2022.
19. B. Bennett, J. Chang and A. J. Bard, *Electrochimica Acta*, 2016, **219**, 1-9.
20. J. Bujes-Garrido, D. Izquierdo-Bote, A. Heras, A. Colina and M. Arcos-Martínez, *Analytica chimica acta*, 2018, **1012**, 42-48.
21. J. Wang, *Analytical electrochemistry*, John Wiley & Sons, 2023.
22. J.-M. Savéant, *Elements of molecular and biomolecular electrochemistry: an electrochemical approach to electron transfer chemistry*, John Wiley & Sons, 2006.
23. A. A. Ensafi and P. Nasr-Esfahani, in *Biosensors*, CRC Press, 2023, pp. 27-56.
24. G. Wilson, *Journal*, 1994.
25. G. Barker, *Analytica Chimica Acta*, 1958, **18**, 118-131.
26. A. Chen and B. Shah, *Analytical Methods*, 2013, **5**, 2158-2173.
27. A. J. Bard and L. R. Faulkner, *Electrochemical methods*, 2001, **2**, 580-632.
28. N. Elgrishi, K. J. Rountree, B. D. McCarthy, E. S. Rountree, T. T. Eisenhart and J. L. Dempsey, *Journal of chemical education*, 2018, **95**, 197-206.
29. P. N. Bartlett, *Bioelectrochemistry: fundamentals, experimental techniques and applications*, John Wiley & Sons, 2008.
30. O. D. Renedo, M. Alonso-Lomillo and M. A. Martinez, *Talanta*, 2007, **73**, 202-219.
31. J. P. Metters, R. O. Kadara and C. E. Banks, *Analyst*, 2011, **136**, 1067-1076.
32. H. F. C. da Silva, Universidade da Beira Interior (Portugal), 2014.
33. M. Li, Y.-T. Li, D.-W. Li and Y.-T. Long, *Analytica chimica acta*, 2012, **734**, 31-44.
34. N. Sandhyarani, in *Electrochemical Biosensors*, Elsevier, 2019, pp. 45-75.
35. A. Chen and S. Chatterjee, *Chemical Society Reviews*, 2013, **42**, 5425-5438.
36. A. C. Power, B. Gorey, S. Chandra and J. Chapman, *Nanotechnology Reviews*, 2018, **7**, 19-41.
37. B.-R. Adhikari, M. Govindhan and A. Chen, *Sensors*, 2015, **15**, 22490-22508.

38. S. K. Vashist, D. Zheng, K. Al-Rubeaan, J. H. Luong and F.-S. Sheu, *Biotechnology advances*, 2011, **29**, 169-188.
39. S. Cinti and F. Arduini, *Biosensors and Bioelectronics*, 2017, **89**, 107-122.
40. M. Briones, E. Casero, M. Petit-Domínguez, M. Ruiz, A. Parra-Alfambra, F. Pariente, E. Lorenzo and L. Vázquez, *Biosensors and Bioelectronics*, 2015, **68**, 521-528.
41. O. A. Loaiza, P. J. Lamas-Ardisana, L. Añorga, E. Jubete, V. Ruiz, M. Borghei, G. Cabañero and H. J. Grande, *Bioelectrochemistry*, 2015, **101**, 58-65.
42. K. L. Kelly, E. Coronado, L. L. Zhao and G. C. Schatz, *Journal*, 2003.
43. K. Alaqad and T. A. Saleh, *J. Environ. Anal. Toxicol*, 2016, **6**, 525-2161.
44. H. Wei, C. Chen, B. Han and E. Wang, *Analytical chemistry*, 2008, **80**, 7051-7055.
45. J.-S. Lee, A. K. Lytton-Jean, S. J. Hurst and C. A. Mirkin, *Nano letters*, 2007, **7**, 2112-2115.
46. P. Tan, H. Li, J. Wang and S. C. Gopinath, *Biotechnology and Applied Biochemistry*, 2021, **68**, 1236-1242.
47. S. Hassanpour, N. Niaei and J. Petr, *Chemosensors*, 2023, **11**, 29.
48. D. Liu, K. Lu, C. Poon and W. Lin, *Inorganic chemistry*, 2014, **53**, 1916-1924.
49. A. Koyun, E. Ahlatcolu, Y. Koca and S. Kara, *A Roadmap of Biomedical Engineers and Milestones*, 2012, 117-142.
50. P. S. Panesar and J. F. Kennedy, *Journal*, 2006.
51. J. Wang, *Chemical reviews*, 2008, **108**, 814-825.
52. S. D'souza, *Applied biochemistry and biotechnology*, 2001, **96**, 225-238.
53. B. R. Eggins, *Chemical sensors and biosensors*, John Wiley & Sons, 2008.
54. A. Sassolas, L. J. Blum and B. D. Leca-Bouvier, *Biotechnology advances*, 2012, **30**, 489-511.
55. R. Das, M. K. Sharma, V. K. Rao, B. Bhattacharya, I. Garg, V. Venkatesh and S. Upadhyay, *Journal of biotechnology*, 2014, **188**, 9-16.
56. W. Sun, P. Qin, H. Gao, G. Li and K. Jiao, *Biosensors and Bioelectronics*, 2010, **25**, 1264-1270.
57. K. Wang, Y. Lei, G.-X. Zhong, Y.-J. Zheng, Z.-L. Sun, H.-P. Peng, W. Chen, A.-L. Liu, Y.-Z. Chen and X.-H. Lin, *Biosensors and Bioelectronics*, 2015, **71**, 463-469.
58. T. Arakawa, D. V. Dao and K. Mitsubayashi, *IEEJ Transactions on Electrical and Electronic Engineering*, 2022, **17**, 626-636.
59. R. Monošík, M. Stred'anský and E. Šturdík, *Journal of clinical laboratory analysis*, 2012, **26**, 22-34.
60. R. Malviya, V. Bansal, O. P. Pal and P. K. Sharma, *Journal of global pharma technology*, 2010, **2**, 22-26.
61. G. L. Glish and R. W. Vachet, *Nature reviews drug discovery*, 2003, **2**, 140-150.
62. R. M. Lequin, *Clinical chemistry*, 2005, **51**, 2415-2418.
63. S. Hassanpour, A. Mokhtarzadeh, M. Hasanzadeh, M. Hejazi and B. Baradaran, *Handbook of Smart Materials in Analytical Chemistry*, 2019, 243-271.
64. R. Gui, H. Jin, H. Guo and Z. Wang, *Biosensors and Bioelectronics*, 2018, **100**, 56-70.
65. M. Shaban and M. Hasanzadeh, *RSC advances*, 2020, **10**, 37116-37133.
66. M. Lindauer and A. Hochhaus, in *Small Molecules in Hematology*, Springer, 2018, pp. 29-68.
67. M. Talpaz, N. P. Shah, H. Kantarjian, N. Donato, J. Nicoll, R. Paquette, J. Cortes, S. O'Brien, C. Nicaise and E. Bleickardt, *New England Journal of Medicine*, 2006, **354**, 2531-2541.
68. Z. Nekoukar, M. Moghimi and E. Salehifar, *Blood Res*, 2021, **56**, 229-242.
69. H. X. Chen and J. N. Cleck, *Nature reviews Clinical oncology*, 2009, **6**, 465.
70. A. Moghaddam, H. A. Zamani and H. Karimi-Maleh, *Micromachines (Basel)*, 2021, **12**, 437.
71. P. K. Kalambate, Y. Li, Y. Shen and Y. Huang, *Analytical Methods*, 2019, **11**, 443-453.
72. N. S. Lakka, C. Kuppan, K. S. Srinivas and R. Yarra, *Chromatographia*, 2020, **83**, 947-962.
73. C. S. Jesus and V. C. Diculescu, *Journal of Electroanalytical Chemistry*, 2015, **752**, 47-53.
74. P. Kissinger and W. R. Heineman, *Laboratory Techniques in Electroanalytical Chemistry, revised and expanded*, CRC press, 2018.
75. S. Hassanpour, A. Saadati and M. Hasanzadeh, *J Mol Recognit*, 2020, **33**, e2817.

76. M. Feyziazar, M. Hasanzadeh, F. Farshchi, A. Saadati and S. Hassanpour, *Reactive and Functional Polymers*, 2020, **146**, 104402.
77. A. S. Nahr, S. Hassanpour and M. Hasanzadeh, *Analytical Methods*, 2020.
78. A. J. Bard, *W iley, New York*, 1980.
79. E. Laviron, *Journal of Electroanalytical Chemistry and Interfacial Electrochemistry*, 1979, **101**, 19-28.
80. M. G. García and A. C. García, *Bioelectrochemistry and bioenergetics*, 1995, **38**, 389-395.
81. B.-G. Lee, K.-B. Rhyu and K.-J. Yoon, *Bulletin of the Korean Chemical Society*, 2009, **30**, 2457-2460.
82. C. M. Brett, O. Brett and A. Electrochemistry, 1993.
83. L. R. Faulkner and A. J. Bard, *Electrochemical methods: fundamentals and applications*, John Wiley and Sons, 2002.
84. S. A. Alavi-Tabari, M. A. Khalilzadeh and H. Karimi-Maleh, *Journal of electroanalytical chemistry*, 2018, **811**, 84-88.
85. F. Tahernejad-Javazmi, M. Shabani-Nooshabadi and H. Karimi-Maleh, *New Journal of Chemistry*, 2018, **42**, 16378-16383.
86. D. E. BAYRAKTEPE, K. POLAT and Z. YAZAN, *Journal of the Turkish Chemical Society Section A: Chemistry*, 2018, **5**, 381-392.
87. H. Karimi-Maleh, A. F. Shojaei, K. Tabatabaeian, F. Karimi, S. Shakeri and R. Moradi, *Biosensors and Bioelectronics*, 2016, **86**, 879-884.
88. J. R. Gilsdorf, C. F. Marrs and B. Foxman, *Infection and immunity*, 2004, **72**, 2457-2461.
89. M. P. SLACK, H. J. AZZOPARDI, R. M. HARGREAVES and M. E. RAMSAY, *The Pediatric infectious disease journal*, 1998, **17**, S204-S207.
90. P. D. Butler and E. R. Moxon, *Microbiology*, 1990, **136**, 2333-2342.
91. J. Puri, V. Talwar, M. Juneja, K. Agarwal and H. Gupta, *Indian pediatrics*, 1999, **36**, 1029-1031.
92. W. Kennedy, S. Chang, K. Purdy, T. Le, P. Kilgore, J. Kim, D. Anh, P. Huong, B. Dong and D. Tan, *Epidemiology & Infection*, 2007, **135**, 1217-1226.
93. A. Mobed, B. Baradaran, M. de la Guardia, M. Agazadeh, M. Hasanzadeh, M. A. Rezaee, J. Mosafer, A. Mokhtarzadeh and M. R. Hamblin, *TrAC Trends in Analytical Chemistry*, 2019.
94. M. L. Yola, T. Eren and N. Atar, *Electrochimica Acta*, 2014, **125**, 38-47.
95. M. H. Abdalhai, A. n. M. Fernandes, X. Xia, A. Musa, J. Ji and X. Sun, *Journal of agricultural and food chemistry*, 2015, **63**, 5017-5025.
96. S. Dash and A. Kumar, *J Bacteriol Mycol Open Access*, 2017, **4**, 00095.
97. V. V. Kumar and S. P. Anthony, *Sensors and Actuators B: Chemical*, 2014, **191**, 31-36.
98. Y. He, B. Xu, W. Li and H. Yu, *Journal of agricultural and food chemistry*, 2015, **63**, 2930-2934.
99. Y. Zhou, W. Huang and Y. He, *Sensors and Actuators B: Chemical*, 2018, **270**, 187-191.
100. A. Ravindran, V. Mani, N. Chandrasekaran and A. Mukherjee, *Talanta*, 2011, **85**, 533-540.
101. R. Kanjanawarut and X. Su, *Analytical chemistry*, 2009, **81**, 6122-6129.
102. S. Shrivastava and D. Dash, *Nano-Micro Letters*, 2010, **2**, 164-168.
103. X. Xu, J. Wang, F. Yang, K. Jiao and X. Yang, *Small*, 2009, **5**, 2669-2672.
104. X. Chen, S. G. Parker, G. Zou, W. Su and Q. Zhang, *ACS nano*, 2010, **4**, 6387-6394.
105. I. E. Paul, D. N. Kumar, A. Rajeshwari, S. A. Alex, D. Karthiga, A. M. Raichur, N. Chandrasekaran and A. Mukherjee, in *Nanobiosensors*, Elsevier, 2017, pp. 129-165.
106. J. Homola, *Chemical reviews*, 2008, **108**, 462-493.
107. G. H. Woehrle, J. E. Hutchison, S. Özkar and R. G. FINKE, *Turkish Journal of Chemistry*, 2006, **30**, 1-13.
108. S. Wang and H. Xin, *The Journal of Physical Chemistry B*, 2000, **104**, 5681-5685.
109. H. Fissan, S. Ristig, H. Kaminski, C. Asbach and M. Epple, *Analytical Methods*, 2014, **6**, 7324-7334.
110. W. W. Cleland, *Biochemistry*, 1964, **3**, 480-482.
111. M. C. Alliegro, *Analytical biochemistry*, 2000, **282**, 102-106.

112. K. Yano and I. Karube, *TrAC Trends in Analytical Chemistry*, 1999, **18**, 199-204.
113. Q.-Q. Gai, F. Qu, Z.-J. Liu, R.-J. Dai and Y.-K. Zhang, *Journal of Chromatography A*, 2010, **1217**, 5035-5042.
114. R. Gao, L. Zhang, Y. Hao, X. Cui, D. Liu, M. Zhang and Y. Tang, *Talanta*, 2015, **144**, 1125-1132.
115. E. Verheyen, J. P. Schillemans, M. Van Wijk, M.-A. Demeniex, W. E. Hennink and C. F. Van Nostrum, *Biomaterials*, 2011, **32**, 3008-3020.
116. N. B. Messaoud, A. A. Lahcen, C. Dridi and A. Amine, *Sensors and Actuators B: Chemical*, 2018, **276**, 304-312.
117. S. J. Neill, R. Desikan, A. Clarke, R. D. Hurst and J. T. Hancock, *Journal of experimental botany*, 2002, **53**, 1237-1247.
118. K. M. Mullaugh, R. J. Kieber, J. D. Willey and G. B. Avery Jr, *Environmental science & technology*, 2011, **45**, 9538-9542.
119. C. Chen, X. Hong, T. Xu, A. Chen, L. Lu and Y. Gao, *Journal of The Electrochemical Society*, 2015, **162**, H699.
120. N. C. Veitch, *Phytochemistry*, 2004, **65**, 249-259.
121. C. Kühlmeyer and J. Klein, *Enzyme and microbial technology*, 2003, **32**, 99-106.
122. Q. Wang, R. Xue, H. Guo, Y. Wei and W. Yang, *Journal of Electroanalytical Chemistry*, 2018, **817**, 184-194.
123. M. Hasanzadeh, F. Mokhtari, N. Shadjou, A. Eftekhari, A. Mokhtarzadeh, V. Jouyban-Gharamaleki and S. Mahboob, *Materials Science and Engineering: C*, 2017, **75**, 247-258.
124. M. Hasanzadeh, S. Hassanpour, A. Saadati, N. Shadjou and A. Mokhtarzadeh, *Nano Life*, 2017, **7**, 1750006.
125. M. Hasanzadeh, F. Mokhtari, V. Jouyban-Gharamaleki, A. Mokhtarzadeh and N. Shadjou, *Journal of Molecular Recognition*, 2018, **31**, e2717.
126. A. Yarman, K. J. Jetzschmann, B. Neumann, X. Zhang, U. Wollenberger, A. Cordin, K. Haupt and F. W. Scheller, *Chemosensors*, 2017, **5**, 11.
127. C. Dong, H. Shi, Y. Han, Y. Yang, R. Wang and J. Men, *European Polymer Journal*, 2021, **145**, 110231.
128. D. Nie, D. Jiang, D. Zhang, Y. Liang, Y. Xue, T. Zhou, L. Jin and G. Shi, *Sensors and Actuators B: Chemical*, 2011, **156**, 43-49.
129. S. Sardaremelli, M. Hasanzadeh and H. Razmi, *Journal of Molecular Recognition*, 2021, **34**, e2884.
130. J. Xu, F. Shang, J. H. Luong, K. M. Razeeb and J. D. Glennon, *Biosensors and Bioelectronics*, 2010, **25**, 1313-1318.
131. J. Kärger and D. M. Ruthven, *New Journal of Chemistry*, 2016, **40**, 4027-4048.
132. A. L. Eckermann, D. J. Feld, J. A. Shaw and T. J. Meade, *Coordination chemistry reviews*, 2010, **254**, 1769-1802.
133. H. A. Harbury, *Journal of Biological Chemistry*, 1957, **225**, 1009-1024.
134. T.-C. Chou, K.-Y. Wu, F.-X. Hsu and C.-K. Lee, *journal of food and drug analysis*, 2018, **26**, 662-669.
135. K. Thenmozhi and S. S. Narayanan, *Materials Science and Engineering: C*, 2017, **70**, 223-230.
136. M. Dai, T. Huang, L. Chao, Q. Xie, Y. Tan, C. Chen and W. Meng, *Talanta*, 2016, **149**, 117-123.
137. J. Zbiljić, O. Vajdle, V. Guzsvány, J. Molnar, J. Agbaba, B. Dalmacija and K. Kalcher, *Journal of Hazardous Materials*, 2015, **283**, 292-301.
138. W. Xu, J. Liu, M. Wang, L. Chen, X. Wang and C. Hu, *Analytica chimica acta*, 2016, **913**, 128-136.
139. Y. Xiong, C. Wang, Y. Wu, C. Luo, D. Zhan and S. Wang, *Molecules*, 2022, **27**, 8599.
140. L. Campos-Arias, R. del Olmo, N. Peřinka, N. Casado, J. L. Vilas-Vilela, D. Mecerreyes, F. J. del Campo and S. Lanceros-Méndez, *Electrochimica Acta*, 2023, **439**, 141615.
141. D. Chen, X. Zhuang, J. Zhai, Y. Zheng, H. Lu and L. Chen, *Sensors and Actuators B: Chemical*, 2018, **255**, 1500-1506.

142. S. Komathi, A. I. Gopalan, S.-K. Kim, G. S. Anand and K.-P. Lee, *Electrochimica Acta*, 2013, **92**, 71-78.
143. R. Karthik, N. Karikalan and S.-M. Chen, *Carbohydrate polymers*, 2017, **164**, 102-108.
144. L. Naderi, S. Shahrokhian, M. K. Amini and M. Hafezi Kahnamouei, *ACS Applied Nano Materials*, 2023.
145. S. Nandini, S. Nalini, R. Manjunatha, S. Shanmugam, J. S. Melo and G. S. Suresh, *Journal of Electroanalytical Chemistry*, 2013, **689**, 233-242.
146. E. Erçarıkcı, K. D. Kıranşan and E. Topçu, *IEEE Sensors Journal*, 2023.
147. M.-H. Yeh, Y.-S. Li, G.-L. Chen, L.-Y. Lin, T.-J. Li, H.-M. Chuang, C.-Y. Hsieh, S.-C. Lo, W.-H. Chiang and K.-C. Ho, *Electrochimica Acta*, 2015, **172**, 52-60.
148. C. Chen, X. Hong, T. Xu, A. Chen, L. Lu and Y. Gao, *Synthetic Metals*, 2016, **212**, 123-130.
149. Y. Wang, Z. Wang, Y. Rui and M. Li, *Biosensors and Bioelectronics*, 2015, **64**, 57-62.
150. Z. Yu, H. Li, X. Zhang, N. Liu and X. Zhang, *Talanta*, 2015, **144**, 1-5.
151. M. Sheikholeslam, P. Nanda, A. Sanati, M. Pritzker and P. Chen, *Materials Letters*, 2023, **335**, 133799.
152. M. Ye, C. Yang, Y. Sun, J. Wang, D. Wang, Y. Zhao, Z. Zhu, P. Liu, J. Zhu and C. Li, *ACS Applied Nano Materials*, 2022, **5**, 10922-10932.
153. S. Kubendhiran, B. Thirumalraj, S.-M. Chen and C. Karuppiah, *Journal of colloid and interface science*, 2018, **509**, 153-162.
154. Y. Pan, Z. Hou, H. Yang and Y.-N. Liu, *Materials Science in Semiconductor Processing*, 2015, **40**, 176-182.
155. J. Alvarez-Paguay, L. Fernández, D. Bolaños-Méndez, G. González and P. J. Espinoza-Montero, *Sensing and Bio-Sensing Research*, 2022, **37**, 100514.
156. M. Shafa, I. Ahmad, S. Hussain, M. Asif, Y. Pan, R. Zairov, A. A. Alothman, M. Ouladsmane, Z. Ullah and N. Ullah, *Surfaces and Interfaces*, 2023, **36**, 102616.
157. C. van der Horst, B. Silwana, E. Iwuoha and V. Somerset, *Procedia technology*, 2017, **27**, 179-182.
158. S. Yang, C. Bai, Y. Teng, J. Zhang, J. Peng, Z. Fang and W. Xu, *Canadian Journal of Chemistry*, 2019, **97**, 833-839.
159. S. Sardaremelli, H. Razmi, M. Hasanzadeh and N. Shadjou, *International journal of biological macromolecules*, 2020, **145**, 311-324.

Presentation (small booklet)

PALACKÝ UNIVERSITY IN OLOMOUC

Faculty of Science

Department of Analytical Chemistry

DOCTORAL THESIS

Novel electrochemical sensors for analysis of biological active compounds

Author of the thesis: Soodabeh Hassanpour, MSc.

Field of study: Analytical Chemistry

Supervisor: Assoc. Prof. RNDr. Jan Petr, Ph.D.

Olomouc 2023

Novel electrochemical sensors for analysis of biological active compounds

Abstract

Recently, medical organizations and research disciplines have switched to employing affordable biosensors. Biosensors have become more critical in drug development, drug identification, bio-medicine, food safety, security, protection, and ecological research. It has directly contributed to developing specialized and reliable diagnostic equipment that uses biological sensing components as biosensors. Different analytes, biological receptors, and transducer concepts are used in biosensors. In recent years, innovative sensing platforms have been developed employing screen-printed electrodes (SPEs), which are inexpensive, simple, and quick mass production through thick film technology.

During my Ph.D., I concentrated on designing, constructing, and validating several SPE-based (bio)sensors to identify biologically active compounds important for healthcare applications, demonstrating their significant potential as a suitable sensing platform. I created (bio)sensors for a variety of analytes, from nucleic acid to small molecules, with specific modification strategies to endow the platforms with selectivity toward the species of interest. I developed disposable electrochemical (bio)sensors in two papers based on modifying with single-walled carbon nanotubes (SWCNT) and molecularly imprinted polymers. In the first case, SWCNT-modified SPCE as disposable electrochemical sensors was proposed for quick determination of dasatinib in pharmaceutical formulations, demonstrating an excellent boosting effect on the oxidation response of dasatinib. The sensor was able to monitor different dasatinib concentrations with a limit of detection of 0.06 µM. In the second paper, the SPE surface was modified with poly tyrosine-chitosan and combined with a self-assembly surface molecular imprinting approach to develop horseradish peroxidase (HRP)-imprinted biosensor. Additionally, the molecularly imprinted electrochemical biosensor for determination of HRP was expanded for the detection of H_2O_2 as enzymatic substrates. The HRP-imprinted biosensor was determined H_2O_2 and HRP with detection limits of 2.18 nM and 9.39×10^{-8} mg/ml (2.34 pM), respectively.

The last paper was related to developing a DNA-based bio-assay for determining *Haemophilus influenza* through bioconjugation of citrate-capped silver nanoparticles with pDNA toward target sequences detection. The ultra-sensitive fabricated optical genosensor was detected the synthesized probe (SH-5′-AAT TTT CCA ACT TTT TCA CCT GCA T-3') of *Haemophilus influenza* with great selectivity and sensitivity after hybridization with cDNA with the low limit of quantification of 1 ZM. Finally, the designed genosensor is a significant diagnostic strategy for detecting *Haemophilus influenza* with great selectivity.

Contents

1 INTRODUCTION

Biosensors as analytical instruments connect a biological, biochemical, or chemical recognition element with a transducer in which the recognition part can interact directly or indirectly with an analyte [1]. The use of sensors and biosensors in detecting and monitoring different analytes in clinical analysis, medical diagnosis, environmental monitoring, and food safety has grown in popularity in recent years. They are preferred over traditional methods like immunoassays, spectroscopy, and chromatography techniques because of their high sensitivity, quick analysis time, and lower cost [2, 3]. Additionally, they may be utilized by the general population to examine complicated materials without tedious sample preparation. Such sensors can be found in various powerful devices, including glucose biosensors, cholesterol test kits, and some blood analyzers [4].

The versatility, low cost, small size, and portability for *in-situ* applications provided by screen-printed technology added significant merits to electrochemical biosensors. Nowadays, the creation of miniaturized electrochemical biosensors for detecting various analytes is made possible by disposable screen-printed carbon electrodes (SPCEs) produced using thick-film technology [5, 6]. SPCEs, as an alternative to the standard electrochemical setups using conventional electrodes, are available for electrochemical applications due to their easy and quick activating procedure, disposability, small size, high chemical stability, portability, wide electrochemical window, low background current with an economical substrate, and no need for time-consuming processes. One of the most notable benefits of SPCEs, besides the significant cost reduction, is the ability to analyze a trace amount of sample solution by replacement of large cells and bulky electrodes [7, 8]. In light of these indications, the works presented herein pursued the development of electrochemical SPCEs-based sensors and biosensors to monitor a number of biologically active compounds.

2 THEORETICAL PART

2.1 Sensors and Biosensors

Biosensors are often classified into three main parts: biorecognition elements (bioreceptor), transducers, and a signal processor (Fig. 2.1). The most crucial step in the manufacture of a biosensor is the selection of an appropriate transducer, bioreceptor, and their immobilization on a sensing platform during detection of analyte (such as proteins, DNAs, metabolites, human samples, food, or environmental samples). We can modify the sensing platform throughout the construction process by functionalizing any component according to the conditions of our experiment [9]. The biorecognition component is an important part of a biosensor that selectively reacts with the target analyte, lessens interferences from other species in a sample, and needs careful consideration throughout the selection and immobilization processes. Bioreceptors can be made in a lab or directly taken from live systems (such as an antibody, aptamer, nucleic acid, whole cells, or enzyme). Transducers are an extremely important parts of a biosensor since they are known to transform the produced biological signals into detectable signal that may be either optical or electrochemical. The analyte concentration often affects the signal strength produced during biological contact with it. Then, the signal is then collected, amplified, and displayed by a signal processor. Depending on the transducer or biorecognition element biosensors may be divided into numerous categories [10]. Biosensors are categorized into electrochemical, optical, thermal, and piezoelectric biosensors based on the transducer surface employed to create the sensing platform. Electrochemical biosensors are the most commonly studied among the other four due to their outstanding sensitivity, speed, and cost-effectiveness for identifying analytes [9].

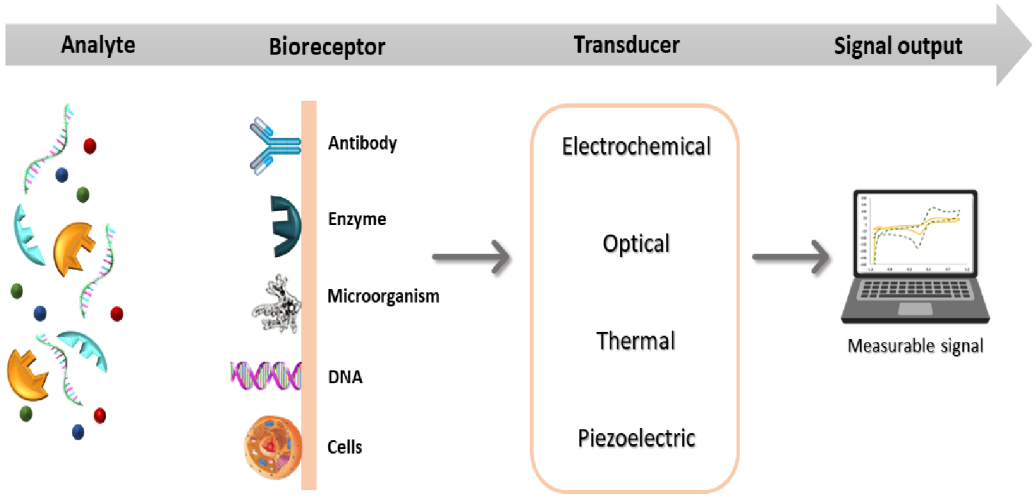

Fig. 2.1 | Biosensor components. Schematic illustration of biosensor operation principles: target analyte detection by the corresponding biorecognition element followed by signal transduction method and output.

2.2 Electrochemical Sensors and Biosensors

In electrochemical sensors and biosensors, the electrode functions as a transducer [11]. The sensing ability of a sensor depends on the measurement of currents and/or voltages that are produced by a recognition event between the interest analytes and the immobilized or chemically modified receptor on the electrode [12]. The main methods used to operate electrochemical transducers include cyclic voltammetry (CV), differential pulse voltammetry (DPV), square wave voltammetry (SWV), linear sweep voltammetry (LSV), electrochemical immittance/impedance spectroscopy (EIS), amperometry, etc [13]. The electrochemical sensors and biosensors are shown in Fig. 2.2, together with the measurable signals they produce using various transduction methods. The following sections describe the transduction techniques used in this research.

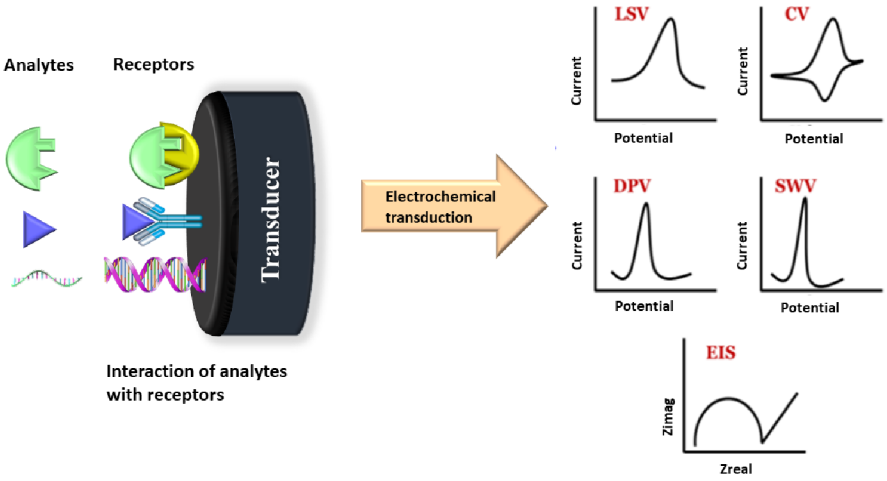

Fig. 2.2 | Electrochemical (bio)sensor and its measurable signals.

2.3 Electrochemical Platform Setup

Electrochemical platforms are typically made up of three electrodes including working electrode (WE), auxiliary or counter electrode (CE), and reference electrode (RE) that are part of an electrochemical cell. An ionic material, usually a salt in solution, is needed for electrochemical experiments since it serves as the supporting electrolyte and ensures conductivity [14, 15]. To conduct electrochemical studies, a variety of setup and equipment options are available. The most popular configuration relies on the usage of a standard three-electrode cell. However, the analytical field's demands forced this configuration to downsize, become more portable, and combine all the components into a single system, leading to screen-printed electrodes-based systems.

2.4 Conventional three-electrode system

A three-electrode cell arrangement typically consists of a beaker with a capacity of 5 to 50 mL that contains the three electrodes including Ag/AgCl reference electrode, platinum counter electrode, and working electrode submerged in supporting electrolyte. There are also more comprehensive systems that include gas management, such as oxygen removal, temperature control, and magnetic stirrers together with the correct cover (Fig. 2.3). Due to the considerable adaptability of these systems, it is simple to change the cell components based on the analytical goal and/or the kind of sample. Glass is frequently used as a cell material because it is inexpensive, transparent, chemically inert, and impermeable; however, quartz and teflon are potential alternative materials [15].

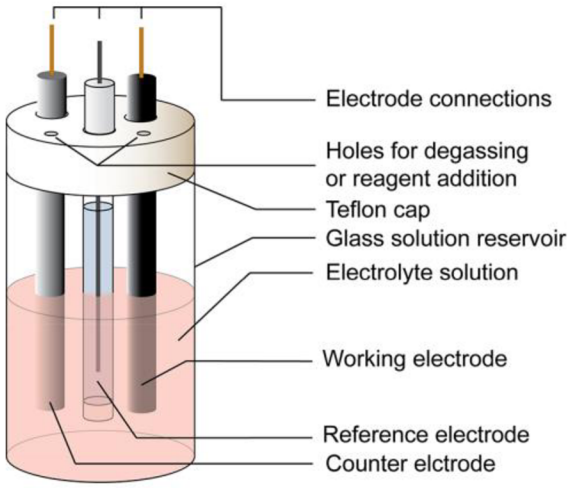

Fig. 2.3 | Schematic illustration of the conventional electrochemical cell. The electrodes are inserted through holes in the cell cover [16].

2.5 Screen-printed electrodes system

Screen-printed electrodes (SPE), a new class of compact, disposable, sensitive, and selective devices, have emerged due to the electroanalytical limitations and practical challenges related to the traditional solid electrodes. Nowadays, electroanalysis uses these transducers extensively to create biosensors and electrochemical sensors, demonstrating their usefulness for a variety of applications. The thick-film method used to create SPEs involves sequentially depositing conductive and nonconductive layers onto an insulating support (printing substrate) with the help of the right screen-printing equipment. This approach enables the large-scale manufacture of low-cost, highly repeatable devices, which is particularly beneficial in fabricating numerous electrodes or electrode array structures [17, 18]. Various inks or

pastes are deposited on the printing substrate using a suitable screen with open-mesh areas. The ability to employ multiple screens and inks results in different SPE types that may be created based on the analytical goal.

The rising reputation of SPEs as effective electroanalytical instruments has resulted in many commercially accessible electrodes of various materials and designs throughout the years. Figure 2.4 depicts a typical commercially available SPEs arrangement employed in our experiment. These SPEs have a three-electrode configuration, with an Ag/AgCl reference electrode, an auxiliary carbon electrode, and a working electrode (4-mm diameter) made of carbon, gold, platinum, silver, or other types of conductive inks. Besides design adaptability, the SPE configuration has remarkable advantages in the electroanalytical sector. SPEs are affordable and may be used either as disposable or reusable devices. Additionally, because they do not require highly experienced staff or time-consuming sample preparation methods, these platforms are simple and suited for *in-situ* and real-time applications outside the laboratory. Moreover, the low power consumption, rapid response, high sensitivity, and ability to function at room temperature broaden the variety of applications for these devices. Furthermore, the appropriate modifications to SPEs give a chance to increase the devices' specificity and sensitivity to the target analytes [17, 19].

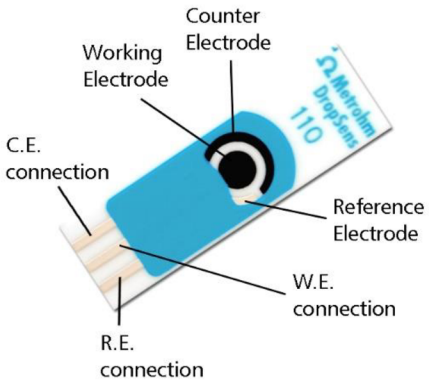

Fig. 2.4 | Commercially available screen-printed carbon electrodes used in this PhD thesis (WE 4-mm diameter).

2.6 Modifications of (bio)sensors

Achieving high selectivity, sensitivity, repeatability, and stability is a significant problem in the creation of biosensors. Surface modifications are crucial for the appropriate immobilization of bioreceptors, noise reduction, and improved sensitivity. Furthermore, surface functionalization reduces unintended non-specific binding of the analyte or other components to the surface [20]. Furthermore, the biomolecules' conformation on the surface significantly impacts the selectivity and sensitivity of a biosensor. In other words, the performance of biosensors is greatly affected by the materials utilized for surface modification and the surface chemistry or functionalization approach employed in bioreceptor immobilization [20]. The

analytical performance of the biosensors can also be marked by metal coatings, nanoparticles, molecularly imprinted polymers, metal-organic frameworks, enzymes, and reactive groups, among other things. Several different electrode modifications and combinations have been developed recently as a result of numerous research with the goal of achieving a reasonable selectivity and sensitivity [21].

3 AIMS

The primary objective of the research presented herein is to develop new sensors and biosensors for determining biologically active compounds with interest in the analytical field. This Ph.D. thesis entails achieving the following objectives:

- Development of method for determination of anticancer drug Dasatinib based on single-walled carbon nanotube-modified SPCEs

- Development of biosensing method for detection of *haemophilus influenza* based on citrate capped silver nanoparticles conjugated with pDNA

- Development of horseradish peroxidase bound to poly(tyrosine)-chitosan polymeric scaffold as a molecularly imprinted polymer for monitoring of hydrogen peroxide

4 EXPERMINTAL PART

4.1 Results and Discussion- A disposable electrochemical sensor based on single-walled carbon nanotubes for the determination of anticancer drug dasatinib

Characterization of SPCEs

SEM images of SPCEs were performed to investigate the surface morphology of the working electrode modified with nanoparticles. Fig. 4.1A shows the surface of a bare screen-printed carbon electrode with a smooth morphology. But modification of the electrode surface with graphene oxide (GPHOX)/graphene nanoparticles (GPH) demonstrates stable and monolayer structures (Fig. 4.1B-C). Notably, carbon nanotube (CNT)/single-walled carbon nanotubes modified SPCEs exhibit a compact film with a tubular distribution structure of nanotubes on the surface of the screen-printed carbon electrodes (Fig. 4.1D-E). The surface of the SWCNT-SPCE was very uneven, which can be helpful in the enhancement of the electrode surface area. Subsequently, these results confirmed that the SPCE was modified with single-walled carbon nanotubes, which altered the electrode surface activity. Also, these results validate that the dispersion of SWCNT on the surface of the screen-printed carbon electrode was performed successfully. Also, the EDS of the SWCNT-modified working electrode is presented in Fig. 4.1F.

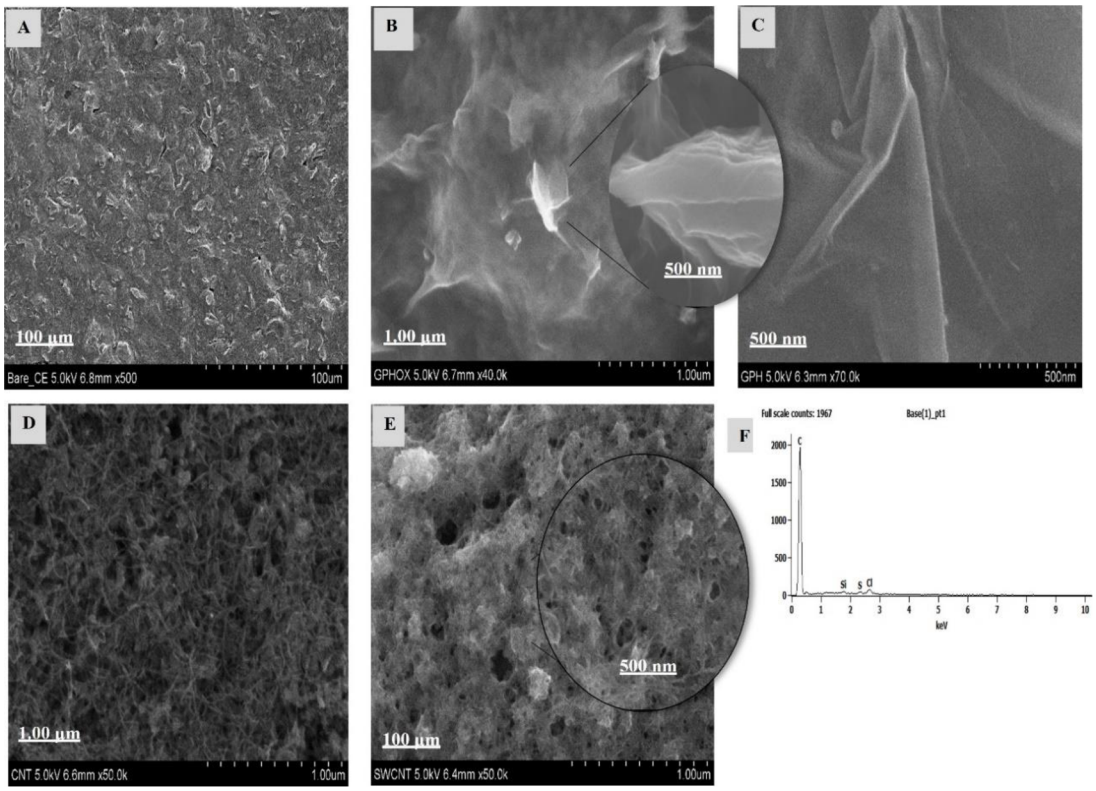

Fig. 4.1 | SEM images of working electrodes: (A) Bare carbon electrode; (B) Graphene oxide modified carbon electrode; (C) Graphene modified carbon electrode; (D) Carbon nanotubes modified carbon electrode; (E) Single-walled carbon nanotubes modified carbon electrode, and (F) EDS spectra of SWCNT.

SWCNT-modified SPCE as the optimal SPCE for dasatinib quantitation

This work aims to select the best SPCE for studying DAS oxidation behavior and fast determination of it in a pharmaceutical sample. The electrochemical behavior of DAS has been analyzed by measuring the cyclic voltammetry at different modified SPCEs at various pHs. In cyclic voltammetry, 100 M DAS showed an oxidation peak at 0.6 V to 0.8 V depending on the pH and type of SPCE when the potential range was between -1.5 and 1.5 V, with a scan rate of 100 mV s^{-1} in a 40 mM Britton–Robinson (BR) buffer. The absence of a reduction peak for DAS on the reverse scan, as shown in Fig. 4.2, indicated that the oxidation process is irreversible. These peaks refer to the anodic oxidation of dasatinib using bare and modified SPCEs.

Various types of SPCEs, including those based on bare carbon, modified SWCNTs, CNTs, GPH, or GPHOX, were evaluated as different working electrodes. The signal intensity obtained using various electrodes in accordance with the applicable approach is shown in Fig. 4.2A. The SWCNT-modified SPCE was shown to give a greater peak intensity with a sharper peak. In contrast, the others exhibited broadened peaks, especially GPH and GPHOX-modified SPCEs. Hence, this kind of electrode proved to be the best. The difference in the electric charges of SWCNT-COOH-SPCE (negative charge due to the loss of the carboxylic group's proton) and the positive charge of DAS at this pH (pH 5.0) could explain the sensitivity of this compound's behavior over the electrode. The anodic peak current rose at the SWCNT-modified SPCE compared to the bare SPCE in Fig. 4.2B, showing the critical function of single-walled carbon nanotubes. This can be related to the increment of the active surface area of the electrode due to modification with SWCNTs which has a large surface area of about 600 m^2g^{-1}, high electrical conductivity, and the accumulation of DAS on the surface of the modified SPCE. It shows the crucial role of SWCNTs in the oxidation process and electrode activity. SWCNTs can accelerate the electron transfer rate with excellent electrocatalytic behavior toward the oxidation of dasatinib.

To comprehend the interaction and oxidation behavior of DAS over the SPCE, it is crucial to understand how the positive charge of the DAS molecule changes with pH. Dasatinib API has two basic ionization constants (pKa), which are 6.8 and 3.1, and one weakly acidic pKa, which is 10.8, in a saturated solution in water with a pH of approximately 6.0 [22]. In this way, this study evaluated the effect of the pH values over a broad range from 3.0 to 10.0 of the BR buffer on the 100 µM dasatinib electrochemical behavior through cyclic voltammetry. It was observed that for DAS compound, peak 1_a broadened as the supporting electrolyte's pH rose, and the voltammogram

at pH 9.0 and pH 10.0 revealed two successive charge transfer processes, peak 1_a at E_p1_a = +0.61 V and peak 2_a at E_p2_a = +0.94 V for pH 9.0 and peak 1_a at E_p1_a = +0.46 V and peak 2_a at E_p2_a = +0.81 V for pH 10.0 (Fig. 4.4A). The buffer pH considerably influenced the anodic peak currents (*Ipa*) at the surface of SWCNT-COOH-SPCE. It was observed that with increasing pH, the peak current of the modified SWCNT electrode at pH 5.0 is higher than that of other types of SPCE and pH (Fig. 4.2B), probably related to the large effective surface area of SWCNTs. The *Ipa* of dasatinib steadily increased with the increment of pH from 3.0 to 5.0. They decreased afterward because of the peak broadening. The anodic peak current of dasatinib reaches a maximum at pH 5.0 (Fig. 4.3C). Also, with a rise in pH, the anodic peak potential of dasatinib slightly shifted toward the negative. According to these findings, protons have participated in their electrode reaction processes. Ep versus pH was plotted with a slope of approximately −0.0602 V. (Fig. 4.3B). Therefore, it was concluded that both peaks signify irreversible processes involving two protons and two electrons.

This finding is consistent with the known electrochemical reactions of dasatinib, as demonstrated by other research. It is well known that two electron and two proton processes contribute to the oxidation of dasatinib. It is suggested that dasatinib's thiazole moiety is involved in its oxidation. This may be referred to the creation of sulfoxide due to the transfer of two electrons and two protons from the sulfur atom of the thiazole ring in the presence of Britton-Robinson buffer (Fig. 4.2C) [23].

Then, the carryover effect was evaluated on bare and SWCNT-modified electrodes. The Britton–Robinson buffer and dasatinib signals were assessed on the same electrode. The RSD of the peak current was 14% for the bare carbon electrode and 0.2% for the SWCNT-modified electrode. Therefore, SWCNT-COOH-SPCEs were used in further studies.

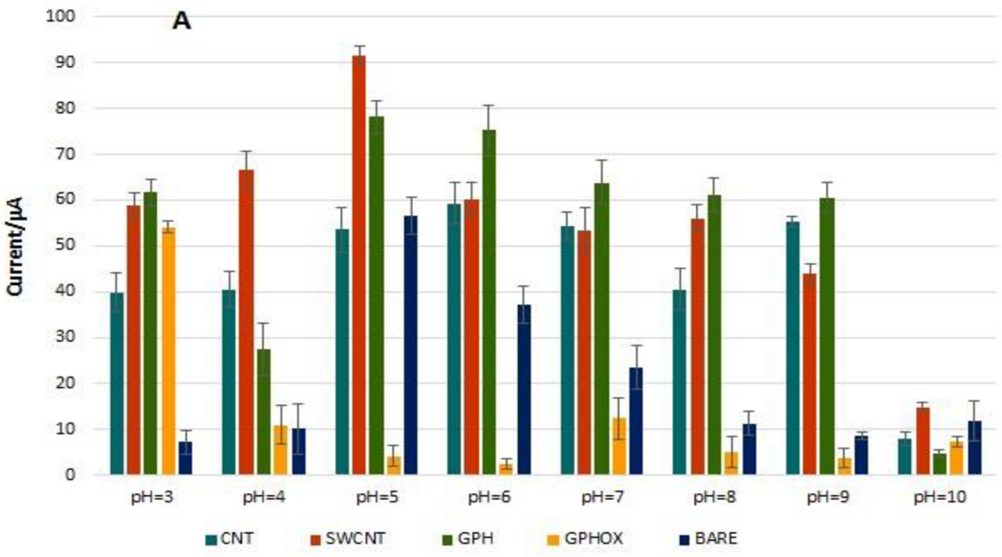

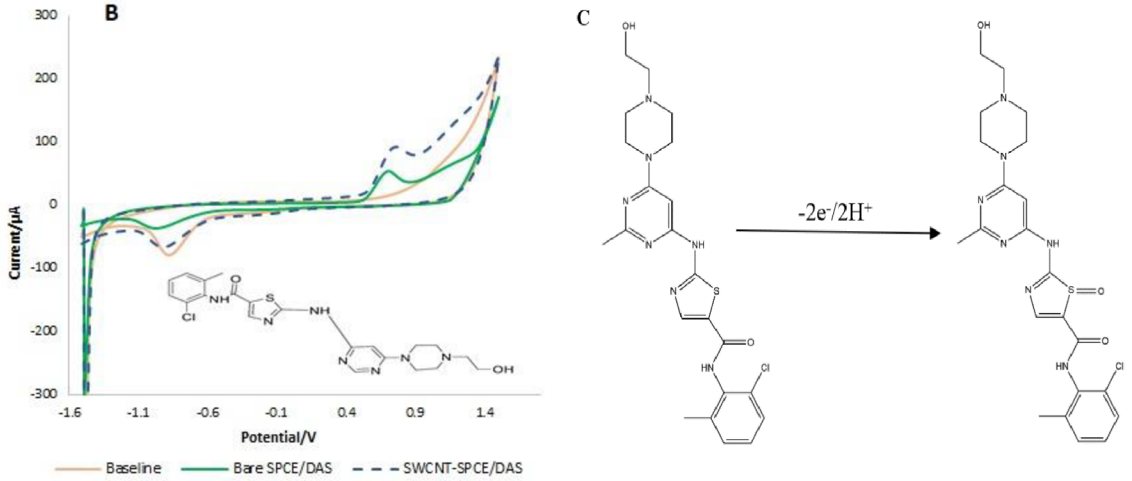

Fig. 4.2 | (A) Histogram of various types of SPCE at different pHs of Britton-Robinson buffer for detection of DAS using CV techniques. (B) The CVs of bare and SWCNT-modified SPCE in the presence (b) of 100 µM DAS (pH 5.0). (C) Electrochemical oxidation mechanism of dasatinib at SWCNT-modified SPCE.

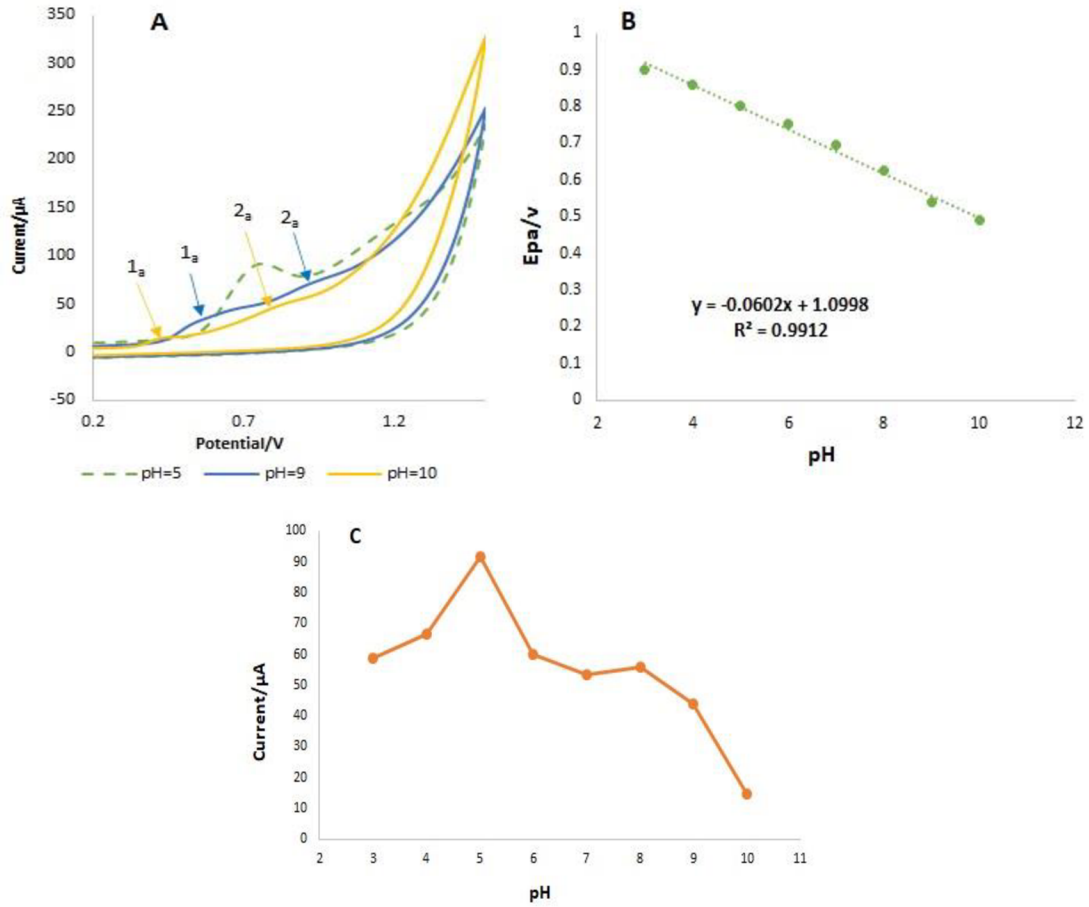

Fig. 4.3 | (A) Cyclic voltammograms in 100 µM DAS at pH 5.0, 9.0, and 10.0. (B) Effect of pH (pH 3.0–10.0) on the peak potential obtained at SWCNT- modified SPCE in Britton-Robinson buffer solution at a scan rate of 100mV.s^{-1}. (C) Variation in the peak potentials of DAS with pH of the buffer at SWCNT- modified SPCE.

Effect of scan rate at SWCNT-modified SPCE

The effect of the scan rate on DAS electrooxidation was evaluated in the range of 20–200 mVs^{-1} on the surface of the SWCNT-modified electrode using the CV technique (Fig. 4.4A). The dependence of Neperian logarithm of peak current on the Neperian logarithm of sweep rate (*ln* I_p *versus ln v*) is linear in which slope is 0.7499 ± 0.02 (Fig. 4.4B). It is indicated that the kinetics of the electrode process was controlled by adsorption, so the anodic oxidation of DAS on the surface of the SWCNT-COOH-SPCE is an adsorption-controlled electrochemical process. It is established that a slope is less than 0.5 is related to diffusion-controlled electrode processes, but if the slope is close to 1.0, the electrode process is adsorption-controlled [2, 15, 24-27]. It is described by the following equation [28]:

$\ln I_p/\mu A = 0.7499 \ln v(V/s) + 5.5469$ ($R^2 = 0.9947$) Eq. 1

According to Fig. 4.4C, the peak currents were found to increase with increasing the scan rate, with a shift in the oxidation peak potential of DAS towards a more positive window (anodic area) which confirms the irreversible nature of electrode processes. Fig. 4.4C shows the dependence of *Epa* on the Neperian logarithm of the scan rate (*Epa versus ln v*). If the electrochemical reaction is irreversible, then the *Epa* is independent of the scan rate. Therefore, it can be deduced that heterogeneous electron transfer in DAS electrooxidation is irreversible because *Epa* increases with increasing scan rate. By increment of scan rate, the anodic peak potential (*Epa*) shifted towards more positive values, and a linear relationship was witnessed in the range of 20–200 $mVs^{-1,}$ as shown in Fig. 4.4C. The equation of this behaviour can be expressed as:

$Epa\ (V) = 0.0449\ Ln\ v(V\ s^{-1}) + 0.8526$ ($R^2 = 0.9954$) Eq. 2

Additionally, for an adsorption-controlled and irreversible electrode process, the following Laviron equation between E_{pa} *versus ln v* can be used to determine the value of the reaction's total electron transfer coefficient [29]:

$$Ep = \left(\frac{RT}{2\alpha nF}\right) \ln v + \text{constant} \quad \text{Eq. 3}$$

Where α is the electron-transfer coefficient, n is the number of electrons, and v is the potential sweep rate. The other symbols have their usual meaning. Taking F = 96485 C mol−1, T = 298 K, and R = 8.314J K−1 mol−1, in this study, employing the dependence of anodic peak potential on the logarithm of the potential sweep rate (the slope = 0.0449), the value of total electron transfer coefficient (αn) was calculated to be 0.28 for DAS electrooxidation.

α can be calculated based on the equation Ep/2−Ep=1.875 (RT/αF) [29, 30], where Ep and Ep/2 are the peak potential and the potential at which the current (Ip) is equal to half its peak value (Ip/2) in cyclic voltammogram, respectively. The value of α equals 0.13. Furthermore, the shape factor in the irreversible system is given by |Ep − Ep/2| = 47.7/αn (mV) [31-33], from which the number of electrons transferred in the electrochemical reaction of DAS (in the presence of Britton-Robinson buffer) were found to be approximately 2 (n=2.1).

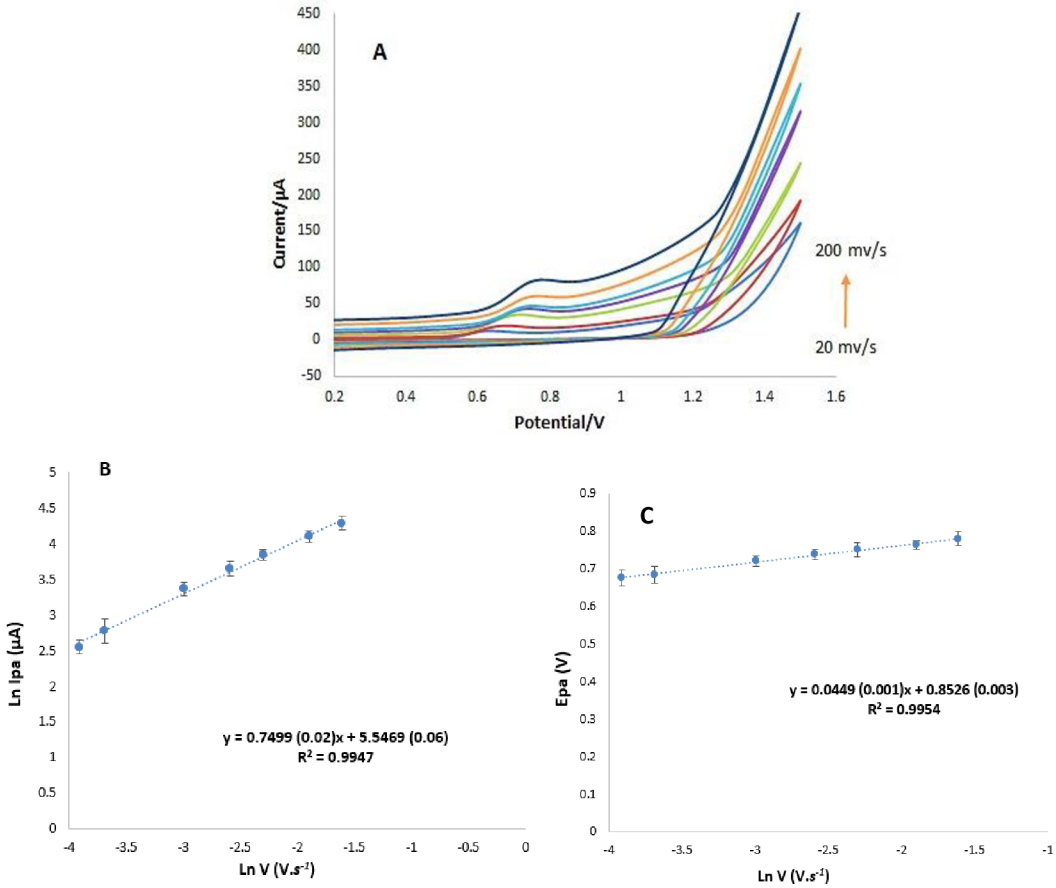

Fig. 4.4 | The effect of scan rate (A) CV of 100 µM dasatinib at SWCNT-modified SPCE; Britton-Robinson buffer pH 5.0; scan rates 20, 25, 50, 75, 100, 150, 200 mV.s^{-1}. (B) The plot of ln Ipa (Napierian logarithm of oxidation peak currents) versus ln V (Napierian logarithm of scan rates). (C) Dependency of oxidation Epa (peak potentials) versus ln V.

Optimized experimental SWCNT-modified SPCE

The calibration curve in Fig. 4.5A-B shows that the oxidation signal is linearly associated with dasatinib in the concentrations range of 0.1 - 100 µM, with a correlation coefficient of 0.9975. The limit of detection (LOD), calculated as signal/noise = 3.3, was estimated to be 0.06 µM. The limit of quantitation (LOQ), calculated as signal/noise = 10, was 0.19 µM. Based on the obtained results, the developed electrochemical sensor had relatively high sensitivity and good linearity. The

linear range for determining DAS tablet solutions (as actual samples) was investigated from 0.1 to 100 µM with a correlation coefficient of 0.999 (Fig. 4.5C). The LOD, calculated as signal/noise = 3.3, and LOQ, calculated as signal/noise = 10, were estimated to be 0.07 µM and 0.22 µM, respectively (Table. 4.1). The amount of dasatinib found was 70 mg/tablet, representing a relative error of 6 %.

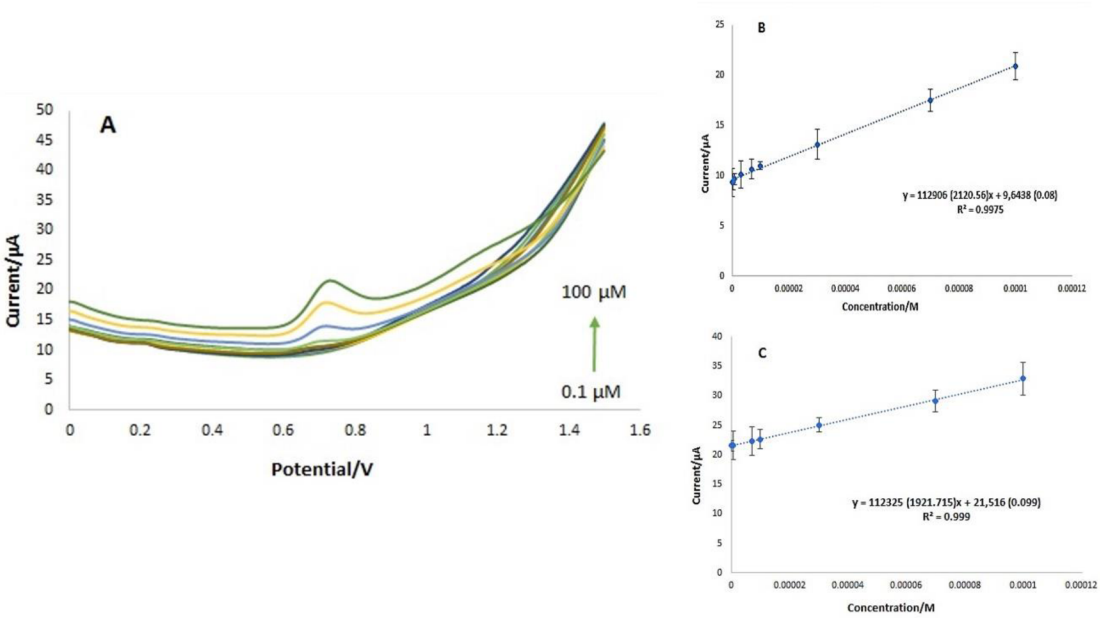

Fig. 4.5 | (A) Concentration effect of DAS detection by SWV method in concentration range (100, 70, 30, 10, 7, 3, 0.7, 0.3, and 0.1 µM) in Britton-Robinson buffer pH 5.0 by SWCNT-modified SPCEs. Step potential= 0.005V, Scan rate= 100mV/s. (B) Calibration curve related to SWV analysis of DAS. (C) Calibration curve related to SWV analysis of real sample dasatinib tablet solutions.

Table. 4.1 | Linear range, limits of detection, limits of quantification and correlation coefficient (R^2) calculated from DAS calibration curves obtained in BR buffer pH 5.0, and tablet sample.

Sample	Linear range (µM)	LOD (µM)	LOQ (µM)	R^2
Buffer	0.1 - 100	0.06	0.19	0.9975
Tablet	0.1 - 100	0.07	0.22	0.999

Therefore, the carbon-based screen-printed electrodes, a new generation of electrodes, were used to determine the anticancer drug dasatinib. According to the obtained results, modification of SPCEs with nanomaterials resulted in a better response for dasatinib than the bare ones. And among the different types of modified SPCEs, single-walled carbon nanotube-modified electrodes gave the highest peak currents for dasatinib detection. SWCNTs improve the electrochemically active area

and enhance the electronic transfer attributes. The tubular structure of SWCNTs on the SPCE surface was very uneven, which led to the enhancement of the surface area of the electrode. The developed platform showed a good electrochemical response towards dasatinib with LODs of 0.06 µM. The established electrochemical sensor is among the superior reported electrochemical sensors (Table. 4.2) in terms of repeatability, low detection limit, and broad linear range. It should be highlighted that the excellent performance of the SWCNT was related to its outstanding properties like high electrical conductivity and large surface area, which pave the way for fast electrons. The results showed that the developed electrochemical sensor also had relatively high sensitivity and good linearity in detecting dasatinib in actual samples, too. Consequently, the single-walled carbon nanotube-modified screen-printed electrodes could be used for the sensitive and quick analysis of electrochemically active pharmaceutical substances.

Table. 4.2 | Comparison of developed electrochemical sensors for the sensitive determination of Dasatinib.

Type of electrode	Modification	pH	RSD	Linear range	Limit of detection	Ref.
Carbon paste	ZnO NP/1-butyl-3-methylimidazolium tetrafluoroborate	5.0	3.78%	1.0–1200 µM	0.5 µM	[34]
Glassy carbon	Au-NPs/rGO/ds-DNA	4.80	3.1%	0.03–5.5 µM	0.009 µM	[35]
Pencil graphite	-	3.0	5.80%	0.0092 – 1.0 µM	0.0028 µM	[36]
Glassy carbon	-	3.4	2.1%	0.2–2.0 µM	0.13 µM	[23]
Carbon paste	Pt/MWCNTs-1-butyl-3-methylimidazoliumhexafluoro phosphate-	8.0	-	5.0– 500 µM	1.0 µM	[37]
Screen-printed carbon	SWCNT	5.0	1.89%	0.1-100 µM	0.06 µM	This work

Reproducibility, Selectivity, and Stability of the sensor

Six sensors were chosen randomly to detect dasatinib under the same experimental conditions. The proposed method's repeatability (relative standard deviation) was assessed by measuring SWVs of 100 µM DAS in Britton–Robinson buffer pH 5.0 (intraday stability) through a SWCNT-modified electrode. The relative standard deviation (RSD%) was 1.89% to determine DAS in one day.

The interference study serves a significant role in analytical chemistry. To this end, the sensor's selectivity for determining DAS was investigated through the influences of some co-existing interferences like different organic and inorganic compounds such as lactose, sucrose, glucose, SO_4^{2-}, and CO_3^{2-} in the real samples. Fig. 4.6 displays the SWV measurements of DAS and its mixtures with various interfering species. As can be seen, these compounds had almost no effect on the peak current of DAS, with a difference of less than 1.8% in peak current (%ΔI) between the peak current of DAS with and without interference. It demonstrated that the suggested sensor is highly selective for dasatinib detection. It should be noted that using glucose as an interfering agent broadened the DAS peak and showed two consecutive charge transfer reactions (Fig. 4.6A).

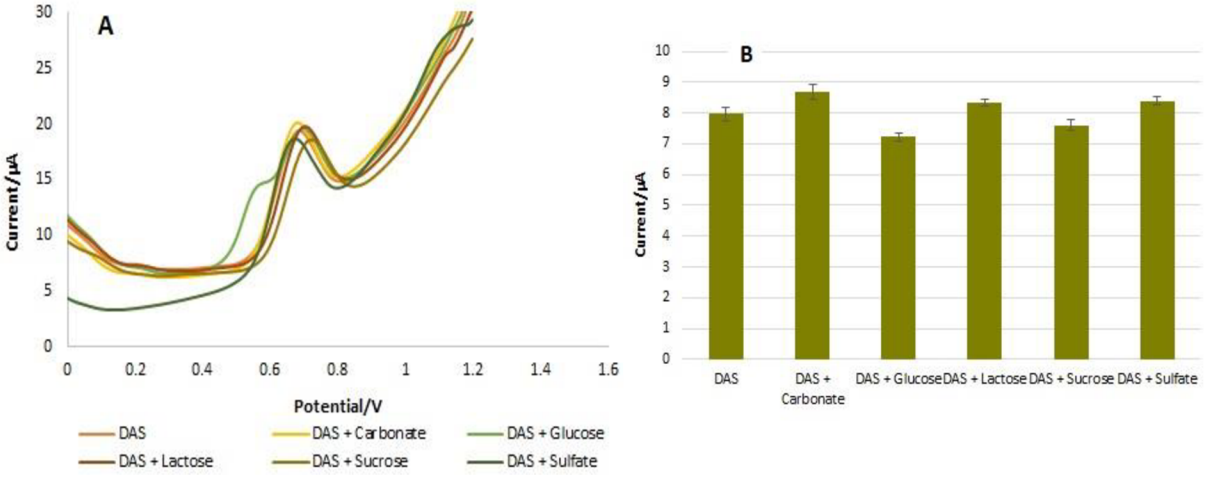

Fig. 4.6 | (A) Interference effect of lactose, sucrose, glucose, SO_4^{2-}, and CO_3^{2-} on determination of DAS by SWV method on SWCNT-COOH-SPCEs in supporting electrolyte Britton-Robinson buffer pH 5.0. (B) Histogram of interference effect.

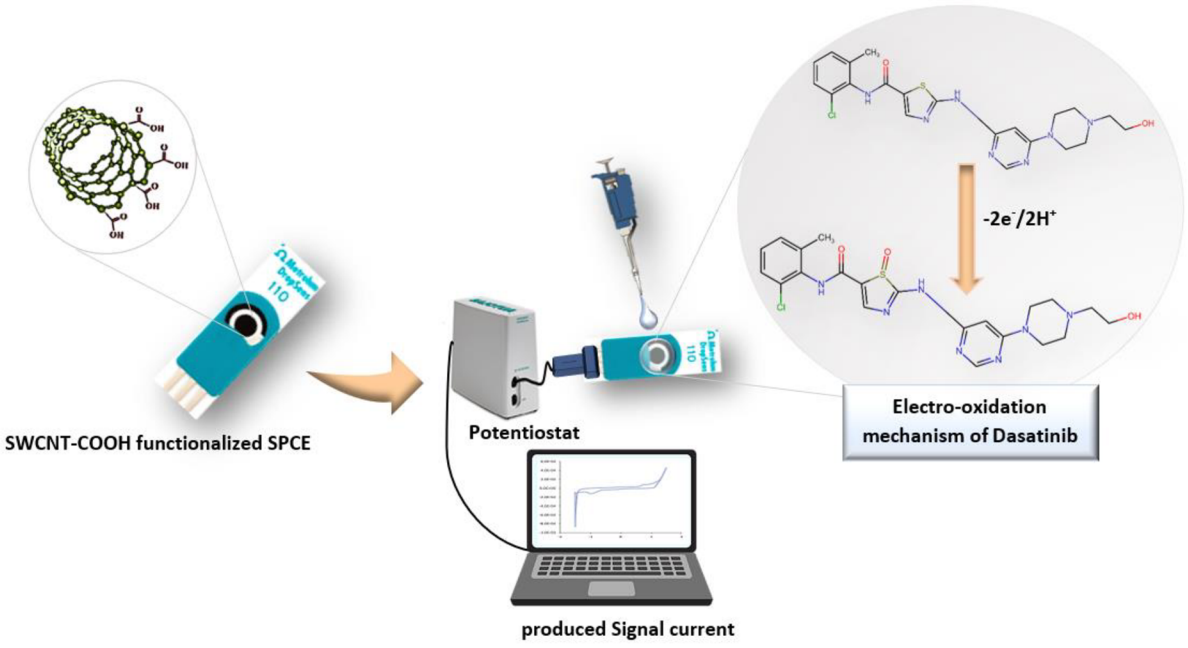

Scheme. 4.1 | *Electrochemical sensing of Dasatinib with SWCNT-modified screen-printed carbon electrode.*

4.2 Results and Discussion- pDNA conjugated with citrate capped silver nanoparticles towards ultrasensitive bio-assay of haemophilus influenza in human biofluids: A novel optical biosensor

TEM, FE-SEM and DLS analysis of citrate capped AgNPs

The mechanism of Cit/AgNPs formation and supportive proof of morphologies and characteristics of silver nanoparticles was provided by TEM (transmission electron microscopy). TEM is continuously the first method employed for determination of the size and nanoparticle size distribution [38]. TEM images recorded using the holey carbon grid which are shown in Fig. 4.7. The TEM micrographs of synthesized citrate capped silver nanoparticles clearly show the AgNPs are discrete, monodisperse, and spherical in environment with average particle size under 10 nm.

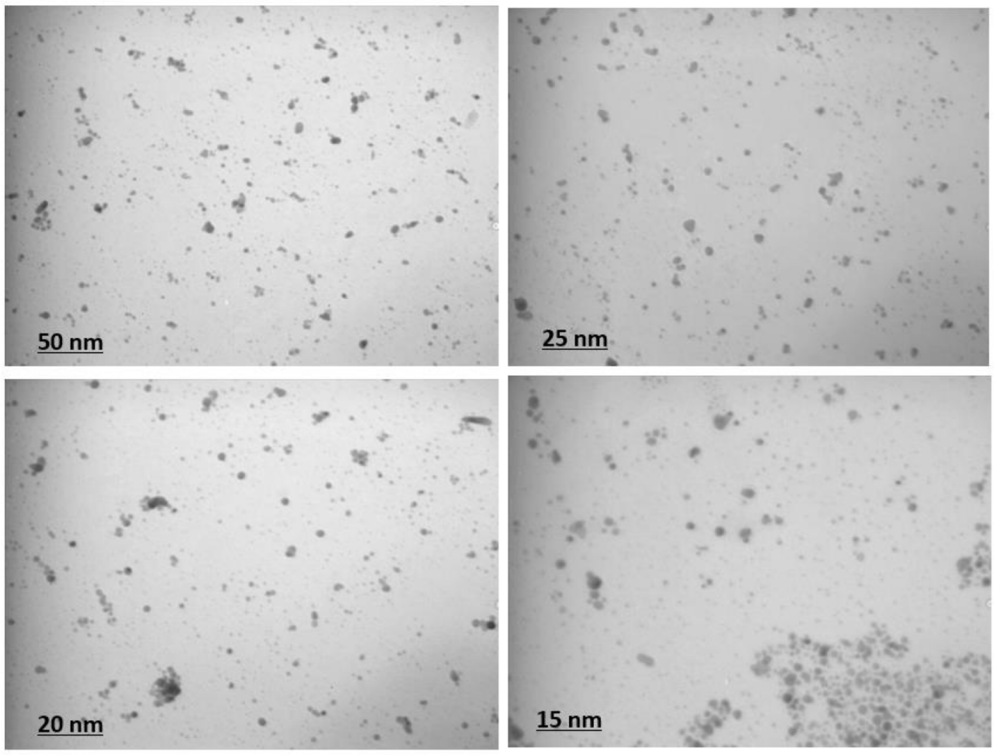

Fig. 4.7 | TEM images of Cit/AgNPs in various magnifications.

Surface morphology of Cit/AgNPs was characterized by FE-SEM (field emission scanning electron microscope) and chemical compositions of nanoparticles were analyzed by EDS (energy dispersive spectroscopy). As shown in Fig. 4.8A, AgNPs have uniform spherical structure. According to the standard theory of colloids, the stability of colloids depends on the equilibrium between the van der Waals interaction and the coulombic repulsion of the charged particles the charged particles [39]. According to Fig. 4.8B, sharp and large peaks from citrate and sodium appear due to the existence of sodium citrate and sodium borohydride in the structure of Cit/AgNPs.

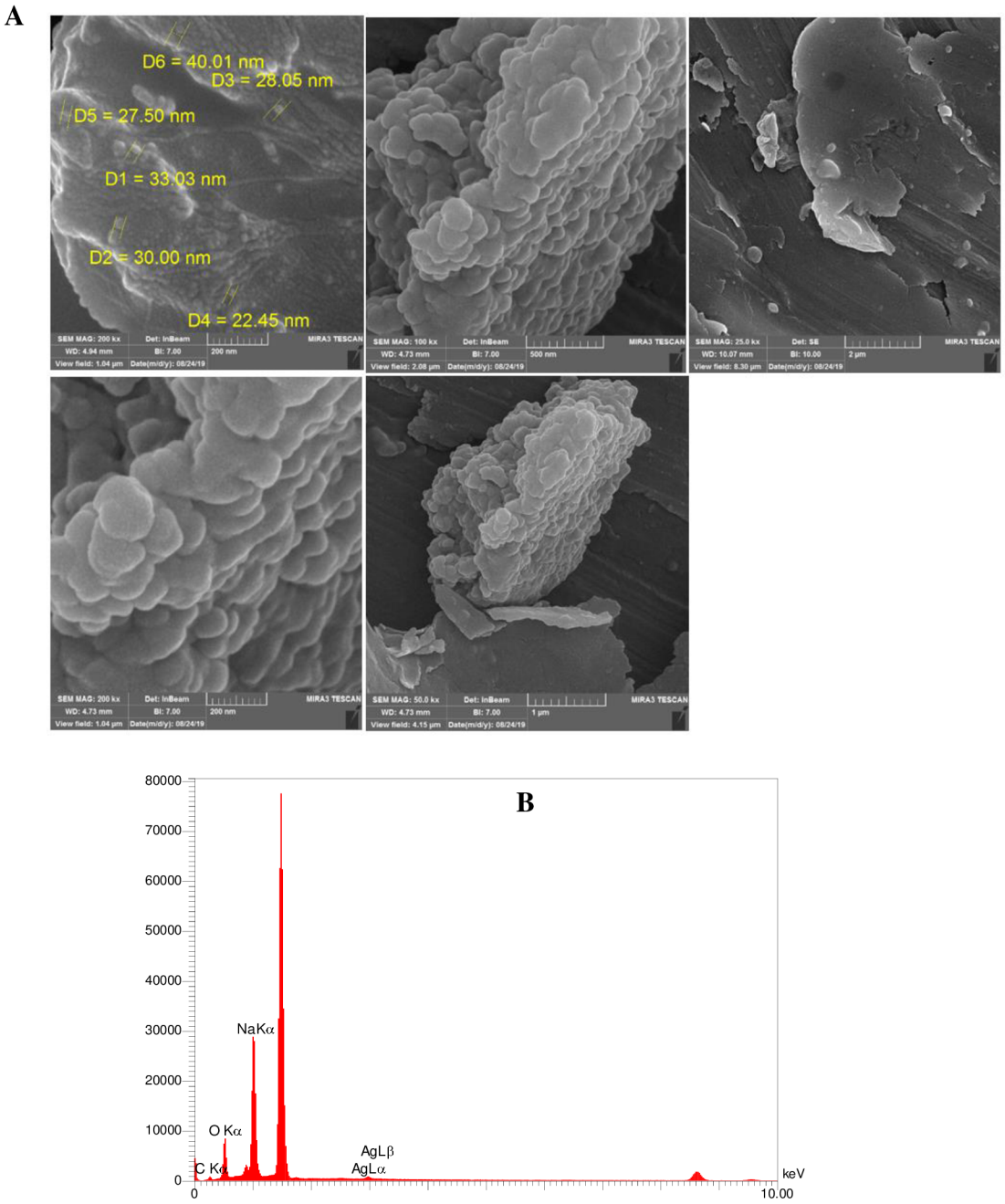

Fig. 4.8 | (A). FE-SEM images of Cit/AgNPs in various magnification. (B). EDS spectra of Cit/AgNPs.

DLS (dynamic light scattering) is a powerful technique which depends on the interaction of light with particles. This technique can be employed for measurements of narrow particle size distributions especially in the range of 2–500 nm [40]. For determination of citrate capped AgNPs hydrodynamic sizes and zeta potential were evaluated (Fig. 4.9). The average particle size of synthesized Cit/AgNPs was 2.27 nm. Furthermore, Cit-AgNPs exhibits fluorescence emission in the range of 400–

600 nm. This may be due to citrate in the structure of this probe with the maximum excitation and emission wavelength at 370 nm and 420 nm, respectively UV–Vis spectra revealed that maximum absorption of Cit-AgNPs is around 397 nm.

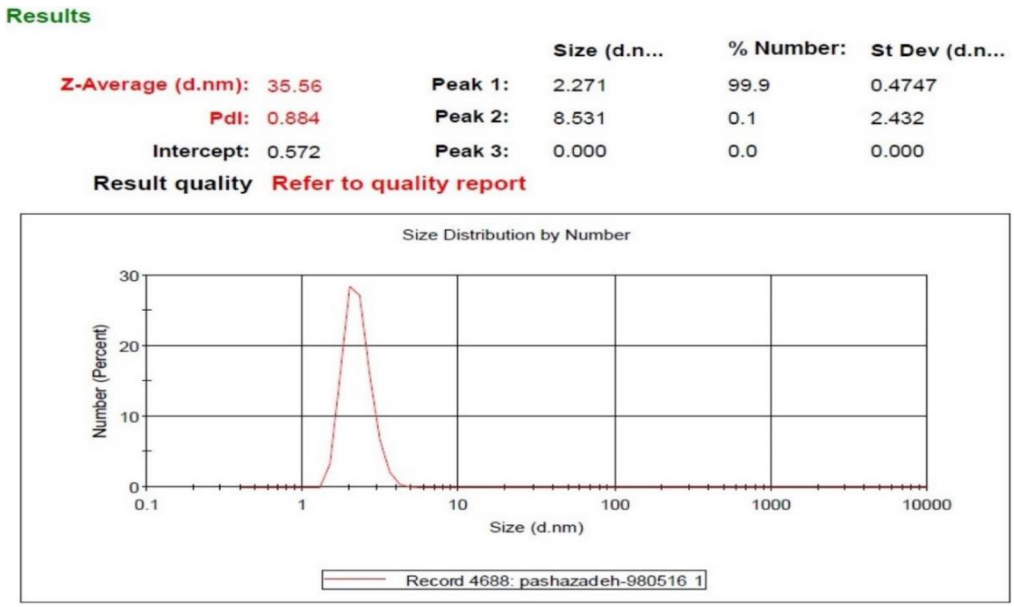

Fig. 4.9 | Size distribution analysis of Cit/AgNPs via DLS.

Preparation of optical biosensor

pDNA is one of the most significant element in genosensing. For this purpose, pDNA was activated through combination with DTT. DTT (dithiotrietol) is usually employed as a deprotecting or decreasing agent for thiolated-probe DNA. The sulfur atoms in terminal of thiolated DNA have potential for forming dimers especially in the existence of oxygen. Thiol groups oxidation prevented by DTT. So, it is applied as a protecting agent [41, 42]. Therefore, DTT (0.01 M) and sodium acetate (0.01 M) were prepared with deionized water. Then, 15 µL of pDNA (SH-5′-AAT TTT CCA ACT TTT TCA CCT GCA T-3') was mixed with 100 µL DTT/sodium acetate solution. After 15 min, 200 µLof ethyl acetate was added and for 5 min vortexed. The prepared solution was centrifuged for 10 min at 8000 rpm and supernatant was removed. Subsequently, 200 µL of Cit/AgNPs was added to the prepared pDNA solution and incubated for 2 h at 45$^{\circ C}$ for spectrofluorometery and 200 µL of diluted Cit/AgNPs (1/2 concentration) was also another microtube of prepared pDNA and incubated which was applied for UV–vis spectrophotometery. 10 µL of NaCl (1 M) was added to 300 µL of mixed Cit/AgNPs-pDNA and Cit/AgNPs for increment of quality and stability of nanoparticles. Then, the prepared solutions were pipetted in the cuvettes and data was recorded both by spectrofluorometer in range of 400−750 nm wavelength and UV-VIS spectrophotometer in range of 250−700 nm spectral range. Fluorescence emission and excitation spectra of Cit/AgNPs and Cit/AgNPs-

pDNA are demonstrated in Fig. 4.10A. The excitation peaks for Cit/AgNPs and Cit/AgNPs-pDNA were observed at 439 and 438 nm, respectively. The fluorescence spectrum of Cit/AgNPs was similar to that of Cit/AgNPs-pDNA; although, the fluorescence intensity was declined by pDNA. As can be seen in Fig. 4.10B, momentous alteration in UV–vis spectra was happened after addition of pDNA which appeared at 470 nm. All of the genosensor preparation steps was shown in Scheme. 4.2.

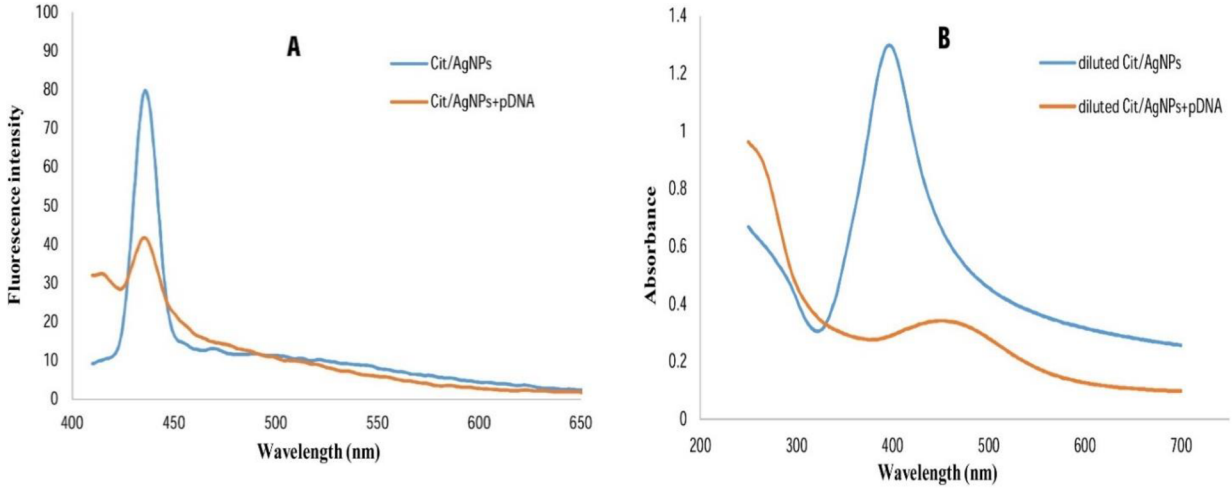

Fig. 4.10 | A) Fluorescence spectra of Cit/AgNPs and Cit/AgNPs-pDNA. B) UV/Vis absorbance spectrum of Cit/AgNPs and Cit/AgNPs-pDNA.

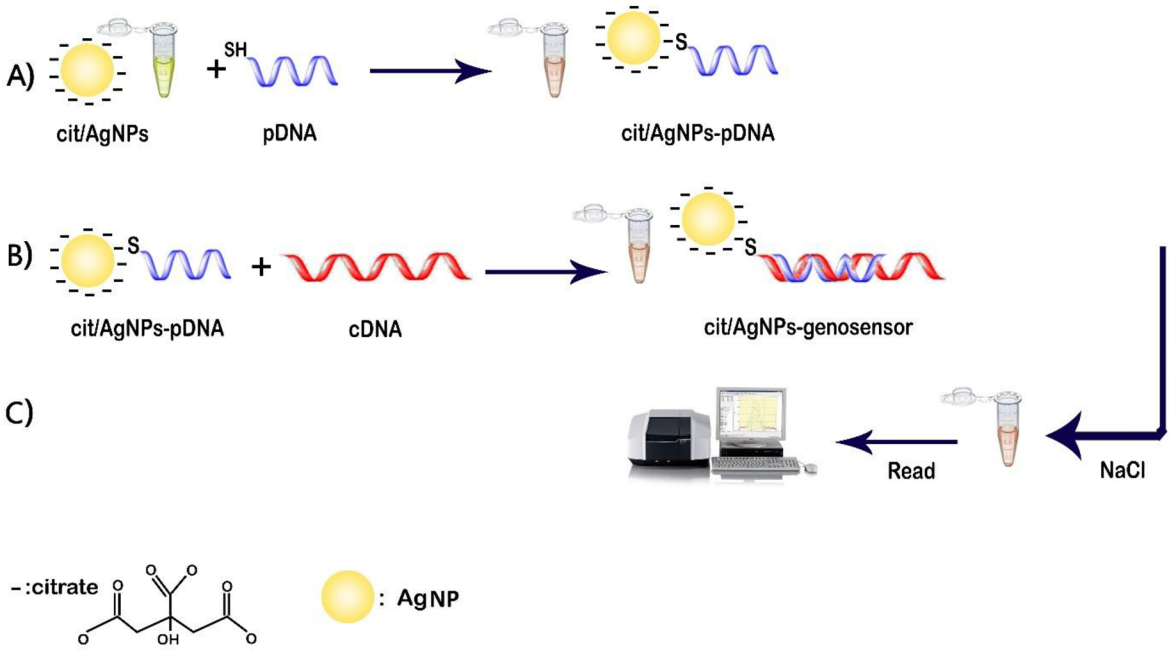

Scheme. 4.2 | Illustration of preparation steps of genosensor.

Optimization of hybridization time

Hybridization leads to quick and effective binding of DNA strands. In this study, pDNA hybridized with its specific DNA (cDNA (complementary target sequences)). Oligonucleotides were successfully immobilized on the surface of Cit/AgNPs due to interaction of AgNPs surface with oligonucleotides binding groups. Thiol groups of oligonucleotides result in increment of binding affinity of them to the surface of nanoparticles, which leads to greater stability of Ag nanoparticle probes [43]. The Cit/AgNPs have stability toward salt concentration (NaCl). So, they are stable against aggregation by NaCl concentration. This hybridization process was associated with color alteration, red-shifting as a result of assembly of particle which can be seen by naked eye in the form of yellow to pale red color change (Fig. 4.11A). To evaluate the hybridization and optimum incubation time, Cit/AgNPs functionalized with pDNA (SH-5′-AAT TTT CCA ACT TTT TCA CCT GCA T-3') solution (Cit/AgNPs-pDNA) and incubated with 15 µL of cDNA (5′-ATG CAG GTG AAA AAG TTG GAA AAT T-3') at different incubation times (2, 5, 10, 15, and 20 min). In this part, 10 µL of NaCl was added to enhance the AgNPs stability and inhibted their aggregration. After insertion of 10 µl NaCl, UV–vis spectra were recorded at different time (251,015 and 20 min). Obtained results demonstrated that the optimum cDNA incubation time was 2 min. As revealed in Fig. 4.11, the location of peak is absolutely similar with previous section.

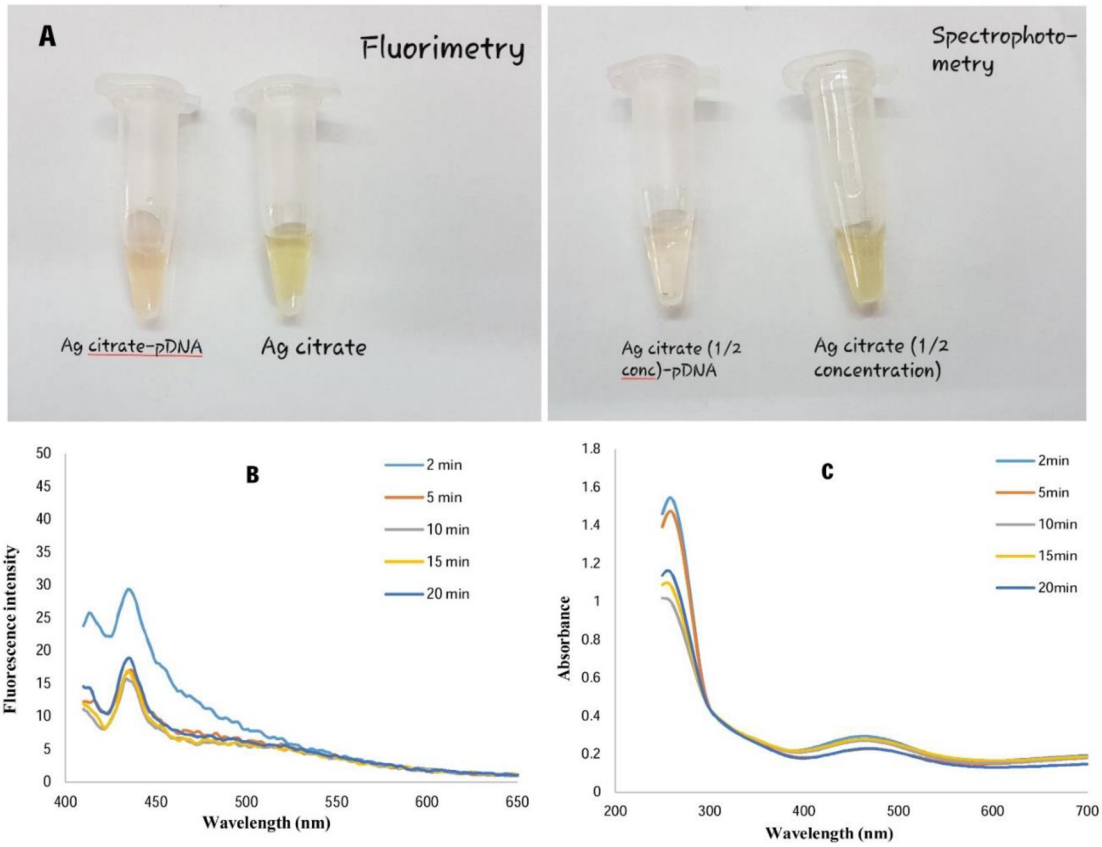

Fig. 4.11 | (A) color alteration of Cit/AgNPs from yellow to pale red after hybridization with pDNA. Fluorescence excitation (B) and UV/Vis absorbance (C) spectrum in various hybridization time (2,5,10,15, and 20 min).

Analytical study

Sensitivity is one of the significant parts of the genosensors. In order to evaluate the sensitivity of prepared genosensor, various concentration of cDNA (10^{-6},10^{-9},10^{-12},10^{-15},10^{-17} and 10^{-21} M) was applied with 2 min incubation time. Same as the previous section, 10 µL of NaCl was added for increasing quality and stability of AgNPs. 15 µL of these concentrations were added to the prepared Cit/AgNPs-pDNA and incubated at 37$^{\circ C}$ for 2 min. As exhibited in Fig. 4.12, the maximum peak was recorded for concentration 10^{-6} M and it was thoroughly predictable. According to decrease of cDNA concentration, the intensity of the excited fluorescence and absorbed signal was decreased. According to the results, in spite of recorded signals downward mobility, the developed optical genosensor can be employed for determination of cDNA, target sequence, up to the concentration of 1 ZM for both spectrofluorometer and UV–vis spectrophotometer. Dynamic linear ranges for both were between 1 µM-1 zM and regression equations recorded for spectrofluorometery and UV–vis spectrophotometery respectively were:

$y = -1.7625$ (*Haemophilus influenza*) $+ 23.969$ $R^2 = 0.8412$ Eq. 4

$y = -0.0885$ (*Haemophilus influenza*) $+ 1.1295$ $R^2 = 0.8692$ Eq. 5

Briefly, the designed DNA based biosensor not only possess great sensitivity but also has easy and low-cost construction.

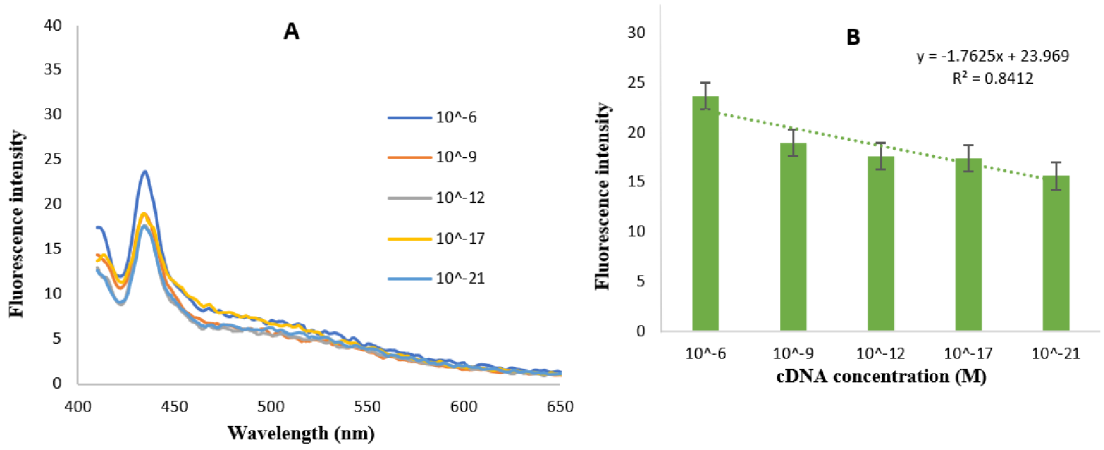

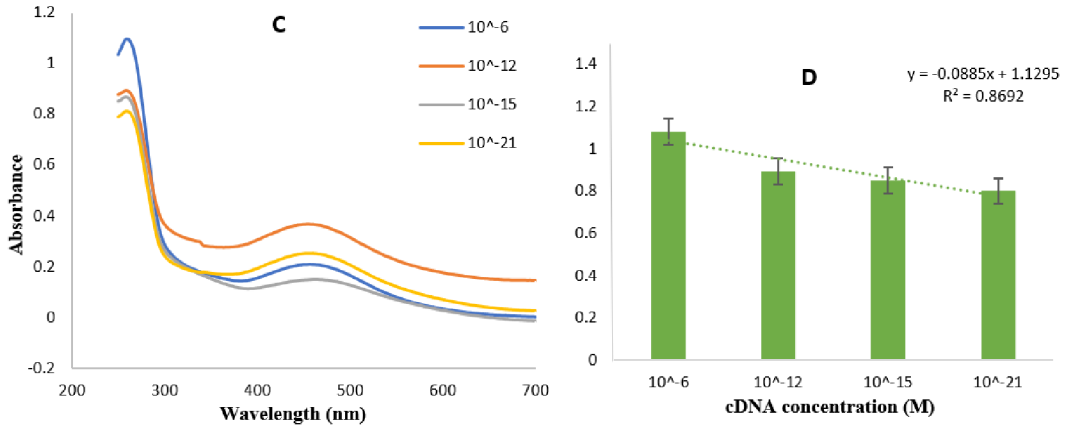

Fig. 4.12 | Fluorescence excitation (A) and UV/Vis absorbance (C) spectrum of genosensor after hybridization with a variety of cDNA concentrations (10^{-6},10^{-9},10^{-12},10^{-15},10^{-17} and 10^{-21} M) in the 400−750 nm and 250−700 nm spectral ranges, respectively. Histograms of peak intensity versus concentration of cDNA (C and D).

Selectivity

One of the remarkable merits of biosensors is its selectivity. Hence, a perfect biosensor should have power to distinguish similar analytes. For evaluate the selectivity, we designed three mismatch sequences (mismatch 1: 5′-ATG GAG GTG AAA AAG TTG GAA AAT T-3', mismatch 2: 5′-AGG GAG GTG AAA AAG TTG GAA AAT T-3', mismatch 3: 5′-AGG GAG GTG AGA AAG TTG GAA AAT T-3'). Alike with analytical study, the designed genosensor was incubated with 15 µL mismatch primers and fluorescence excitation and UV/Vis absorbance was recorded for comparison with cDNA hybridization. The selectivity of genosensor was evaluated in spectral ranges 400−750 nm and 250−700 nm, respectively. As showed in Fig. 4.13, in the presence of mismatched DNAs, fluorescence excitation had significant reduction, whereas, UV/Vis absorbance was considerably increased from mismatch one to mismatch three. These results has exact agreement with different reported studies that the dsDNA intensity is more than that of ssDNA.

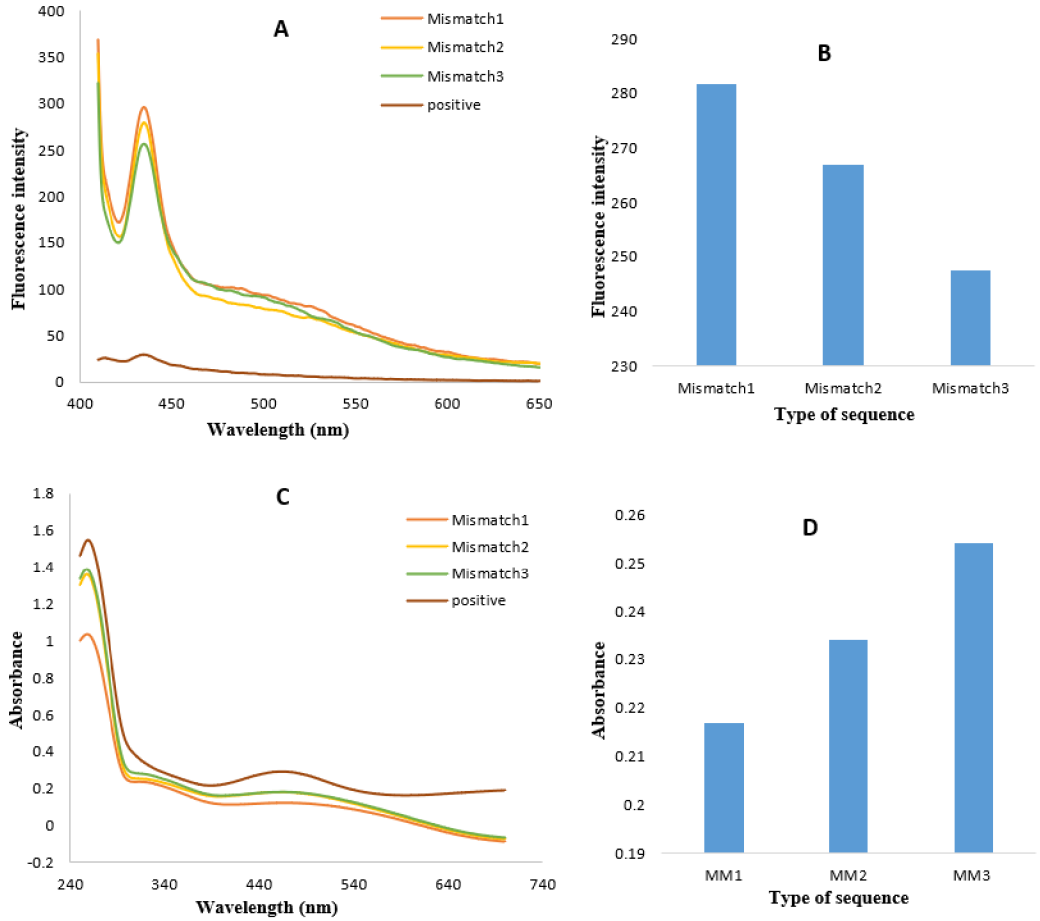

Fig. 4.13 | Fluorescence excitation (A) and UV/Vis absorbance (C) spectrum of hybridization with mismatch cDNAs (Mismatch1, Mismatch2, Mismatch3) in the 400−750 nm and 250−700 nm spectral ranges, respectively. Histograms of peak intensity versus type of sequence (B and D).

Stability

One of the ways to increase the genosensors stability is employing silver nanoparticles. Silver nanoparticles draw a lot of attention in optical biosensors because of their simple and low-cost fabrication as well as great extinction coefficients. In addition, AgNPs has great superficial area which can be suitably modified [43, 44]. The stability of developed genosensor was measured in two steps. At first, intraday stability of synthesized Cit/AgNPs was examined at regular 2 -h interval time. According to Fig. 4.14A-B, the fluorescence excitation and UV/Vis absorbance of Cit/AgNPs were decreased respectively during each 2 -h interval time. In the second step, the stability of developed genosensor was evaluated similar to that of Cit/AgNPs. As displayed in Fig. 4.14C-D, the fluorescence excitation of engineered genosensor was increased respectively during each 2 -h interval time; whereas, its UV/Vis absorbance was decreased.

Therefore, the synthesized Cit/AgNPs has acceptable stability. The genosensor has stability for use within 4 -h. Finally, designed platform has appropriate stability despite its easy fabrication.

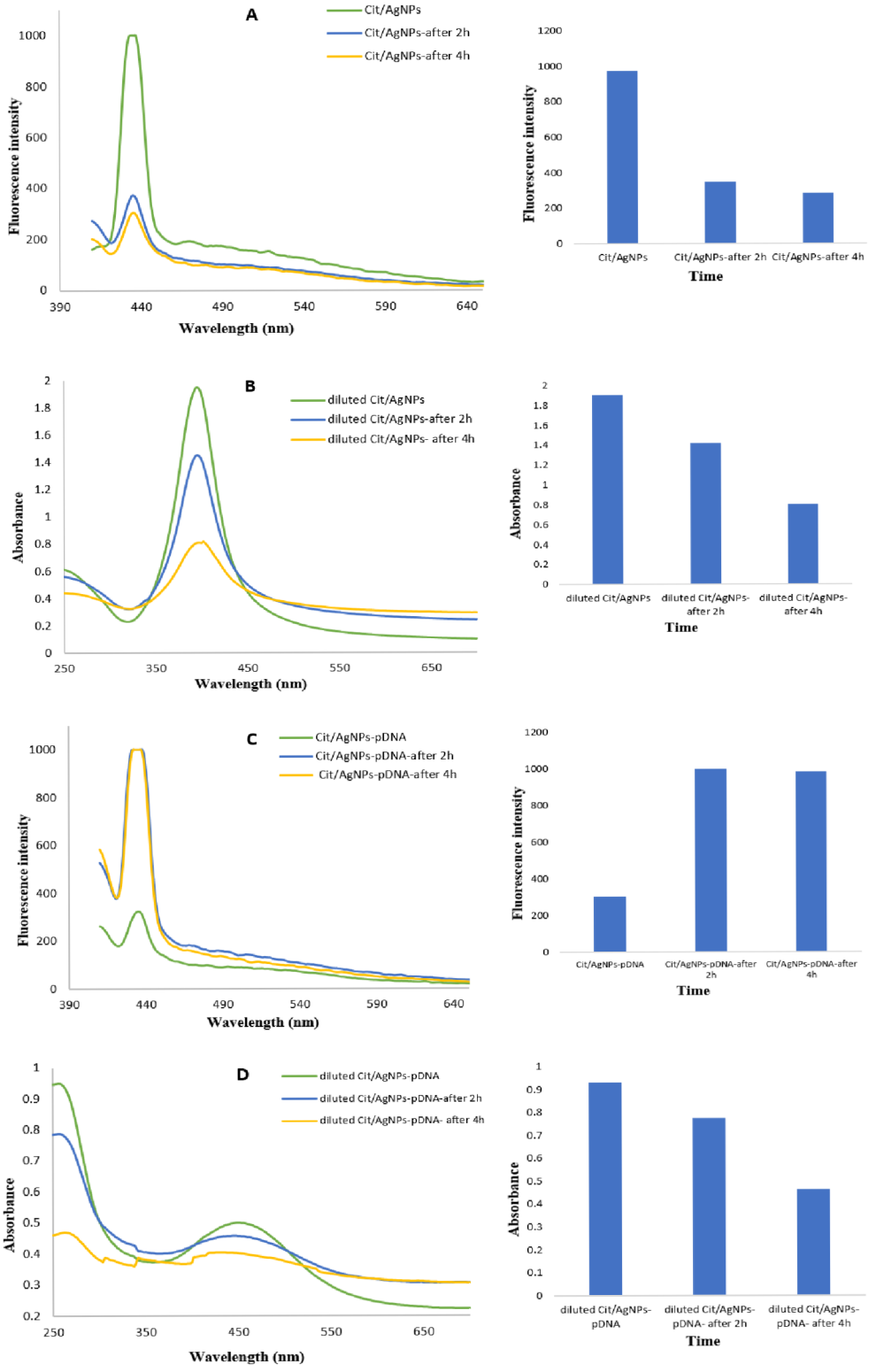

Fig. 4.14 | Fluorescence excitation (A–C) and UV/Vis absorbance (B–D) of Cit/AgNPs and Cit/AgNPs-pDNA, respectively, at regular 2 -h interval time.

4.3 Results and Discussion- Bioelectrocataytic behavior horseradish peroxidase bound to green polymeric scaffold of poly(tyrosine)-chitosan as molecularly imprinted polymer toward monitoring of H_2O_2 in human biofluids

Electropolymerization of L-Tyr supported CS on the SPCE surface

The electropolymerization of 10 mM L-Tyr in PBS (pH = 7.4) utilizing the CV method produced poly(Tyr). The modification procedure was performed in the potential range of -1.0 to 1.0 V (10 repetitive cycles), and the scan rate was 100 $mV.s^{-1}$. After the electropolymerization of poly(Tyr) on the SPCE surface, deionized water was used to rinse the modified electrode to remove any unabsorbed substances. According to Fig. 4.15A, the creation of poly(Tyr) led to an anodic peak at 0.6 V and a reduction peak at -0.8 V. As the number of CV scans rose, the peak current also increased, exhibiting the formation of an electroconductive polymer film on the electrode surface. In the second step, the SPCE was moved into 0.1 M HCl containing 2 mg/mL CS, and 20 repetitive cycles were performed in the potential range from -1.0 V to 0.15 V and sweep rate of 100 $mV.s^{-1}$ (Fig. 4.15B). A thin film of poly(Tyr)-CS film was created on the surface of a screen-printed carbon electrode.

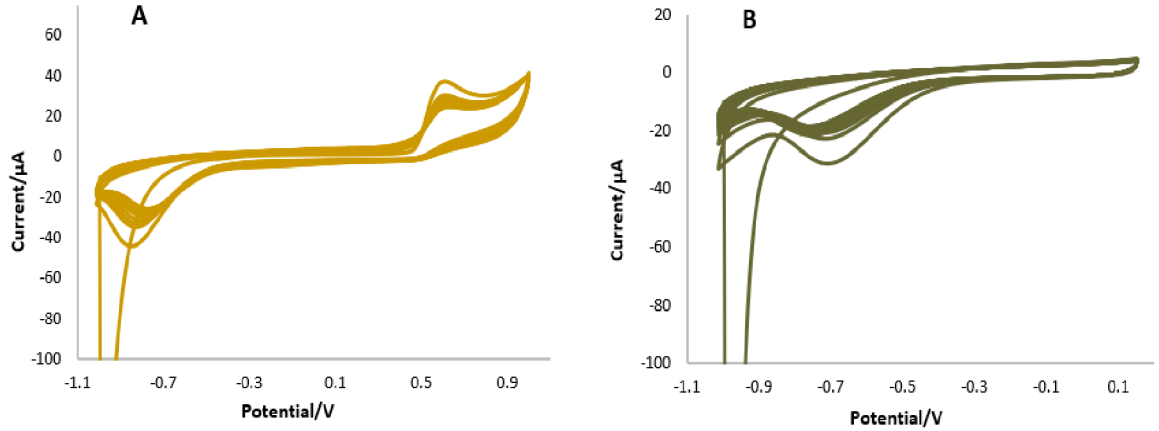

Fig. 4.15 | A) CVs of poly(Tyr) on the surface of SPCE in the presence of 0.1 M *PBS* (pH=7.4) containing 27 mM *L-Tyr* at scan rate of 100 mV s^{-1}. Number of cycles is 10. B) CVs of CS on the surface of SPCE in the presence of 0.1 M *HCl* containing 2 mg/mL CS at scan rate of 100 mV s^{-1}. Number of cycles is 20.

Preparation of MIP/ poly(Tyr)-CS modified biosensors

The combination of poly(Tyr)-CS electropolymerization with the self-assembly surface molecular imprinting approach led to the protein (HRP) imprinting in poly(Tyr)-CS. The poly(Tyr)-CS/SPCE were

submerged in PBS (pH=6) containing 1 mg/mL HRP after the electropolymerization. They lasted 24 hours in a refrigerator at 4°C. The HRP template molecules were easily immobilized on the poly(Tyr)-CS matrix through hydrogen binding interaction. The modified electrode (HRP/poly(Tyr)-CS/SPCE) was immersed in 1.0 M hydrochloric acid solution for a period to eliminate the binding template HRP. The imprinted electrode (MIP/poly(Tyr)-CS/SPCE) was thoroughly rewashed with ultrapure water after that. Electrochemical techniques like CV and DPV were applied to ensure that the template had been properly removed. Prior to usage, the MIP/poly(Tyr)-CS/SPCE electrode was kept at 4 °C in a refrigerator.

Morphological and structural characterization of prepared imprinted biosensor

The morphology of the modified SPCE and the imprinted layer was further examined using SEM. EDS was used to perform an elementary analysis as well. Fig. 4.16 display the SEM image of the poly(Tyr)-CS/SPCE, HRP/poly(Tyr)-CS/SPCE, MIP/poly(Tyr)-CS/SPCE, and bare SPCE. The surface of bare SPCE was smooth and flat, as seen in Fig. 4.16D. A notable homogeneous monodispersed spherical structure was seen when poly(Tyr)-CS was modified on SPCE (Fig. 4.16A), which is ideal for macromolecular loading effectiveness, and the average size of spherical beads was around 60 nm. Such polymer's monodispersed spherical beads have increased surface area and pore volume, which results in high imprinting effectiveness and enhanced noncovalent bonding interaction strength. Fig. 4.16B exhibits that HRP protein molecules have been assembled on the surface of the monodispersed spherical poly(Tyr)-CS film, which made the surface uneven and undulant. Additionally, the EDX demonstrates that P and Fe elements were not initial polymer film, and P and Fe peaks can be seen in the enzyme-immobilized film. These alterations showed that HRP had been successfully immobilized on the poly(Tyr)-CS film. The change in film shape caused by eliminating the HRP template molecules is apparent in Fig. 4.16C.

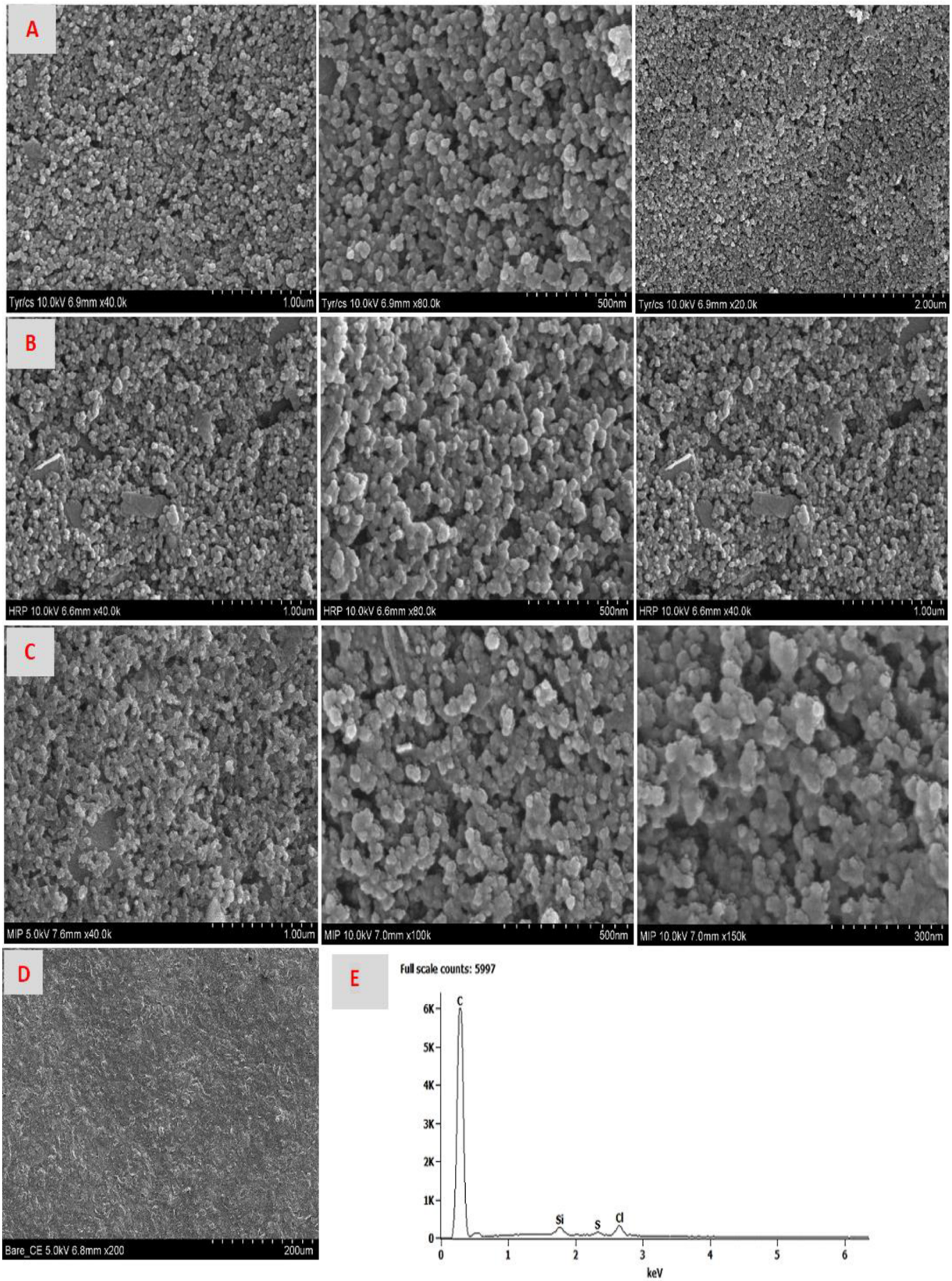
A
Tyr/cs 10.0kV 6.9mm x40.0k 1.00um
Tyr/cs 10.0kV 6.9mm x80.0k 500nm
Tyr/cs 10.0kV 6.9mm x20.0k 2.00um
B
HRP 10.0kV 6.6mm x40.0k 1.00um
HRP 10.0kV 6.6mm x80.0k 500nm
HRP 10.0kV 6.6mm x40.0k 1.00um
C
MIP 5.0kV 7.6mm x40.0k 1.00um
MIP 10.0kV 7.0mm x100k 500nm
MIP 10.0kV 7.0mm x150k 300nm
D
Bare_CE 5.0kV 6.8mm x200 200um
E
Full scale counts: 5997
C
Si
S
Cl
6K
5K
4K
3K
2K
1K
0
0
1
2
3
4
5
6
keV

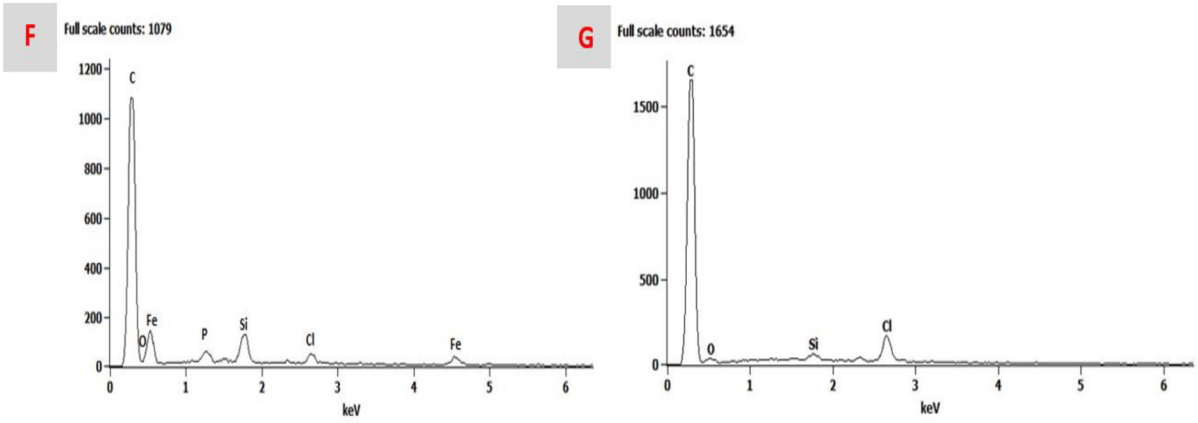

Fig. 4.16 | Scanning electron microscopy of (A) poly(Tyr)-CS/SPCE, (B) HRP/poly(Tyr)-CS/SPCE, and (C) MIP/poly(Tyr)-CS/SPCE, (D) bare SPCE, and EDXs of (E) poly(Tyr)-CS/SPCE, (F) HRP/poly(Tyr)-CS/SPCE, and (G) MIP/poly(Tyr)-CS/SPCE, respectively.

The possible mechanisms of the electropolymerization of poly(Tyr)-CS film

The suggested process of electropolymerization of poly(Tyr)-CS is that L-tyrosine polymerization starts in the first step by providing an oxidation potential, leading to the production of a radical cation on the carbon-containing amine group. It has been demonstrated that an NH group-containing monomer may be electropolymerized on the SPCE surface to create a conducting film by the formation of a covalent bond (N-C) between the NH group and carbon electrode [45, 46]. Since CS is positively charged when dissolved in acid (HCl in the current study), the electron-withdrawing oxygen-containing groups on poly(Tyr) in the second step are advantageous to the combination with CS from an electrostatic point of view. The findings, therefore, demonstrate that tyrosine may interact with hydrophilic CS via $-NH_3^+$ and -OH side groups, allowing for the formation of a specific self-assembly network between the tyrosine monomer and CS chains (Scheme. 4.3)[46, 47].

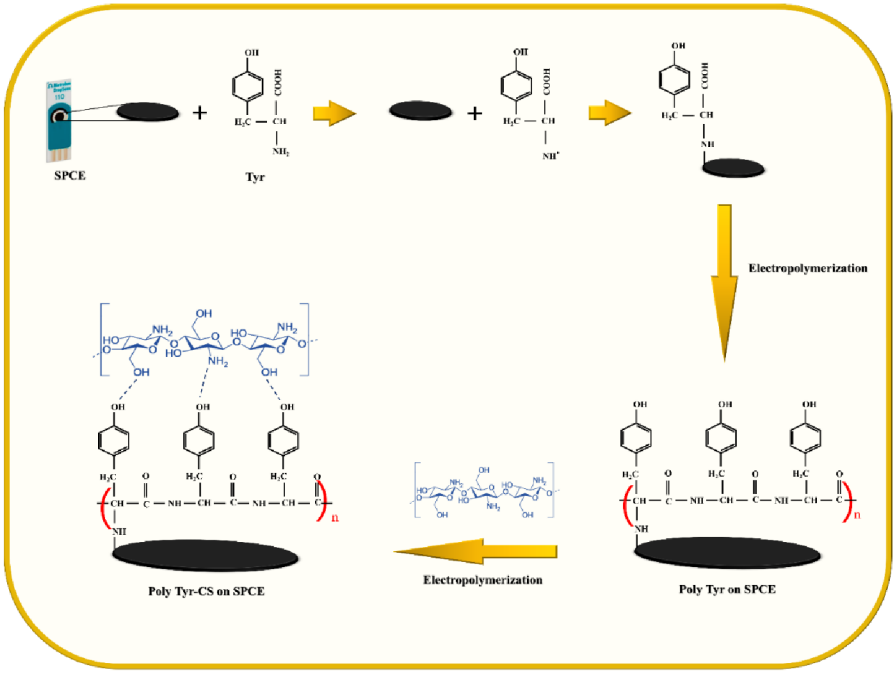

Scheme. 4.3 | *Electropolymerization procedure of tyrosine supported chitosan on the screen-printed carbon electrode.*

Optimization of biosensor responses

Electrochemical characterization of developed imprinted biosensor

Scheme 4.4 depicts the fabrication of the HRP electrochemical imprinted biosensor (MIP/poly(Tyr)-CS/SPCE). A new imprinting preparation method was used to ensure the diffusion and elution of the HRP biomacromolecule on the surface of the created modified electrode [48-52]. In this strategy, pre-assembly of the poly(Tyr)-CS film onto the SPCE surface before binding of HRP rather than the conventional method of tyrosine and CS electropolymerization in the presence of the HRP template was carried out. CV was employed for the characterization of preparation procedures of the imprinted biosensor in a 0.01 M $Fe(CN)_6^{4-}/Fe(CN)_6^{3-}$ solution containing 0.1 M KCl as a supporting electrolyte. Fig. 4.17 showed that the redox peaks were enhanced when SPCE was modified by poly(Tyr)-CS compared to the bare SPCE, suggesting that the high electrical conductivity and unique characteristics of the poly(Tyr)-CS/SPCE *can* expedite the electron flow of probe involving $Fe(CN)_6^{4-}/Fe(CN)_6^{3-}$. Template HRP molecules were trapped in the poly(Tyr)-CS matrix through hydrogen bond interaction between the –NH groups of the poly(Tyr)-CS film and the -COOH groups of the HRP template molecules. Consequently, when the HRP molecule was bounded, the peak current of the prepared electrode reduced drastically, implying the successful assembly of HRP that allows electron transport to be retarded because of weak conductivity. However, after the removal of the template protein molecules from the polymer matrix, the specific imprinting cavity for

HRP molecule determination was reconstructed. The imprinted sites were evidently generated following the elution of the template protein, which let the probe molecules diffuse into the electrode surface via the imprinted layer's pores [50-52]. As a result, the peak current was enhanced, indicating that HRP biomacromolecules were successfully removed. CV can keep track of the template elution from the matrix.

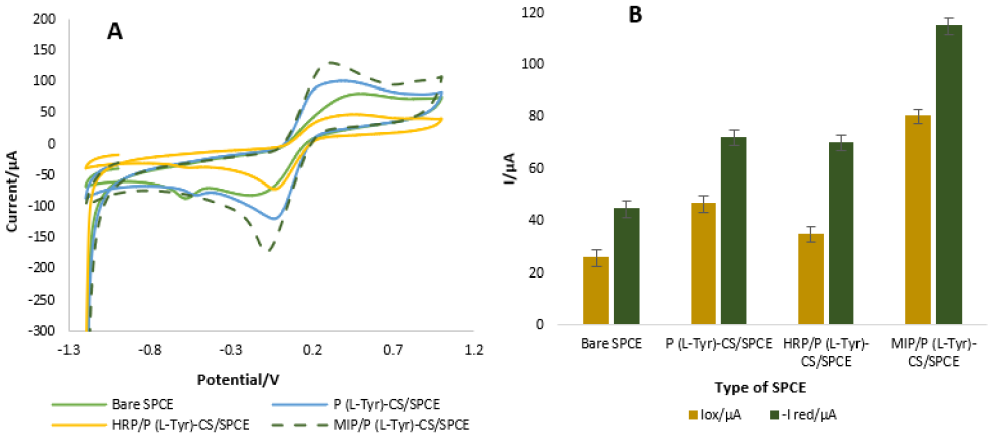

Fig. 4.17 | A) CVs of preparation steps of imprinted polymer in 0.01 M $Fe(CN)_6^{4-}/Fe(CN)_6^{3-}$+0.1 M KCl at a sweep rate of 30 mV/s. B) peak currents variation versus type of modified electrodes (n = 3, SD = 3.01).

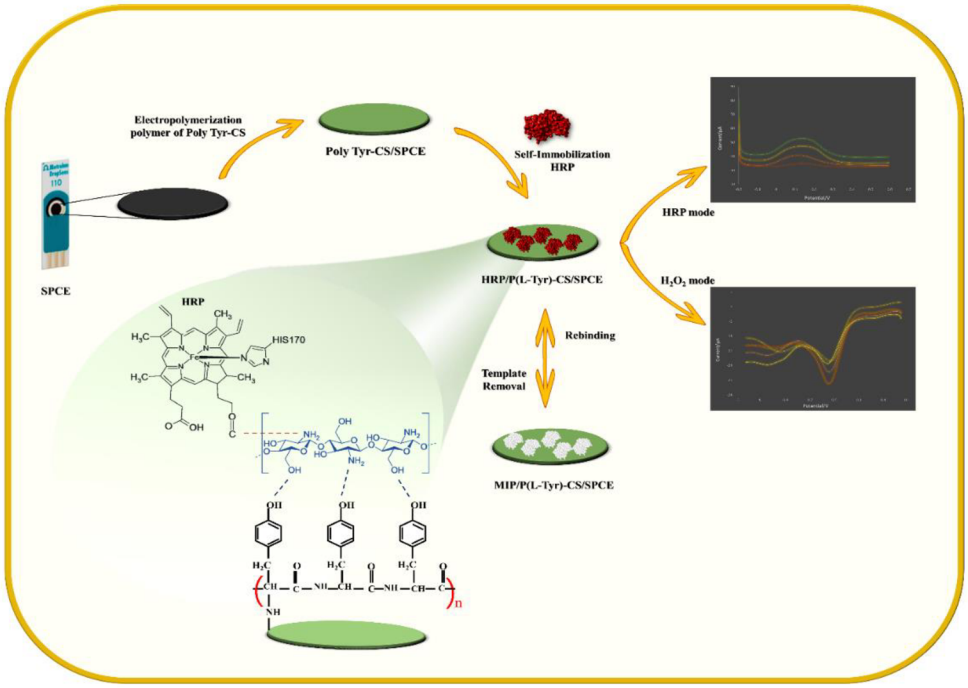

Scheme. 4.4 | *The preparation process of MIP/poly(Tyr)-CS/SPCE biosensor.*

The template removal time is critical in achieving the optimal MIP-based sensor. The adequate time allows for the template extraction from the polymeric matrix. The electrode surface was exposed to

1.0 M HCl, and the exposure time was between 5 and 40 min (Fig. 4.18). The peak current rose when the electrode surface was soaked in 1.0 M HCl for 20 minutes. These findings show that the HRP has begun to be removed from the polymeric matrix. However, after 20 min, the CV current fell and remained stable until 40 min. As shown in Fig. 4.18B, a 20-min immersion in 1.0 M HCl was sufficient to remove HRP from the polymeric matrix.

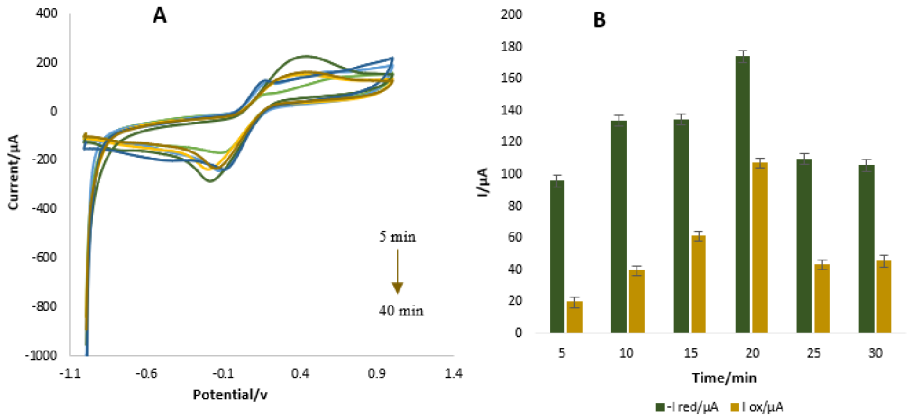

Fig. 4.18 | A) CVs of HRP/poly(Tyr)-CS/SPCE imprinted polymer at different *removal time (5,10,15,20,30, and 40 min)* in 0.01 M $Fe(CN)_6^{4-}/Fe(CN)_6^{3-}$+0.1 M KCl at a sweep rate of 0.1 V/s. B) peak currents variation versus template removal time with HCl (n = 3, SD = 3.33).

Kinetic studying

CVs of poly(Tyr)-CS modified SPCE were obtained at various sweep rates in the range of 10 to 500 mV.s^{-1} in $Fe(CN)_6^{4-}/Fe(CN)_6^{3-}$ solution for the kinetic study. Peak currents increased with increasing scan rate, as shown in Fig. 4.19. According to Fig. 4.19D, the dependence of the Neperian logarithm of peak current on the Neperian logarithm of sweep rate (*ln Ip versus ln v*) is linear ln Ip_a = 0.1845 ln v + 5.1798 (R^2 = 0.9951), in which the slope is 0.1845 ± 0.003. A slope close to 1.0 is believed to be the electrode process is adsorption-controlled, and a slope less than 0.5 is thought to be diffusion-controlled by Fick's law [53, 54]. Hence, this indicates that the electrochemical reaction at poly(Tyr)-CS/SPCE surface was controlled by diffusion. Fig. 4.19C demonstrates the dependence of peak potential on the Neperian logarithm of the scan rate (E_{pa} *versus ln v*) and that the electron transfer has an irreversible nature with a positive shifting in the anodic and cathodic peak positions, respectively. The linear relation between E_{pa} *versus ln v* can be expressed as E_{pa} = 0.0932 ln *v* + 0.6717 (R^2 = 0.9843). As for a diffusion-controlled and irreversible electrode process, according to Laviron [29], E_{pa} can be calculated using the following equation:

$$Ep = \left(\frac{RT}{2\alpha nF}\right) \ln v + \text{constant} \qquad \text{Eq. 6}$$

In the above equation, E_p is the peak potential, α is the electron-transfer coefficient, n is the number of electrons, T is the temperature (298 K), F is the Faraday constant (96485 C mol^{-1}), and R is the universal

gas constant (8.314 J K^{-1} mol^{-1}). In this study, the value of αn was calculated to be 0.13 for $[Fe(CN)_6]^{3-/4-}$. Furthermore, the value obtained for n from $|Ep - E_p/2| = 47.7/\alpha n$ (mV) irreversible system [31-33] is $1.03 \approx 1$.

Moreover, the special surface of SPCE covered with poly(Tyr)-CS should be investigated to assess the effective electrode surface coverage. To calculate the value of Γ^* as surface coverage of a modified electrode, the slope of peak currents on scan rates (I_p *vs.* V) was examined using Equation. 5 (Fig. 4.19B) [55]:

$$I_p = (n^2 F^2/4RT)\, \nu A\Gamma^* \qquad \text{Eq. 7}$$

Where A is the electrode surface area ($A=\pi r^2=0.1256$ cm^2), ν is the potential sweep rate, and Γ* represents the surface coverage of the modified electrode (M/cm^2). The surface coverage of poly(Tyr)-CS/SPCE was attained as 1.25×10^{-5} $cm^2 \cdot s^{-1}$, which supplies an effective surface for the HRP immobilization and generation of the imprinted polymer.

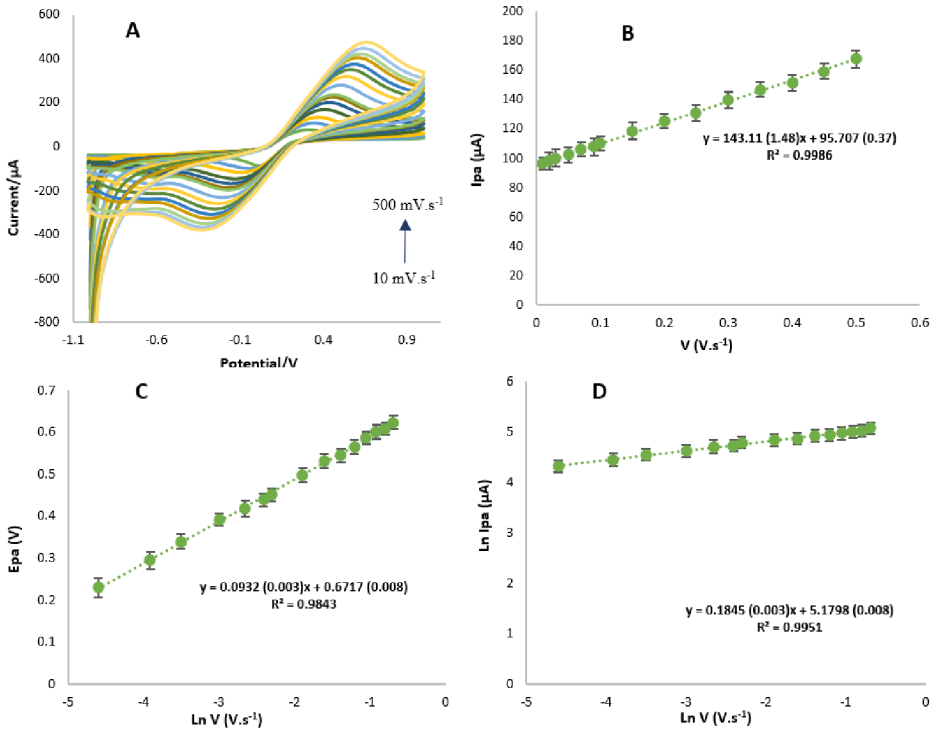

Fig. 4.19 | A) CVs of poly(Tyr)-CS/SPCE in 0.01 M $Fe(CN)_6^{3-}$/$Fe(CN)_6^{4-}$ + 0.1M KCl at various sweep rates (10, 20, 30, 50, 70, 90, 100, 150, 200, 250, 300, 350, 400, 450, and 500 mV/s). B) The dependency of I_p versus v. C) Variation of E_p versus Lnv. D) Variation of lnIp versus Lnv.

HRP determination by the MIP/poly(Tyr)-CS/SPCE

Highly sensitive determination of the target is critical for molecularly imprinted sensors. This study has investigated the application of MIP/poly(Tyr)-CS/SPCE to detect HRP at various concentrations using the DPV method with 0.01 M $Fe(CN)_6^{3-}$/$Fe(CN)_6^{4-}$ containing 0.1 M KCl as an electrochemical probe.

According to Fig. 4.20A, the current response of the imprinted biosensor reduced as HRP concentration rose. This was caused by the entrance of the template molecule into imprinted sites, retarding electron transfer to the created cavity and obstructing the probe molecule's ability to diffuse through the imprinting layer. A correlation exists between the concentration of HRP and the decreased peak current. As exhibited in Fig. 4.20B, there was a good dynamic linear range from 1.0 $\times 10^{-8}$ to 1.0 $\times 10^{-1}$ mg/mL to be displayed with a linear regression equation ΔI (μA)=0.1679 C_{HRP}+2.8954 (R^2=0.9729) with the LOD of 9.39 × 10^{-8} mg/ml (2.34 pM) (S/N=3.3) and a quantitation limit (LOQ) of 2.84 × 10^{-7} mg/ml (7.11 pM) (S/N=10).

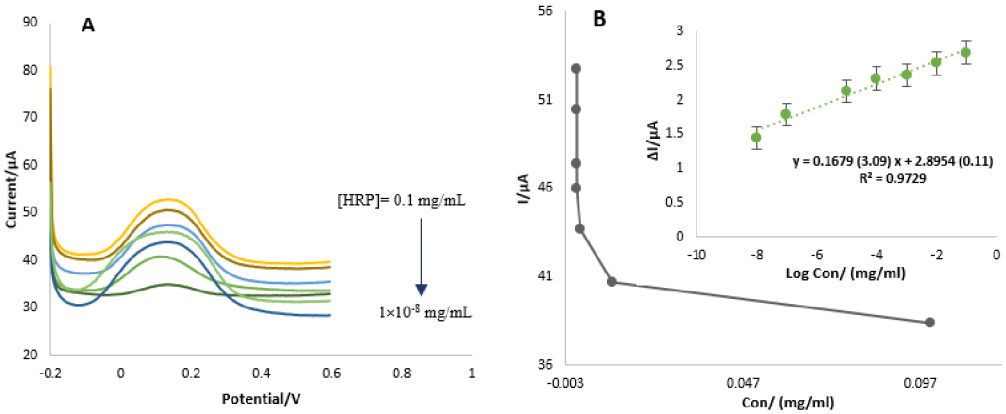

Fig. 4.20 | A) DPV of MIP/poly(Tyr)-CS/SPCE in different concentration of HRP (0.1, 10^{-2}, 10^{-3}, 10^{-4}, 10^{-5}, 10^{-7}, and 10^{-8} mg/mL in 0.01M $Fe(CN)_6^{3-}/Fe(CN)_6^{4-}$ + 0.1M KCl. B) Calibration curve of the corresponding peak currents of MIP/poly(Tyr)-CS/SPCE versus concentrations of HRP (n = 3, SD = 2.03).

Bioelectrocatalytic *activity* of HRP-imprinted biosensor

Anaerobic oxidase via the ferric-ferrous cycle provides the basis for the bioelectrocatalytic activity of HRP. A typical reduction substrate for the HRP process is H_2O_2. The bioelectrocatalytic mechanism of HRP for H_2O_2 reduction comprises two fundamental steps: i) Through two-electron oxidation, the heme moiety transforms into an intermediate known as compound I, and ii) two sequential one-electron reductions allow the enzyme to return to its resting state utilizing compound II, a second intermediate [56]. Using CV and DPV techniques (Fig. 4.21), the electrocatalytic performance of the HRP-imprinted biosensor (1 mg/ml HRP) for H_2O_2 reduction was investigated in 0.1 M PBS solution with different concentrations of H_2O_2. The influence of pH on the biosensing behavior of the HRP-imprinted biosensor was examined in the pH range of 4.0 to 8.0 in the presence of H_2O_2 to develop effective biosensing for H_2O_2 reduction. The current response reached its maximum at pH 8.0, as shown in Fig. 4.21C. Thus, HRP's enzyme activity reached its peak. Consequently, 0.1 M PBS solution pH 8.0 has been used to investigate H_2O_2 reduction for the first time. The CV curve represented -0.66 V as the reduction potential for H_2O_2 (Fig. 4.21D). Using the DPV method, the current response was studied at H_2O_2 concentrations ranging from

10 nM to 1 mM. The reduction peak current progressively rose as the concentration of H_2O_2 successively increased, demonstrating that the immobilized HRP/poly(Tyr)-CS/SPCE had a bioelectrocatalytical activity to H_2O_2 reduction in 0.1 M PBS with pH 8.0 (Fig. 4.21A). The obtained linear range by DPV was 10 nM to 1 mM with regression equation $-I(\mu A) = 1.061\ C_{[H2O2]}(mM) + 7.4934$ ($R^2 = 0.9945$). The limit of detection for the detection of H_2O_2 using the HRP-imprinted biosensor was estimated to be 2.18 nM (S /N=3.3), and LOQ was 6.60 nM (S/N=10) for DPV.

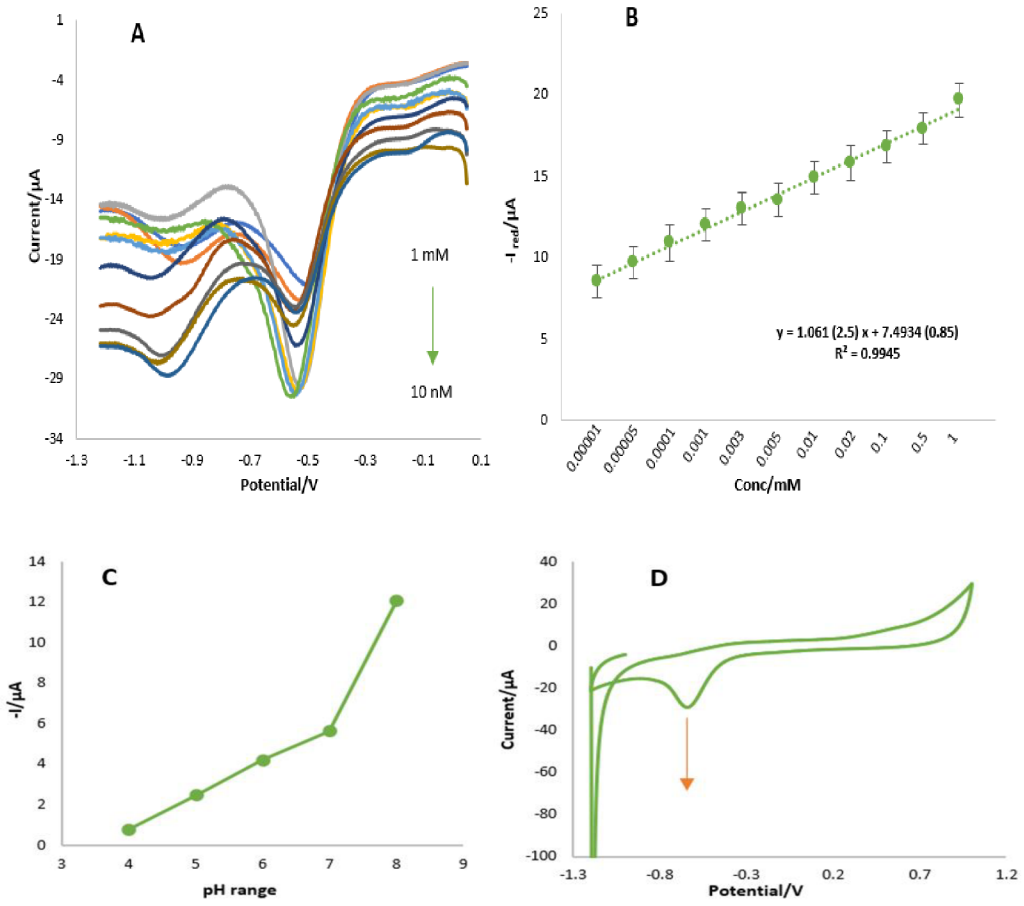

Fig. 4.21 | A) DPVs of HRP/poly(Tyr)-CS/SPCE to different concentrations of H_2O_2 from 10 nM to 1 mM in 0.1 M PBS (pH = 8.0). B) Histogram of HRP/poly(Tyr)-CS/SPCE (n = 3, SD = 1.01). C) Calibration of pH effect on H_2O_2 reduction by HRP-imprinted biosensor in 1 mM H_2O_2 solution including 0.1 M PBS with different pH (4.0 - 8.0) at a sweep rate of 30 mV/s (n = 3, SD = 0.6). D) CV of HRP/poly(Tyr)-CS/SPCE in 1 mM H_2O_2 solution including 0.1 M PBS (pH = 8.0) at a sweep rate of 30 mV/s.

H_2O_2 measurement using electrochemical biosensors has been the subject of several investigations (Table. 4.3). A few studies have employed molecularly imprinted polymer-electrochemical biosensors to determine H_2O_2. However, most researchers have used different types of nanoparticles as matrices for

biosensor development. It should be noted that creating these platforms takes more time and involves more procedures, including creating working electrodes such as carbon paste and carbon cloth electrodes and synthesizing nanoparticles. However, the environmentally friendly poly(Tyr)-CS film offers a simple, accessible, and affordable matrix for the creation of molecularly imprinted polymer-electrochemical biosensors. As shown in Table. 4.3, the performance of the proposed molecularly imprinted biosensor has a lower LOD than those of previously published electrochemical biosensors for the precise determination of trace amounts of H_2O_2.

Table. 4.3 | Analytical performance comparison of the available biosensors for determination of H_2O_2.

Materials	Electrodes	Detection methods	Linear range	LOD	Ref.
Pt-MWCNT	SPCE	Chronoamperometry	10–100 µM	10 µM	[57]
HRP/toluidine blue/graphite	Ceramic electrode		0.429 µM–0.455 mM	0.171 µM	[58]
CS/HRP-poly(L-DOPA)	Au-plated Au (Au_{plate}/Au) electrodes		0.001–1.25 mM	0.1 µM	[59]
MnO_2	CPE[1]		0.04–1.91 µM	0.012 µM	[60]
MnOOH nanorod arrays	Carbon cloth electrode		20 µm–9.67 mM	3.2 µM	[61]
HRP/NH_2-Hf-BTB-MOL[2]/MWNTs			7.5 µM to 1500 µM	0.87 µM	[62]
PEDOT:PSS[3]	SPCE		1-100 µM	0.97 µM	[63]
PtNPs-CDs/IL-GO	GCE[5]	Amperometry	1–900 µM	0.1 µM	[64]
HRP/PTMSPA[4]@GNR			1×10^{-5}–1×10^{-3} M	0.06 µM	[65]
PtNPs/ethyl cellulose			0.05 µM–2.22 mM	0.01 µM	[66]
$Co_3S_4/CuCo_2O_4$			0.001–4.03 mM	17 µM	[67]
Pd/HRP/f-GR	Graphite electrode		25 µM–3.5 mM	0.05 µM	[68]
AgNiNP/RGO	Paper electrode		0.003–13 mM	0.91 µM	[69]
Boron-doped graphene nanosheets	RDE[6]		1.0–20.0 mM	3.8 µM	[70]
HRP/PAN-PNMThH	GCE	Chronoamperometry	5.0 µM–60.0 mM	3.2 µM	[71]
HRP/C-Dots/LDHs			0.1–23.1 µM	0.04 µM	[72]
NiO/GR			0.25–4.75 mM	0.7664 µM	[73]
EFK8-SWNT- hemoglobin			20–960 µM	7.54 µM	[74]
MIP/P(β-CD)			1–15 µM	0.4 µM	[52]
$ZnFe_2O_4/g\text{-}C_3N_4$			5–200 µM	1 µM	[75]
CoS/RGO			0.1–2542.4 µM	42 nM	[76]

Nanographene-coated rice-like manganese dioxide nanorods/graphene			0.002–4.44 mM	0.2 µM	[77]
HRP/Hap5-fCNT			1.0×10^{-5} – 2.34×10^{-4} M	1.91 µM	[78]
Ag-Cu nanoalloys		Cyclic voltammetry – Electrochemical impedance spectroscopy	2.0 – 9.61 mM	152 µM	[79]
HRP/Bi-AgNPs		Differential pulse voltammetry	0.02–1.0 µM	0.06 µM	[80]
MIP/MPBA[7]/AuNPs			0.6–20 µM	0.16 µM	[81]
MIP/polyaniline nanotubes			0–10 µM and 10–90 µM	0.01 µM	[50]
MIP/Poly toluidine blue			1 µM –40 mM	1 µM	[82]
MIP/poly(Tyr)-CS	SPCE		10 nM–1 mM	2.18 nM	This work

Real sample analysis

Using the DPV technique, the developed HRP-imprinted biosensor was also successfully employed toward the sensitive detection of H_2O_2 in unprocessed human plasma samples (Fig. 4.22A). Different concentrations of H_2O_2, ranging from 5 nM to 1 mM, were spiked into human plasma samples to examine the practical use of the MIP-based biosensor. These concentrations were then measured using the DPV method. As shown in Fig. 4.22B, the HRP-imprinted biosensor is capable of measuring H_2O_2 in the concentration range of 5 nM to 1 mM, and the calibration curve for the linear regression equation is $-I(\mu A) = 0.8822\ C_{[H2O2]}(mM) + 2.0266$ ($R^2 = 0.994$). The LOD (S/N=3.3) for the detection of H_2O_2 in unprocessed human plasma samples using HRP-imprinted biosensor was calculated to be 1.50 nM, and the LOQ (S/N=10) was 4.56 nM.

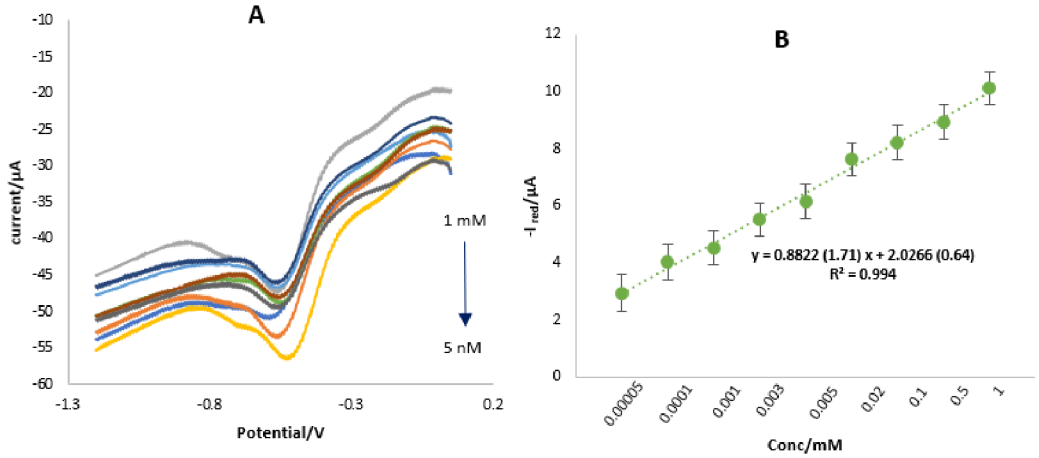

Fig. 4.22 | A) DPV response of HRP/poly(Tyr)-CS/SPCE towards sensitive determination of H_2O_2 in untreated human plasma samples with different concentration. B) Calibration curve (n = 3, SD = 0.6).

Stability, repeatability, and selectivity of the developed molecularly imprinted biosensor

The imprinted biosensor showed good stability and repeatability. CVs of poly(Tyr)-CS/SPCE were measured in 0.01 M $Fe(CN)_6^{3-}$ /$Fe(CN)_6^{4-}$ containing 0.1 M KCl at different cycles (1,5,10, and 50) to evaluate the stability of the polymer layer on the SPCE surface. Good stability was found after 10 cycles, as shown in Fig. 4.23A-B, indicating that the suggested polymer film is stable. The findings show that the peak current of poly(Tyr)-CS/SPCE remained almost steady after 10 cycles. However, after 50 cycles, there was a drastic change in the oxidation and reduction potentials of the proposed polymer film. Redox peak currents and potentials were discovered to have altered, confirming the limited stability of poly(Tyr)-CS after 50 cycles. The findings show that the electropolymerization of poly(Tyr)-CS is highly stable throughout a range of 10 sweep rates. Hence, after 10 cycles, this polymer is not an acceptable matrix for subsequent applications. poly(Tyr)-CS can therefore be employed in the disposal. The repeatability of MIP/poly(Tyr)-CS/SPCE was examined using 0.1 mg/ml HRP by the DPV method in six cycles of a binding-elution-rebinding test of the protein-modified electrode, and the calculated RSD (relative standard deviation) was 3.96% (Fig. 4.23C-D).

The selectivity of the HRP/poly(Tyr)-CS/SPCE for H_2O_2 was investigated in the presence of potential interfering electroactive agents such as ascorbic acid (AA), dopamine (DA), uric acid (UA), and glucose (GL) with DPV technique. Fig. 4.23E-F shows the voltammetric response signals of 1mM H_2O_2 in PBS solution (pH 8.0) by the addition of 0.1 mM of each interfering specie. The HRP-imprinted biosensor reduced the interference effect to 1 mM H_2O_2 by GL 16.41 %, UA 17.21 %, and AA 23.76 %, which exhibited negligible effects on the H_2O_2 response. This implies that the interfering agents have almost no effect on the analyte response. Therefore, it displayed the high selectivity of the designed HRP-imprinted biosensor toward the determination of H_2O_2. However, voltammetric responses can be detected by dopamine (1 mM H_2O_2), indicating dopamine can engage in the redox process of H_2O_2 (51.11 %), thus interfering with H_2O_2 measurement.

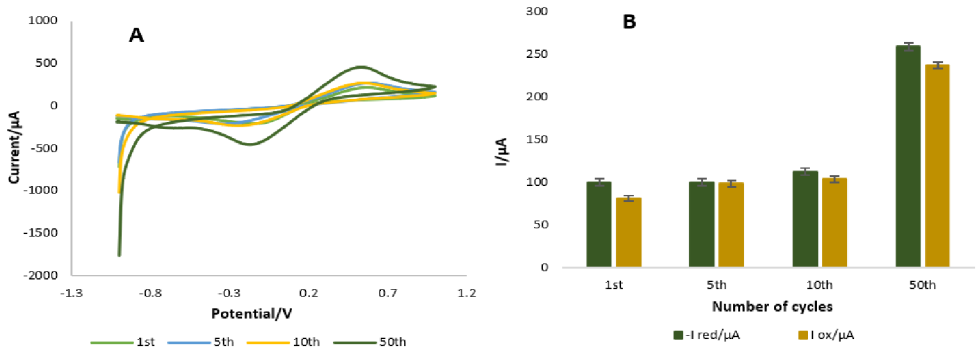

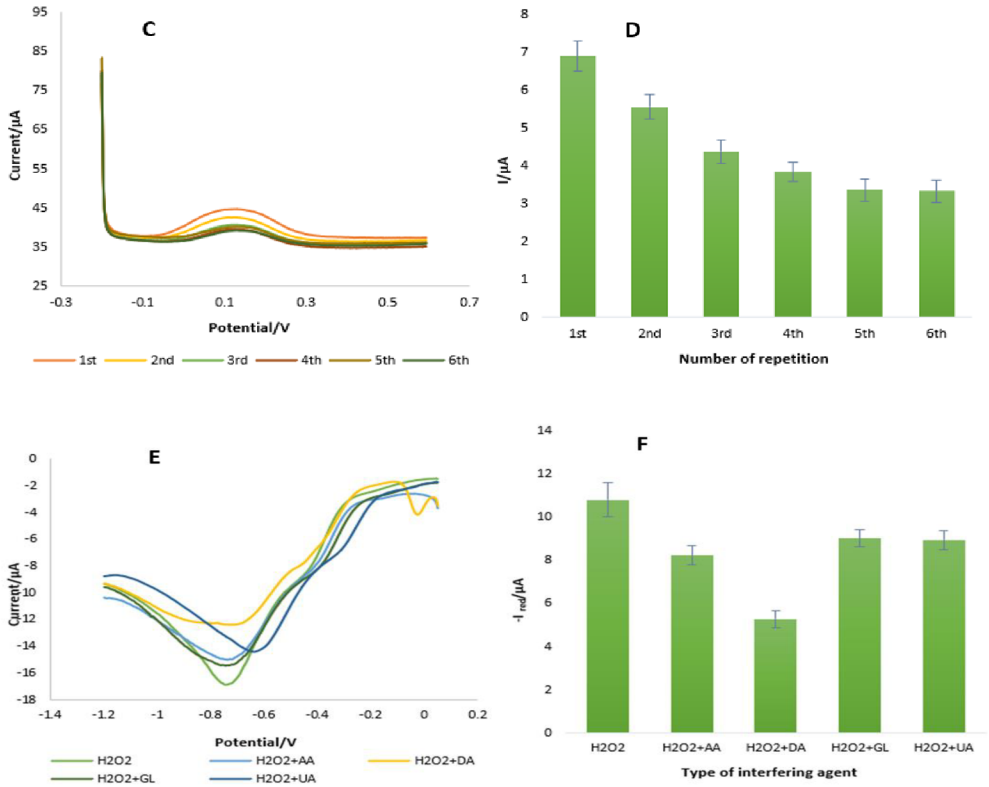

Fig. 4.23 | A) Stability of poly(Tyr)-CS/SPCE were recorded in 0.01 M $Fe(CN)_6^{3-}$ /$Fe(CN)_6^{4-}$ + 0.1M KCl at a sweep rate of 100 mV/s with different cycle numbers (1,5,10, and 50). B) variation of current versus cycle number (n = 3, SD = 3.86). C) Repeatability of MIP/poly(Tyr)-CS/SPCE was recorded in 0.1 mg/ml HRP solution for six cycles. D) Current versus cycle number variation (n = 3, SD = 0.31). E) Effects of interfering species on the voltammetric determination of 1 mM H_2O_2 with HRP/poly(Tyr)-CS/SPCE in PBS solution pH=8 in the presence of ascorbic acid, glucose, dopamine, and uric acid as interfering agents. F) Variation of I_p H_2O_2 versus the type of interfering agents (n = 3, SD = 0.5).

5 CONCLUSIONS

This thesis briefly describes screen-printed electrodes and devices with potential applications in bioelectronics. I focused on the development of portable and disposable (bio)sensors for detecting distinct biologically active compounds important for biomedical applications.

In the first part, SWCNT-modified SPCE as disposable electrochemical sensors was suggested for fast quantification of dasatinib in pharmaceutical formulations, demonstrating an excellent boosting effect on the oxidation response of dasatinib. At optimized pH 5.0 Britton-Robinson buffer, SWCNT-modified SPCEs showed 94% recovery with optimum electrooxidation activity. The oxidation currents exhibited linear relation with dasatinib concentration in the 0.1–100 μM. Based on the results, a limit of detection of 0.06 μM was obtained in the standard solution. The SWCNT-modified SPCEs have been applied to analyze dasatinib in pharmaceutical tablet samples.

In the second part, a sensitive and specific approach was developed for the determination of *Haemophilus influenza* using DNA based bio-assay through bioconjugation of citrate capped silver nanoparticle with pDNA toward target sequences detection. The synthesized probe (SH-5′-AAT TTT CCA ACT TTT TCA CCT GCA T-3') of *Haemophilus influenza* was detected with great sensitivity and selectivity after hybridization with cDNA (5′-ATG CAG GTG AAA AAG TTG GAA AAT T-3'). The ultra-sensitive fabricated optical DNA-based bio-assay was showed the low limit of quantification of 1 ZM for DNA sample using 15 μL of probe and 200 μL of Cit/AgNPs. It has potential for bacterial determination both in clinical and environmental specimens. To evaluate the selectivity of developed DNA based biosensor, three mismatch sequences were applied. Finally, the designed genosensor is a significant diagnostic strategy for detection of *Haemophilus influenza* with great selectivity.

The last part of the thesis focused on the development a highly selective and sensitive electrochemical horseradish peroxidase-imprinted biosensor based on the combination of poly tyrosine-chitosan film electropolymerization on the surface of screen-printed electrodes and a self-assembly surface molecular imprinting approach. The HRP-imprinted biosensor showed a highly bioelectrocatalytical behavior toward hydrogen peroxide reduction in 0.1 M PBS with pH 8.0 and could be used in the voltammetric determination of H_2O_2 in the linear range of 10 nM to 1 mM with a limit of detection and limit of quantification of 2.18 nM and 6.60 nM, respectively. The molecularly imprinted biosensor also exhibited great sensitivity for HRP and was successfully applied for recognition with various concentration ranges of HRP from 1.0×10^{-8} to 1.0×10^{-1} mg/mL with LOD and LOQ of 9.39×10^{-8} mg/ml (2.34 pM) and 2.84×10^{-7} mg/ml (7.11 pM) by differential pulse voltammetry, respectively. The designed electrochemical imprinted biosensor was utilized to detect H_2O_2 in an unprocessed human plasma sample.

To conclude, I concentrated on creating functionalization techniques to design sensitive and selective (bio)sensors for specific analytes and demonstrated their detection in complex media. The screen-printed electrodes were employed to develop cost-effective disposable and portable devices for home care or in-field applications accompanied by various modification techniques for more selective target detection. I investigated numerous factors to enhance the functionalization approach and sensing range, resulting in highly effective (bio)sensors for all applications.

6 APPENDIX

Soodabeh Hassanpour, MSc.

Czech Republic | soodabeh.hassanpour01@upol.cz, soodabehhassanpour@yahoo.com | +420 605-881-208 | Linkedin | Google Scholar

RESEARCH INTERESTS

-Development of electrochemical biosensors for POC applications
-Developing micro/nanosensors
-Biosensors integrated into microfluidics
-Screen printing
-Designing flexible, printable, and wearable biosensors
-Application of nanomaterials for designing biosensors
-BioMEMS

EDUCATION

11/2019-Present **Ph.D. Candidate in Analytical Chemistry**
Palacký University Olomouc, Czech Republic
Dissertation: Novel electrochemical (bio)sensors for analysis of biologically active compounds

10/2015–10/2017 **MSc. Cellular and Molecular Biology-Biochemistry,** Top-Researcher honors
University of Tabriz, Iran
Thesis: Preparation of electrochemical sensors based on functionalized mesoporous silica nanoparticles with amine/iron oxide nanoparticles and their application for the detection of some small biomolecules

10/2010–01/2014 **BSc. Cellular and Molecular Biology-Biotechnology**
University of Tabriz, Iran

PROFESSIONAL EXPERIENCES

2019 - Present **Ph.D. Student**
Palacký University Olomouc, Czech Republic
• Developed innovative MIP (molecularly imprinted polymer) based biosensors for high-precision diagnosis.
• Designed protocols for enantioselective electrochemical biosensors to detect D-amino acids.
• Proficient in utilizing Capillary Electrophoresis for chiral separation of antidepressant and antihistamine drugs.
• Skilled in designing 3D models of microfluidics using Autodesk Fusion 360 software and fabricating them using 3D printers.
• Synthesized nanoparticles and prepared nanocomposites and polymeric films for electrode modification.
• Entrapped enzymes into dendritic silica nanoparticles to create enzymatic biosensors.
• Designed protocols for enzymatic and nonenzymatic electrochemical biosensors to detect cancer biomarkers, viruses, drugs, and pesticides.
• Crafted compelling project proposals and secured funding from reputable agencies.
• Conducted statistical analysis on data sets to derive meaningful insights for the research projects.
• Led a group of researchers in a project that resulted in one published review paper and two under-review original research papers.

2016 - 2019 **Research Assistant**
Pharmaceutical Analysis Research Center, Tabriz University of Medical Sciences, Iran
• Designed and developed a range of biosensors, including electrochemical, paper-based, and optical sensors using AUTOLAB and PalmSens 4c systems.
• Entrapped enzymes into mesoporous silica nanoparticles to create enzymatic biosensors.
• Developed immunosensors for cancer biomarker detection and genosensors for virus detection.
• Designed and fabricated various electrochemical sensors for detecting drugs, amino acids, and pesticides.
• Synthesized and utilized various conductive inks to create flexible and wearable sensors.
• Synthesized nanoparticles and prepared nanocomposites for electrode modification.
• Conducted statistical analysis on data sets using Excel.
• Managed lab inventory and procurement of equipment and services through negotiations.
• Mentored and trained undergraduate and postgraduate students in biosensor development and analysis techniques.

TEACHING EXPERIENCE

2021 – 2022	"Imunoanalytics" course to MSc. Students, Palacký University Olomouc, Czech Republic
2020-2021	"Immunoanalysis of low-molecular-weight compounds" course to MSc. Students, Palacký University Olomouc, Czech Republic

PROJECTS, GRANTS AND AWARDS

	As Principal Investigator (PI)	
2022	The Ministry of Education, Youth and Sports Czech Republic, Doctoral Student Grant Competition, "Chirality-based electrochemical sensors: new approaches for enantiomer discrimination project", DSGC-2021-0176	56,397.655 Euro
	As Main Applicant	
2019-2023	Fischer Scholarship, Palacký University Olomouc	12,610.831 Euro per year
2022	Erasmus+ Scholarship for the research stay at the University of Copenhagen, Denmark	2.2K Euro
	As Member	
2023	Palacký University Olomouc, project IGA_PrF	
2022	Palacký University Olomouc, project IGA_PrF	
2020-2021	Czech Science Foundation, Improving sensitivity in chiral separations by capillary electrophoresis connected with ESI-MS or ICP-MS project	
2021	Palacký University Olomouc, project IGA_PrF	
2020	Palacký University Olomouc, project IGA_PrF	
2018-2019	Tabriz University of Medical Sciences, Conductive nano/bio-inks for the design of different biosensors project	

CONFERENCES

09/2022	12th International Symposium of Drug Analysis, 32nd International Symposium on Pharmaceutical and Biomedical Analysis, DA-PBA 2022, Mons, Belgium (Poster) "A new platform for enzymatic enantioselective biosensing of amino acids in human plasma using the D-amino acid oxidase enzyme encapsulated in dendritic silica"
06/2022	Advances in Chromatography and Electrophoresis & Chiranal 2022, Olomouc, Czech Republic (Poster) "Enzymatic chiral biosensing of tyrosine in human plasma using the D-amino acid oxidase enzyme entrapped in dendritic silica nanoparticles"
04/2022	4th Cross-Border Seminar on Electroanalytical Chemistry (CBSEC), Prague, Czech Republic (Oral) "Nanomaterials modified conductive ink-based electrochemical immunosensor for monitoring CA125 protein in plasma samples"
07/2021	e-MSB 2021: 37th International Symposium on Microscale Separations and Bioanalysis (Poster) "Preconcentration of DNA in A 3D-Printed Microfluidic Device"
10/2020	24th International Conference on Miniaturized Systems for Chemistry and Life Sciences (MicroTAS 2020) online workshop

TECHNICAL SKILLS

-Autodesk Fusion 360
-Chem Draw
-Corel
-NOVA 1.10 and NOVA 2.1.2
-ChemStation Agilent
-Microsoft Office

TRAINING

11/2022-04/2023	Electro-membrane extraction (EME) with chiral Capillary Electrophoresis, University of Copenhagen, Denmark Supervisors: Prof. Jorg P. Kutter and Prof. Stig Pedersen-Bjergaard

THESIS PUBLICATIONS

1 **S. Hassanpour**, J. Petr, *A disposable electrochemical sensor based on single-walled carbon nanotubes for the determination of anticancer drug dasatinib*, Monatshefte für Chemie-Chemical Monthly (2023) 1-9.

2 **S. Hassanpour**, N. Niaei, J. Petr, *Metal–Organic Frameworks-Based Analytical Devices for Chiral Sensing and Separations: A Review (2012–202.* Chemosensors 11(1) (2023) 29.

3 **S. Hassanpour**, A. Saadati, M. Hasanzadeh, *pDNA conjugated with citrate capped silver nanoparticles towards ultrasensitive bio-assay of haemophilus influenza in human biofluids: A novel optical biosensor*, Journal of Pharmaceutical and Biomedical Analysis 180 (2020) 113050.

4 **S. Hassanpour**, M. Hasanzadeh, J. Petr, *Bioelectrocataytic behavior horseradish peroxidase bound to green polymeric scaffold of poly(tyrosine)-chitosan molecularly imprinted polymer toward monitoring of H_2O_2 in human biofluids*, RSC advances, submitted.

SELECTED PUBLICATIONS (GOOGLE SCHOLAR H INDEX 16, 7190 citations)

1 M.B. Behyar, H. Kholafazad-kordasht, **S. Hassanpour**, M. Hasanzadeh, *An innovative electrically conductive biopolymer based on poly (β-cyclodextrin) towards recognition of ascorbic acid in real sample: Utilization of biocompatible advanced materials in biomedical analysis*, Journal of Molecular Recognition 35(5) (2022) e2953.

2 **S. Hassanpour**, M. Hasanzadeh, *Label-free electrochemical-immunoassay of cancer biomarkers: Recent progress and challenges in the efficient diagnosi.* *of cancer employing electroanalysis and based on point of care (POC)*, Microchemical Journal 168 (2021) 106424.

3 **S. Hassanpour**, B. Behnam, B. Baradaran, M. Hashemzaei, F. Oroojalian, A. Mokhtarzadeh, M. de la Guardia, *Carbon based nanomaterials for the detection of narrow therapeutic index pharmaceuticals*, Talanta 221 (2021) 121610.

4 A. Saadati, **S. Hassanpour**, M. Hasanzadeh, *Lab-on-fruit skin and lab-on-leaf towards recognition of trifluralin using Ag-citrate/GQDs nanocomposite stabilized on the flexible substrate: A new platform for the electroanalysis of herbicides using direct writing of nano-inks and pen-on paper technology*, Heliyon 6(12) (2020) e05779.

5 **S. Hassanpour**, H.J. Kim, A. Saadati, P. Tebon, C. Xue, F.W. van den Dolder, J. Thakor, B. Baradaran, J. Mosafer, A. Baghbanzadeh, *Thrombolytic agen.* *nanocarriers in controlled release*, Small 16(40) (2020) 2001647.

6 H. kholafazad Kordasht, **S. Hassanpour**, B. Baradaran, R. Nosrati, M. Hashemzaei, A. Mokhtarzadeh, M. de la Guardia, *Biosensing of microcystins in water samples; recent advances*, Biosensors and Bioelectronics 165 (2020) 112403.

7 A. Saadati, **S. Hassanpour**, M. Hasanzadeh, N. Shadjou, *Binding of pDNA with cDNA using hybridization strategy towards monitoring of Haemophilus influenza genome in human plasma samples*, International journal of biological macromolecules 150 (2020) 218-227.

8 F. Farshchi, M. Hasanzadeh, M. Feyziazar, A. Saadati, **S. Hassanpour**, *Electropolymerization of chitosan in the presence of CuNPs on the surface of a copper electrode: an advanced nanocomposite for the determination of mefenamic acid and indomethacin in human plasma samples and prevention of drug poisoning*, Analytical Methods 12(9) (2020) 1212-1217.

9 **S. Hassanpour**, A. Saadati, M. Hasanzadeh, *Sensitive monitoring of riboflavin in commercial multivitamins using poly (chitosan)-based nanocomposite*, Journal of Molecular Recognition 33(2) (2020) e2817.

10 F. Bahavarnia, A. Mobed, M. Hasanzadeh, A. Saadati, **S. Hassanpour**, A. Mokhtarzadeh, *Bio-assay of Acintobacter baumannii using DNA conjugated with gold nano-star: A new platform for microorganism analysis*, Enzyme and microbial technology 133 (2020) 109466.

11 A. Saadati, **S. Hassanpour**, F. Bahavarnia, M. Hasanzadeh, *A novel biosensor for the monitoring of ovarian cancer tumor protein CA 125 in untreated human plasma samples using a novel nano-ink: a new platform for efficient diagnosis of cancer using paper based microfluidic technology*, Analytical Methods 12(12) (2020) 1639-1649.

12 A. Mobed, M. Hasanzadeh, A. Saadati, **S. Hassanpour**, *Synthesis and electroanalytical behaviour of AgNPs/graphite conductive nano-ink towards biosensing of bacteria genome in human biofluids*, Analytical Methods 12(9) (2020) 1218-1228.

13 M. Feyziazar, M. Hasanzadeh, F. Farshchi, A. Saadati, **S. Hassanpour**, *An innovative method to electrochemical branching of chitosan in the presence of copper nanocubics on the surface of glassy carbon and its electrical behaviour study: A new platform for pharmaceutical analysis using electrochemical sensors*, Reactive and Functional Polymers 146 (2020) 104402.

14 A. Mobed, M. Hasanzadeh, N. Shadjou, **S. Hassanpour**, A. Saadati, M. Agazadeh, *Immobilization of ssDNA on the surface of silver nanoparticles-graphene quantum dots modified by gold nanoparticles towards biosensing of microorganism*, Microchemical Journal 152 (2020) 104286.

15 A. Mobed, F. Nami, M. Hasanzadeh, **S. Hassanpour**, A. Saadati, A. Mokhtarzadeh, *A novel nucleic acid based bio-assay toward recognition of Haemophilus influenza using bioconjugation and DNA hybridization method*, International journal of biological macromolecules 139 (2019) 1239-1251.

16 F. Bahavarnia, A. Saadati, **S. Hassanpour**, M. Hasanzadeh, N. Shadjou, A. Hassanzadeh, *Paper based immunosensing of ovarian cancer tumor protein CA 125 using novel nano-ink: a new platform for efficient diagnosis of cancer and biomedical analysis using microfluidic paper-based analytical devices (µPAD)*, International journal of biological macromolecules 138 (2019) 744-754.

17 A. Mobed, M. Hasanzadeh, **S. Hassanpour**, A. Saadati, M. Agazadeh, A. Mokhtarzadeh, *An innovative nucleic acid based biosensor toward detection of Legionella pneumophila using DNA immobilization and hybridization: A novel genosensor*, Microchemical Journal 148 (2019) 708-716.

18 A. Saadati, **S. Hassanpour**, M. Hasanzadeh, N. Shadjou, A. Hassanzadeh, *Immunosensing of breast cancer tumor protein CA 15-3 (carbohydrate antigen 15.3) using a novel nano-bioink: A new platform for screening of proteins in human biofluids by pen-on-paper technology*, International journal of biological macromolecules 132 (2019) 748-758.

19 A. Saadati, **S. Hassanpour**, M. de la Guardia, J. Mosafer, M. Hashemzaei, A. Mokhtarzadeh, B. Baradaran, *Recent advances on application of peptide nucleic acids as a bioreceptor in biosensors development*, TrAC Trends in Analytical Chemistry 114 (2019) 56-68.

20 **S. Hassanpour**, M. Hasanzadeh, A. Saadati, N. Shadjou, J. Soleymani, A. Jouyban, *A novel paper based immunoassay of breast cancer specific carbohydrate (CA 15.3) using silver nanoparticles-reduced graphene oxide nano-ink technology: A new platform to construction of microfluidic paper-based analytical devices (µPADs) towards biomedical analysis*, Microchemical Journal 146 (2019) 345-358.

21 M. Jafari, M. Hasanzadeh, E. Solhi, **S. Hassanpour**, N. Shadjou, A. Mokhtarzadeh, A. Jouyban, S. Mahboob, *Ultrasensitive bioassay of epitope of Mucin-16 protein (CA 125) in human plasma samples using a novel immunoassay based on silver conductive nano-ink: A new platform in early stage diagnosis of ovarian cancer and efficient management*, International journal of biological macromolecules 126 (2019) 1255-1265.

22 H. Ashrafi, **S. Hassanpour**, A. Saadati, M. Hasanzadeh, K. Ansarin, S.A. Ozkan, N. Shadjou, A. Jouyban, *Sensitive detection and determination of benzodiazepines using silver nanoparticles-N-GQDs ink modified electrode: A new platform for modern pharmaceutical analysis*, Microchemical Journal 145 (2019) 1050-1057.

23 **S. Hassanpour**, A. Saadati, M. Hasanzadeh, N. Shadjou, A. Mirzaie, A. Jouyban, *Direct writing of biocatalytic materials based on pens filled with high-tech enzymatic inks:"Do-it-Yourself"*, Microchemical Journal 145 (2019) 266-272.

24 F. Nami, A. Saadati, **S. Hassanpour**, M. Hasanzadeh, A. Hassanzadeh, *Bioassay of ovarian cancer tumor protein CA 125 using novel nano-ink on the flexible paper substrate: A new platform for efficient diagnosis of cancer*, International journal of biological macromolecules (2019).

25 A. Mirzaie, A. Saadati, **S. Hassanpour**, M. Hasanzadeh, M. Siahi-Shadbad, A. Jouyban, *Determination of proline in human plasma samples using the encapsulation of proline dehydrogenase enzyme in dendritic silica: a new platform for the enzymatic biosensing of amino acids*, Analytical Methods 11(36) (2019) 4609-4619.

26 A. Mobed, M. Hasanzadeh, M. Aghazadeh, A. Saadati, **S. Hassanpour**, A. Mokhtarzadeh, *The bioconjugation of DNA with gold nanoparticles towards the spectrophotometric genosensing of pathogenic bacteria*, Analytical Methods 11(33) (2019) 4289-4298.

27 A. Mobed, M. Hasanzadeh, **S. Hassanpour**, A. Saadati, M. Agazadeh, A. Mokhtarzadeh, *An innovative nucleic acid based biosensor toward detection of Legionella pneumophila using DNA immobilization and hybridization: A novel genosensor*, Microchemical Journal 148 (2019) 708-716.

28 **S. Hassanpour**, B. Baradaran, M. de la Guardia, A. Baghbanzadeh, J. Mosafer, M. Hejazi, A. Mokhtarzadeh, M. Hasanzadeh, *Diagnosis of hepatitis via nanomaterial-based electrochemical, optical or piezoelectrical biosensors: a review on recent advancements*, Microchimica Acta 185(12) (2018) 1-24.

29 M. Hasanzadeh, A.S. Nahar, **S. Hassanpour**, N. Shadjou, A. Mokhtarzadeh, *Immobilization of proline dehydrogenase on functionalized silica mesoporous nanomaterial towards preparation of a novel thermostable enzyme biosensor*, Journal of Nanoscience and Nanotechnology 18(11) (2018) 7786-7796.

30 M. Hasanzadeh, **S. Hassanpour**, A.S. Nahr, N. Shadjou, A. Mokhtarzadeh, S. Mahboob, *Electropolymerization of proline supported beta cyclodextrin inside amino functionalized magnetic mesoporous silica nanomaterial: one step preparation, characterization and electrochemical application*, Anal. Bioanal. Electrochem 10(1) (2018) 77-97.

31 **S. Hassanpour**, B. Baradaran, M. Hejazi, M. Hasanzadeh, A. Mokhtarzadeh, M. de la Guardia, *Recent trends in rapid detection of influenza infections by bio and nanobiosensor*, TrAC Trends in Analytical Chemistry 98 (2018) 201-215.

32 M. Hasanzadeh, **S. Hassanpour**, A. Saadati, N. Shadjou, A. Mokhtarzadeh, *Magnetic mesoporous silica/chitosan/polyproline: a novel nanocomposite toward sensing of some clinically relevant biomolecules*, Nano Life 7(03n04) (2017) 1750006.

33 A. Mokhtarzadeh, **S. Hassanpour**, Z.F. Vahid, M. Hejazi, M. Hashemi, J. Ranjbari, M. Tabarzad, S. Noorolyai, M. de la Guardia, *Nano-delivery system targeting to cancer stem cell cluster of differentiation biomarkers*, Journal of Controlled Release 266 (2017) 166-186.

34 M. Hasanzadeh, A.S. Nahar, **S. Hassanpour**, N. Shadjou, A. Mokhtarzadeh, J. Mohammadi, *Proline dehydrogenase-entrapped mesoporous magnetic silica nanomaterial for electrochemical biosensing of L-proline in biological fluids*, Enzyme and microbial technology 105 (2017) 64-76.

BOOK PUBLICATIONS

Book	A. Saadati, **S. Hassanpour**, N. Shadjou, M. Hasanzadeh, *Conductive inks: Synthesis and electroanalytical application*, LAP LAMBERT academic publishing (2022).
Book chapter	**S. Hassanpour**, A. Mokhtarzadeh, M. Hasanzadeh, M. Hejazi, B. Baradaran, *Nanomaterials for Use in Apta-Assays*, Handbook of Smart Materials in Analytical Chemistry (2019) 243-271.

REFERENCES

Dr. Jan Petr	secjpetr@gmail.com	Ph.D. supervisor, Palacký University Olomouc, Czech Republic
Dr. Petr Bednář	petr.bednar@upol.cz	Head of the Analytical Chemistry department, Palacký University Olomouc, Czech Republic
Prof. Jorg P. Kutter	jorg.kutter@sund.ku.dk	Erasmus+ traineeship supervisor, University of Copenhagen, Denmark
Prof. Stig Pedersen-Bjergaard	stig.pedersen-bjergaard@farmasi.uio.no	Erasmus+ traineeship supervisor, University of Copenhagen, Denmark
Dr. Mohammad Hasanzadeh	mhmmd_hasanzadeh@yahoo.com	MSc. supervisor, Tabriz University of Medical science, Iran

7 REFERENCES

1. F. Bettazzi, G. Marrazza, M. Minunni, I. Palchetti and S. Scarano, *Comprehensive Analytical Chemistry*, 2017, **77**, 1-33.
2. S. Hassanpour, B. Baradaran, M. de la Guardia, A. Baghbanzadeh, J. Mosafer, M. Hejazi, A. Mokhtarzadeh and M. Hasanzadeh, *Microchimica Acta*, 2018, **185**, 1-24.
3. S. Hassanpour, B. Baradaran, M. Hejazi, M. Hasanzadeh, A. Mokhtarzadeh and M. de la Guardia, *TrAC Trends in Analytical Chemistry*, 2018, **98**, 201-215.
4. J. J. Gooding, *Electroanalysis: An International Journal Devoted to Fundamental and Practical Aspects of Electroanalysis*, 2008, **20**, 573-582.
5. L. M. Santiago, D. Bejarano-Nosas, P. Lozano-Sanchez and I. Katakis, *Analyst*, 2010, **135**, 1276-1281.
6. D. Mata, D. Bejarano, M. Botero, P. Lozano, M. Constantí and I. Katakis, *Electrochimica Acta*, 2010, **55**, 4261-4266.
7. Y. Koç, U. MORALI, S. Erol and H. AVCI, *Turkish Journal of Chemistry*, 2021, **45**, 1895-1915.
8. K. Mahato and J. Wang, *Sensors and Actuators B: Chemical*, 2021, **344**, 130178.
9. U. Jain, N. Chauhan and K. Saxena, *Multifaceted Bio-Sensing Technology*, 2023, 31-44.
10. A. Saadati, S. Hassanpour, M. de la Guardia, J. Mosafer, M. Hashemzaei, A. Mokhtarzadeh and B. Baradaran, *TrAC Trends in Analytical Chemistry*, 2019, **114**, 56-68.
11. O. A. Farghaly, R. A. Hameed and A.-A. H. Abu-Nawwas, *Int. J. Electrochem. Sci*, 2014, **9**, 3287-3318.
12. D. R. Thévenot, K. Toth, R. A. Durst and G. S. Wilson, *Analytical Letters*, 2001, **34**, 635-659.
13. H. R. S. Lima, J. S. da Silva, E. A. de Oliveira Farias, P. R. S. Teixeira, C. Eiras and L. C. C. Nunes, *Biosensors and Bioelectronics*, 2018, **108**, 27-37.
14. A. A. Ensafi and P. Nasr-Esfahani, in *Biosensors*, CRC Press, 2023, pp. 27-56.
15. A. J. Bard and L. R. Faulkner, *Electrochemical methods*, 2001, **2**, 580-632.
16. N. Elgrishi, K. J. Rountree, B. D. McCarthy, E. S. Rountree, T. T. Eisenhart and J. L. Dempsey, *Journal of chemical education*, 2018, **95**, 197-206.
17. O. D. Renedo, M. Alonso-Lomillo and M. A. Martinez, *Talanta*, 2007, **73**, 202-219.
18. J. P. Metters, R. O. Kadara and C. E. Banks, *Analyst*, 2011, **136**, 1067-1076.
19. M. Li, Y.-T. Li, D.-W. Li and Y.-T. Long, *Analytica chimica acta*, 2012, **734**, 31-44.
20. N. Sandhyarani, in *Electrochemical Biosensors*, Elsevier, 2019, pp. 45-75.
21. A. Chen and S. Chatterjee, *Chemical Society Reviews*, 2013, **42**, 5425-5438.
22. N. S. Lakka, C. Kuppan, K. S. Srinivas and R. Yarra, *Chromatographia*, 2020, **83**, 947-962.
23. C. S. Jesus and V. C. Diculescu, *Journal of Electroanalytical Chemistry*, 2015, **752**, 47-53.
24. P. Kissinger and W. R. Heineman, *Laboratory Techniques in Electroanalytical Chemistry, revised and expanded*, CRC press, 2018.
25. S. Hassanpour, A. Saadati and M. Hasanzadeh, *J Mol Recognit*, 2020, **33**, e2817.
26. M. Feyziazar, M. Hasanzadeh, F. Farshchi, A. Saadati and S. Hassanpour, *Reactive and Functional Polymers*, 2020, **146**, 104402.
27. A. S. Nahr, S. Hassanpour and M. Hasanzadeh, *Analytical Methods*, 2020.
28. A. J. Bard, *W iley, New York*, 1980.
29. E. Laviron, *Journal of Electroanalytical Chemistry and Interfacial Electrochemistry*, 1979, **101**, 19-28.
30. M. G. García and A. C. García, *Bioelectrochemistry and bioenergetics*, 1995, **38**, 389-395.
31. B.-G. Lee, K.-B. Rhyu and K.-J. Yoon, *Bulletin of the Korean Chemical Society*, 2009, **30**, 2457-2460.
32. C. M. Brett, O. Brett and A. Electrochemistry, 1993.
33. L. R. Faulkner and A. J. Bard, *Electrochemical methods: fundamentals and applications*, John Wiley and Sons, 2002.
34. S. A. Alavi-Tabari, M. A. Khalilzadeh and H. Karimi-Maleh, *Journal of electroanalytical chemistry*, 2018, **811**, 84-88.
35. F. Tahernejad-Javazmi, M. Shabani-Nooshabadi and H. Karimi-Maleh, *New Journal of Chemistry*, 2018, **42**, 16378-16383.
36. D. E. BAYRAKTEPE, K. POLAT and Z. YAZAN, *Journal of the Turkish Chemical Society Section A: Chemistry*, 2018, **5**, 381-392.

37. H. Karimi-Maleh, A. F. Shojaei, K. Tabatabaeian, F. Karimi, S. Shakeri and R. Moradi, *Biosensors and Bioelectronics*, 2016, **86**, 879-884.
38. G. H. Woehrle, J. E. Hutchison, S. Özkar and R. G. FINKE, *Turkish Journal of Chemistry*, 2006, **30**, 1-13.
39. S. Wang and H. Xin, *The Journal of Physical Chemistry B*, 2000, **104**, 5681-5685.
40. H. Fissan, S. Ristig, H. Kaminski, C. Asbach and M. Epple, *Analytical Methods*, 2014, **6**, 7324-7334.
41. W. W. Cleland, *Biochemistry*, 1964, **3**, 480-482.
42. M. C. Alliegro, *Analytical biochemistry*, 2000, **282**, 102-106.
43. J.-S. Lee, A. K. Lytton-Jean, S. J. Hurst and C. A. Mirkin, *Nano letters*, 2007, **7**, 2112-2115.
44. H. Wei, C. Chen, B. Han and E. Wang, *Analytical chemistry*, 2008, **80**, 7051-7055.
45. M. Hasanzadeh, F. Mokhtari, N. Shadjou, A. Eftekhari, A. Mokhtarzadeh, V. Jouyban-Gharamaleki and S. Mahboob, *Materials Science and Engineering: C*, 2017, **75**, 247-258.
46. M. Hasanzadeh, S. Hassanpour, A. Saadati, N. Shadjou and A. Mokhtarzadeh, *Nano Life*, 2017, **7**, 1750006.
47. M. Hasanzadeh, F. Mokhtari, V. Jouyban-Gharamaleki, A. Mokhtarzadeh and N. Shadjou, *Journal of Molecular Recognition*, 2018, **31**, e2717.
48. A. Yarman, K. J. Jetzschmann, B. Neumann, X. Zhang, U. Wollenberger, A. Cordin, K. Haupt and F. W. Scheller, *Chemosensors*, 2017, **5**, 11.
49. C. Dong, H. Shi, Y. Han, Y. Yang, R. Wang and J. Men, *European Polymer Journal*, 2021, **145**, 110231.
50. Q. Wang, R. Xue, H. Guo, Y. Wei and W. Yang, *Journal of Electroanalytical Chemistry*, 2018, **817**, 184-194.
51. D. Nie, D. Jiang, D. Zhang, Y. Liang, Y. Xue, T. Zhou, L. Jin and G. Shi, *Sensors and Actuators B: Chemical*, 2011, **156**, 43-49.
52. S. Sardaremelli, M. Hasanzadeh and H. Razmi, *Journal of Molecular Recognition*, 2021, **34**, e2884.
53. J. Xu, F. Shang, J. H. Luong, K. M. Razeeb and J. D. Glennon, *Biosensors and Bioelectronics*, 2010, **25**, 1313-1318.
54. J. Kärger and D. M. Ruthven, *New Journal of Chemistry*, 2016, **40**, 4027-4048.
55. A. L. Eckermann, D. J. Feld, J. A. Shaw and T. J. Meade, *Coordination chemistry reviews*, 2010, **254**, 1769-1802.
56. H. A. Harbury, *Journal of Biological Chemistry*, 1957, **225**, 1009-1024.
57. T.-C. Chou, K.-Y. Wu, F.-X. Hsu and C.-K. Lee, *journal of food and drug analysis*, 2018, **26**, 662-669.
58. K. Thenmozhi and S. S. Narayanan, *Materials Science and Engineering: C*, 2017, **70**, 223-230.
59. M. Dai, T. Huang, L. Chao, Q. Xie, Y. Tan, C. Chen and W. Meng, *Talanta*, 2016, **149**, 117-123.
60. J. Zbiljić, O. Vajdle, V. Guzsvány, J. Molnar, J. Agbaba, B. Dalmacija and K. Kalcher, *Journal of Hazardous Materials*, 2015, **283**, 292-301.
61. W. Xu, J. Liu, M. Wang, L. Chen, X. Wang and C. Hu, *Analytica chimica acta*, 2016, **913**, 128-136.
62. Y. Xiong, C. Wang, Y. Wu, C. Luo, D. Zhan and S. Wang, *Molecules*, 2022, **27**, 8599.
63. L. Campos-Arias, R. del Olmo, N. Peřinka, N. Casado, J. L. Vilas-Vilela, D. Mecerreyes, F. J. del Campo and S. Lanceros-Méndez, *Electrochimica Acta*, 2023, **439**, 141615.
64. D. Chen, X. Zhuang, J. Zhai, Y. Zheng, H. Lu and L. Chen, *Sensors and Actuators B: Chemical*, 2018, **255**, 1500-1506.
65. S. Komathi, A. I. Gopalan, S.-K. Kim, G. S. Anand and K.-P. Lee, *Electrochimica Acta*, 2013, **92**, 71-78.
66. R. Karthik, N. Karikalan and S.-M. Chen, *Carbohydrate polymers*, 2017, **164**, 102-108.
67. L. Naderi, S. Shahrokhian, M. K. Amini and M. Hafezi Kahnamouei, *ACS Applied Nano Materials*, 2023.
68. S. Nandini, S. Nalini, R. Manjunatha, S. Shanmugam, J. S. Melo and G. S. Suresh, *Journal of Electroanalytical Chemistry*, 2013, **689**, 233-242.
69. E. Erçarıkcı, K. D. Kıranşan and E. Topçu, *IEEE Sensors Journal*, 2023.
70. M.-H. Yeh, Y.-S. Li, G.-L. Chen, L.-Y. Lin, T.-J. Li, H.-M. Chuang, C.-Y. Hsieh, S.-C. Lo, W.-H. Chiang and K.-C. Ho, *Electrochimica Acta*, 2015, **172**, 52-60.
71. C. Chen, X. Hong, T. Xu, A. Chen, L. Lu and Y. Gao, *Synthetic Metals*, 2016, **212**, 123-130.
72. Y. Wang, Z. Wang, Y. Rui and M. Li, *Biosensors and Bioelectronics*, 2015, **64**, 57-62.
73. Z. Yu, H. Li, X. Zhang, N. Liu and X. Zhang, *Talanta*, 2015, **144**, 1-5.
74. M. Sheikholeslam, P. Nanda, A. Sanati, M. Pritzker and P. Chen, *Materials Letters*, 2023, **335**, 133799.
75. M. Ye, C. Yang, Y. Sun, J. Wang, D. Wang, Y. Zhao, Z. Zhu, P. Liu, J. Zhu and C. Li, *ACS Applied Nano Materials*, 2022, **5**, 10922-10932.

76. S. Kubendhiran, B. Thirumalraj, S.-M. Chen and C. Karuppiah, *Journal of colloid and interface science*, 2018, **509**, 153-162.
77. Y. Pan, Z. Hou, H. Yang and Y.-N. Liu, *Materials Science in Semiconductor Processing*, 2015, **40**, 176-182.
78. J. Alvarez-Paguay, L. Fernández, D. Bolaños-Méndez, G. González and P. J. Espinoza-Montero, *Sensing and Bio-Sensing Research*, 2022, **37**, 100514.
79. M. Shafa, I. Ahmad, S. Hussain, M. Asif, Y. Pan, R. Zairov, A. A. Alothman, M. Ouladsmane, Z. Ullah and N. Ullah, *Surfaces and Interfaces*, 2023, **36**, 102616.
80. C. van der Horst, B. Silwana, E. Iwuoha and V. Somerset, *Procedia technology*, 2017, **27**, 179-182.
81. S. Yang, C. Bai, Y. Teng, J. Zhang, J. Peng, Z. Fang and W. Xu, *Canadian Journal of Chemistry*, 2019, **97**, 833-839.
82. S. Sardaremelli, H. Razmi, M. Hasanzadeh and N. Shadjou, *International journal of biological macromolecules*, 2020, **145**, 311-324.